UNIVERSIDADE FEDERAL DO RIO GRANDE DO SUL

INSTITUTO DE QUÍMICA

PROGRAMA DE PÓS-GRADUAÇÃO EM QUÍMICA

ALEXANDRE DELLA FLORA

Avaliação do acoplamento de processos fotocatalíticos solares e processo de adsorção para amitigação de fármacos em efluente hospitalar

TESE DE DOUTORADO

Porto Alegre

2022

UNIVERSIDADE FEDERAL DO RIO GRANDE DO SUL

INSTITUTO DE QUÍMICA

PROGRAMA DE PÓS-GRADUAÇÃO EM QUÍMICA

ALEXANDRE DELLA FLORA

Avaliação do acoplamento de processos fotocatalíticos solares e processo de adsorção para amitigação de fármacos em efluente hospitalar

Tese apresentada como requisito parcial para a obtenção do grau de Doutor em Química

Prof. Dra. Carla Sirtori
Orientadora

Prof. Dr. Éder Claudio Lima
Co-orientador

Porto Alegre, novembro de 2022

AGRADECIMENTOS

acompanhar nessa trajetória nesses últimos anos, e por sua causa, consegui terminar. Te amo, minha amada esposa.

Sumário

LISTA DE FIGURAS

Capítulo 1.

Capítulo 2.

LISTA DE TABELAS

Capítulo 1.

Capítulo 2

Capítulo 3.

ABREVIAÇÕES

ANA	= Agência Nacional de Águas
ANVISA	= Agência Nacional de Vigilância Sanitária
AOPs	= Processos Avançados de Oxidação, do inglês: *Adanced Oxidantion Process*
CONAMA	= Conselho Nacional do Meio Ambiente
DBE	= do inglês: *Double Bond Equivalence*
DBO	= Demanda Bioquímica de Oxigênio
DQO	= Demanda Química de Oxigênio
ETA	= Estação de Tratamento de Águas
ETAR	= Estação de Tratamento de Águas Residuais
FLUT	= Flutamida
PBT	= Persistência, Bioacumulação e Toxicidade
(Q)SAR	= do inglês: *(quantitative) structure-activity relationship*
TPs	= produtos de transformação, do inglês: *Transformation Products*

RESUMO

A presença de contaminantes de interesse emergente no meio ambiente vem aumentando nos últimos anos devido ao amplo uso de fármacos, produtos de higiene pessoal, agrotóxicos, retardantes de chamas, organoclorados e organobromados, entre outros. Nesse sentido, especial atenção tem sido dada aos fármacos, uma vez que tais compostos, quando presentes nos diferentes compartimentos ambientais, podem causar efeitos adversos variados e, até mesmo, gerar ou ampliar a resistência bacteriana em organismos aquáticos e nos seres humanos. Além disso, as estações de tratamentos de efluentes geralmente empregam tratamentos biológicos. Tais sistemas não foram projetados para o tratamento de fármacos. Isso porque estes contaminantes não são biodegradáveis e, em muitos casos, podem ser tóxicos ou inibir o consórcio de microrganismos que constitui os diferentes processos biológicos convencionalmente empregados nos sistemas de tratamento convencionais. Assim, surge a necessidade de realizar novos estudos que avaliem o emprego de diferentes tecnologias de tratamentos para a degradação e remoção desses contaminantes de interesse emergente. Dentre os tratamentos mais promissores para o tratamento de efluentes e águas residuais complexas pode-se destacar os Processos Avançados de Oxidação (AOPs), em especial o processo Fenton e foto-Fenton em pH próximo da neutralidade. Por sua vez, técnicas cromatográficas acopladas à espectrometria de massas de alta resolução são uma alternativa instrumental válida para o monitoramento dos contaminantes de interesse emergente e, também, para poder realizar a identificação de produtos de transformação (TPs). Quando combinadas a modelagem *in silico*, por métodos de relações quantitativas entre a estrutura e atividade ((Q)SAR), ajudam na tomada de decisão sobre quais os contaminantes e TPs de maior risco ambiental e até que ponto os tratamentos avaliados devem perdurar. Por sua vez, quando os AOPs têm sua aplicação limitada por diferentes fatores, os processos de adsorção, em especial, os tratamentos que empregam carvão ativo produzido através de biomassas, se apresentam como uma alternativa interessante para, mediante um sistema de tratamentos alternativos acoplados, viabilizara remoção de diferentes contaminantes ou TPs recalcitrantes/tóxicos gerados nos processos de AOPs. Considerando essas questões, a presente tese está dividida em três capítulos, detalhados a seguir.

O Capítulo 1 apresenta o estudo individualizado da Flutamida via degradação por processo foto-Fenton solar (SPF). O fármaco selecionado para estudo é utilizado no

tratamento do câncer da próstata. As identificações dos TPs foram realizadas por cromatografia líquida de alta eficiência acoplada ao analisador de massas híbrido quadrupolo-tempo de voo. Ainda, associadas às ferramentas de predições *in silico*, foram preditos parâmetros de ecotoxicidade desses TPs. Na condição otimizada do processo foto-Fenton solar, um total de 13 TPs nunca antes relatados na literatura científica atual, foram preditos e os resultados da avaliação *in sílico* indicam que tais TPs são persistentes, mutagênicos e carcinogênicos, além de não serem biodegradáveis.

O Capítulo 2 apresenta o tratamento de um efluente hospitalar contaminado com a Flutamida. Nesse estudo, priorizou-se a identificação dos TPs no efluente, utilizando análise não-alvo (*non-target screening*) por meio de uma base de dados construída especificamente para identificação dos TPs da Flutamida, e a remoção da Flutamida e seus TPs por combinação de processos solar foto-Fenton e de adsorção utilizando carvão ativo. Ainda, foi otimizado o processo de adsorção para remoção dos analitos em estudo. O acople dos processos permitiu remover com segurança a grande maioria dos TPs, com altas taxas de remoção. Contudo, para os TPs que apresentam abertura do anel aromático, taxas inferiores foram obtidas em decorrência de serem TPs com uma polaridade maior.

O Capítulo 3 é o estudo do tratamento de um efluente hospitalar real fortificado com uma mistura de 9 compostos farmacêuticos (cloranfenicol, fluconazol, flutamida, furosemida, gemfibrozil, ibuprofeno, losartana, nimesulida e paracetamol) de diferentes classes. Inicialmente foram comparadas quatro abordagens de degradação por foto-Fenton solar. Ao mesmo tempo, os TPs gerados por essas diferentes abordagens foram identificados mediante o uso de uma base de dados especialmente construída que continha informações de 127 TPs provenientes dos 9 fármacos selecionados. As diferentes abordagens geraram um total de 38 TPs, sendo que duas novas estruturas foram pospostas para os TPs de nimesulida. Ainda, ao realizar a combinação de processos, altas taxas de remoção foram alcançadas para os fármacos e TPs, exceto no caso de TPs que apresentam uma polaridade maior.

Ao longo dos diferentes estudos realizados, estratégias para a degradação dos compostos farmacêuticos aliadas à remoção dos TPs foram propostas. Adicionalmente, novas estruturas de TPs, que nunca haviam sido identificados e publicados, foram divulgadas por meio dos estudos que compõe essa Tese, evidenciando que o presente trabalho apresenta relevância na temática de remoção de fármacos e TPs presentes em efluentes hospitalares.

Palavras chave: Fármacos, efluente hospitalar, processo foto-Fenton solar, produtos de transformação, (Q)SAR, adsorção.

ABSTRACT

The presence of emerging contaminants into the environment has increased in recent years due to the widespread use of pharmaceuticals, personal care products, pesticides, flame retardants, organochlorines and organobromines, among others. In this sense, special attention has been given to pharmaceuticals, since such compounds, when present in different environmental compartments, can cause adverse effects, and even generate or increase bacterial resistance in aquatic organisms and humans. In addition, wastewater treatment plants employ biological treatments. Such systems are not designed for pharmaceutical treatment as these contaminants are non-biodegradable. Moreover, in many cases, they can be toxic or inhibit the consortium of microorganisms that constitute the different biological processes conventionally used. Thus, novel studies must be proposed to evaluate the use of different treatments for the degradation and removal of pharmaceuticals. Advanced Oxidation Processes (AOPs) are among the most promising treatments for effluents and complex wastewaters, especially Fenton and photo-Fenton processes at circumneutral pH. In turn, chromatographic techniques coupled with high resolution mass spectrometry are a valid instrumental alternative to monitor contaminants of emerging interest and also to identify transformation products (TPs). When combined with in silico modeling by methods of quantitative structure-activity relationship ((Q)SAR), these analyses help to decide which contaminants and TPs pose the greatest environmental risk and how long the evaluated treatments should last. On the other hand, when AOPs have their application limited by different factors, the adsorption processes, in particular, treatments that use active carbon produced from biomass, present themselves as an interesting alternative. This is because an alternative system of coupling treatments enables the removal of different contaminants or recalcitrant/toxic TPs generated in AOPs processes. Taking this into consideration, the present thesis is divided into three chapters, detailed below.

Chapter 1 presents the individualized study of Flutamide via solar photo-Fenton degradation. The drug selected for this study is used in the treatment of prostate cancer. The identifications of the PTs were performed by high performance liquid chromatography coupled with hybrid mass analyzer (quadrupole-time-of-flight). Additionally, associated with in silico prediction tools, ecotoxicity parameters of these new PTs were predicted. In the optimized condition of the solar photo-Fenton process, a total of 13 TPs never before

reported in the current scientific literature were identified. Furthermore, the results of the *in silico* evaluation indicate that these TPs are persistent, mutagenic and carcinogenic, in addition to being non-biodegradable.

Chapter 2 presents the treatment of a hospital effluent contaminated with Flutamide. In this study, priority was given to the identification of TPs in the effluent, applying non-target screening and using a purpose built database to identify the TPs of Flutamide, and the removal of Flutamide and its TPs by combining photo-Fenton solar processes and adsorption using active carbon. Furthermore, the adsorption process was optimized to remove the analytes under study. The coupling of the processes allowed to safely remove the vast majority of TPs, with high removal rates. However, for TPs that present aromatic ring opening, lower rates were obtained as a result of TPs having a higher polarity.

Chapter 3 focuses on the study of the treatment of a real hospital effluent fortified with a mixture of nine pharmaceuticals (chloramphenicol, fluconazole, flutamide, furosemide, gemfibrozil, ibuprofen, losartan, nimesulide and paracetamol) from different classes. Initially, four degradation approaches by solar photo-Fenton were compared. At the same time, the TPs generated by these different approaches were identified using a specially constructed database that contained information on 127 TPs from the nine selected drugs. The different approaches generated a total of 38 TPs, with two new chemical structures being proposed for the nimesulide TPs. In addition, when performing the combination of processes, high removal rates were achieved for initial pharmaceuticals and TPs, except in the case of TPs that have a higher polarity.

Throughout the different studies carried out, strategies for the degradation of pharmaceutical compounds allied to the removal of TPs were proposed. Additionally, new structures of TPs, which had never been identified and published, were disclosed through the studies that make up this Thesis, showing that the present work is relevant in the theme of removal of drugs and TPs present in hospital effluents.

Keywords: Pharmaceuticals, hospital effluent, solar photo-Fenton process, transformation products, (Q)SAR, adsorption.

INTRODUÇÃO

Os fármacos compreendem uma classe de microcontaminantes de interesse emergente muito importante, pois seu consumo é contínuo e crescente. Além disso, trata-se de um grupo muito numeroso e heterogêneo de compostos, os quais são sintetizados com o propósito de tratar enfermidades, prevenir infecções e reduzir sintomas. Segundo informações publicadas no Diário Oficial da União, até o ano de 2019, existiam cerca de 3729 medicamentos genéricos registrados, e dentro desses números, existem as formas de combinação (associações de dois ou mais compostos) ou isolados que chegam a 644 princípios ativos registrados no Brasil[1]. Por muito tempo os fármacos foram lançados no meio ambiente com pouquíssima atenção. Porém, a partir da década de 1990, observa-se um crescente interesse por parte de pesquisadores na realização de estudos referentes à ocorrência, destino ambiental, quantificação, monitoramento e remoção de fármacos dos diferentes compartimentos ambientais, em especial em ambientes aquáticos[2].

Acredita-se que a maior fonte de poluição das águas por fármacos seja pela excreção de humanos e animais, tanto na sua forma inalterada, quanto metabolizada[3]. Desta forma, em regiões que não apresentam um sistema de saneamento básico eficaz, como é o caso do Brasil, verifica-se a introdução continuada de fármacos nos diferentes compartimentos ambientais, em especial nas águas superficiais. Dados da ANA (Agência Nacional de Águas) revelam que, infelizmente, o esgoto gerado por 45% de toda a população brasileira não recebe qualquer tipo de tratamento. Assim, diariamente, 5,5 mil toneladas de esgoto não tratado, onde certamente uma gama importante de fármacos está presente, chegam aos rios e, em menor quantidade vão parar em reservatórios de água, mananciais e lagos do nosso país[4]. Além disso, por muitas vezes o esgoto gerado em unidades de saúde, como por exemplo os efluentes hospitalares, são incorporados ao sistema de tratamento de esgoto doméstico, sem nenhum tratamento prévio[5–8], o que amplia ainda mais a liberação de fármacos no meio ambiente. A Figura 1 representa um esquema da rota de inserção dos fármacos em especial nas águas superficiais, uma vez que as estações de tratamentos de águas residuais são projetadas para o tratamento de macropoluentes (nitratos, fosfatos, DQO, DBO, entre outros) e não para viabilizar a degradação/remoção dos fármacos que costumam estar na ordem de µg-ng L^{-1}[9–11]. Ainda, mesmo em concentrações traço ou ultra-traço, os fármacos podem apresentar risco ambiental, como persistência (resistência a degradação

pelos organismos aquáticos ou microorganismos), bioacumulação (acúmulo no tecido adiposo dos organismos aquáticos) e toxicidade (potencial para levar a morte diferentes organismos)[10,12,13].
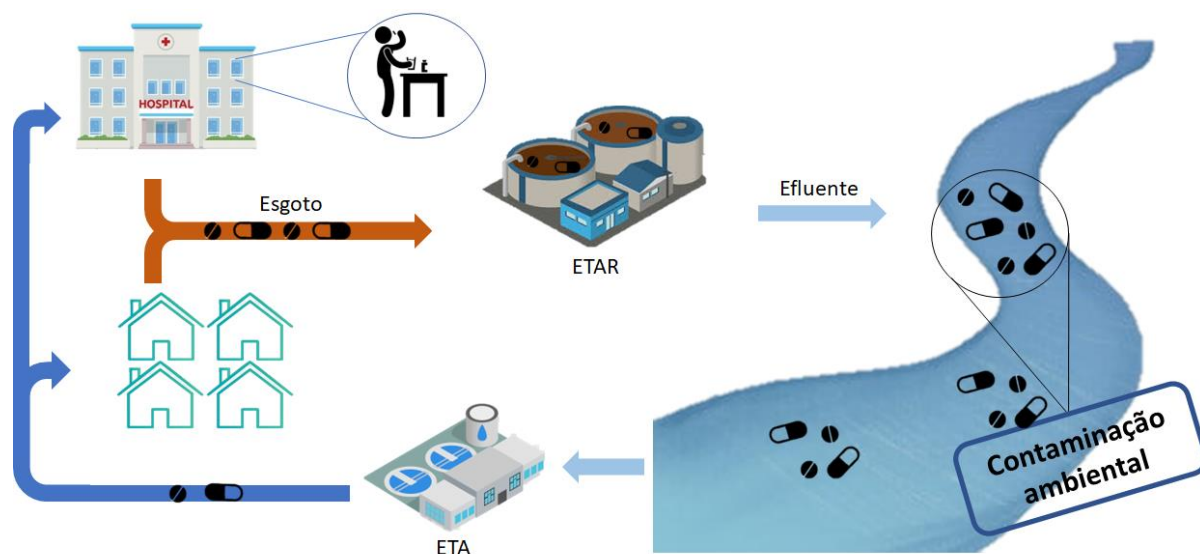
Figura 1. Rota de exposição da contaminação de fármacos no meio ambiente devido ao esgoto doméstico. ETAR: Estação de Tratamentos de Águas Residuais; ETA: Estação de Tratamento de Águas. Fonte: o Autor.

Estudos recentes detectaram mais de 80 compostos com atividade farmacológica em diferentes matrizes aquosas ambientais em concentrações que podem variar desde ng L^{-1} a µg L^{-1}[7,14]. Além disso, de acordo com estes trabalhos, os níveis mais altos se encontram em lugares próximos aos vertedouros de águas residuais[3]. Neste contexto, os fármacos que podem ser comercializados sem prescrição médica, como os analgésicos e anti-inflamatórios, são os que se detectam mais frequentemente e em concentrações mais altas no meio ambiente[15]. Por outro lado, os antibióticos são os fármacos mais estudados, devido a dois fatores principais: pela possibilidade de gerar fenômenos de resistência bacteriana, reduzindo o seu potencial terapêutico[16–18]; e pela porcentagem de eliminação destes compostos ser pequena nas plantas de tratamento que em geral empregam sistemas convencionais. Para se ter uma ideia da importância dessa questão, atualmente, a propagação da resistência

bacteriana foi classificada pela Organização Mundial da Saúde como uma das três maiores ameaças para a saúde pública no século XXI[18].

O efluente hospitalar por sua vez apresenta características semelhantes ao efluente doméstico, quando são comparados em parâmetros físico-químicos, contudo o que diferencia é a presença de fármacos e outros microcontaminantes[19]. A quantidade desses compostos presentes no efluente hospitalar é alta, e isso está relacionado às diferentes áreas que o hospital tem, como por exemplo: lavanderia, cozinha, análises clínicas, sanitários, ambulatórios, setores de rádio químicos e outros. Segundo o Conselho Nacional do Meio Ambiente (CONAMA), o efluente hospitalar deve sofrer algum tipo de tratamento ou serem liberados diretamente na rede doméstica, para serem tratados [20,21]. Dessa maneira, a gama de produtos químicos liberados é enorme e acaba impactando no meio ambiente, uma vez que esse efluente é misturado com o efluente doméstico, sendo uma fonte de contaminação ambiental de fármacos e outros contaminantes[6,22,23].

Embora no Brasil, não exista nenhuma legislação e/ou instrumento legal que controle, limite ou monitore fármacos nos ambientes naturais (efluentes, águas superficiais, subterrâneas e destinadas a consumo humano, solo ou sedimento), os inúmeros inconvenientes gerados pela presença destas substâncias nos diferentes compartimentos ambientais têm levado ao desenvolvimento de diferentes metodologias analíticas onde, sem dúvida, as técnicas cromatográficas têm uma relevância destacada já que permitem separar, identificar e/ou quantificar a presença desses micropoluentes em diferentes matrizes ambientais. Desta maneira, a União Europeia, em sua última Decisão 2020/1161, aumentou o número de fármacos que devem ser monitorados por cromatografia líquida acoplada ao analisador de massas do tipo triploquadrupolo. Assim, dentre os fármacos e metabólitos que devem ser monitorados estão: amoxicilina, ciprofloxacina, sulfametoxazol, trimetoprim, venlafaxina e o-desmetilvenlafaxina, clotrimazol, fluconazol e miconazol[24].

O tratamento convencional de águas residuais não é adequado para remoção de fármacos. Assim, surge a necessidade de empregar processos mais eficazes para esses compostos, como é o caso dos Processos Avançados de Oxidação (AOPs). Os AOPs são novas tecnologias para remoção de uma gama compostos orgânicos, e principalmente os fármacos, pois esses processos apresentam uma característica importante, que é a possibilidade de degradação não seletiva de compostos recalcitrantes e/ou transformá-los em espécies biodegradáveis[25,26].

Os AOPs têm a capacidade de detoxificar, ou seja, reduzir a toxicidade e, também, promover a desinfecção de matrizes aquosas, oxidando os microrganismos causadores de doenças em efluentes ou águas residuais[27]. Um processo que vem ganhando destaque é o Fenton por causa de sua simplicidade. Os radicais hidroxila são gerados *in situ* através da reação de íons de ferro II com o peróxido de hidrogênio para gerar radicais hidroxila e íons ferro III, com pH no intervalo de 2,7 a 3,0. Quando o processo Fenton é aplicado sob radiação UV ou solar, potencializa a geração de radicais hidroxila, isto é, a radiação UV ou solar aumenta a cinética da regeneração do íon ferro III para íon ferro II, restaurando o catalisador do processo, que nesse ciclo gera um mol adicional de radicais hidroxila(Figura 2). A busca por melhorar esse processo, e torná-lo ambientalmente mais sustentável, trouxe desafios para a comunidade cientifica, o principal foi sair da zona do pH ótimo no intervalo de 2,7 - 3,0, para um pH próximo da neutralidade, pois a partir de pH 3,5 o Fe(III) começa a precipitar, diminuindo assim a eficiência do tratamento[26]. Nesse contexto, a inserção de pequenas modificações no processo, mediante o uso de complexos de Fe(III)-EDDS (ácido etileno diamina-N,N'-dissuccínico), Fe(III)-citrato e Fe(III)-EDTA em pH neutro, pode-se conseguir boas porcentagens de degradação[28–30].Alternativamente, outra estratégia válida para viabilizar o trabalho em pH próximo à neutralidade, é mediante o uso de múltiplas adições de íons Fe(II) em intervalos de tempos próximos, por exemplo de 5 em 5 mim ou de 10 em 10 min, para aumentar a geração de radicais hidroxila no meio reacional e assim minimizar os custos de acidificação do efluente e neutralização do mesmo pós tratamento[31–33]. Além disso, a aplicação da radiação solar torna o processo mais atrativo do ponto de vista ambiental [26,34–36] e, em especial, é de bastante interesse para países como o Brasil onde a radiação solar é abundante.
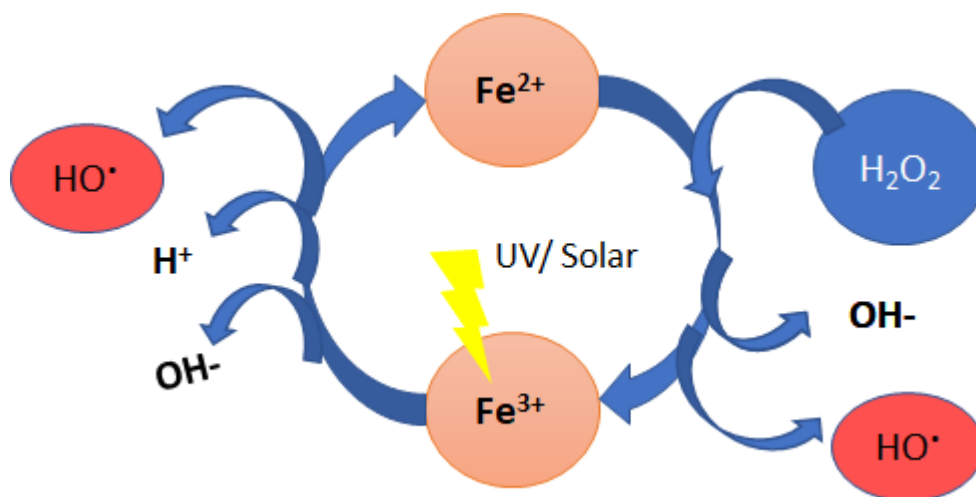
Figura 2. Esquema simplificado da formação de radicais hidroxila pelo processo foto-Fenton. Fonte: o Autor.

Todos estes tipos de processos têm inúmeras vantagens e sua utilização varia com a matriz ambiental que se esteja trabalhando, mas é importante sinalizar que existem fatores que influenciam a eficácia dos AOPs, como a concentração do(s) contaminante(s) e reagentes, pH, temperatura e presença de carbonatos[37], bicarbonatos, cloretos, brometos, fosfatos, sulfatos[30] e cátions como Mg^{2+}, Ca^{2+}[29].

Por sua vez, os processos de adsorção se constituem em método "universal" de remoção de micropoluentes. Nesse processo, ocorre a acumulação de substâncias na interface entre duas fases (líquida-líquida, gasosa-líquida, gasosa-sólida ou líquida-sólida). A substância que se acumula na interface é chamada de adsorvato e o material em que a adsorção ocorre é o adsorvente[38].

O fenômeno de adsorção pode ser classificado em dois tipos, dependendo da natureza das forças envolvidas. No caso da fisissorção (ou adsorção física), o adsorvato está ligado à superfície do adsorvente por forças de van der Waals, interação π–π, ligações de hidrogênio, hidrofobicidade e interações dipolares induzidas por dipolo relativamente fracas. A quimisorção (ou adsorção química), por sua vez, envolve troca ou compartilhamento de elétrons entre as moléculas de adsorvato e a superfície do adsorvente, resultando em reação química[38]. Nesse caso a interação química é mais voltada para remoção de íons metálicos e para remoção de micropoluentes, como os fármacos, prevê-se que o mecanismo de interação é o físico[39]. O mecanismo de adsorção de um adsorvato em fase líquida geralmente envolve quatro etapas: (1) transporte do interior da solução, (2) difusão externa, (3) difusão

intra-partícula e (4) adsorção, a qual ocorre nos poros menores do material sorvente até atingir o equilíbrio[40].

As principais vantagens do processo de adsorção residem no fato de que costumam ter baixo custo inicial de implementação, são altamente eficientes na remoção de diferentes contaminantes e tem desenho operacional simples que facilmente poderia viabilizar o acople desses métodos a outros processos de tratamento. Estudos recentes demonstraram que a aplicação de diferentes materiais adsorventes, tais como carvão ativado, biocarvões modificados, nanoadsorventes (nanotubos de carbono e grafeno), adsorventes compósitos, e outros estão sendo usados para a remoção de micropoluentes presentes em água e efluentes aquosos[39].

De acordo com Saucier[40], dentre todos os materiais sorventes, os carvões ativos apresentam um lugar de destaque, pois são excelentes materiais sorventes e, também muito versáteis. De acordo com a literatura, os carvões ativos geralmente demonstram alta capacidade de adsorver contaminantes orgânicos. Também, nesse caso não são gerados produtos farmacologicamente ativos ou tóxicos durante o processo de adsorção. Além disso, carvões ativos produzidos a partir de resíduos agroindustriais são uma alternativa de baixo custo em relação aos carvões ativos comerciais, apresentando capacidade de adsorção similar ou melhor que estes. Entre esses materiais alternativos como fonte de carbono para a produção de carvão ativado, podem ser citados: cascas, caroços e sementes de frutas e caules de plantas. Não cabe dúvida que o aproveitamento desses resíduos para produção de carvão ativo é uma alternativa ambientalmente interessante que cumpre requisitos da economia circular e que evita ou reduz os problemas ambientais oriundos da disposição inadequada dessa matéria prima (resíduos agroindustriais). A Figura 03 apresenta alguns exemplos de resíduos renováveis para a produção do carvão ativo[41].

Figura 3. Exemplos de biomassas que podem sem utilizadas como fonte de carbono para a produção de carvão ativo. Fonte: adaptada de Wong e Colaboradores [41].

Tendo em conta o exposto anteriormente, a combinação de AOPs e processos de adsorção para o tratamento de diferentes classes de micropoluentes, se converte em uma estratégia muito interessante visto que as vantagens singulares de cada um dos processos podem ser associadas e promover um tratamento integrado mais eficiente.

Adicionalmente, outro aspecto que deve ser levado em conta provem do fato de que há casos onde a aplicação de AOPs na degradação de microcontaminantes pode gerar um "coquetel" de TPs, especialmente quando taxas de mineralização discretas são observadas. Em geral, esses TPs tendem a ser mais polares que os compostos de origem e, por essa razão, tendem a permanecer no meio aquoso e, algumas vezes são mais recalcitrantes e/ou tóxicos[42–44]. Assim, outro ponto muito importante é que os TPs formados são novos compostos químicos, dos quais se têm muito pouca informação sobre suas estruturas químicas, seus efeitos ao meio ambiente e aos seres humanos.

Estudos que permitam avaliar e associar o risco toxicológico, predição da biodegradabilidade e o potencial carcinogênico e mutagênico dos TPs são fundamentais para ampliar a informação sobre os TPs e, também, orientar a melhor forma de acoplamento dos diferentes processos de tratamento. Como os fármacos e os TPs estão presentes em uma mistura de multicomponentes, o que inviabiliza a realização de testes individualizados de toxicidade e de destino ambiental. Dessa forma, modelos de *(Quantitative) Structure-Activity Relationship* ((Q)SAR) têm sido empregados para auxiliar na avaliação da toxicidade e destino ambiental destes compostos desconhecidos e dos quais, na maior parte dos casos, não se dispõe de padrão analítico comercial[45,46]. Nesse sentido, os modelos de (Q)SAR fornecem predições mais rápidas, econômicas e livres de testes de animais. Além disso, modelos de (Q)SAR são adequados para trabalhar com grandes quantidades de dados, permitindo, inclusive, discernir entre as tendências de dados existentes e de relevância ambiental[47]. De acordo com Abramenko e colaboradores[48] a modelagem (Q)SAR está baseada no princípio deque a estrutura química de um composto, determina suas propriedades físicas, químicas e biológicas. Dessa forma, partindo da estrutura química de um fármaco e ou de um TP, é possível determinar informações sobre a ecotoxidade, mesmo quando dados experimentais não estão disponíveis. Assim, os modelos (Q)SAR são a ferramenta ideal para auxiliar na predição de toxicidade, carcinogenicidade, mutagenicidade, biodegradabilidade, e outros parâmetros para os TPs[49,50].

Portanto, a proposição de metodologias analíticas avançadas, de processos de degradação baseados em AOPs mediados pela radiação solar, sua avaliação operacional, de identificação de TPs e proposição de caminhos de degradação para os contaminantes de partida, assim como a avaliação de risco ambiental por (Q)SAR são temas recorrentes e que merecem atenção e precisam ser avaliadas de forma conjunta, conforme se propõe na presente tese.

Finalmente, cabe destacar que o uso isolado de ambos os processos (AOPs e adsorção) está bastante estudado, porém, a associação de ambos os processos ainda é considerada em poucas situações[51,52]. Um levantamento recente realizado na plataforma "*Clarivate Analytics-Web of Science*", para a última década, pode ser visto na Figura 4. O referido levantamento evidencia que as publicações de estudos visando o acoplamento e processos (AOPs e adsorção) não são expressivas embora estejam aumentando, em especial a partir de 2019. Esse aspecto destaca um dos pontos que confere caráter inovador à presente

tese. Adicionalmente, o trabalho com fármacos ainda pouco estudados (por exemplo flutamida), com estudos de degradação em matriz real (efluente hospitalar) e a identificação de TPs mediante a estratégia de uso de bases de dados especialmente construídas são outros aspectos relevantes contidos no presente estudo. Assim, em consonância com o indicado por Verlicchi [53], a presente tese espera contribuir para que o debate sobre o tratamento mais adequado para a matriz de efluente hospitalar seja contínuo e constantemente alimentado por novos *insights*.
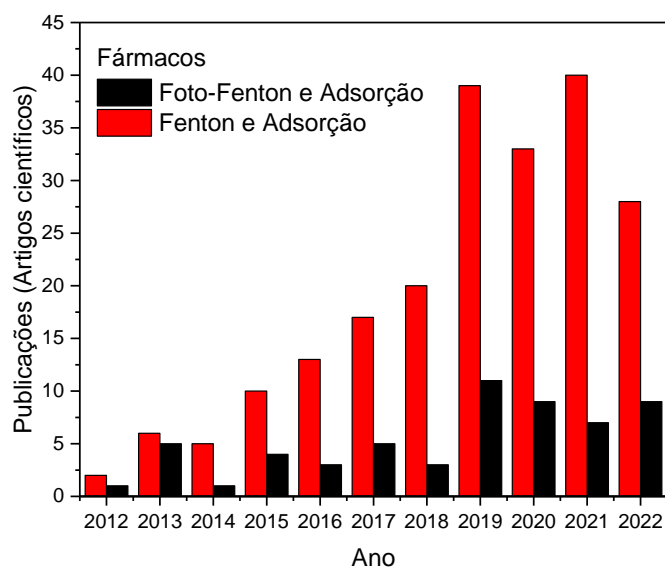
Figura 4. Publicações de artigos científicos, durante a última década, relacionadas com os termos: fármacos (em vermelho: "pharmaceuticals" + "Fenton" + "Adsorption", em preto: "pharmaceuticals" + "photo-Fenton" + "Adsorption"). Fonte: o Autor com resultados do *Clarivate Analytics-Web of Science*.

Capítulo 1

Degradação do fármaco anticancerígeno flutamida por tratamento foto-Fenton solar em pH próximo da neutralidade: Identificação de produtos de transformação e avaliação de risco *in silico* (Q)SAR

INTRODUÇÃO

A Flutamida (FLUT) é um fármaco não esteriodal antiandrógeno que é utilizado principalmente no tratamento de câncer de próstata[54]. Alguns estudos indicam que a Flutamida pode ser considerado um desregulador endócrino[55–57].No ano de 2010, o consumo anual da Flutamida na comunidade autônoma da Catalunha – Espanha foi de aproximadamente 94,6 kg, que corresponde a aproximadamente 18,4% dos fármacos utilizados para tratamentos endócrinos[58]. No Brasil, segundo dados de 2017 da Agência Nacional de Vigilância Sanitária (ANVISA) o consumo do fármaco foi de aproximadamente 100 mil caixas de comprimidos, que equivale ao consumo de 3% de fármacos citostáticos[59]. A presença desse fármaco já foi relatada em concentrações na ordem de ng L^{-1} em amostras aquosas[60].

Os AOPs surgem como uma alternativa para a degradação de fármacos recalcitrantes e podem ser acoplados a diferentes sistemas de tratamento, seja como pré ou pós-tratamentos. Dentre os AOPs, o processo Fenton é considerado um dos processos mais simples, pois para sua execução se requer o reagente Fenton (Fe(II) e H_2O_2) em pH ácido(2,8–3,0) para geração de radicais hidroxilas[61]. Esses radicais(HO•) são espécies altamente reativas e não seletivas, que devem ser gerados *in situ* no meio reacional[27]. Por sua vez, Afshar e colaboradores[62] avaliaram o processo Fenton heterogêneo, que é uma modificação do processo Fenton tradicional, através do uso de um catalisador de $CoFe_2O_4$ e H_2O_2. Tal processo proporcionou uma degradação de aproximadamente de 67,7% de Flutamida para um tratamento de30 minem pH 4,32, partindo de uma concentração inicial de Flutamida de 150μM, ou seja, o equivalente a 41 mg L^{-1}. Para melhorar o processo de tratamento, os autores combinaram ao processo de ozônio, e alcançaram uma remoção máxima de Flutamida de 93,0%, observando também a presença de 5 TPs. Por sua vez, o processo foto-Fenton solar em meio ácido ou próximo à neutralidade se constitui em uma alternativa atrativa para viabilizar a degradação de uma ampla gama de microcontaminantes[63,64].

Adicionalmente, outro aspecto relevante e que deve ser monitorado ao se avaliar novas alternativas de tratamento diz respeito à avaliação de TPs gerados durante o tratamento. Esse seguimento ao longo do processo em estudo permite identificar o comportamento das espécies formadas, ou seja, se são facilmente degradados ou persistentes durante o processo em estudo e, também, em muitas situações é possível realizar uma

proposta de sua estrutura química bem como inferir sobre as principais rotas de degradação que têm lugar

Nos casos onde ser observe a persistência de TPs é importante tentar conhecer os efeitos que tais TPs podem causar ao meio ambiente, para assim criar estratégias para minimizar esse impacto (seja ampliando o tempo de tratamento até sua degradação completa ou reduzindo o tempo de tratamento até um ponto onde os TPs gerados não apresentem toxicidade ou sejam biodegradáveis). Como os TPs estão presentes em uma mistura de compostos, o estudo individualizado de cada um deles é um processo extremamente complexo, ou até mesmo inviável, pois não se dispõe de padrões analíticos comerciais dos TPs. Dessa forma, modelagens computacionais (*in sílico*) são ferramentas poderosas que vem surgindo, para avaliar os efeitos de ecotoxidade, uma vez que são baseadas na abordagem de (Q)SAR)[65–67]. Assim, efeitos de toxicidade, carcinogenicidade, mutagenicidade, PBT (persistência-bioacumulação-toxicidade) são algumas das previsões que as modelagens *in sílico* podem nos facilitar para cada um dos TPs identificados desde que se obtenha uma proposta de estrutura química do mesmo[46,47,68].

OBJETIVO

Esse capítulo tem como objetivo realizar a degradação da Flutamida por processo foto-Fenton solar em água ultrapura em pH 5 (pH próximo à neutralidade). Será realizada a identificação dos TPs formados durante o tratamento. Ainda, a avaliação da ecotoxicidade e comportamento ambiental da Flutamida e seus TPs será realizada por diferentes métodos *in silico* ((Q)SAR) mediante o uso de softwares livres.

PRINCIPAIS RESULTADOS

Durante a degradação da Flutamida foram observados 13 novos TPs nunca antes proposto na literatura científica. A identificação desses TPs é um processo complexo, uma vez que não existem padrões analíticos comerciais disponíveis. Para realizar a identificação desses TPs, foi adotada uma estratégia de identificação baseada na abordagem "clássica", onde o surgimento de novos sinais cromatográficos no cromatograma de íon totais (TIC) pode ser usado como um indicativo de formação de TPs. Concomitantemente, são analisados os espectros de massa de alta resolução adquiridos em modo MS e *broad band-CID*(MS/MS

automatizado) para cada pico cromatográfico observado no TIC. Assim, o sistema Q-TOF MS permite conhecer a formula, massa exata experimental, massa exata calculada, erro de massa, *double bond equivalence* (DBE), e perfil isotópico (se houver)de cada TP. De conhecimento de tais informações, foi possível realizar uma elucidação estrutural propositiva para os 13 TPs da Flutamida.

Para todos os TPs identificados propositivamente nesse trabalho, foram adotados os seguintes critérios de análise: verificação da composição elemental do íon molecular e de cada fragmento com um erro de massa inferior a 5 ppm, análise do perfil de fragmentação do TP e do valor do DBE. Deste modo, foi possível propor os 13 TPs e, adicionalmente, a partir destes um caminho de degradação da Flutamida durante o processo foto-Fenton solar. Assim, as principais reações que tiveram lugar foram: hidroxilação e abstração de hidrogênio seguido pela formação de dupla ligação.

A eliminação do peróxido de hidrogênio residual que permanecia ao final do processo de tratamento no meio reacional, foi realizada através da adição de um excesso de bissulfito de sódio. Possivelmente por ter realizado essa etapa, foram observados em alguns TPs a apresenta de gruposSO_3^-. Segundo Chen e colaboradores[69] grupos sulfônicos podem reagir com o Fe^{2+}para formação de radicais $SO_3^{-\cdot}$ e Fe^{3+}. Esse argumento corrobora com os resultados observados nesse estudo.

Os resultados da avaliação *in silico* (Q)SAR dos TPs identificados nesse estudo, indicam que o tratamento foto-Fenton solar não foi eficiente para mitigar os riscos associados à Flutamida para o meio ambiente. Os novos TPs formados são compostos não biodegradáveis, potencialmente mutagênicos e carcinogênicos, de acordo com os resultados das predições *in silico*. Portanto, um tratamento complementar, após o processo foto-Fenton solar deveria ser aplicado para diminuir os riscos associados a esses compostos.

Todos os métodos, resultados e conclusões estão apresentados no **Artigo 1** e **Material Suplementar 1**.

Degradation of the anticancer drug flutamide by solar photo-Fenton treatment at near-neutral pH: Identification of transformation products and *in silico* (Q)SAR risk assessment

Alexandre Della-Flora, Marcelo L. Wilde, Igor D.F. Pinto, Éder C. Lima, Carla Sirtori[*]

Instituto de Química, Universidade Federal Do Rio Grande Do Sul, Av. Bento Gonçalves 9500, CEP 91501-970, Porto Alegre, RS, Brazil

ABSTRACT

Flutamide (FLUT) is a non-steroidal drug mainly used in the treatment of prostate cancer and has been detected in the aquatic environment at ng L^{-1} levels. The environmental fate and effects of FLUT have not yet been studied. Conventional treatment technologies fail to completely remove pharmaceuticals, so the solar photo-Fenton process (SPF) has been proposed as an alternative. In this study, the degradation of FLUT, at two different initial concentrations in ultra-pure water, was carried out by SPF. The initial SPF conditions were pH_0 5, $[Fe^{2+}]_0 = 5$ mg L^{-1}, and $[H_2O_2]_0 = 50$ mg L^{-1}. Preliminary elimination rates of 53.4% and 73.4%. The kinetics of FLUT degradation could be fitted by a pseudo-first order model and the k_{obs} were 6.57×10^{-3} and 9.13×10^{-3} min^{-1} t_{30W} and the half-life times were 95.62 and 73.10 min t_{30W} were achieved for $[FLUT]_0$ of 5 mg L^{-1} and 500 µg L^{-1}, respectively. Analysis using LC-QTOF MS identified thirteen transformation products (TPs) during the FLUT degradation process. The main degradation pathways proposed were hydroxylation, hydrogen abstraction, demethylation, NO_2 elimination, cleavage, and aromatic ring opening. Different *in silico* (quantitative) structure-activity relationship ((Q)SAR) freeware models were used to predict the toxicities and environmental fates of FLUT and the TPs. The *in silico* predictions indicated that these substances were not biodegradable, while some TPs were classified near the threshold point to be considered as PBT compounds. The *in silico* (Q)SAR predictions gave positive alerts concerning the mutagenicity and carcinogenicity endpoints. Additionally, the (Q)SAR toolbox software provided structural alerts corresponding to the positive alerts obtained with the different mutagenicity and carcinogenicity models, supporting the positive alerts with more proactive information.

1. Introduction

Pharmaceuticals are chemicals with high, continuous, and widespread consumption worldwide (Rodriguez-Narvaez et al., 2017). Environmental contamination by pharmaceuticals is problematic, since they are not entirely removed in conventional wastewater treatment plants (WWTPs), prior to discharge of the treated effluent into streams and rivers (Li et al., 2016; Sim et al., 2011). Furthermore, pharmaceuticals may be toxic and bioaccumulate in aquatic organisms, even at trace or ultra-trace levels (Brooks et al., 2005; Michael et al., 2013).

Flutamide (FLUT) is a drug that is mainly used in the treatment of prostate cancer (Brogden and Clissold, 1991) and has been indicated as an endocrine disruptor (Knapczyk-Stwora et al., 2019; Tian et al., 2017; Yin et al., 2017). The annual consumption of FLUT in Catalonia (Spain) in the year 2010 was approximately 94.6 kg (corresponding to ~18.4%

of the pharmaceuticals consumed for endocrine therapy) (Franquet-Griell et al., 2015). According to (Ortiz de García et al., 2013) the FLUT was estimated in 521 kg y^{-1} and 1987.4 kg y^{-1} in France and Spain, respectively. In addition, the consumption in Brazil in the year 2017 was approximately 100 thousand pills box this equates the amount of consumed 3% of the cytostatic drugs (ANVISA, 2018). FLUT has been found in the aquatic environment at ng L^{-1} levels (Miller et al., 2019).

Advanced oxidation processes (AOPs) have been proposed as an alternative to conventional treatments, due to their ability to degrade recalcitrant organic compounds (Ribeiro et al., 2015). Among AOPs, photocatalysts have been employed for pharmaceuticals degradation (Fakhri et al., 2017a, 2017b; 2016, 2015; Fakhri and Behrouz, 2015a, 2015b; Fakhri and Kahi, 2017; Fakhri and Khakpour, 2015; Fakhri and Nejad, 2016; Mohammadi et al., 2016). However, the processes using solar photo-Fenton (SPF) have been growing in attention aiming the

---

degradation of different pharmaceuticals active compounds (Chong et al., 2010; Giannakis et al., 2017; Ioannou-Ttofa et al., 2019; Klamerth et al., 2010; Lumbaque et al., 2019b, 2019a; Malato et al., 2009; Méndez-Arriaga et al., 2010; Pignatello et al., 2006). Pharmaceuticals are usually present in wastewaters and the aquatic environment under near-neutral pH conditions that are suitable for application of the photo-Fenton process (Amildon Ricardo et al., 2018; Clarizia et al., 2017; Papoutsakis et al., 2016; Soriano-Molina et al., 2019).

However, AOPs may not lead to complete mineralization, resulting in a series of new and unknown TPs that can be stable, persistent, and sometimes more toxic than the parent compounds, causing new and undesirable biological effects (Fatta-Kassinos et al., 2011; Koltsakidou et al., 2019; Rücker and Kümmerer, 2012). Pharmaceuticals and their TPs do not occur as isolated compounds, but in multicomponent mixtures, which makes it unfeasible to perform separate tests concerning their environmental fates and toxicities. *In silico* (quantitative) structure-activity relationship ((Q)SAR) models have been employed to assist in evaluating the toxicities and environmental fates of unknown compounds such as TPs (Leder et al., 2015; Rastogi et al., 2014; Wilde et al., 2018, 2016).

The only study reported on FLUT degradation in AOPs was conducted by Afshar et al. (2018). This study was performed using a higher initial concentration of FLUT (150 μmol L^{-1} = 41.4 mg L^{-1}) using the heterogeneous Fenton process combined with ozonation, with CoFe$_2$O$_4$ nanoparticles as catalyst. It was possible to remove up to 93% of the FLUT and five TPs were proposed. However, no ecotoxicity evaluations were performed.

To the best of our knowledge, this is the first study considering the degradation of FLUT in lower concentration and further assessment of environmental risk and hazardous of FLUT and TPs formed by SPF process by combining experimental and *in silico* tools. Besides, the degradation of FLUT employing SPF processes was carried out at pH near to neutrality. The chemical structures of the TPs generated during the treatment was proposed by using a non-target approach in LC-QTOF MS. Additionally, the ecotoxicities and environmental fates of FLUT and the TPs were assessed utilizing different *in silico* (Q)SAR models.

2. Materials and methods

2.1. Chemicals

Flutamide (99.45%) was purchased from Shangqiu Chemry Chemicals (China). 1,10-Phenanthroline, ammonium metavanadate, citric acid, and solvents (LC-MS grade) were purchased from Merck. H$_2$O$_2$ (35% w/v) was purchased from Labsynth. FeSO$_4$.7H$_2$O was acquired from Reagen. All other chemicals used were analytical grade.

2.2. Solar photo-fenton experiments

A stock solution was prepared by dissolving 100 mg of FLUT in 1 mL of methanol. Working solutions (5 mg L^{-1} and 500 μg L^{-1}) were then prepared by diluting the stock solution in ultrapure water (18.2 MΩ cm). The solar photo-Fenton (SPF) process was carried out in an open 1 L cylindrical borosilicate glass batch reactor, under constant magnetic stirring. Aliquots were removed at predetermined times, in order to monitor the degradation of FLUT and the formation of TPs. The residual H$_2$O$_2$ was quenched by adding a 200 μL aliquot of NaHSO$_3$ (28% w/v). The initial pH of the solution was adjusted to pH 5 with 0.05 mol L^{-1} NaOH. The initial concentrations of Fe^{2+} and H$_2$O$_2$ were 5 mg L^{-1} and 50 mg L^{-1}, respectively. In a first step, 5 mg L^{-1} of Fe^{2+} were added to the FLUT's solution at the dark under stirring for 5 min. After that, the solution was exposed to solar irradiation and 50 mg L^{-1} of H$_2$O$_2$ was added. In addition, experiments were carried out to evaluate hydrolysis and possible complex formation between FLUT and Fe^{2+}/Fe^{3+}. For this, 5 mg L^{-1} of Fe^{2+} was added to the solution, with continuous stirring for 120 min (in the dark). Aliquots were withdrawn

for analysis by LC-QTOF MS (see Section 2.4). The solar UV radiation (W m^{-2}) was monitored using a solar energy meter (ICEL SP-2000), with measurements at 2 min intervals. The data provided by the solar energy meter were used to calculate t_{30W}, according to Eq. (1) (Prieto-Rodriguez et al., 2012).

$$t_{30W,n} = t_{30W,n-1} + \Delta t_n \frac{UV}{30} \frac{V_I}{V_t} \qquad \Delta t_n = t_n - t_{n-1} \tag{1}$$

where $t_{30W,n}$ and $t_{30W,n-1}$ are the adjusted experimental times according to UV irradiation (kJ/L) monitored at experimental times of t_n and t_{n-1}, respectively, Δt_n is the experimental time between two samples, V_I and V_t represent the irradiated and total volumes, respectively, and UV is the average incident solar ultraviolet irradiation measured between two experimental times. The value of 30 refers to a constant solar UV power of 30 W m^{-2}, which corresponded to the typical solar UV power at around noon on a sunny day. A scheme of the experimental section was added to Text S1 (supplementary material).

2.3. Degradation kinetics and photonic efficiency

The degradation of organic compounds by HO· follows second order kinetics (Eq. (2)).

$$\frac{dC}{dt} = -k \cdot [C][HO\bullet] \tag{2}$$

where [C] is the concentration of the organic compound, [HO·] is the hydroxyl radical concentration, and k is the reaction rate constant.

Assuming that HO· is highly reactive and in excess relative to the concentration of the target compound, a pseudo-stationary state is reached, so Eq. (2) can be simplified to give pseudo-first order kinetics (Eq. (3)), represented by an apparent pseudo-first order constant (k_{obs}) (Sun et al., 2007).

$$\frac{dC}{dt} = -k \cdot [C][HO\bullet] = k_{obs}[C] \tag{3}$$

Integration of Eq. (3) results in an exponential decay equation (Eq. (4)).

$$[C] = [C_0] \cdot e^{-k_{obs} \cdot t} \tag{4}$$

The half-life ($t_{1/2}$) for FLUT degradation was calculated according to Eq. (5).

$$t_{1/2} = \ln 2 \big/ k_{obs} \tag{5}$$

The degradation rate constant was determined by fitting of the experimental data using a nonlinear regression model, performed with SigmaPlot 12 software (Systat Software, USA). Statistical analysis of the fitting was performed using ANOVA.

The photonic efficiency of the SPF process for degradation of FLUT was calculated according to Eq. (6).

$$\xi = \frac{\Delta C \cdot V}{\Delta t \cdot J_0 \cdot A} \cdot 100 \tag{6}$$

where ΔC is the concentration change in the time interval Δt, V is the irradiated volume (1 L), J_0 is the photonic flux (mol m^{-2} s^{-1}), and A is the irradiated surface area (0.012 m^2) (Faisal et al., 2015).

2.4. Instrumental analysis by LC-QTOF MS

Monitoring of the degradation of FLUT and elucidation of the TPs formed during the SPF process employed a Shimadzu Nexera X2 LC system coupled to a QTOF mass spectrometer (Impact II, Bruker Daltonics). The LC system was equipped with a Hypersil GOLD® C18 reverse phase analytical column (150 mm × 2.1 mm, 3 μm particle diameter). The mobile phase was a mixture of acetonitrile acidified with 0.1% formic acid (eluent A) and ultrapure water acidified with 0.1% formic acid (eluent B), at a flow rate of 0.5 mL min^{-1}. The elution

A. Della-Flora, et al.   Environmental Research 183 (2020) 109223

16
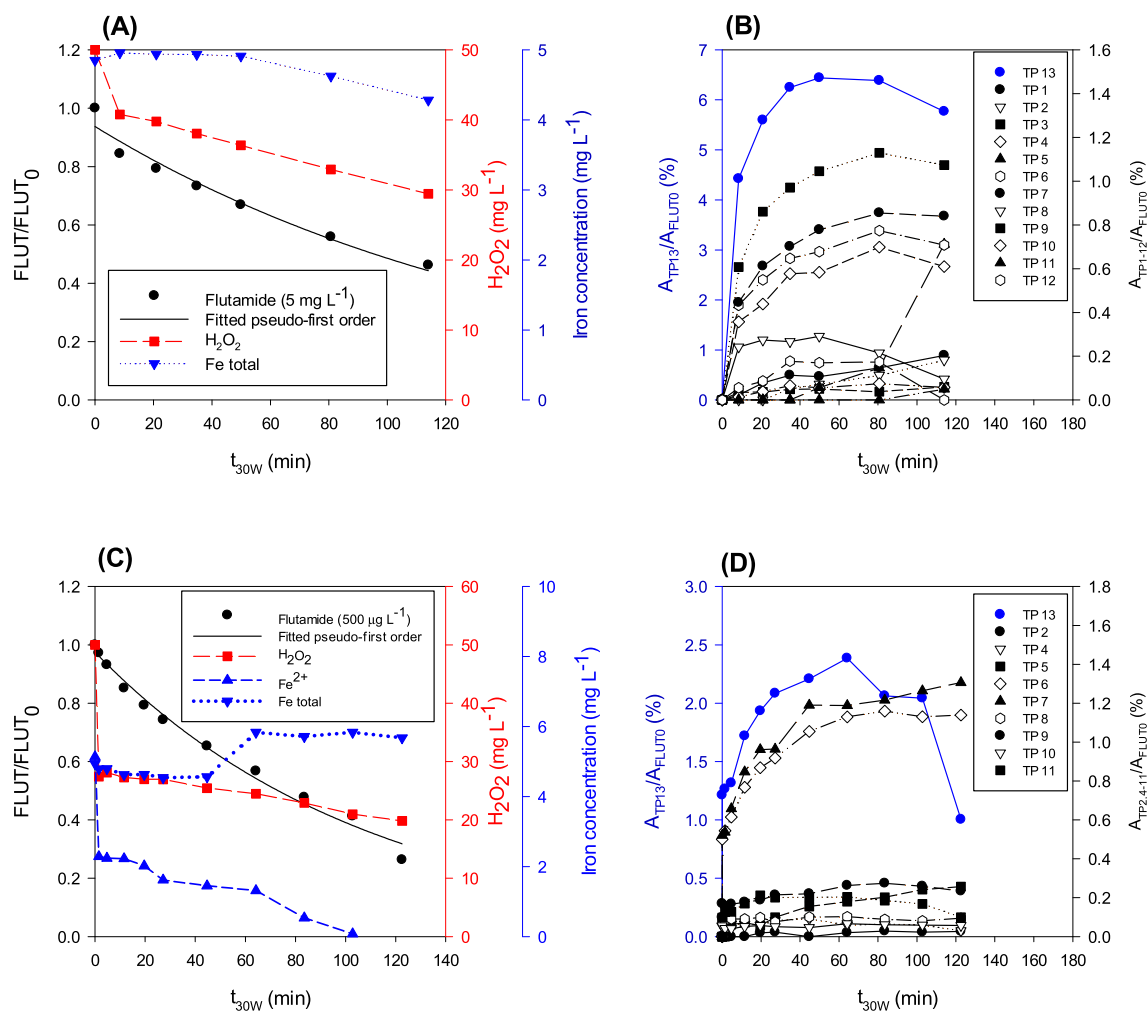
Fig. 1. Primary elimination of FLUT and profile of Fe^{2+}, Fe total, H_2O_2 through the SPF process at FLUT's initial concentration of (A) 5 mg L^{-1} and (C) 500 μg L^{-1}. Profile of the normalized area (A/A$_0$ (%), where A is the TPs area, and A$_0$ is the initial area of FLUT) ofthe Transformation Products (TPs) during the SPFprocess at FLUT′ initial concentration of (B) 5 mg L^{-1} and (D) 500 μg L^{-1}.

gradient was 5% A to 95% A in 11 min, held for 1 min, followed by return to 5% A in 15 min, held for a further 5 min. The QTOF MS was operated in negative ionization mode, with the following conditions: capillary at 2500 V, nebulizer at 4.5 bar, drying gas at 10 L min^{-1}, and gas temperature at 200 °C. The broadband collision-induced dissociation (bbCID) acquisition mode was used, with two collision energies (25 and 50 eV), which provided simultaneous MS and MS/MS spectra. All the MS information was obtained in scan mode, in the m/z range from 50 to 1000. A non-target approach was employed for elucidation of the TPs. DataAnalysis v. 4.2 software (Bruker Daltonik GmbH) was used for analysis of the MS/MS data.

2.5. Determination of total iron and hydrogen peroxide

Ferrous and total iron were determined by the colorimetric method employing 1,10-phenanthroline (ISO 6332, 1988). Hydrogen peroxide was determined spectrophotometrically by the ammonium metavanadate method (Nogueira et al., 2005). These measurements were performed using a Cary 50 UV–Vis spectrophotometer.

2.6. In silico quantitative structure-activity relationship ((Q)SAR) model predictions

The chemical structures of FLUT and the proposed TPs were converted into SMILES code, using ChemBioDraw Ultra (v. 12), and were

subjected to *in silico* predictions using different models. Freely available (Q)SAR software packages considering different endpoints were used for the predictions: (i) EPIWEB v. 4.1 (EPI suite, USEPA), (ii) VEGA v. 1.1.4-binaries (http://www.vega-qsar.eu/) (Pizzo et al., 2013), (iii) Prometheus v. 1.0-binaries (Pizzo et al., 2016), and (iv) OECD (Q)SAR Toolbox v. 4.3.1 (http://www.qsartoolbox.org/).

Different endpoints were considered using BIOWIN 1 and 2 (linear and non-linear biodegradation models), BIOWIN 3 and 4 (ultimate and primary biodegradation models), BIOWIN 5 and BIOWIN 6 (linear and non-linear MITI biodegradation models), and BIOWIN 7 (anaerobic biodegradation model). With the exception of BIOWIN models 3 and 4, which express the results as weeks and days, the *in silico* predictions of each tested compound ranged from 0 (not biodegradable) to 1 (biodegradable). The biodegradability predicted by the combined BIOWIN models was rated as "yes" or "no", based on the following criteria: "Yes" if the BIOWIN 3 result was "weeks", "days", or "days to weeks", and if the probability was ≥0.5 in the case of the BIOWIN 5 model. If these criteria were not met, the prediction was "No" (USEPA, 2012). BIOWIN models have been used for the prediction of biodegradability in several studies (Hübner et al., 2014; Pizzo et al., 2013). The *in silico* prediction of biodegradability provided by VEGA v. 1.1.4 is based on the modified MITI test (I), with a compound being considered readily biodegradable if the biodegradation rate is 60% or more within 28 days (Pizzo et al., 2013). The output of the biodegradability model (IRFMN v. 1.0.9) provided by VEGA (http://www.vega-qsar.eu) is in the form of

Table 1
Accurate mass measurements of FLUT and the main TPs found by LC-QTOFMS by bbCID in negative ionization mode.

Compound	Rt (min)	Formula	Ion mass (m/z) Experimental	Calculated	Error (ppm)	mSigma	DBE	Aqueous solution [FLUT] 5 mgL^{-1}	[FLUT] 500 µg L^{-1}
TP1	2.0	$C_9H_{11}F_3NO_7S$	334.02160	334.0214	−0.5	6.4	3.5	✓	–
		$C_8H_{11}F_3NO_5S$	290.03180	290.0316	−0.7	NA	2.5		
		$C_8H_9F_3NO_2$	208.05950	208.0591	−2,2	14.4	3.5		
TP-2	3.3	$C_9H_{11}F_3NO_7S$	334.02160	334.0214	−0.9	12.2	3.5	✓	✓
		$C_9H_{11}F_3NO_5S$	302.03260	302.0316	−1.4	52.0	3.5		
		$C_8H_{11}F_3NO_5S$	290.03200	290.0316	−1.6	90.8	2.5		
		$C_8H_9F_3NO_3$	224.05370	224.0540	1.3	NA	3.5		
		$C_8H_9F_3NO_2$	208.05960	208.0591	2.5	39.5	3.5		
TP-3	3.5	$C_{11}H_{13}F_3NO_{10}S$	408.02240	408.0218	−1.5	28.6	4.5	✓	–
		$C_{11}H_8F_3NO_3$	259.0429	259.0462	12.6	NA	7.0		
		$C_7H_2F_3O_3$	190.9957	190.9962	2.6	5.2	5.5		
TP-4	4.1	$C_{11}H_{12}F_3N_2O_5S$	341.03840	341.0425	−0.1	9.5	5.5	✓	✓
		$C_{11}H_{10}FN_2O_5S$	301.03030	301.0300	−1.0	43.3	7.5		
		$C_{11}H_{12}F_3N_2O_2$	261.08550	261.0856	0.4	67.5	5.5		
		$C_{11}H_{10}FN_2O_3$	237.06880	237.0681	−2.8	16.4	7.5		
TP-5	4.7	$C_{10}H_6F_3N_2O_4$	275.02850	275.0285	−0.1	6.0	7.5	✓	✓
		$C_7H_4F_3N_2O_3$	221.0177	221.0180	0.9	11.8	5.5		
		$C_7H_4F_3N_2O_2$	205.0231	205.0230	−0.3	11.3	5.5		
TP-6	4.8	$C_{11}H_8F_3N_2O_4$	289.04380	289.0442	1,1	3.3	7.5	✓	✓
		$C_8H_4F_3N_2O_3$	233.01700	233.0180	0.5	14.9	6.5		
		$C_7H_4F_3N_2O_3$	221.01690	221.0177	4.6	115.5	5.5		
		$C_7H_4F_3N_2O_2$	205.02300	205.0230	0.0	2.5	5.5		
TP-7	4.9	$C_{11}H_8F_3N_2O_4$	289.04410	289.0442	0.2	2.9	7.5	✓	✓
		$C_8H_4F_3N_2O_3$	233.0178	233.0180	0.5	14.9	6.5		
		$C_7H_4F_3N_2O_2$	205.0232	205.0232	−0.9	20.0	5.5		
TP-8	5.2	$C_{11}H_{11}F_3NO_2$	246.0750	246.0747	−0.8	6.8	5.5	✓	✓
		$C_{11}H_{10}F_2NO_2$	226.0689	226.0685	−1.9	30.0	6.5		
		$C_8H_3F_2NO_2$	183.0141	183.0137	−0.2	52,1	7.0		
		$C_7H_4F_2NO$	156.0261	156.0266	3.5	n.a.	5.5		
TP-9	5.7	$C_{11}H_{10}F_3N_2O_4$	291.0598	291.0598	−0.1	13.3	6.5	✓	✓
		$C_7H_4F_3N_2O_2$	205.0231	205.023	−0.2	3.1	5.5		
TP-10	5.8	$C_{11}H_{10}F_2N_2O_7S$	371.0166	371.0165	0.0	11.4	6.5	✓	✓
		$C_{11}H_{10}F_3N_2O_5$	307.0534	307.0547	4.2	23.7	6.5		
		$C_{11}H_{10}F_3N_2O_4$	291.0599	291.0598	−0.3	5.3	6.5		
		$C_7H_4F_3N_2O_2$	205.0230	205.0230	0.2	6.9	5.5		
		$C_7H_4F_3NO$	175.0239	175.0239	6.3	N.A	5.0		
TP-11	6.5	$C_{11}H_{10}F_3N_2O_4$	291.0593	291.0598	1.9	2.3	6.5	✓	✓
		$C_{11}H_9F_3N_2O_3$	274.0570	274.0571	0.3	212.2	7.0		
TP-12	6.6	$C_{10}H_6F_3N_2O_4$	275.0295	275.0285	−2.0	11.5	7.5	✓	–
		$C_7H_4F_2N_2O_2$	205.0230	205.0230	2.0	14.8	5.5		
TP-13	6.9	$C_{11}H_{10}F_3N_2O_4$	291.05590	291.0598	−0.2	1.8	6.5	✓	✓
		$C_{11}H_8F_3N_2O_3$	273.04950	273.0493	−0.8	197.5	7.5		
		$C_{11}H_{10}F_3NO_2$	245.06660	245.0669	1.2		6.0		
		$C_7H_4F_3N_2O_3$	221.01800	221.018	−0.6	4.6	5.5		
FLUT	7.1	$C_{11}H_{10}F_3N_2O_3$	275.0654	275.0649	1.8	2.6	6.5	✓	✓
		$C_{10}H_6F_3N_2O_3$	259.0333	259.0336	1.3	na	7.5		
		$C_8H_3F_3N_2O_3$	232.0101	232.0101	0.0	7.1	7.0		
		$C_{11}H_{10}F_3NO$	229.0719	229.0718	0.5	7.4	6.0		
		$C_7H_4F_3N_2O_2$	205.0230	205.0230	0.0	1.1	5.5		
		$C_7H_3F_3NO_2$	190.0121	190.0117	2.4	216.0	5.5		
		$C_7H_5F_3N$	160.0371	160.0380	5.4	na	4.5		

the following categories: readily biodegradable, possibly readily biodegradable, possibly not readily biodegradable, not readily biodegradable, and not assigned (Pizzo et al., 2013). The VEGA 1.1.4 software has also been used to predict mutagenicity, according to the Ames test (CONSENSUS model v. 1.0.2), and includes four different carcinogenicity models (IRFMN/Antares v. 1.0.0, CAESAR v. 2.1.9, ISS v. 1.0.2, and IRFMN/ISSCAN-CGX v. 1.0.0). Complementary to the above mutagenicity predictions, QSAR Toolbox v. 4.3.1 was used to assess the mutagenicity alerts generated for the investigated structures. The following models were used: (A) DNA alerts for Ames: alerts on interaction of chemicals with DNA, extracted from the Ames mutagenicity model (given by OASIS); (B) DNA alerts for CA and MNT: alerts for interaction of chemicals with DNA extracted from chromosomal aberrations (OASIS); (C) *in vitro* mutagenicity (Ames test) by ISS: mutagenicity/carcinogenicity module of the Toxtree software; (D) *in vitro*

mutagenicity (micronucleus) alerts by ISS: ToxMic rulebase of the Toxtree software. Complementary assessment was made of the repeated dose (HESS) hepatotoxicity.

In addition to the *in silico* (Q)SAR predictions of mutagenic activities, CASE Ultra v. 1.7.0.5 was employed (MultiCASE Inc., www.multicase.com/case-ultra) (Chakravarti et al., 2012; Saiakhov et al., 2013, 2014). The mutagenic models (GT_EXPERT and GT1_BMUT) included both statistical and rule-based systems, as recommended in the ICH M7 guidelines (International Conference on Harmonization, 2014).

A description of the main functionalities of TPs was added to the supplementary materials (Text S2, Table S1).

3. Results and discussion

3.1. Flutamide degradation

The [FLUT]$_0$ level of 5 mg L^{-1} was used to enable elucidation of the TPs directly using the LC-QTOF MS system, without any previous pre-concentration techniques. The values obtained for primary elimination of FLUT, at the two different initial concentrations, were 53.4% (t$_{30W}$ = 114 min) and 73.4% (t$_{30W}$ = 122.6 min) for [FLUT]$_0$ of 5 mg L^{-1} and 500 μg L^{-1}, respectively (Fig. 1A and C). Although SPF processes are very efficient for the degradation of pharmaceuticals, the incomplete primary elimination of FLUT provided evidence of its re-calcitrance. The profile for total dissolved iron in the experiment with [FLUT]$_0$ of 5 mg L^{-1} showed a slight decrease of 0.5 mg L^{-1} after 45 min of the SPF process (Fig. 1A), indicating that the iron might undergo further reactions such as complex formation and even minor precipitation. On the other hand, with [FLUT]$_0$ of 500 μg L^{-1}, there was an increase of total iron after 45 min of SPF, which could be explained by the occurrence of complexation and dissolution. For both initial concentrations, the temperature increased by an average of 10 °C between the start and end of the SPF experiment. The Fe^{2+} profile (Fig. 1C) indicated that there was fast consumption during the first minutes, with complete oxidation to Fe^{3+} after the process. For both initial concentrations, the H$_2$O$_2$ consumption indicated the extent of hydroxyl generation throughout the process. Approximately 21 mg L^{-1} and 30.18 mg L^{-1} of H$_2$O$_2$ were consumed after treatment times of t$_{30W}$ = 114 min and t$_{30W}$ = 122.6 min for [FLUT]$_0$ at 5 mg L^{-1} and 0.50 mg L^{-1}, respectively.

Hydrolysis experiments were also performed in the same batch reactor using [FLUT]$_0$ of 5 mg L^{-1}, but without adding Fe^{2+} and H$_2$O$_2$. Iron complexation experiments were carried out using the same initial conditions as the SPF process, but without adding H$_2$O$_2$. Both experiments were conducted for 120 min, in the dark. Aliquots were periodically removed for determination of the FLUT concentration. No hydrolysis and formation of iron complexes with FLUT was observed.

As shown in Fig. 1 (A and C), the kinetics of primary elimination of FLUT followed a pseudo-first order exponential decay. For [FLUT]$_0$ of 5 mg L^{-1}, k$_{obs}$ was 6.57 × 10^{-3} min^{-1} t$_{30W}$ (95% CI: [4.97 × 10^{-3}-0.82 × 10^{-3}]), with r^2 of 0.998 (p < 0.0001) and a half-life time (t$_{1/2}$) of t$_{30W}$ = 95.62 min. For [FLUT]$_0$ of 500 μg L^{-1}, k$_{obs}$ was 9.13 × 10^{-3} min^{-1} t$_{30W}$ (95% CI: [8.19 × 10^{-3}-1.0 × 10^{-2}]), with r^2 of 0.999 (p < 0.0001) and a half-life time (t$_{1/2}$) of t$_{30W}$ = 73.10 min. Similar pseudo-first order kinetics was observed elsewhere for the SPF degradation of emerging contaminants in aqueous solution (Michael et al., 2010, 2019). The calculated ξ(%) values were 1.04 × 10^{-2} and 3.41 × 10^{-3} for the initial FLUT concentrations of 5 mg L^{-1} and 0.5 mg L^{-1}, respectively. These values were of the same order of magnitude as the photonic efficiencies reported by Celeiro et al. (2018).

3.2. Structural elucidation of the TPs and proposal of a degradation pathway

Elucidation of the TPs formed during the SPF process employed LC-QTOF MS in negative ionization mode. Based on the non-target approach results, 13 possible TPs were initially proposed. Table 1 shows the exact masses, the molecular ions ([M−H]$^-$), the ppm errors, and the double bond equivalents (DBE) obtained using the DataAnalysis v. 4.2 software (Bruker Daltonics). In most cases, the correlation between the exact mass and the molecular ion [M−H]$^-$ was very good (error < 5 ppm), providing a degree of certainty for the proposed TPs (see Table 2).

Prediction of the structures of the TPs was based on elemental composition, DBE, and the fragmentation patterns. The fragmentation patterns of the proposed TPs are provided in Text S3 (Figs. S2-S16, Supplementary Material). The EPI Suite™ software (US EPA, 2012) was used to further validate the proposed structures, by predicting the

theoretical log K$_{OW}$ values (Fig. S15, Supplementary Material). The separation using a C$_{18}$ reverse phase chromatographic column enabled correlation between log K$_{OW}$ and the retention time (Rt). A lower log K$_{OW}$ value indicated that the molecule had higher polarity and was therefore eluted earlier, compared to other proposed structures with higher log K$_{OW}$ values.

The observed TPs were more polar than FLUT (Table 1), since they presented shorter retention times. The presence of constitutional isomers was evidenced by the fact that some of the TPs had different Rt values, but the same molecular ion ([M−H]$^-$) *m/z*: 291.098 (TP-9, TP-11, and TP-13), 289.04380 (TP-6 and TP-7), 275.0285 (TP-5 and TP-12), and 334.0214 (TP-1 and TP-2).

Hydroxylation at different positions in the FLUT molecule was the primary mechanism involved in the SPF degradation process. Hydroxylation at the tertiary carbon of the side chain produced TP-11, which is the primary active metabolite of FLUT (Brogden and Clissold, 1991). TP-11 showed a product ion with *m/z* 274.0570 (C$_{11}$H$_9$F$_3$N$_2$O$_3$), indicating the loss of H$_2$O and formation of a double bond, which could be explained by the DBE value of 7.0 (odd configuration). Based on its fragmentation pattern, the most intense peak detected was for TP-13, which resulted from hydroxylation on the aromatic ring of FLUT. As can be seen in Fig. 1A, the fragment with *m/z* 221.0180 Da (C$_7$H$_4$F$_3$N$_2$O$_3$) indicated the loss of C$_4$H$_7$O of the side chain, evidencing the presence of a hydroxyl group somewhere in the aromatic ring of TP-13. For prediction of the position of the hydroxyl in TP-11, a comparison of log K$_{OW}$ was made between the tertiary carbon and the methyl carbon of the isobutyl moiety in the side chain. In order to compare different proposed structures, log K$_{OW}$ was predicted for TP-13 (log K$_{OW}$ = 3.80), which was used as a reference value. When the hydroxyl group was bonded to the tertiary carbon of the isobutyl moiety, log K$_{OW}$ was 2.80, while log K$_{OW}$ of 2.04 was predicted when the HO was bonded to a terminal methyl group. This suggested that the HO group of TP-11 was bonded to the tertiary carbon, due to the lower K$_{OW}$ value. Accordingly, with a log K$_{OW}$ value of 2.04, the hydroxyl position for TP-9 was predicted as being at the terminal methyl group. Another hydroxylated TP was TP-9, which only presented one product ion with *m/z* 205.0231 Da (C$_7$H$_4$F$_3$N$_2$O$_2$). In this case, the hydroxyl could be located at the terminal methyl group or on the nitrogen of the amide group. However, possible attachment at the amide group was discarded, due to its log K$_{OW}$ value of 3.80.

As the reaction process was interrupted at predetermined times by the addition of NaHSO$_3$ to quench the residual H$_2$O$_2$, several TPs with sulfonic groups attached to their structures were proposed, supported by the exact mass analyses and the fragmentation patterns. According to Chen et al. (2019), the presence of sulfonic groups attached to the TPs could be explained by the fact that bisulfite anions can react with ferric iron, with subsequent decomposition to produce ferrous iron and SO$_3^-$· (Eqs. (10) and (11)).

$$Fe^{3+} + HSO_3^- \rightleftharpoons FeSO_3^+ + H^+ \tag{10}$$

$$FeSO_3^+ \rightarrow Fe_2^+ + SO_3^- \tag{11}$$

As can be seen in Fig. 1, [Fe^{2+}] decays over time, increasing [Fe^{3+}], while the addition of NaHSO$_3$ leads to SO$_3^-$·, generating TP-1, TP-2, TP-3, TP-4, and TP-10. The products TP-1, TP-2, and TP-3 were formed according to different steps of hydroxylation, aromatic ring opening, demethylation, and further SO$_3$ attachment to the structure. TP-4 was formed by SO$_3$ addition at the oxygen position of the carboxamide moiety in the FLUT side chain. The fragment with *m/z* 261.0856 Da (C$_{11}$H$_{12}$F$_3$N$_2$O$_2$) indicated the elimination of HSO$_3$. According to its fragmentation pattern, TP-10 (Fig. 2B) was proposed to be formed by HSO$_3$ addition at the beta position of the carbonyl, with addition of a hydroxyl group in the aromatic ring. The fragment with *m/z* 307.0548 Da (C$_{11}$H$_{10}$F$_3$N$_2$O$_5$) indicated that there was elimination of SO$_2$, while the fragment with *m/z* 291.0597 Da (C$_{11}$H$_{10}$F$_3$N$_2$O$_4$) reflected the elimination of hydroxyl in the aromatic ring. This

Table 2

In silico (Q)SAR predictions for mutagenicity and carcinogenicity of FLUT and TPs formed during SPF process.

Comp.	SMILES code	VEGA[a]					QSAR Toolbox[b]						CASE Ultra	
		A	B	C	D	E	A	B	C	D	E	F	A	B
FLUT	O=C(Nc1ccc(c(c1)C(F)(F)F)[N+](=O)[O-])C(C)C	+	+	–	+	+	R/SN1	NA	NiAr	NiAr	+	7.38*	–	–
TP-1	O=S(O)OC(C(=CO)NC(O)CO) = C(C=CO)C(F)(F)F	+	+	–	–	+	NA	NA	NA	H	NC	NC	OD	OD
TP-2 a	O=S(O)OC(C(=CO)N(O)C(O)C) = C(C=CO)C(F)(F)F	+	+	–	–	+	NA	NA	NA	H	NC	NC	IN	OD
TP-2 b	O=S(O)OC(=C(C=CO)N(O)C(O)C)C(=CO)C(F)(F)F	+	+	+	–	+	R/AN2/SN1/SN2	R/AN2/SN1/SN2	NA	H	NC	NC	IN	OD
TP-3 a	O=CC(O) = C(C(O) = C(C=O)NC(O)(O)C(OS(=O)O)(C)CO)C(F)(F)F	+	+	–	+	+	R/AN2/SN1/SN2	R/AN2/SN1/SN2	NA	H/α,β	NC	NC	IN	+
TP-3 b	O=CC(O) = C(NC(O)C(OS(=O)O)(C)CO)C(O) = C(C=O)C(F)(F)F	+	+	–	+	+	NA	NA	α,β	H/α,β	NC	NC	+	+
TP-4	O = [N+]([O-])c1ccc(cc1C(F)(F)F)NC(OS(=O)O)C(C)C	+	+	+	+	+	R/SN1	NA	NiAr	NiAr	+	NC	IN	OD
TP-5	O=C(C=C)N(O)c1ccc(c(c1)C(F)(F)F)[N+](=O)[O-]	+	+	+	+	+	R/AN2/SN1/SN2	R/AN2/SN1/SN2	α,β/NiAr/PriArAm	H/α,β/NiAr/PriArAm	+	NC	+	–
TP-6/7 a	O = [N+]([O-])c1c(O)cc1C(F)(F)F)NCC(=C)C	+	+	–	+	+	NA	NA	NA	H	+	NC	IN	–
TP-6/7 b	O = [N+]([O-])c1cc(O)cc1C(F)(F)F)NCC(=C)C	+	+	–	+	+	R/SN1	NA	NiAr	H/NiAr	+	4.26*	+	–
TP-6/7 c	O = [N+]([O-])c1ccc(NCC(=C)C)c(O)c1C(F)(F)F	+	+	–	+	+	R/SN1	NA	NiAr	H/NiAr	+	4.26*	+	–
TP-8 a	O=C(Nc1ccc(O)c(c1)C(F)(F)F)C(C)C	–	+	–	–	+	NA	NA	NA	NA	+	47.4*	–	–
TP-8 b	O=C(Nc1cc(O)cc(c1)C(F)(F)F)C(C)C	–	+	–	–	+	NA	NA	NA	NA	+	47.4*	–	–
TP-8 c	O=C(Nc1cc(ccc1O)C(F)(F)F)C(C)C	–	+	–	–	+	NA	NA	NA	H	+	28.1*	–	–
TP-8 d	O=C(Nc1cccc(c1O)C(F)(F)F)C(C)C	–	+	–	–	+	NA	NA	NA	H	+	28.1*	–	–
TP-9	O=C(Nc1ccc(c(c1)C(F)(F)F)[N+](=O)[O-])C(C)CO	+	+	+	+	+	R/SN1	NA	NiAr	H/NiAr	+	253***	+	–
TP-10 a	O=C(Nc1ccc(O)c(c1)C(F)(F)F)[N+](=O)[O-])C(OS(=O) = O)(C)C	+	+	+	+	+	NA	NA	NA	H	+	346**	IN	OD
TP-10 b	O=C(Nc1cc(ccc1(O))[N+](=O)[O-])C(F)(F)F)C(OS(=O) = O)(C)C	+	+	+	+	+	R/SN1	NA	NiAr	H/NiAr	+	203**	+	OD
TP-10 c	O=C(Nc1ccc(c(c1(O))C(F)(F)F)[N+](=O)[O-])C(OS(=O) = O)(C)C	+	+	+	+	+	R/SN1	NA	NiAr	H/NiAr	+	203**	+	OD
TP-11	O=C(Nc1ccc(c(c1)C(F)(F)F)[N+](=O)[O-])C(O)(C)C	+	+	+	+	+	R/SN1	NA	NiAr	H/NiAr	+	22.8**	+	–
TP-12 a	O=C(C=C)Nc1cc(c(c1)C(F)(F)F)[N+](=O)[O-]	+	+	+	+	+	NA	NA	α,β	H/α,β	+	NC	IN	–
TP-12 b	O=C(C=C)Nc1cc(c(cc1(O))[N+](=O)[O-])C(F)(F)F	+	+	+	+	+	R/SN1	NA	α,β/NiAr	H/α,β/NiAr	+	NC	+	–
TP-12 c	O=C(C=C)Nc1ccc(c(c1(O))C(F)(F)F)[N+](=O)[O-]	+	+	+	+	+	R/SN1	NA	α,β/NiAr	H/α,β/NiAr	+	NC	+	–
TP-13 a	O=C(Nc1cc(O)c(c1)C(F)(F)F)[N+](=O)[O-])C(C)C	+	+	+	+	+	NA	NA	NA	H	+	11.6*	–	–
TP-13 b	O=C(Nc1cc(cc1(O))[N+](=O)[O-])C(F)(F)F)C(C)C	+	+	+	+	+	R/SN1	NA	NiAr	H/NiAr	+	6.78*	IN	–
TP-13 c	O=C(Nc1ccc(c(c1(O))C(F)(F)F)[N+](=O)[O-])C(C)C	+	+	+	+	+	R/SN1	NA	NiAr	H/NiAr	+	6.78*	IN	–

+: positive alert; −: negative alert.

* Phenol and anilines strict; **Reactive unspecific strict; Basesurface narcotics Strict.

Type of alerts: R: radical via ROS formation; AN2: Carbamoylation after isocyanate formation; SN1: Nucleophilic attack after nitrenium ion formation; SN2: Acylation. NiAr: Nitro-aromatic; H: H-acceptor-path3-H-acceptor; α,β: α,β-unsaturated carbonyls; PriAm: Primary aromatic amine; NA: no alert found; NC: Not categorized.

[c] **CASE Ultra models:** (A) GT1_BMUT and (B) GT_EXPERT.

[a] **VEGA models:** Mutagenicity (A) Ames test CONSENSUS model; Carcinogenicity models: (B) IRFMN/Antares; (C) CAESAR; (D) ISS; (E) IRFMN/ISSCAN-CGX.

[b] **QSAR toolbox models:** (A) DNA alerts for AMES by OASIS; (B) DNA alerts for CA and MNT by OASIS; (C) *in vitro* mutagenicity (Ames test) alerts by ISS; (D) *in vitro* mutagenicity (micronucleus) alerts by ISS; (E) Hepatotoxicity; (F) Ecotoxicological Endpoint Fish [LC50 (EC50) at 96 h *Pimephales promelas*].

elimination was evidenced by the product ion with m/z 205.0232 Da ($C_7H_4F_3N_2O_2$), with elimination of the $C_4H_6O_2$ group.

For TP-6 and TP-7, the DBE and log K_{OW} values were compared in order to predict their structures. These constitutional isomers had the same m/z, but different Rt values, and had predicted DBE values of 7.5. The higher DBE, compared to FLUT (DBE = 6.5), was due to hydrogen abstraction and the formation of a double bond in the FLUT side chain. TP-6 and TP-7 could have been formed from TP-13 by hydrogen abstraction in the side chain, forming a double bond. According to the EPI-Suite™ predictions, the log K_{OW} values predicted for TP-6 and TP-7 were 3.35 and 3.60, respectively. The difference among the predicted values was lower than expected, so the exact position of the hydroxylation could not be accurately ascertained, based only on the MS/MS data.

TP-5 and TP-12 were identified as secondary TPs formed from TP-9 and TP-13, respectively. TP-5 was proposed to be produced from TP-9 by the elimination of CH_3OH on the isobutyl moiety, followed by formation of a double bond and hydroxylation on the nitrogen of the carboxamide group. The proposal of hydroxyl in TP-5 was based on the fragmentation pattern and the predicted log K_{OW}. Accordingly, there were three possibilities for the OH position: (i) attached to α- or β-carbon, (ii) attached to the amide group, or (iii) attached to the aromatic ring. The product ion with m/z 221.0177 Da ($C_7H_4F_3N_2O_3$) excluded the possibility that the OH was attached to α- or β-carbon. The OH bonded to the nitrogen of the carboxamide group was predicted by log K_{OW} of 2.19, compared to log K_{OW} of 2.70 and 3.05 for OH in different positions of the aromatic ring. Therefore, the proposed OH attachment was on the nitrogen of the carboxamide group. This was supported by comparison of the Rt values for TP-5 and its constitutional isomer TP-12, with a difference of approximately 1.9 min. This difference suggested that the HO was attached on the aromatic ring, since the log K_{OW} values for HO attached on the aromatic ring were high (Figure S15, Supplementary Material).

TP-8 was proposed to be formed from FLUT by loss of the nitro group and a further hydroxylation at some position on the aromatic ring. The TP-8 structure could be explained by the product ion with m/z
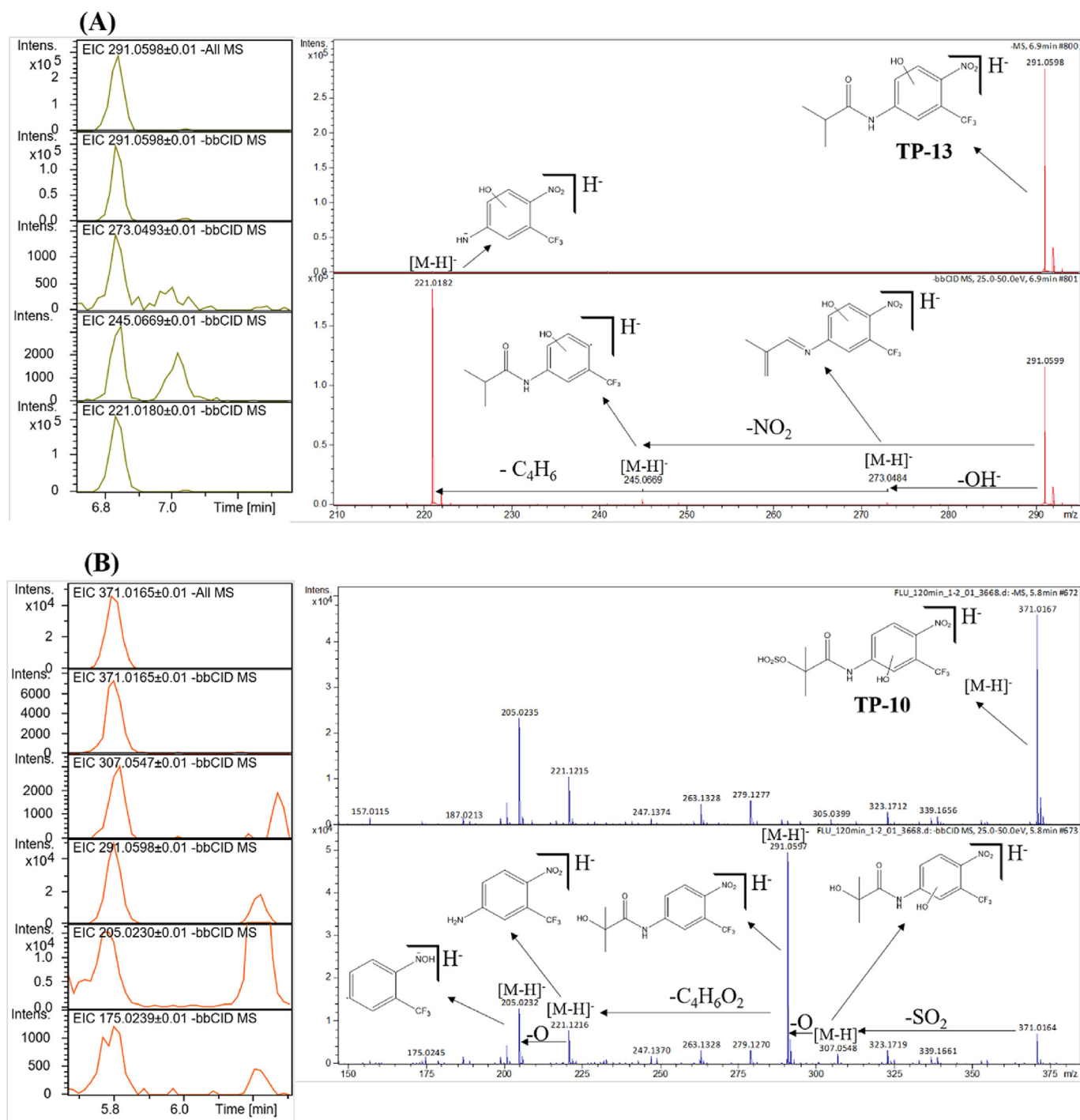
Fig. 2. Extracted ion chromatograms (EIC) and bbCID fragmentation pattern in negative ionization mode of (A) TP-13 and (B) TP-10.

226.0689 Da ($C_{11}H_{10}F_2NO_2$), where there was the loss of HF, forming a double bond and stabilizing resonance through the structure. A degradation pathway could therefore be proposed (Fig. 3).

Fig. 1 (C and D) shows the TPs profile during the SPF process, normalized by the initial area for FLUT. Increases of the TPs areas were observed for both FLUT concentrations, while some of the TPs underwent further transformation, evidenced by decreased areas. At the lower initial FLUT concentration, it was not possible to identify some of the TPs, which could be explained by different degradation pathways, faster elimination kinetics, and the occurrence of some TPs only under certain conditions, as well as lower sensitivity and poorer detection limits (Herrmann et al., 2015).

A table comparing the results of SPF process to the degradation of FLUT was added to supplementary materials (Text S4, Table S2).

3.3. Assessment of environmental fate and ecotoxicity using in silico (Q)SAR predictions

The SMILES code and all the (Q)SAR predictions from the different (Q)SAR models can be seen in Text S5 (Supplementary Material). The environmental fates of FLUT and the TPs, considering their persistence, were assessed by *in silico* biodegradability predictions based on BIOWIN 1–7 and VEGA (IRFM model). The results of the BIOWIN 1–7 (six aerobic models and one anaerobic model) predictions for all possible

21

A. Della-Flora, et al.   Environmental Research 183 (2020) 109223
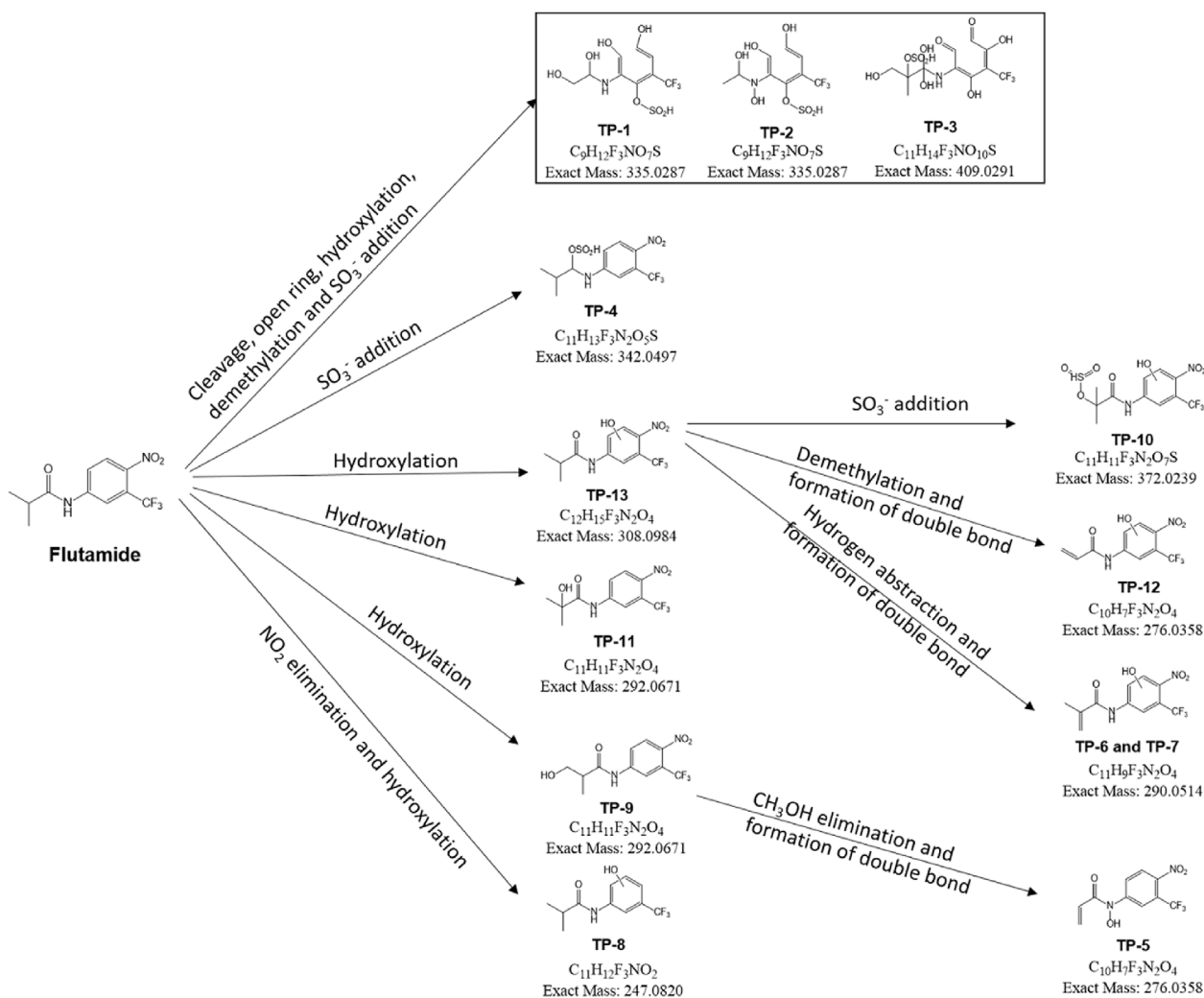
Fig. 3. Proposed degradation pathway of FLUT through solar photo-Fenton.

proposed structures of the TPs indicated that the compounds were not biodegradable. Similar *in silico* predictions were obtained using the VEGA model for ready biodegradability (IRFM model). Fig. 4A shows the VEGA IRFM model for ready biodegradability and the *in silico* predictions of BIOWIN 5 (linear MITI model), which is directly comparable to the OECD 301C biodegradability test. Even considering the TPs formed by cleavage, ring-opening, and further hydroxylation, the values were below the threshold value of 0.5. The biodegradability predictions provided by the VEGA IRFM model were in agreement with the values predicted using BIOWIN 5. An exception was for TP-3, which was predicted as biodegradable by BIOWIN 5, but not readily biodegradable by the VEGA model.

The BIOWIN 5 model is not directly comparable to OECD 301D (closed bottle test), as it is considers a high bacterial density, which increases the probability of biodegradation. The *in silico* predictions performed by BIOWIN do not indicate whether the structures assessed lie within the applicability domains (ADs) of the models. In contrast, the VEGA models provide information about the reliability of the predictions. For the TPs assessed, most of the predictions produced by the VEGA model for biodegradability were of moderate reliability. Pizzo et al. (2013) reported that the biodegradability predictions provided by VEGA gave more accurate results for a group of chemicals, compared to the use of other software. Although the general rule for the structure/biodegradability relationship is that the attachment of groups with electron-donating character (such as hydroxyls) might increase biodegradability (Boethling et al., 2007), most of the TPs of FLUT presented a

CF$_3$ moiety, which is an electron-withdrawing group and tends to increase persistence (Boethling et al., 2007).

The *in silico* (Q)SAR predictions provided by the Prometheus software were used to rank the TPs as possible PBT compounds. A threshold value of 0.5 for the total score was used to differentiate the potentially PBT and non-PBT (< 0.5) or vPvB (≥ 0.5) compounds (Pizzo et al., 2016). Fig. 4B shows that some of the proposed structures had scores near the threshold value of 0.5. The proposed structures for TP-6 and TP-7 (*b* and *c*) exceeded the limit value of 0.5 and could be identified as PBT or vPvB, which would deserve further attention. In general, TPs that still maintained the basic structure of FLUT and had undergone hydroxylation, demethylation, and hydrogen abstraction to form double bonds were ranked around the value of 0.5, as potentially PBT compounds. Conversely, the TPs that had undergone cleavage of the aromatic ring, hydroxylation, and attachment of the HSO$_3$ group were predicted to be non-PBT compounds.

The CONSENSUS model was used in the Ames mutagenicity test predictions performed with the VEGA v. 1.1.4 software. FLUT and most of the TPs were predicted to be mutagenic compounds (Table S6, Supplementary Material). Nevertheless, the CONSENSUS scores for the structures of TP-1 to TP-5, as well as TP-10, were < 0.35, indicating that these structures might not be within the ADs of the models. The other structures showed scores > 0.5, indicating that these structures were within the ADs of the models. The four carcinogenicity models applied for FLUT and the TPs gave positive alerts for FLUT and the TPs from TP-9 to TP-13. These compounds should therefore undergo further
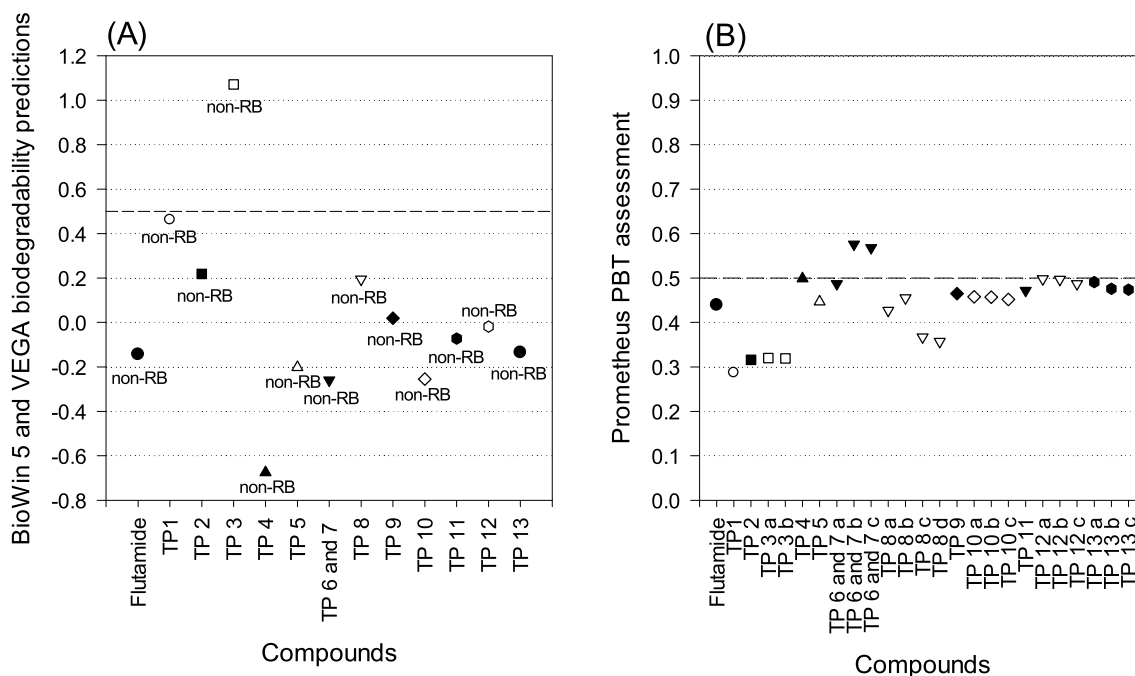
Fig. 4. (A) *In silico* (Q)SAR predictions of BIOWIN 5 (linear MITI model) and VEGA (IRFM model) for the biodegradability of FLUT and TPs; (B) *In silico* (Q)SAR prediction of PBT values by the Prometheus software. (- - -) reference line concerning the threshold value BIOWIN 5 for biodegradability and Prometheus for PBT/ *vP*v*B* compounds.

studies regarding their environmental risk.

The QSAR Toolbox provided a series of complementary alerts concerning the endpoints assessed. The OASIS models delivered DNA alerts for Ames and DNA alerts for CA and MNT, while the ISS models provided alerts for *in vitro* mutagenicity (Ames and micronucleus tests), based on the ADs. The alerts provided by the OASIS models were for radicals formed in reactions involving reactive oxygen species (ROS) and carbamoylation after isocyanate formation.

Fig. 5 shows the QSAR *in silico* alerts, obtained using the ISS models, for the *in vitro* mutagenicities (Ames and micronucleus tests) of the main TPs of FLUT. The structural alerts provided by ISS models C and D were due to the presence of nitroaromatic, α,β-unsaturated carbonyl, and H-acceptor-path3-H-acceptor moieties in the structures. Such structural alerts identify possibly mutagenic and carcinogenic compounds. The TPs with most alerts were those that still maintained the basic structure of FLUT and had undergone few structural changes.

Nitroaromatic compounds have been reported as giving positive results in Ames tests using *Salmonella typhimurium* strains, which could be due to mechanisms involving radicals (including ROS), heterocyclic processes, and metabolic activation (Nelson, 1982). Compounds presenting α,β-unsaturated carbonyls in their structures may also present positive alerts for mutagenicity, since they can interact with electron-rich biological macromolecules. The α,β-unsaturated carbonyls can undergo different interactions with DNA, such as the formation of saturated cyclic adducts and metabolic epoxidation, leading to mutagenic and carcinogenic effects (Eder et al., 1990). The alert produced by $H_{acceptor}$-path3-$H_{acceptor}$ indicates the possibility that the compound might interact with DNA by means of non-covalent binding or groove binding (Snyder et al., 2006). This structural alert was found for all the TPs. The TPs that had undergone aromatic ring cleavage presented various $H_{acceptor}$-path3-$H_{acceptor}$ structural alerts within the same molecule. These included TP-1 (4 alerts), TP-2a (3 alerts), TP-2b (2 alerts), TP-3a (8 alerts), TP-3b (9 alerts), TP-10a and TP-10 b (4 alerts), and TP-11 (2 alerts), as shown in Fig. 5. For TP-5, ISS alerts were found related to primary aromatic amines in the *in vitro* Ames and micronucleus mutagenicity tests. The mutagenic potential of primary aromatic amines occurs when amines are metabolized to reactive electrophiles

via cytochrome P-450 (Benigni et al., 2000). Additionally, TPs with structures similar to that of FLUT presented predicted positive alerts towards hepatotoxicity. The structures proposed for TP-6, TP-7a and b, and TP-13 b and c were predicted to have lower LC_{50} towards *Pimephales promelas*, compared to the parent compound.

4. Conclusions

The SPF degradation of FLUT achieved 53.4% and 73.4% primary elimination for 5 mg L^{-1} and 500 μg L^{-1} of $[FLUT]_0$, respectively. A total of 13 TPs were proposed, for the first time, employing LC-QTOF MS. The structures of the TPs were proposed based on HRMS, the MS/ MS fragmentation patterns, and the agreement obtained for the exact masses of the $[M-H]^-$ molecular ions (error < 2 ppm). For most of the TPs, the degradation mechanism was hydroxylation. TPs with attached sulfonic groups were identified and they were not formed through the SPF process, but due to the $NaHSO_3$ employed to quench the residual H_2O_2. Thus such compounds would not be found in SPF treatment applied to WWTP. Prediction of the isomers was achieved by comparing the log K_{OW} values predicted by the EPI Suite™ software, although the exact position of the hydroxylation could not be ascertained.

The *in silico* (Q)SAR approach for evaluating the environmental fates and effects of the TPs indicated that the degradation of FLUT utilizing SPF might not entirely eliminate the risks associated with this type of compound. *In silico* (Q)SAR predictions could be used in screening to enable more proactive risk assessment of TPs. *In silico* (Q)SAR tools should be further developed to fill the gaps in the initial risk assessment of TPs, providing guidance in order to prioritize hazardous TPs for further tests.

A. Della-Flora, et al.   Environmental Research 183 (2020) 109223

23
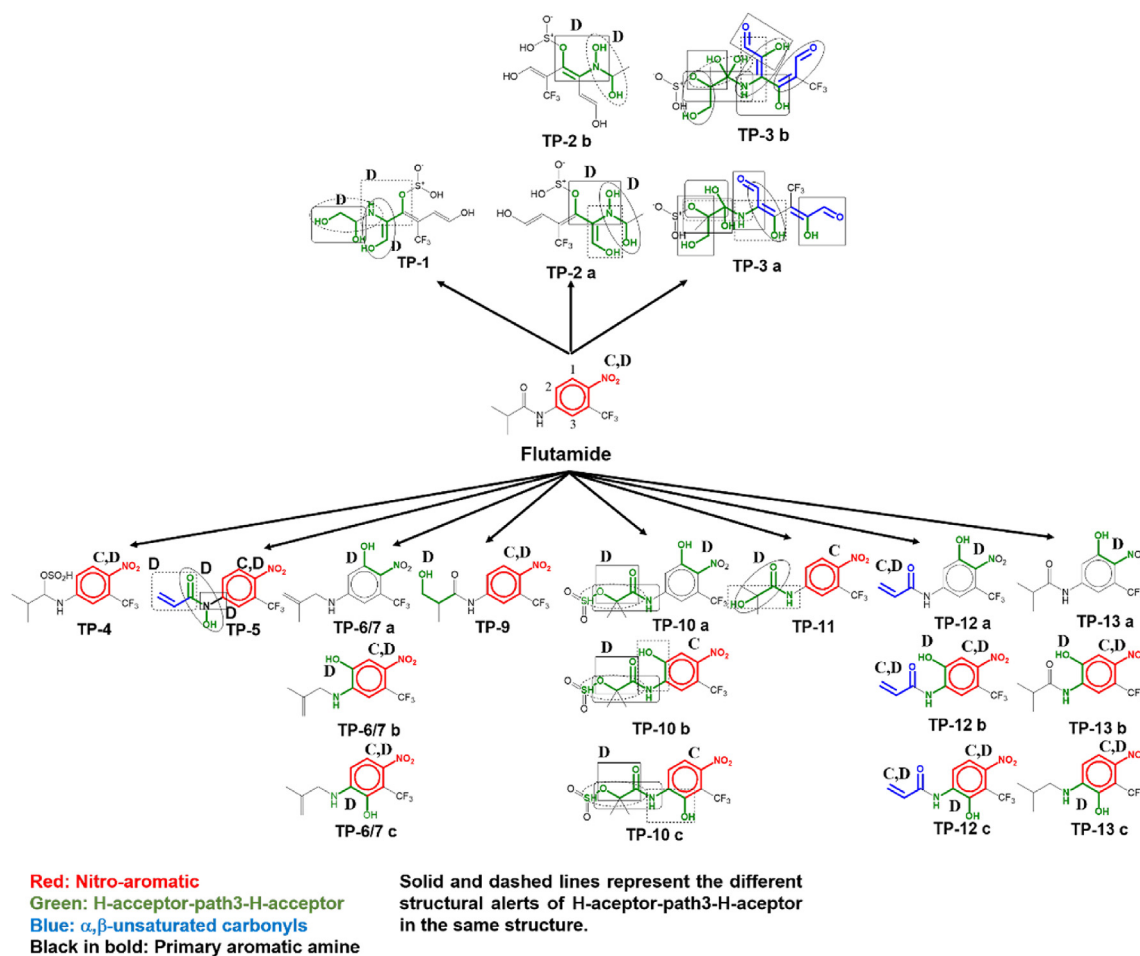
Fig. 5. *In silico* structural alerts predicted by QSAR toolbox ISS models for (C) *in vitro* mutagenicity (Ames test), (D) *in vitro* mutagenicity (micronucleus) found in FLUT, and the different structures proposed for the TPs.

(23811 Chagrin Blvd. Ste. 305, Beachwood, Ohio 44113 USA +1-216-831-3740, sales@multicase.com) for providing a trial version of the software.

Appendix A. Supplementary data

Supplementary data to this article can be found online at https://doi.org/10.1016/j.envres.2020.109223.

References

Afshar, L.E., Chaibakhsh, N., Moradi-Shoeili, Z., 2018. Treatment of wastewater containing cytotoxic drugs by CoFe2O4 nanoparticles in Fenton/ozone oxidation process. Separ. Sci. Technol. 53, 2671–2682. https://doi.org/10.1080/01496395.2018.1461113.

Amildon Ricardo, I., Paiva, V.A.B., Paniagua, C.E.S., Trovó, A.G., 2018. Chloramphenicol photo-Fenton degradation and toxicity changes in both surface water and a tertiary effluent from a municipal wastewater treatment plant at near-neutral conditions. Chem. Eng. J. 347, 763–770. https://doi.org/10.1016/j.cej.2018.04.169.

ANVISA, 2018. Agência Nacional de Vigilância Sanitária. Anuário estatístico do mercado farmacêutico 2017. Brasilia. 2018.

Benigni, R., Giuliani, A., Franke, R., Gruska, A., 2000. Quantitative structure-activity relationships of mutagenic and carcinogenic aromatic amines. Chem. Rev. 100, 3697–3714. https://doi.org/10.1021/cr9901079.

Boethling, R.S., Sommer, E., DiFiore, D., 2007. Designing small molecules for biodegradability. Chem. Rev. 107, 2207–2227. https://doi.org/10.1021/cr050952t.

Brogden, R.N., Clissold, S.P., 1991. Flutamide: a review of its pharmacodynamic and pharmacokinetic properties, and therapeutic use in advanced prostatic cancer. Drup Aging 1, 104–115. https://doi.org/10.2165/00003495-198938020-00003.

Brooks, B.W., Chambliss, C.K., Stanley, J.K., Ramirez, A., Banks, K.E., Johnson, R.D., Lewis, R.J., 2005. Determination of select antidepressants in fish from an effluent-dominated stream. Environ. Toxicol. Chem. 24, 464–469.

Celeiro, M., Vignola Hackbarth, F., Selene, S.M.A.G., Llompart, M., Vilar, V.J.P., 2018.

Assessment of advanced oxidation processes for the degradation of three UV filters from swimming pool water. J. Photochem. Photobiol. Chem. 351, 95–107. https://doi.org/10.1016/j.jphotochem.2017.10.023.

Chakravarti, S.K., Saiakhov, R.D., Klopman, G., 2012. Optimizing predictive performance of CASE Ultra expert system models using the applicability domains of individual toxicity alerts. J. Chem. Inf. Model. 52, 2609–2618. https://doi.org/10.1021/ci300111r.

Chen, M., Zhang, Z., Zhu, L., Wang, N., Tang, H., 2019. Bisulfite-induced drastic enhancement of bisphenol A degradation in Fe3+-H2O2 Fenton system. Chem. Eng. J. 361, 1190–1197. https://doi.org/10.1016/j.cej.2018.12.170.

Chong, M.N., Jin, B., Chow, C.W.K., Saint, C., 2010. Recent developments in photocatalytic water treatment technology: a review. Water Res. 44, 2997–3027. https://doi.org/10.1016/j.watres.2010.02.039.

Clarizia, L., Russo, D., Di Somma, I., Marotta, R., Andreozzi, R., 2017. Homogeneous photo-Fenton processes at near neutral pH: a review. Appl. Catal. B Environ. 209, 358–371. https://doi.org/10.1016/j.apcatb.2017.03.011.

Eder, E., Hoffman, C., Bastian, H., Deininger, C., Scheckenbach, S., 1990. Molecular mechanisms of DNA damage initiated by alfa,beta-unsaturated carbonyl compounds as criteria for genotoxicity and mutagenicity. Environ. Health Perspect. 88, 99–106.

Faisal, M., Bouzid, H., Harraz, F.A., Ismail, A.A., Al-Sayari, S.A., Al-Assiri, M.S., 2015. Mesoporous Ag/ZnO multilayer films prepared by repeated spin-coating for enhancing its photonic efficiencies. Surf. Coating. Technol. 263, 44–53. https://doi.org/10.1016/j.surfcoat.2014.12.063.

Fakhri, A., Azad, M., Tahami, S., 2017a. Degradation of toxin via ultraviolet and sunlight photocatalysis using ZnO quantum dots/CuO nanosheets composites: preparation and characterization studies. J. Mater. Sci. Mater. Electron. 28, 16397–16402. https://doi.org/10.1007/s10854-017-7550-x.

Fakhri, A., Behrouz, S., 2015a. Photocatalytic properties of tungsten trioxide (WO3) nanoparticles for degradation of Lidocaine under visible and sunlight irradiation. Sol. Energy 112, 163–168. https://doi.org/10.1016/j.solener.2014.11.014.

Fakhri, A., Behrouz, S., 2015b. Assessment of SnS2 nanoparticles properties for photocatalytic and antibacterial applications. Sol. Energy 117, 187–191. https://doi.org/10.1016/j.solener.2015.04.016.

Fakhri, A., Kahi, D.S., 2017. Synthesis and characterization of MnS2/reduced graphene oxide nanohybrids for with photocatalytic and antibacterial activity. J. Photochem. Photobiol. B Biol. 166, 259–263. https://doi.org/10.1016/j.jphotobiol.2016.12.017.

Fakhri, A., Khakpour, R., 2015. Synthesis and characterization of carbon or/and boron-doped CdS nanoparticles and investigation of optical and photoluminescence properties. J. Lumin. 160, 233–237. https://doi.org/10.1016/j.jlumin.2014.12.019.

Fakhri, A., Naji, M., Fatolahi, L., Nejad, P.A., 2017b. Synthesis and characterization of Fe3O4 and CdTe quantum dots anchored SnO2 nanofibers and SnO2 nanospheres for degradation and removal of two carcinogen substance. J. Mater. Sci. Mater. Electron. 28, 16484–16492. https://doi.org/10.1007/s10854-017-7560-8.

Fakhri, A., Nejad, P.A., 2016. Antimicrobial, antioxidant and cytotoxic effect of Molybdenum trioxide nanoparticles and application of this for degradation of ketamine under different light illumination. J. Photochem. Photobiol. B Biol. 159, 211–217. https://doi.org/10.1016/j.jphotobiol.2016.04.002.

Fakhri, A., Pourmand, M., Khakpour, R., Behrouz, S., 2015. Structural, optical, photoluminescence and antibacterial properties of copper-doped silver sulfide nanoparticles. J. Photochem. Photobiol. B Biol. 149, 78–83. https://doi.org/10.1016/j.jphotobiol.2015.05.013.

Fakhri, A., Rashidi, S., Tyagi, I., Agarwal, S., Gupta, V.K., 2016. Photodegradation of Erythromycin antibiotic by γ-Fe2O3/SiO2 nanocomposite: response surface methodology modeling and optimization. J. Mol. Liq. 214, 378–383. https://doi.org/10.1016/j.molliq.2015.11.037.

Fatta-Kassinos, D., Vasquez, M.I., Kümmerer, K., 2011. Transformation products of pharmaceuticals in surface waters and wastewater formed during photolysis and advanced oxidation processes - degradation, elucidation of byproducts and assessment of their biological potency. Chemosphere 85, 693–709. https://doi.org/10.1016/j.chemosphere.2011.06.082.

Franquet-Griell, H., Gómez-Canela, C., Ventura, F., Lacorte, S., 2015. Predicting Concentrations of Cytostatic Drugs in Sewage Effluents and Surface Waters of Catalonia (NE Spain), vol. 138. pp. 161–172.

Giannakis, S., Hendaoui, I., Jovic, M., Grandjean, D., De Alencastro, L.F., Girault, H., Pulgarin, C., 2017. Solar photo-Fenton and UV/H2O2 processes against the antidepressant Venlafaxine in urban wastewaters and human urine. Intermediates formation and biodegradability assessment. Chem. Eng. J. 308, 492–504. https://doi.org/10.1016/j.cej.2016.09.084.

Herrmann, M., Menz, J., Olsson, O., Kümmerer, K., 2015. Identification of phototransformation products of the antiepileptic drug gabapentin: biodegradability and initial assessment of toxicity. Water Res. 85, 11–21. https://doi.org/10.1016/j.watres.2015.08.004.

Hübner, U., von Gunten, U., Jekel, M., 2014. Evaluation of the persistence of transformation products from ozonation of trace organic compounds - a critical review. Water Res. 8, 150–170. https://doi.org/10.1016/j.watres.2014.09.051.

International Conference on Harmonization (ICH), 2014. ICH guideline M7. http://www.ich.org/fileadmin/Public_Web_Site/ICH_Products/Guidelines/Multidisciplinary/M7/M7_Step_4.pdf, Accessed date: 11 February 2015.

Ioannou-Ttofa, L., Raj, S., Prakash, H., Fatta-Kassinos, D., 2019. Solar photo-Fenton oxidation for the removal of ampicillin, total cultivable and resistant E. coli and ecotoxicity from secondary-treated wastewater effluents. Chem. Eng. J. 355, 91–102. https://doi.org/10.1016/j.cej.2018.08.057.

ISO 6332, 1988. Water quality - determination of iron - spectrometric method using 1,10-phenanthroline. Int. Organ. Stand.

Klamerth, N., Malato, S., Maldonado, M., Aguery, A., Fernandez-Alba, A., 2010. Application of photo-fenton as a tertiary treatment of emerging contaminants in municipal. Environ. Sci. Technol. 44, 1792–1798.

Knapczyk-Stwora, K., Nynca, A., Ciereszko, R.E., Paukszto, L., Jastrzebski, J.P., Czaja, E., Witek, P., Koziorowski, M., Slomczynska, M., 2019. Flutamide-induced alterations in transcriptional profiling of neonatal porcine ovaries. J. Anim. Sci. Biotechnol. 10, 1–15. https://doi.org/10.1186/s40104-019-0340-y.

Koltsakidou, A., Antonopoulou, M., Evgenidou, E., Konstantinou, I., Lambropoulou, D., 2019. A comparative study on the photo-catalytic degradation of Cytarabine anticancer drug under Fe3+/H2O2, Fe3+/S2O82−, and [Fe(C2O4)3]3−/H2O2 processes. Kinetics, identification, and in silico toxicity assessment of generated transformation products. Environ. Sci. Pollut. Res. 26, 7772–7784. https://doi.org/10.1007/s11356-018-4019-2.

Leder, C., Rastogi, T., Kümmerer, K., 2015. Putting benign by design into practice-novel concepts for green and sustainable pharmacy: designing green drug derivatives by non-targeted synthesis and screening for biodegradability. Sustain. Chem. Pharm. 2, 31–36. https://doi.org/10.1016/j.scp.2015.07.001.

Li, Z., Sobek, A., Radke, M., 2016. Fate of pharmaceuticals and their transformation products in four small European rivers receiving treated wastewater. Environ. Sci. Technol. 50, 5614–5621. https://doi.org/10.1021/acs.est.5b06327.

Lumbaque, E.C., Becker, R.W., Salmoria Araújo, D.S., Dallegrave, A., Ost Fracari, T.O., Lavayen, V., Sirtori, C., 2019a. Degradation of pharmaceuticals in different water matrices by a solar homo/heterogeneous photo-Fenton process over modified alginate spheres. Environ. Sci. Pollut. Res. 26, 6532–6544. https://doi.org/10.1007/s11356-018-04092-z.

Lumbaque, E.C., Salmoria Araújo, D., Moreira Klein, T., Lopes Tiburtius, E.R., Argüello, J., Sirtori, C., 2019b. Solar photo-Fenton-like process at neutral pH: Fe(III)-EDDS complex formation and optimization of experimental conditions for degradation of pharmaceuticals. Catal. Today 328, 259–266. https://doi.org/10.1016/j.cattod.2019.01.006.

Malato, S., Fernández-Ibáñez, P., Maldonado, M.I., Blanco, J., Gernjak, W., Malato, S., Ferna, P., 2009. Decontamination and disinfection of water by solar photocatalysis: recent overview and trends. Catal. Today 147, 1–59. https://doi.org/10.1016/j.cattod.2009.06.018.

Méndez-Arriaga, F., Esplugas, S., Giménez, J., 2010. Degradation of the emerging contaminant ibuprofen in water by photo-Fenton. Water Res. 44, 589–595. https://doi.org/10.1016/j.watres.2009.07.009.

Michael, I., Frontistis, Z., Fatta-Kassinos, D., 2013. Removal of pharmaceuticals from environmentally relevant matrices by advanced oxidation processes (AOPs). Comprehensive Analytical Chemistry, second ed. Elsevier B.Vhttps://doi.org/10.1016/B978-0-444-62657-8.00011-2.

Michael, I., Hapeshi, E., Michael, C., Fatta-Kassinos, D., 2010. Solar Fenton and solar TiO2 catalytic treatment of ofloxacin in secondary treated effluents: evaluation of operational and kinetic parameters. Water Res. 44, 5450–5462. https://doi.org/10.1016/j.watres.2010.06.053.

Michael, S.G., Michael-Kordatou, I., Beretsou, V.G., Jäger, T., Michael, C., Schwartz, T., Fatta-Kassinos, D., 2019. Solar photo-Fenton oxidation followed by adsorption on activated carbon for the minimisation of antibiotic resistance determinants and toxicity present in urban wastewater. Appl. Catal. B Environ. 244, 871–880. https://doi.org/10.1016/j.apcatb.2018.12.030.

Miller, T.H., Ng, K.T., Bury, S.T., Bury, S.E., Bury, N.R., Barron, L.P., 2019. Biomonitoring of pesticides, pharmaceuticals and illicit drugs in a freshwater invertebrate to estimate toxic or effect pressure. Environ. Int. 129, 595–606. https://doi.org/10.1016/j.envint.2019.04.038.

Mohammadi, S., Sohrabi, M., Golikand, A.N., Fakhri, A., 2016. Preparation and characterization of zinc and copper co-doped WO3 nanoparticles: application in photocatalysis and photobiology. J. Photochem. Photobiol. B Biol. 161, 217–221. https://doi.org/10.1016/j.jphotobiol.2016.05.020.

Nelson, S.D., 1982. Metabolic activation and drug toxicity. J. Med. Chem. 25, 753–765. https://doi.org/10.1021/jm00349a001.

Nogueira, R.F.P., Oliveira, M.C., Paterlini, W.C., 2005. Simple and fast spectrophotometric determination of H2O2 in photo-Fenton reactions using metavanadate. Talanta 66, 86–91. https://doi.org/10.1016/j.talanta.2004.10.001.

Ortiz de García, S., Pinto Pinto, G., García Encina, P., Irusta Mata, R., 2013. Consumption and occurrence of pharmaceutical and personal care products in the aquatic environment in Spain. Sci. Total Environ. 444, 451–465. https://doi.org/10.1016/j.scitotenv.2012.11.057.

Papoutsakis, S., Pulgarin, C., Oller, I., Sánchez-Moreno, R., Malato, S., 2016. Enhancement of the Fenton and photo-Fenton processes by components found in wastewater from the industrial processing of natural products: the possibilities of cork boiling wastewater reuse. Chem. Eng. J. 304, 890–896. https://doi.org/10.1016/j.cej.2016.07.021.

Pignatello, J.J., Oliveros, E., MacKay, A., 2006. Advanced oxidation processes for organic contaminant destruction based on the fenton reaction and related chemistry. Crit. Rev. Environ. Sci. Technol. 36, 1–84. https://doi.org/10.1080/10643380500326564.

Pizzo, F., Lombardo, A., Manganaro, A., Benfenati, E., 2013. In silico models for predicting ready biodegradability under REACH: a comparative study. Sci. Total Environ. 463–464, 161–168. https://doi.org/10.1016/j.scitotenv.2013.05.060.

Pizzo, F., Lombardo, A., Manganaro, A., Cappelli, C.I., Petoumenou, M.I., Albanese, F., Roncaglioni, A., Brandt, M., Benfenati, E., 2016. Integrated in silico strategy for PBT assessment and prioritization under reach. Environ. Res. 151, 478–492. https://doi.org/10.1016/j.envres.2016.08.014.

Prieto-Rodriguez, L., Miralles-Cuevas, S., Oller, I., Agüera, A., Puma, G.L., Malato, S., 2012. Treatment of emerging contaminants in wastewater treatment plants (WWTP) effluents by solar photocatalysis using low TiO2 concentrations. J. Hazard Mater. 211–212, 131–137. https://doi.org/10.1016/j.jhazmat.2011.09.008.

Rastogi, T., Leder, C., Kümmerer, K., 2014. Qualitative environmental risk assessment of photolytic transformation products of iodinated X-ray contrast agent diatrizoic acid. Sci. Total Environ 482–483, 378–388. https://doi.org/10.1016/j.scitotenv.2014.02.139.

Ribeiro, A.R., Nunes, O.C., Pereira, M.F.R., Silva, A.M.T., 2015. An overview on the advanced oxidation processes applied for the treatment of water pollutants defined in the recently launched Directive 2013/39/EU. Environ. Int. 75, 33–51. https://doi.org/10.1016/j.envint.2014.10.027.

Rodriguez-Narvaez, O.M., Peralta-Hernandez, J.M., Goonetilleke, A, Bandala, E.R., 2017. Treatment technologies for emerging contaminants in water: a review. Chem. Eng. J. 323, 361–380. https://doi.org/10.1016/j.cej.2017.04.106.

Rücker, C., Kümmerer, K., 2012. Modeling and predicting aquatic aerobic biodegradation – a review from a user's perspective. Green Chem. 14, 875–887. https://doi.org/10.1039/c2gc16267a.

Saiakhov, R., Chakravarti, S., Klopman, G., 2013. Effectiveness of CASE ultra expert system in evaluating adverse effects of drugs. Mol. Inform. 32, 87–97. https://doi.org/10.1002/minf.201200081.

Saiakhov, R., Chakravarti, S., Sedykh, A., 2014. An improved workflow to perform in silico mutagenicity assessment of impurities as per ICH M7 guideline. Toxicol. Lett. 229, S164. https://doi.org/10.1016/j.toxlet.2014.06.563.

Sim, W.-J., Lee, J.-W., Lee, E.-S., Shin, S.-K., Hwang, S.-R., Oh, J.-E., 2011. Occurrence and distribution of pharmaceuticals in wastewater from households, livestock farms, hospitals and pharmaceutical manufactures. Chemosphere 82, 179–186.

Snyder, R.D., Ewing, D., Hendry, L.B., 2006. DNA intercalative potential of marketed drugs testing positive in in vitro cytogenetics assays. Mutat. Res. Genet. Toxicol. Environ. Mutagen 609, 47–59. https://doi.org/10.1016/j.mrgentox.2006.06.001.

Soriano-Molina, P., Plaza-Bolaños, P., Lorenzo, A., Agüera, A., García Sánchez, J.L., Malato, S., Sánchez Pérez, J.A., 2019. Assessment of solar raceway pond reactors for removal of contaminants of emerging concern by photo-Fenton at circumneutral pH from very different municipal wastewater effluents. Chem. Eng. J. 366, 141–149. https://doi.org/10.1016/j.cej.2019.02.074.

Sun, J.H., Sun, S.P., Fan, M.H., Guo, H.Q., Qiao, L.P., Sun, R.X., 2007. A kinetic study on the degradation of p-nitroaniline by Fenton oxidation process. J. Hazard Mater. 148, 172–177. https://doi.org/10.1016/j.jhazmat.2007.02.022.

Tian, J., Liu, L., Han, Y., Yang, Y., Jin, S., Yang, J., 2017. Effects of testosterone and flutamide on reproduction in Brachionus calyciflorus. Sci. Rep. 7, 1–7. https://doi.org/10.1038/s41598-017-05517-4.

US EPA, 2012. U.S. EPA. Estimation Programs Interface Suite™ for Microsoft® Windows

4.11 United States Environmental Protection Agency, Washington, DC, USA.

Wilde, M.L., Menz, J., Leder, C., Kümmerer, K., 2018. Combination of experimental and in silico methods for the assessment of the phototransformation products of the anti-psychotic drug/metabolite Mesoridazine. Sci. Total Environ. 618, 697–711. https://doi.org/10.1016/j.scitotenv.2017.08.040.

Wilde, M.L., Menz, J., Trautwein, C., Leder, C., Kümmerer, K., 2016. Environmental fate and effect assessment of thioridazine and its transformation products formed by photodegradation. Environ. Pollut. 213, 658–670. https://doi.org/10.1016/j.envpol.2016.03.018.

Yin, P., Li, Y.W., Chen, Q.L., Liu, Z.H., 2017. Diethylstilbestrol, flutamide and their combination impaired the spermatogenesis of male adult zebrafish through disrupting HPG axis, meiosis and apoptosis. Aquat. Toxicol. 185, 129–137. https://doi.org/10.1016/j.aquatox.2017.02.013.

Supplementary Material

Degradation of the anticancer drug flutamide by solar photo-Fenton treatment at near-neutral pH: identification of transformation products and *in silico* (Q)SAR risk assessment

Alexandre Della-Flora[a], Marcelo L. Wilde[a], Igor D. F. Pinto[a], Eder C. Lima[a], Carla Sirtori[a*]

[a]Instituto de Química, Universidade Federal do Rio Grande do Sul, Av. Bento Gonçalves 9500, CEP 91501-970 Porto Alegre, RS, Brazil.

* Corresponding author: Prof. Dr. Carla Sirtori – carla.sirtori@ufrgs.br

Text S1. Scheme of the experimental section.
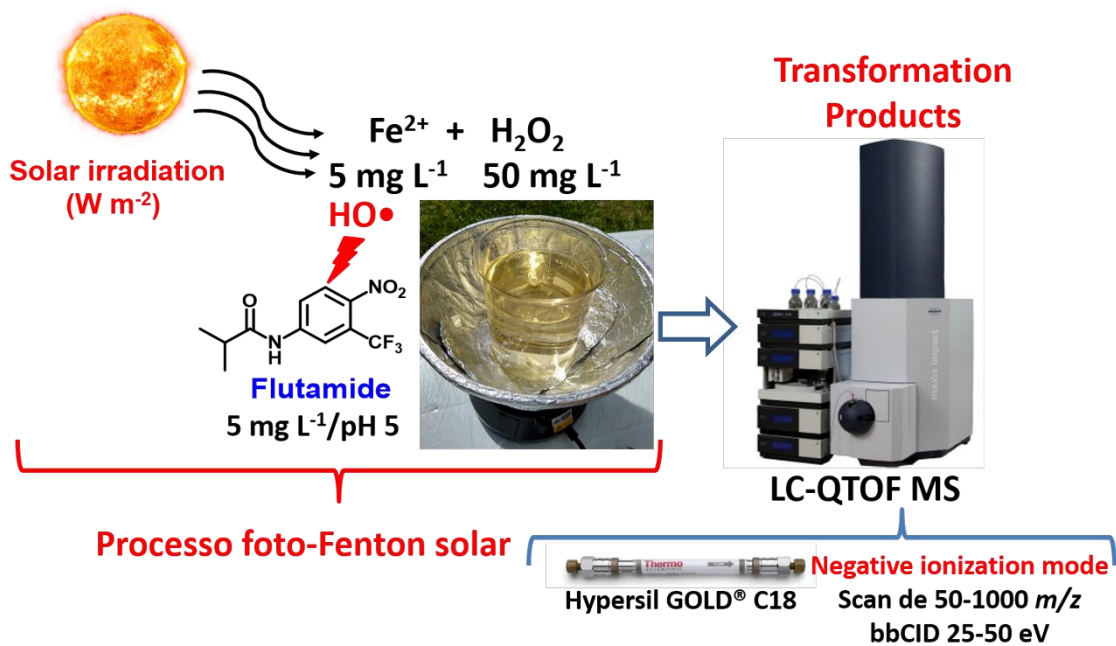
Figure S1. Squeme of the experimental design applyed for the solar photo-Fenton degradation of Flutamide.

Text S2. Description of the QSAR software.

Table S1. Description of the applied QSAR models endpoits assessed for the in silico prediction of FLUT and TPs.

QSAR Software	Model	Description	Endpoint	Reference
Case Ultra V. 1.7.0.5 (MultiCASE Inc.)	GT_EXPERT	Expert Rules for Bacterial Mutagenicity	Mutagenicity	(Chakravarti et al., 2012)
	GT1_BMUT	Bacterial Mutagenicity by OECD 471 Test	Mutagenicity	
VEGA v.1.1.4	CONSENSUS v. 1.0.2	The model provides a qualitative prediction of mutagenicity on Salmonella typhimurium (Ames test), applying a consensus approach based on the four QSAR models currently available in VEGA.	Mutagenicity (Ames test)	(Pizzo et al., 2013) (http://www.vega-qsar.eu)
	CAESAR v.2.1.13	The model provides a qualitative prediction of mutagenicity on Salmonella typhimurium (Ames test).	Mutagenicity (Ames test)	
	SarPy/IRFMN v.1.0.7	The model provides a qualitative prediction of mutagenicity on Salmonella typhimurium (Ames test).	Mutagenicity (Ames test)	
	ISS v.1.0.2	The model provides a qualitative prediction of mutagenicity on Salmonella typhimurium (Ames test).	Mutagenicity (Ames test)	
	KNN/Read-Across v.1.0.0	The model performs a read-across and provides a qualitative prediction of mutagenicity on Salmonella typhimurium (Ames test).	Mutagenicity (Ames test)	
	CAESAR v.2.1.9	The model provides a qualitative prediction of carcinogenic potency according to specific requirements of Chemical regulation.	Carcinogenicity	
	ISS v.1.0.2	The model provides a qualitative prediction of carcinogenic potency according to specific requirements of Chemical regulation.	Carcinogenicity	
	IRFMN/Antares v. 1.0.0	The model provides a qualitative prediction of carcinogenicity (presence of carcinogenic effects in male or female rats).	Carcinogenicity	
	IRFMN/ISSCAN-CGX v. 1.0.0	The model provides a qualitative prediction of carcinogenicity (expert assessment based on carcinogenic effects in different species).	Carcinogenicity	

	IRFMN v. 1.0.9	The model is based on the OECD TG 301C - modified MITI - I test data and provides a qualitative evaluation (binary classification) of ready biodegradability properties.	Ready biodegradability model	
QSAR Toolbox v. 4.3 (OECD)	DNA alerts for AMES by OASIS	Investigate the presence of alerts within the target molecules responsible for interaction with DNA related to Ames mutagenicity.	Mutagenicity (Ames test)	(Dimitrov et al., 2016; Schultz et al., 2018) http://www.qsartoolbox.org
	DNA alerts for CA and MNT by OASIS	Investigate the presence of alerts within the target molecules responsible for interaction with DNA related to Chromosomal aberration and Micronucleus tests.	Mutagenicity (Chromosomal aberration and Micronucleus tests)	
	in vitro mutagenicity (Ames test) alerts by ISS	It works as a decision tree for estimating in vitro (Ames test) mutagenicity. The structural alerts for mutagenicity are molecular functional groups or substructures known to be linked to the mutagenic activity of chemicals.	Mutagenicity (Ames test)	
	in vitro mutagenicity (micronucleus) alerts by ISS	This profiler is based on the ToxMic rulebase of the software Toxtree. This rulebase provides a list of 35 structural alerts (SAs) for a preliminary screening of potentially in vivo mutagens. These SAs are molecular functional groups or substructures that are known to be linked to the induction of effects in the in vivo micronucleus assay.	Mutagenicity (Micronucleus tests)	
	Hepatotoxicity	The profiler contains category boundaries to be expected to induce similar toxicological effects in repeated dose oral toxicity. These category boundaries were developed based on repeated dose toxicity test data in the database of Hazard Evaluation Support System (HESS). Justification for each category (mechanistic or empirical information) is described.	Hepatotoxicity repeated dose	
	Ecotoxicological Endpoint Fish [LC50 (EC50) at 96 h *Pimephales promelas*)	External SAR/QSAR approach for the prediction of ecotoxicological endpoint based on the mortality of *Pimephales promelas* after 96 h test duration	LC50 (mg L^{-1}) at 96 h duration	
EPI Suite v. 4.11	BIOWIN 1 (Linear model)	The fast biodegradation probability for any compound is calculated by summing, for all the fragments present in that compound, the fragment coefficient multiplied by the number of instances of the fragment in the compound (for MW, the value of that parameter is multiplied by its coefficient), and then adding this summation to the equation constant which is	Biodegradability	(Boethling and Costanza, 2010; US EPA, 2012)

	0.7475. The summed values for each fragment coefficient multiplied by the number of instances appear in the "VALUE" column of the linear results screen	
BIOWIN 2 (Non-linear model)	Calculation of the fast biodegradation probability for any compound begins by summing, for all the fragments present in that compound, the fragment coefficient multiplied by the number of instances of the fragment in the compound (for MW, the value of that parameter is multiplied by its coefficient), then adding this summation to the equation constant which is 3.0087. The summed values for each fragment coefficient multiplied by the number of instances appear in the "VALUE" column of the non-linear results screen. The non-linear fast biodegradation probability is then calculated from the logistic equation as follows, where total = 3.0087 + the summation as described above: Non-linear probability = exp(total) / (1 + exp(total))	
BIOWIN 3 and 4 (Ultimate and Primary Biodegradation Models)	These two models estimate the time required for "complete" ultimate and primary biodegradation. Primary biodegradation is the transformation of a parent compound to an initial metabolite. Ultimate biodegradation is the transformation of a parent compound to carbon dioxide and water, mineral oxides of any other elements present in the test compound, and new cell material.	
BIOWIN 5 and 6 (Linear and Non-Linear MITI Biodegradation Model)	BIOWIN produces two separate MITI probability estimates for each chemical. The first estimate is based upon the fragments derived through linear regression. The second estimate is based upon the fragments derived through non-linear regression. Prediction accuracy of the training and validation sets are as shown below. The numbers correspond to correct predictions (either "readily degradable" or "not readily degradable") for the original data.	
BIOWIN 7 (Anaerobic Biodegradation Model)	Biowin7 estimates the probability of fast biodegradation under methanogenic anaerobic conditions; specifically, under the conditions of the "serum bottle" anaerobic biodegradation screening test (Meylan et al. 2007). A total of 169 compounds	

		with serum bottle test data were identified for use in model development. This data set was not separated into separate training and validation sets: all available compounds were used for the regression. Each compound was scored "pass" or "fail" using 60% of theoretical gas production in 56 days (the normal test duration) as the pass criterion; for model regression, Pass=1 and Fail=0.		
	Predicting Ready Biodegradability	Ready Biodegradability Prediction: (YES or NO) The criteria for the YES or NO prediction are as follows: If the Biowin3 (ultimate survey model) result is "weeks" or faster (i.e. days, days to weeks, or weeks) AND the Biowin5 (MITI linear model) probability is >= 0.5, then the prediction is YES (readily biodegradable). If this condition is not satisfied, the prediction is NO (not readily biodegradable).		
	KOWWIN v. 1.69	Estimates the logarithmic octanol-water partition coefficient (log P) of organic compounds. KOWWIN requires only a chemical structure to estimate a log P.	Estimation of the octanol-water partition coefficient log K_{OW}	(EPI suite, USEPA)

Text S3. HRMS elucidation of Flutamide and transformation products formed through solar photo-Fenton
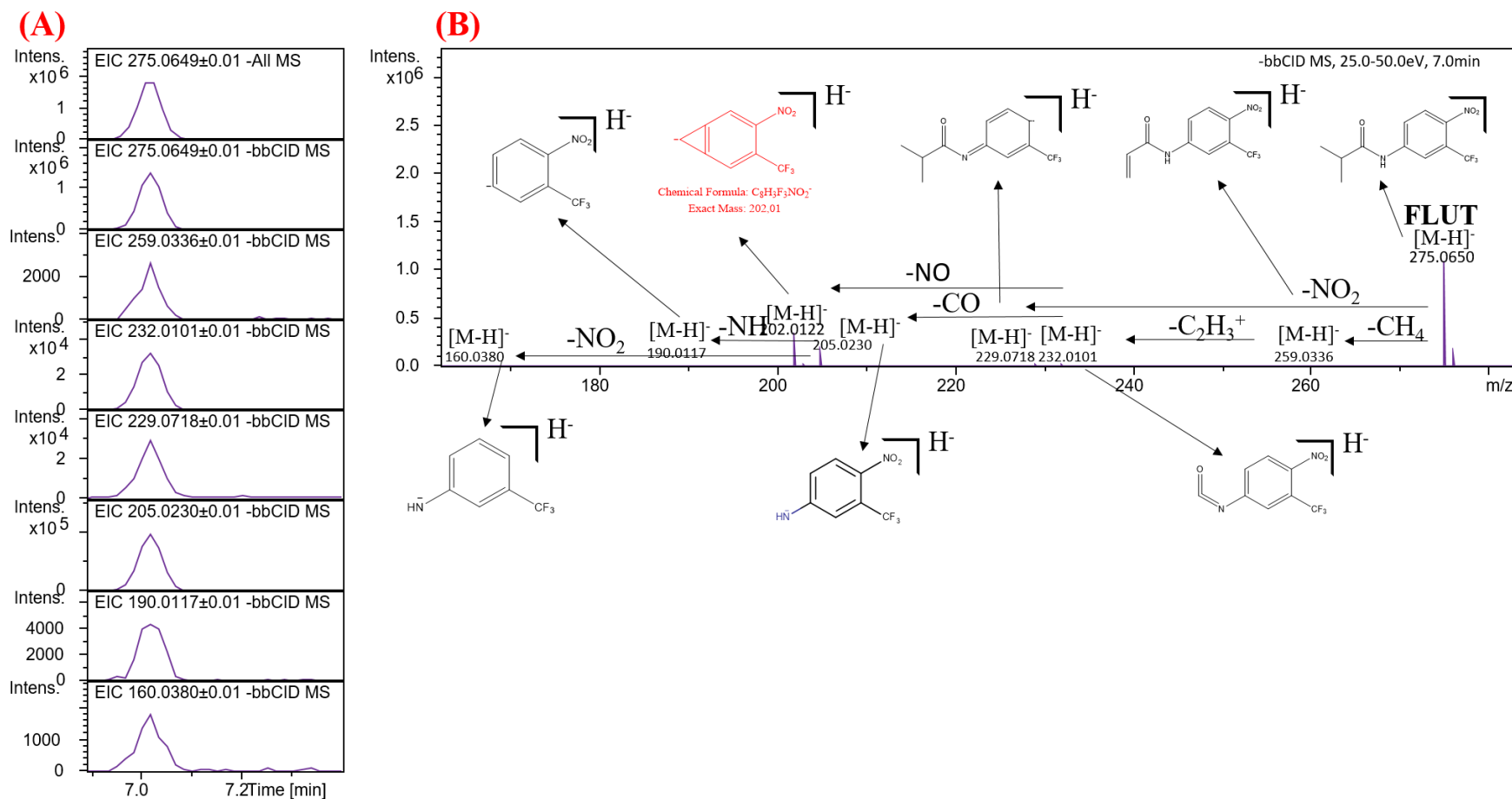
Figure S2. (A)Extraction ions chromatograms (EIC) of each fragment found for FLUT. (B)Mass spectrum, fragmentation pattern, and characteristic losses.
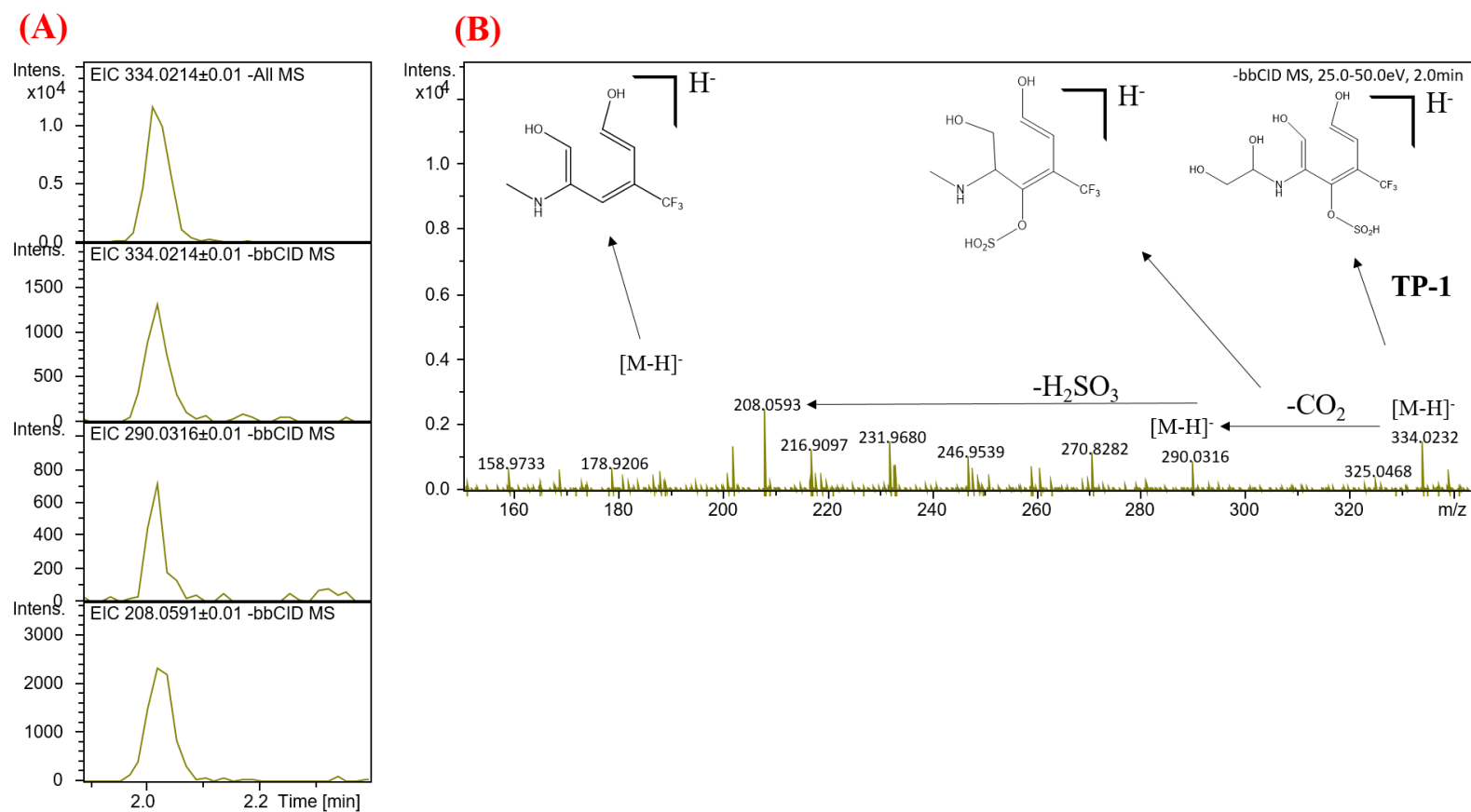
Figure S3. (A)Extraction ions chromatograms (EIC) of each fragment found for TP-1. (B)Mass spectrum, fragmentation pattern, and characteristic losses.
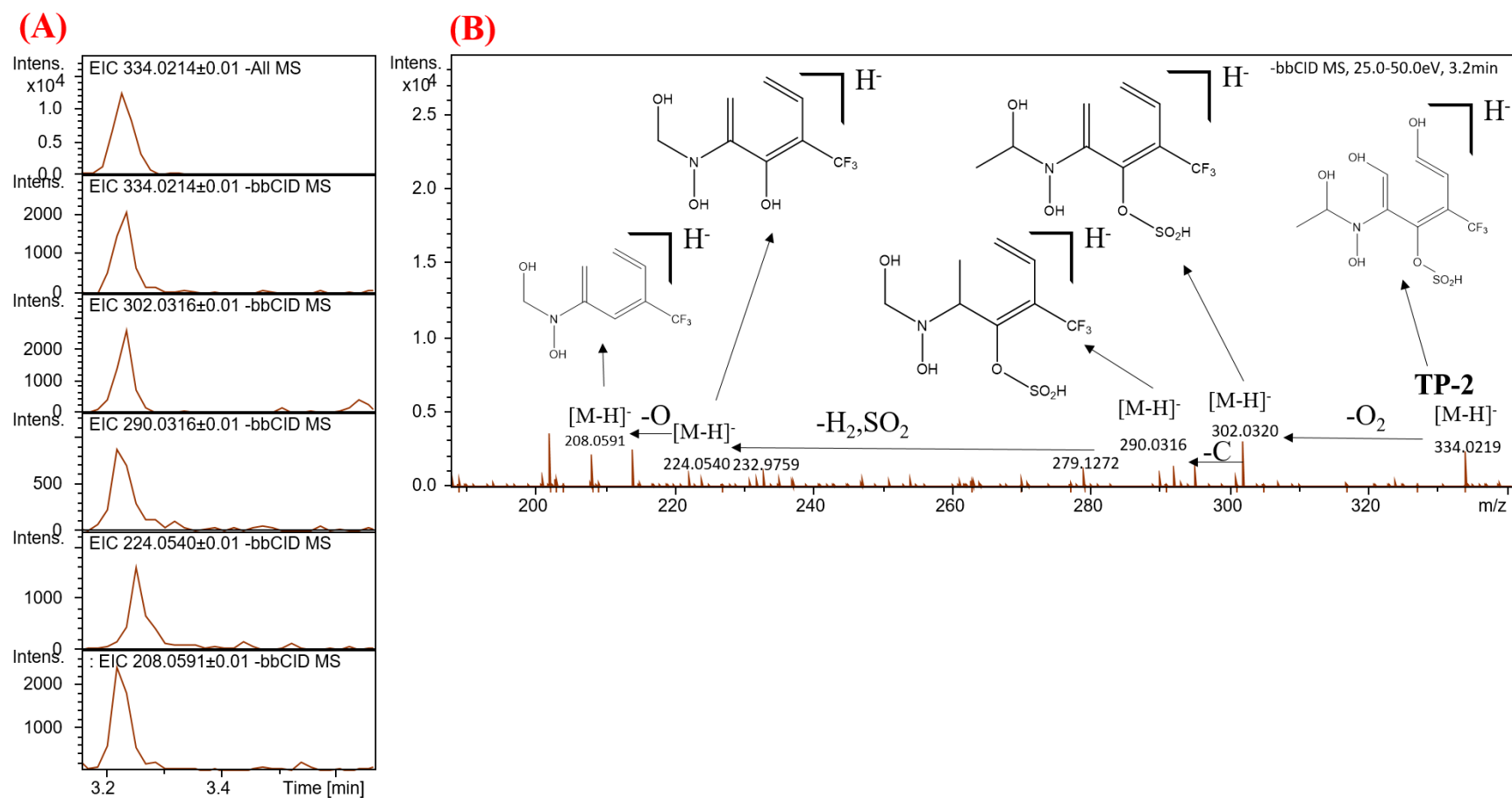
Figure S4. (A)Extraction ions chromatograms (EIC) of each fragment found for TP-2. (B)Mass spectrum, fragmentation pattern, and characteristic losses.
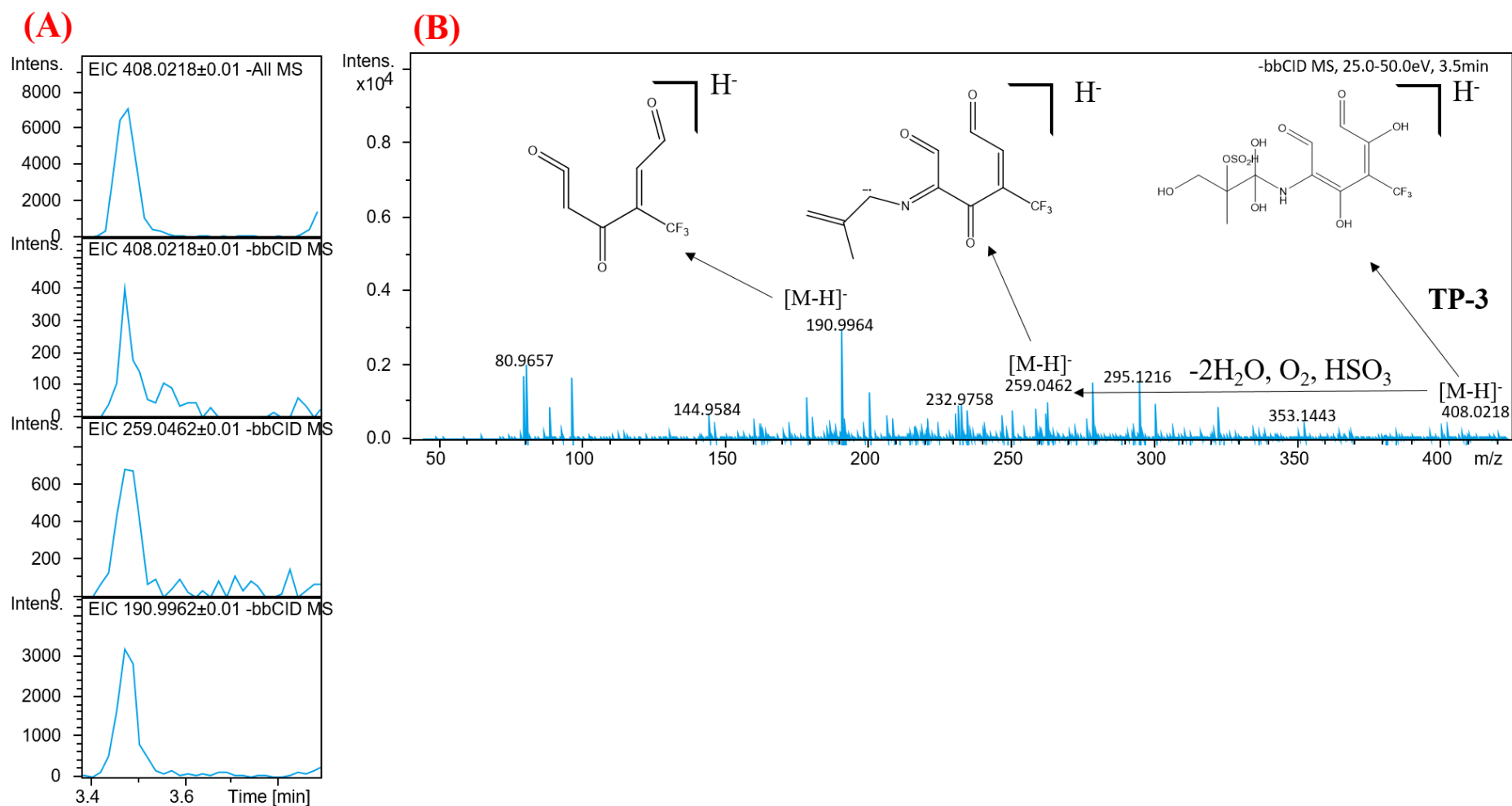
Figure S5. (A)Extraction ions chromatograms (EIC) of each fragment found for TP-3. (B)Mass spectrum, fragmentation pattern, and characteristic losses.

Figure S6.(A)Extraction ions chromatograms (EIC) of each fragment found for TP-4. (B)Mass spectrum, fragmentation pattern, and characteristic losses.
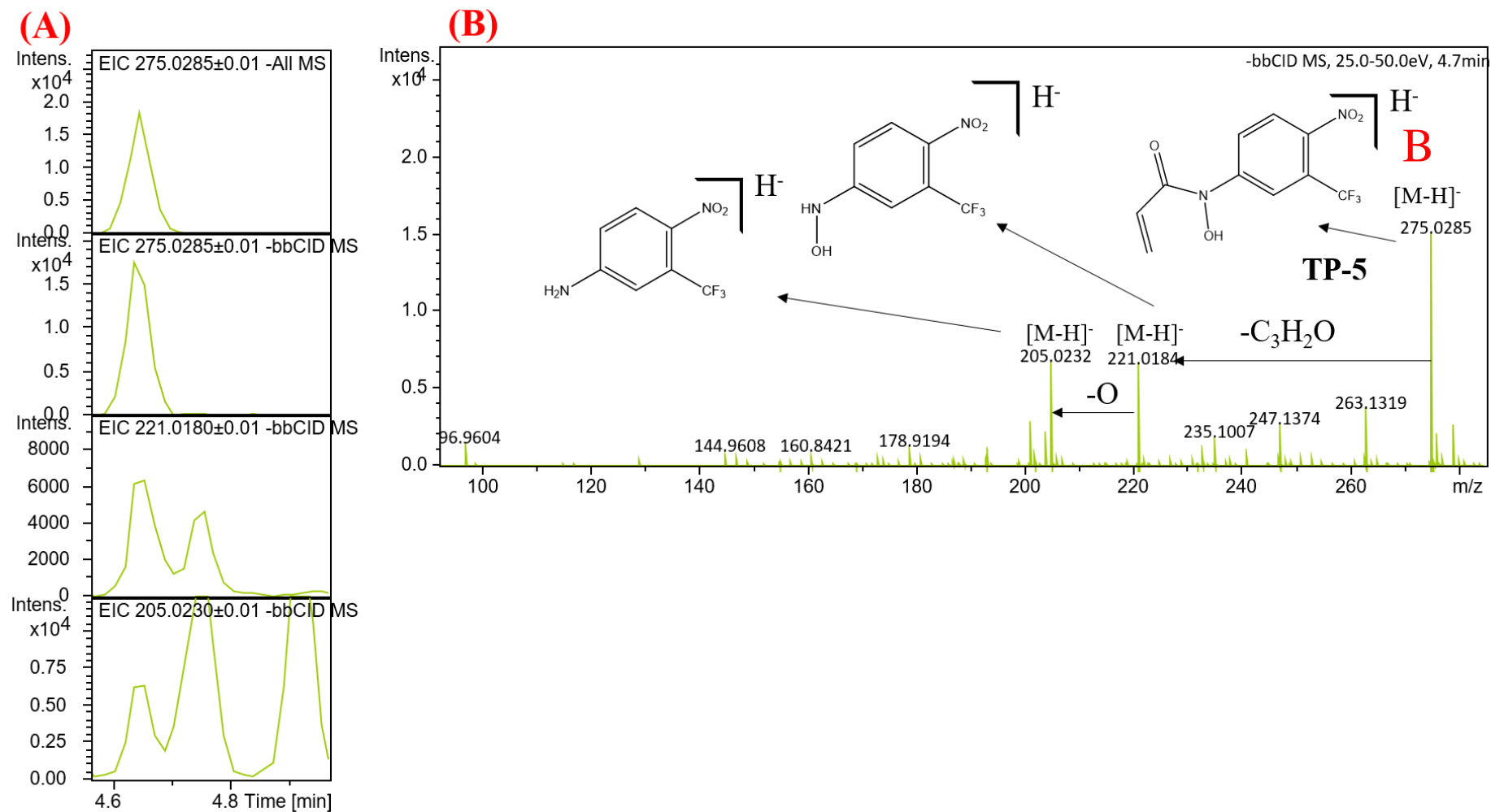
Figure S7.(A)Extraction ions chromatograms (EIC) of each fragment found for TP-5. (B)Mass spectrum, fragmentation pattern, and characteristic losses.

Figure S8.(A)Extraction ions chromatograms (EIC) of each fragment found for TP-6. (B)Mass spectrum, fragmentation pattern, and characteristic losses.

(A)

(B)
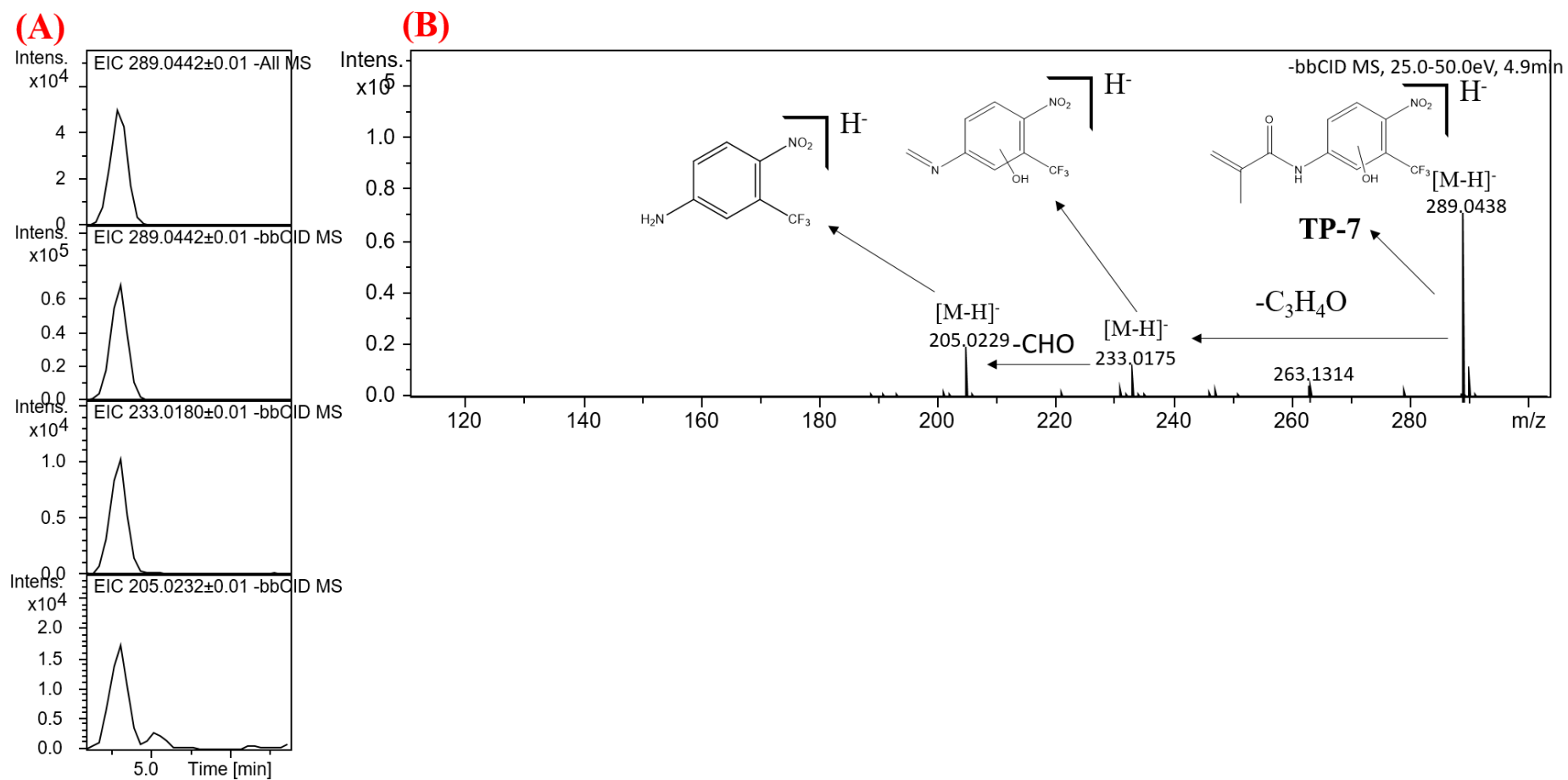
Figure S9.(A)Extraction ions chromatograms (EIC) of each fragment found for TP-7. (B)Mass spectrum, fragmentation pattern, and characteristic losses.

Figure S10.(A)Extraction ions chromatograms (EIC) of each fragment found for TP-8. (B)Mass spectrum, fragmentation pattern, and characteristic losses.
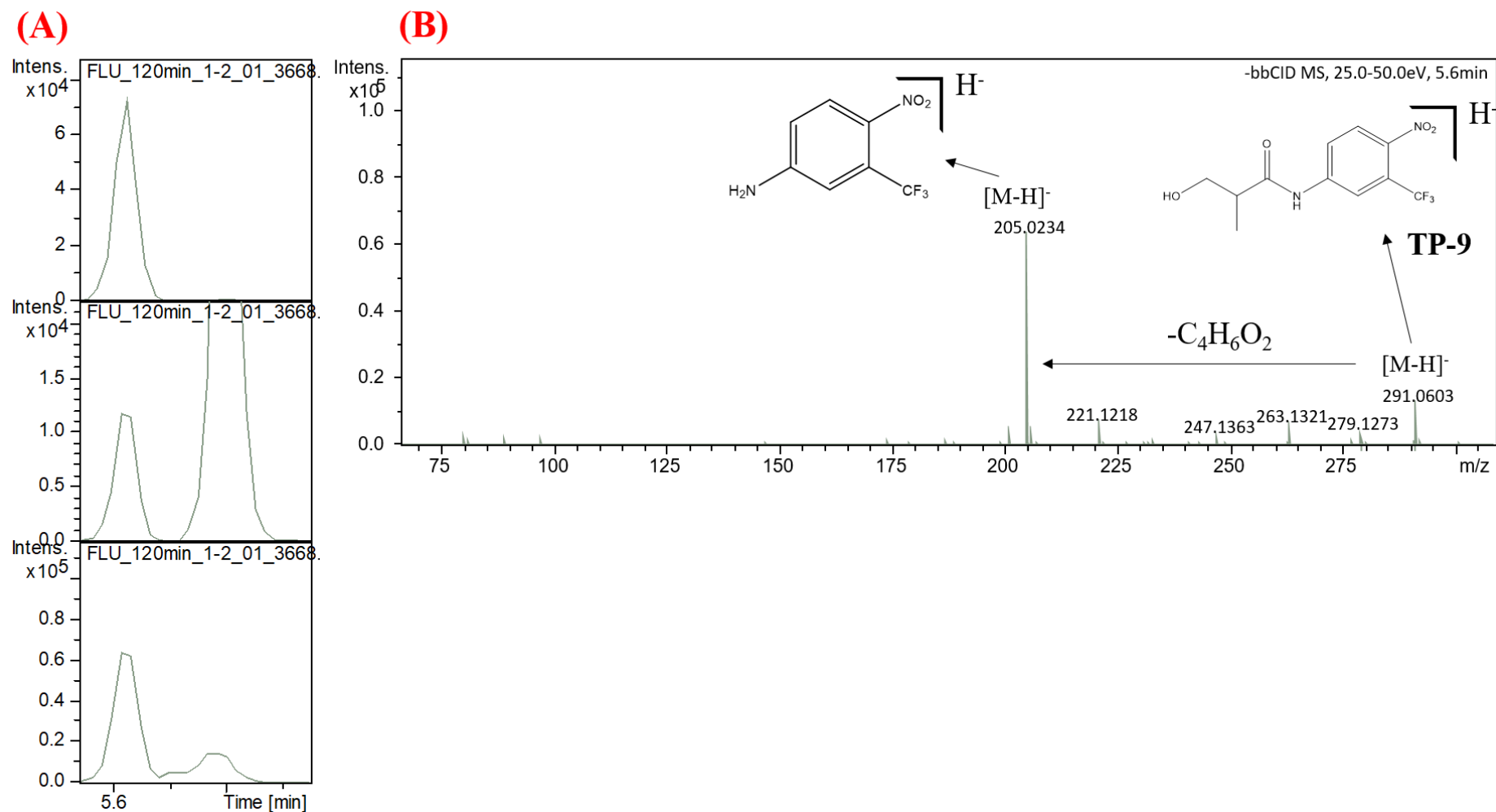
Figure S11.(A)Extraction ions chromatograms (EIC) of each fragment found for TP-9. (B)Mass spectrum, fragmentation pattern, and characteristic losses.
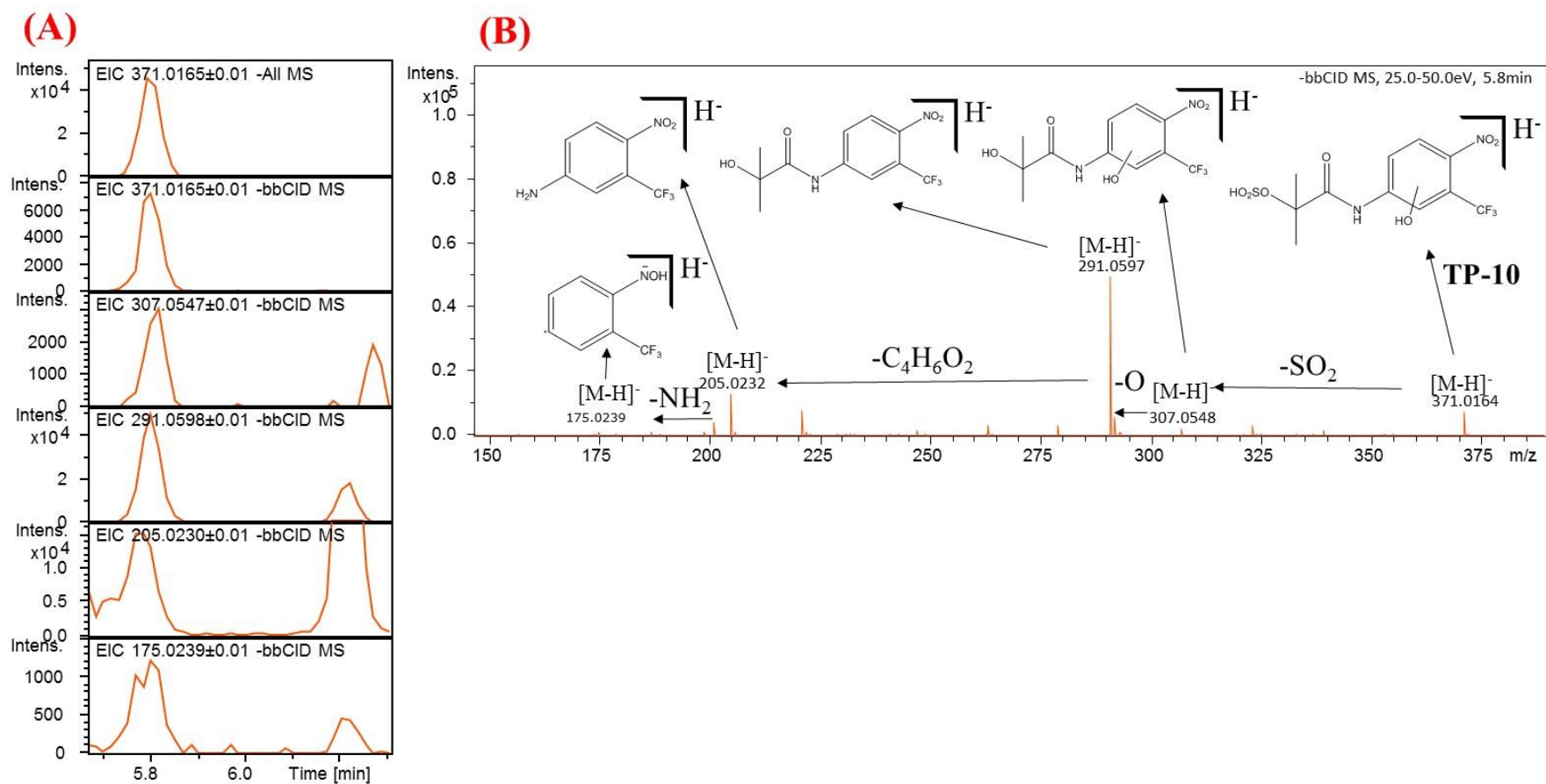
Figure S12.(A)Extraction ions chromatograms (EIC) of each fragment found for TP-10. (B)Mass spectrum, fragmentation pattern, and characteristic losses.
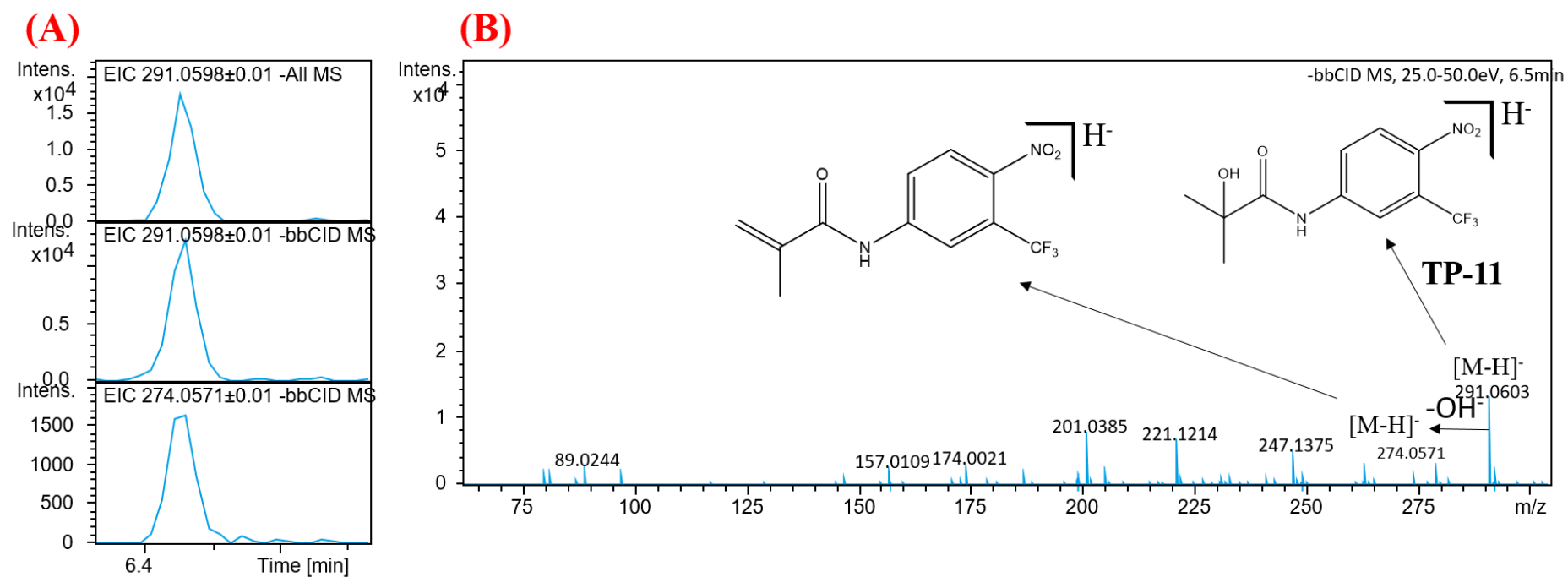
Figure S13. (A)Extraction ions chromatograms (EIC) of each fragment found for TP-11. (B)Mass spectrum, fragmentation pattern, and characteristic losses.
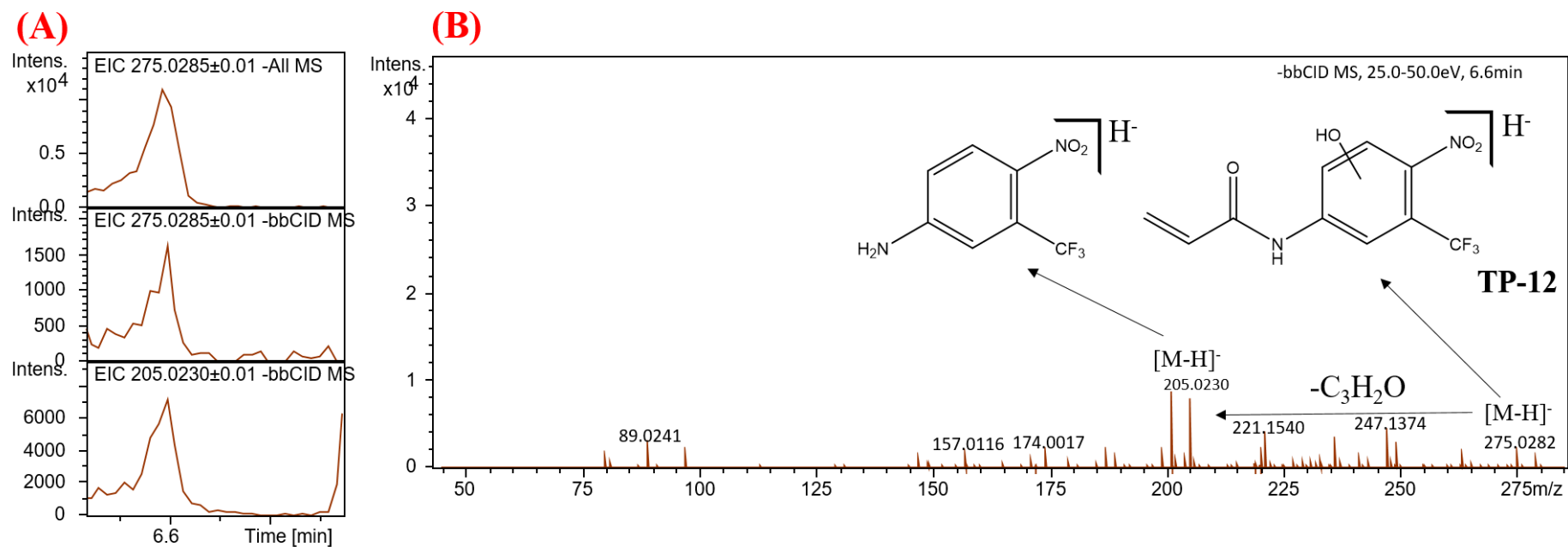
Figure S14. (A)Extraction ions chromatograms (EIC) of each fragment found for TP-12. (B)Mass spectrum, fragmentation pattern, and characteristic losses.
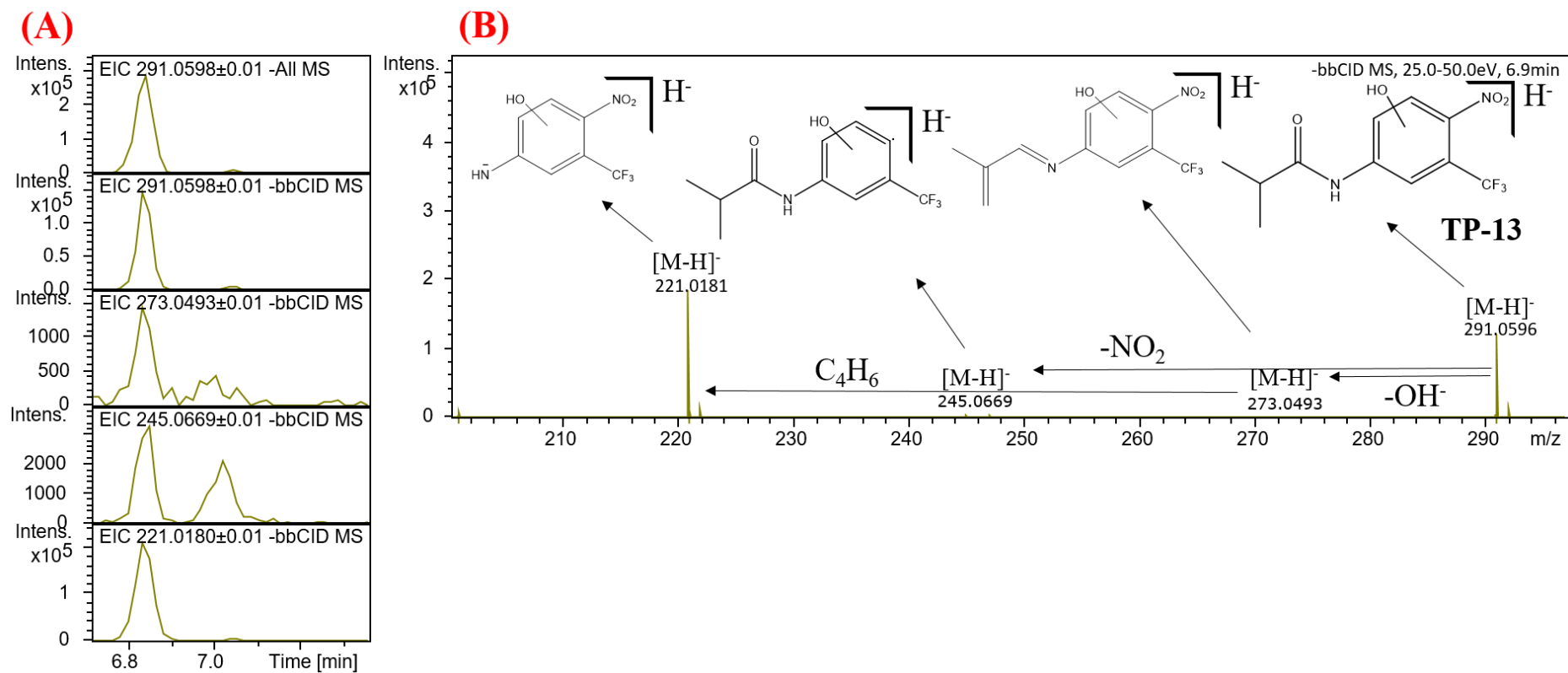
Figure S15. (A)Extraction ions chromatograms (EIC) of each fragment found for TP-13. (B)Mass spectrum, fragmentation pattern, and characteristic losses.
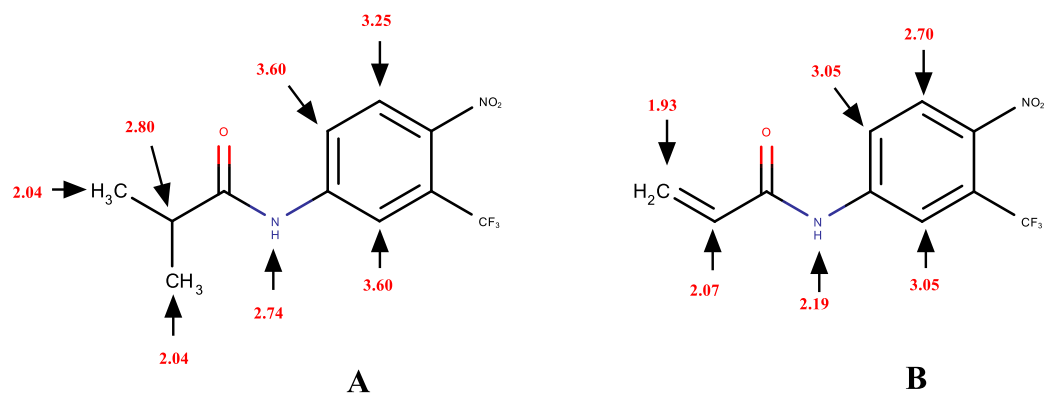
Figure S16. In red, the log K_{OW} values for the possible different hydroxylation positions. A) Referring to TP-9, TP-11, and TP-13. B) Referring to TP-5 and TP-12.

Text S4. Comparison of the main results of SPF process

Table S2. Comparison of the main results of SPF applied to the degradation of FLUT in aqueous medium after t_{30W} = 120 min.

FLUT concentration	Degradation (%)	Consumption of H_2O_2 (mg L^{-1})	Consumption of Fe^{2+} (mg L^{-1})	k_{obs} (min^{-1} t_{30W})	$t_{1/2}$ min t_{30W}	ξ (%)	Number of TPs found
5 mg L^{-1}	53.7	20	*	6.57×10^{-3}	95.62	1.04×10^{-2}	13
500 µg L^{-1}	73.4	30	5	9.13×10^{-3}	73.10	3.41×10^{-3}	10

* not measured

Text S5. *In silico* **QSAR predictions**

Table S4. Representation of FLUT Smiles and their TPs.

Compound	Smiles
Flutamide	O=C(Nc1cc(C(F)(F)F)c([N+]([O-])=O)cc1)C(C)C
TP1	OC(CO)NC(C(OS(O)=O)=C(C(F)(F)F)C=CO)=CO
TP 2 a	OC(C)N(O)C(C(OS(O)=O)=C(C(F)(F)F)C=CO)=CO
TP 2 b	OC(C)N(O)C(C=CO)=C(OS(O)=O)C(C(F)(F)F)=CO
TP 3 a	CC(CO)(OS(O)=O)C(O)(O)NC(C(=O))=C(O)C(C(F)(F)F)=C(O)C=O
TP 3 b	CC(CO)(OS(O)=O)C(O)(O)NC(C(O)=C(C(F)(F)F)C(=O))=C(C(=O))O
TP 4	CC(C(Nc1cc(C(F)(F)F)c([N+]([O-])=O)cc1)OS(O)=O)C
TP 5	C=CC(N(c1ccc([N+]([O-])=O)c(C(F)(F)F)c1)O)=O
TP 6 and 7 a	CC(CNc1cc(C(F)(F)F)c([N+]([O-])=O)c(O)c1)=C
TP 6 and 7 b	CC(CNc1cc(C(F)(F)F)c([N+]([O-])=O)cc1O)=C
TP 6 and 7 c	CC(CNc1c(O)c(C(F)(F)F)c([N+]([O-])=O)cc1)=C
TP 8 a	O=C(C(C)C)Nc1cc(C(F)(F)F)c(O)cc1
TP 8 b	O=C(C(C)C)Nc1cc(C(F)(F)F)cc(O)c1
TP 8 c	O=C(C(C)C)Nc1cc(C(F)(F)F)ccc1O
TP 8 d	O=C(C(C)C)Nc1c(O)c(C(F)(F)F)ccc1
TP 9	O=C(C(C)CO)Nc1cc(C(F)(F)F)c([N+]([O-])=O)cc1
TP 10 a	O=C(C(C)(C)OS(=O)=O)Nc1cc(C(F)(F)F)c([N+]([O-])=O)c(O)c1
TP 10 b	O=C(C(C)(C)OS(=O)=O)Nc1cc(C(F)(F)F)c([N+]([O-])=O)cc1O
TP 10 c	O=C(C(C)(C)OS(=O)=O)Nc1c(O)c(C(F)(F)F)c([N+]([O-])=O)cc1
TP 11	O=C(C(O)(C)C)Nc1cc(C(F)(F)F)c([N+]([O-])=O)cc1
TP 12 a	O=C(Nc1cc(C(F)(F)F)c([N+]([O-])=O)c(O)c1)C=C
TP 12 b	O=C(Nc1cc(C(F)(F)F)c([N+]([O-])=O)cc1O)C=C
TP 12 c	O=C(Nc1c(O)c(C(F)(F)F)c([N+]([O-])=O)cc1)C=C
TP 13 a	O=C(C(C)C)Nc1cc(C(F)(F)F)c([N+]([O-])=O)c(O)c1
TP 13 b	O=C(C(C)C)Nc1cc(C(F)(F)F)c([N+]([O-])=O)cc1O
TP 13 c	O=C(C(C)C)Nc1c(O)c(C(F)(F)F)c([N+]([O-])=O)cc1

Table S4. Log KOW and biodegradability values of FLUT and its TPs provided by EPI Suite from US EPA.

Compound	log Kow theoretical	log Kow experimental	BIOWIN 1	BIOWIN 2	BIOWIN 3	BIOWIN 4	BIOWIN 5	BIOWIN 6	BIOWIN 7	Biodegradability Predictions
Flutamide	3.51	3.35	0.0007	0.0017	1.8520	3.2719	-0.1436	0.0000	-0.5571	NO
TP1	-5.75		0.8563	0.137	2.6097	3.6507	0.462	0.0000	1.1840	NO
TP 2 a	-4.66		0.5437	0.0168	2.4253	3.4780	0.2186	0.0000	0.7684	NO
TP 2 b	-4.66		0.5437	0.0168	2.4253	3.4780	0.2186	0.0000	0.7684	NO
TP 3 a	-6.48		0.8637	0.999	1.9065	3.5009	1.0712	0.0000	0.9348	NO
TP 3 b	-6.48		0.8637	0.999	1.9065	3.5009	1.0712	0.0000	0.9348	NO
TP 4	0.38		-0.4746	0	1.6253	2.8627	-0.6752	0.0000	-0.4329	NO
TP 5	2.19		-0.2094	0.0001	1.9063	3.0665	-0.2017	0.0000	0.1152	NO
TP 6 and 7 a	3.54		-0.3274	0	1.8276	2.9978	-0.2599	0.0000	0.0334	NO
TP 6 and 7 b	3.89		-0.3274	0	1.8276	2.9978	-0.2599	0.0000	0.0334	NO
TP 6 and 7 c	3.89		-0.3274	0	1.8276	2.9978	-0.2599	0.0000	0.0334	NO
TP 8 a	2.14		0.4354	0.071	2.1421	3.4618	0.1945	0.0000	-0.2624	NO
TP 8 b	2.14		0.4354	0.071	2.1421	3.4618	0.1945	0.0000	-0.2624	NO
TP 8 c	2.49		0.4354	0.071	2.1421	3.4618	0.1945	0.0000	-0.2624	NO
TP 8 d	2.49		0.4354	0.071	2.1421	3.4618	0.1945	0.0000	-0.2624	NO
TP 9	2.04		0.1518	0.004	1.9766	3.3782	0.0189	0.0000	-0.3188	NO
TP 10 a	1.18		-0.1131	0.0002	1.4840	3.0195	-0.2551	0.0000	-0.5494	NO
TP 10 b	1.53		-0.1131	0.0002	1.4840	3.0195	-0.2551	0.0000	-0.5494	NO
TP 10 c	1.53		-0.1131	0.0002	1.4840	3.0195	-0.2551	0.0000	-0.5494	NO
TP 11	2.8	2.7	-0.1908	0.0002	1.6045	3.0954	-0.0729	0.0000	-0.7255	NO
TP 12 a	2.7		0.1166	0.0041	1.9085	3.3116	-0.0191	0.0000	-0.2766	NO
TP 12 b	3.05		0.1166	0.0041	1.9085	3.3116	-0.0191	0.0000	-0.2766	NO
TP 12 c	3.05		0.1166	0.0041	1.9085	3.3116	-0.0191	0.0000	-0.2766	NO
TP 13 a	3.25		0.1089	0.0033	1.8730	3.2885	-0.1352	0.0000	-0.381	NO
TP 13 b	3.6		0.1089	0.0033	1.8730	3.2885	-0.1352	0.0000	-0.381	NO
TP 13 c	3.6		0.1089	0.0033	1.8730	3.2885	-0.1352	0.0000	-0.381	NO

Table S5. *In silico* QSAR prediction of PBT values by the Prometheus software for Flutamide and TPs investigated in this study.

Compound	SMILES	LogP	LogP rel.	P	P rel.	B	B rel.	T	T rel.	Score P	Score B	Score T	PBT	PB
Flutamide	O=C(Nc1ccc(c(c1)C(F)(F)F)[N+](=O)[O-])C(C)C	3.35	1	P/vP	0.5	1.88	0.8	0.185	0.4	0.712	0.265	0.458	0.439	0.435
TP1	O=S(O)OC(C(=CO)NC(O)CO)=C(C=CO)C(F)(F)F	-2.59	0.2	nP	0.5	0.27	0.4	5.99	0.3	0.359	0.223	0.305	0.287	0.283
TP 2 a	O=S(O)OC(C(=CO)N(O)C(O)C)=C(C=CO)C(F)(F)F	-1.5	0.2	nP	0.5	0.26	0.4	-	0.5	0.359	0.222	0.5	0.316	0.282
TP 2 b	O=S(O)OC(=C(C=CO)N(O)C(O)C)C(=CO)C(F)(F)F	-1.5	0.2	nP	0.5	0.25	0.4	-	0.5	0.359	0.222	0.5	0.316	0.282
TP 3 a	O=CC(O)=C(C(O)=C(C=O)NC(O)(O)C(OS(=O)O)(C)CO)C(F)(F)F	-5	0.2	nP	0.5	0.41	0.4	-	0.5	0.359	0.228	0.5	0.32	0.286
TP 3 b	O=CC(O)=C(NC(O)(O)C(OS(=O)O)(C)CO)C(O)=C(C=O)C(F)(F)F	-5	0.2	nP	0.5	0.4	0.4	-	0.5	0.359	0.227	0.5	0.319	0.286
TP 4	O=[N+]([O-])c1ccc(cc1C(F)(F)F)NC(OS(=O)O)C(C)C	3.32	0.4	P/vP	0.5	2.05	0.4	0.165	0.3	0.712	0.36	0.47	0.499	0.507
TP 5	O=C(C=C)N(O)c1ccc(c(c1)C(F)(F)F)[N+](=O)[O-]	2.44	0.4	P/vP	0.5	1.56	0.4	0.953	0.3	0.712	0.305	0.376	0.447	0.466
TP 6 and 7 a	O=[N+]([O-])c1c(O)cc(cc1C(F)(F)F)NCC(=C)C	3.12	0.4	P/vP	0.5	2.24	0.8	0.12	0.4	0.712	0.333	0.487	0.487	0.487
TP 6 and 7 b	O=[N+]([O-])c1cc(O)c(cc1C(F)(F)F)NCC(=C)C	3.12	0.4	P/vP	0.5	3.01	0.8	0.121	0.4	0.712	0.506	0.487	0.576	0.6
TP 6 and 7 c	O=[N+]([O-])c1ccc(NCC(=C)C)c(O)c1C(F)(F)F	3.12	0.4	P/vP	0.5	3.02	0.8	0.179	0.6	0.712	0.507	0.451	0.568	0.601
TP 8 a	O=C(Nc1ccc(O)c(c1)C(F)(F)F)C(C)C	2.71	0.4	P/vP	0.5	1.4	0.4	0.828	0.6	0.712	0.29	0.334	0.427	0.454
TP 8 b	O=C(Nc1cc(O)cc(c1)C(F)(F)F)C(C)C	2.52	0.8	P/vP	0.5	1.67	0.4	0.584	0.4	0.712	0.316	0.384	0.455	0.474
TP 8 c	O=C(Nc1cc(ccc1(O))C(F)(F)F)C(C)C	2.63	0.8	P/vP	0.5	1.31	0.8	0.514	0.4	0.712	0.183	0.392	0.367	0.361
TP 8 d	O=C(Nc1cccc(c1(O))C(F)(F)F)C(C)C	2.63	0.8	P/vP	0.5	1.31	0.8	0.745	0.6	0.712	0.183	0.341	0.357	0.361
TP 9	O=C(Nc1ccc(c(c1)C(F)(F)F)[N+](=O)[O-])C(C)CO	2.3	0.4	P/vP	0.5	1.43	0.4	-	0.5	0.712	0.293	0.5	0.465	0.456
TP 10 a	O=C(Nc1cc(O)c(c(c1)C(F)(F)F)[N+](=O)[O-])C(OS(=O)=O)(C)C	2.19	0.4	P/vP	0.5	1.33	0.4	0.115	0.3	0.712	0.284	0.492	0.458	0.45
TP 10 b	O=C(Nc1cc(c(cc1(O))[N+](=O)[O-])C(F)(F)F)C(OS(=O)=O)(C)C	2.19	0.4	P/vP	0.5	1.32	0.4	0.115	0.3	0.712	0.283	0.492	0.457	0.449
TP 10 c	O=C(Nc1ccc(c(c1(O))C(F)(F)F)[N+](=O)[O-])C(OS(=O)=O)(C)C	2.19	0.4	P/vP	0.5	1.33	0.4	0.171	0.4	0.712	0.284	0.463	0.452	0.45
TP 11	O=C(Nc1ccc(c(c1)C(F)(F)F)[N+](=O)[O-])C(O)(C)C	2.7	1	P/vP	0.5	1.72	0.4	0.245	0.3	0.712	0.322	0.447	0.472	0.479
TP 12 a	O=C(C=C)Nc1cc(O)c(c(c1)C(F)(F)F)[N+](=O)[O-]	2.21	0.4	P/vP	0.5	2.43	0.8	0.266	0.4	0.712	0.373	0.434	0.498	0.515
TP 12 b	O=C(C=C)Nc1cc(c(cc1(O))[N+](=O)[O-])C(F)(F)F	2.21	0.4	P/vP	0.5	2.42	0.8	0.261	0.4	0.712	0.371	0.435	0.497	0.514
TP 12 c	O=C(C=C)Nc1ccc(c(c1(O))C(F)(F)F)[N+](=O)[O-]	2.21	0.4	P/vP	0.5	2.42	0.8	0.378	0.6	0.712	0.371	0.391	0.487	0.514
TP 13 a	O=C(Nc1cc(O)c(c(c1)C(F)(F)F)[N+](=O)[O-])C(C)C	2.61	0.4	P/vP	0.5	2.27	0.8	0.117	0.4	0.712	0.339	0.489	0.491	0.491

TP 13 b	O=C(Nc1cc(c(cc1(O))[N+](=O)[O-])C(F)(F)F)C(C)C	**2.61**	0.4	P/vP	0.5	1.73	0.4	0.167	0.4	0.712	0.323	0.465	**0.476**	0.479
TP 13 c	O=C(Nc1ccc(c(c1(O))C(F)(F)F)[N+](=O)[O-])C(C)C	**2.61**	0.4	P/vP	0.5	1.74	0.4	0.174	0.6	0.712	0.323	0.454	**0.474**	0.48

Table S6. *In silico* QSAR predictions for Mutagenicity (Ames test) CONSENSUS model for Flutamide and TPs investigated in the present study according to VEGA QSAR v.1.1.4 software.

Id	SMILES	Assessment	Used models	Predicted Consensus Mutagen activity	Mutagenic Score	Non-Mutagenic Score	Model Caesar assessment	Model ISS assessment	Model SarPy assessment	Model KNN assessment
Flutami de	O=C(Nc1ccc(c(c1)C(F)(F)F)[N+](=O)[O-])C(C)C	Mutagenic (Consensus score: 0.25)	4	Mutagenic	0.25	0.15	Suspect Mutagenic (low reliability)	Mutagenic (moderate reliability)	Mutagenic (low reliability)	NON-Mutagen (moderate reliability)
TP1	O=S(O)OC(C(=CO)NC(O)CO)=C(C=CO)C(F)(F)F	Mutagenic (Consensus score: 0.1)	4	Mutagenic	0.1	0.1	NON-Mutagenic (low reliability)	NON-Mutagenic (low reliability)	Mutagenic (low reliability)	Mutagen (low reliability)
TP 2 a	O=S(O)OC(C(=CO)N(O)C(O)C)=C(C=CO)C(F)(F)F	Mutagenic (Consensus score: 0.1)	4	Mutagenic	0.1	0.1	NON-Mutagenic (low reliability)	NON-Mutagenic (low reliability)	Mutagenic (low reliability)	Mutagen (low reliability)
TP 2 b	O=S(O)OC(=C(C=CO)N(O)C(O)C)C(=CO)C(F)(F)F	Mutagenic (Consensus score: 0.1)	4	Mutagenic	0.1	0.1	NON-Mutagenic (low reliability)	NON-Mutagenic (low reliability)	Mutagenic (low reliability)	Mutagen (low reliability)
TP 3 a	O=CC(O)=C(C(O)=C(C=O)NC(O)(O)C(OS(=O)O)(C)CO)C(F)(F)F	Mutagenic (Consensus score: 0.1)	4	Mutagenic	0.1	0.1	NON-Mutagenic (low reliability)	Mutagenic (low reliability)	Mutagenic (low reliability)	NON-Mutagen (low reliability)
TP 3 b	O=CC(O)=C(NC(O)(O)C(OS(=O)O)(C)CO)C(O)=C(C=O)C(F)(F)F	Mutagenic (Consensus score: 0.15)	4	Mutagenic	0.15	0.05	NON-Mutagenic (low reliability)	Mutagenic (low reliability)	Mutagenic (low reliability)	Mutagen (low reliability)
TP 4	O=[N+]([O-])c1ccc(cc1C(F)(F)F)NC(OS(=O)O)C(C)C	Mutagenic (Consensus score: 0.3)	4	Mutagenic	0.3	0	Suspect Mutagenic (low reliability)	Mutagenic (moderate reliability)	Mutagenic (low reliability)	Mutagen (low reliability)
TP 5	O=C(C=C)N(O)c1ccc(c(c1)C(F)(F)F)[N+](=O)[O-]	Mutagenic (Consensus score: 0.35)	4	Mutagenic	0.35	0.15	Suspect Mutagenic (moderate reliability)	Mutagenic (low reliability)	Mutagenic (moderate reliability)	NON-Mutagen (moderate reliability)
TP 6 and 7 a	O=[N+]([O-])c1c(O)cc(cc1C(F)(F)F)NCC(=C)C	Mutagenic (Consensus score: 0.25)	4	Mutagenic	0.25	0.15	Suspect Mutagenic (low reliability)	Mutagenic (moderate reliability)	Mutagenic (low reliability)	NON-Mutagen (moderate reliability)
TP 6 and 7 b	O=[N+]([O-])c1cc(O)c(cc1C(F)(F)F)NCC(=C)C	Mutagenic (Consensus score: 0.6)	4	Mutagenic	0.6	0	Suspect Mutagenic (moderate reliability)	Mutagenic (moderate reliability)	Mutagenic (moderate reliability)	Mutagen (moderate reliability)
TP 6 and 7 c	O=[N+]([O-])c1ccc(NCC(=C)C)c(O)c1C(F)(F)F	Mutagenic (Consensus score: 0.6)	4	Mutagenic	0.6	0	Suspect Mutagenic (moderate reliability)	Mutagenic (moderate reliability)	Mutagenic (moderate reliability)	Mutagen (moderate reliability)

TP 8 a	O=C(Nc1ccc(O)c(c1)C(F)(F)F)C(C)C	NON-Mutagenic (Consensus score: 0.67)	4	NON-Mutagenic	0	0.67	NON-Mutagenic (moderate reliability)	NON-Mutagenic (moderate reliability)	NON-Mutagenic (moderate reliability)	NON-Mutagen (good reliability)
TP 8 b	O=C(Nc1cc(O)cc(c1)C(F)(F)F)C(C)C	NON-Mutagenic (Consensus score: 0.67)	4	NON-Mutagenic	0	0.67	NON-Mutagenic (moderate reliability)	NON-Mutagenic (moderate reliability)	NON-Mutagenic (moderate reliability)	NON-Mutagen (good reliability)
TP 8 c	O=C(Nc1cc(ccc1(O))C(F)(F)F)C(C)C	NON-Mutagenic (Consensus score: 0.75)	4	NON-Mutagenic	0	0.75	NON-Mutagenic (good reliability)	NON-Mutagenic (moderate reliability)	NON-Mutagenic (moderate reliability)	NON-Mutagen (good reliability)
TP 8 d	O=C(Nc1cccc(c1(O))C(F)(F)F)C(C)C	NON-Mutagenic (Consensus score: 0.67)	4	NON-Mutagenic	0	0.67	NON-Mutagenic (moderate reliability)	NON-Mutagenic (moderate reliability)	NON-Mutagenic (moderate reliability)	NON-Mutagen (good reliability)
TP 9	O=C(Nc1ccc(c(c1)C(F)(F)F)[N+](=O)[O-])C(C)CO	Mutagenic (Consensus score: 0.45)	4	Mutagenic	0.45	0.15	Suspect Mutagenic (moderate reliability)	Mutagenic (moderate reliability)	Mutagenic (moderate reliability)	NON-Mutagen (moderate reliability)
TP 10 a	O=C(Nc1cc(O)c(c(c1)C(F)(F)F)[N+](=O)[O-])C(OS(=O)=O)(C)C	Mutagenic (Consensus score: 0.2)	4	Mutagenic	0.2	0	Suspect Mutagenic (low reliability)	Mutagenic (low reliability)	Mutagenic (low reliability)	Mutagen (low reliability)
TP 10 b	O=C(Nc1cc(c(cc1(O))[N+](=O)[O-])C(F)(F)F)C(OS(=O)=O)(C)C	Mutagenic (Consensus score: 0.2)	4	Mutagenic	0.2	0	Suspect Mutagenic (low reliability)	Mutagenic (low reliability)	Mutagenic (low reliability)	Mutagen (low reliability)
TP 10 c	O=C(Nc1ccc(c(c1(O))C(F)(F)F)[N+](=O)[O-])C(OS(=O)=O)(C)C	Mutagenic (Consensus score: 0.2)	4	Mutagenic	0.2	0	Suspect Mutagenic (low reliability)	Mutagenic (low reliability)	Mutagenic (low reliability)	Mutagen (low reliability)
TP 11	O=C(Nc1ccc(c1)C(F)(F)F)[N+](=O)[O-])C(O)(C)C	Mutagenic (Consensus score: 0.45)	4	Mutagenic	0.45	0.15	Suspect Mutagenic (moderate reliability)	Mutagenic (moderate reliability)	Mutagenic (moderate reliability)	NON-Mutagen (moderate reliability)
TP 12 a	O=C(C=C)Nc1cc(O)c(c(c1)C(F)(F)F)[N+](=O)[O-]	Mutagenic (Consensus score: 0.35)	4	Mutagenic	0.35	0.15	Suspect Mutagenic (moderate reliability)	Mutagenic (low reliability)	Mutagenic (moderate reliability)	NON-Mutagen (moderate reliability)
TP 12 b	O=C(C=C)Nc1cc(c(cc1(O))[N+](=O)[O-])C(F)(F)F	Mutagenic (Consensus score: 0.5)	4	Mutagenic	0.5	0.15	Suspect Mutagenic (good reliability)	Mutagenic (low reliability)	Mutagenic (good reliability)	NON-Mutagen (moderate reliability)
TP 12 c	O=C(C=C)Nc1ccc(c(c1(O))C(F)(F)F)[N+](=O)[O-]	Mutagenic (Consensus score: 0.5)	4	Mutagenic	0.5	0	Suspect Mutagenic (moderate reliability)	Mutagenic (low reliability)	Mutagenic (moderate reliability)	Mutagen (moderate reliability)
TP 13 a	O=C(Nc1cc(O)c(c(c1)C(F)(F)F)[N+](=O)[O-])C(C)C	Mutagenic (Consensus score: 0.6)	4	Mutagenic	0.6	0	Suspect Mutagenic (moderate reliability)	Mutagenic (moderate reliability)	Mutagenic (moderate reliability)	Mutagen (moderate reliability)
TP 13 b	O=C(Nc1cc(c(cc1(O))[N+](=O)[O-])C(F)(F)F)C(C)C	Mutagenic (Consensus score: 0.6)	4	Mutagenic	0.6	0	Suspect Mutagenic (moderate reliability)	Mutagenic (moderate reliability)	Mutagenic (moderate reliability)	Mutagen (moderate reliability)

TP 13 c	O=C(Nc1ccc(c(c1(O))C(F)(F)F)[N+](=O)[O-])C(C)C	Mutagenic (Consensus score: 0.6)	4	Mutagenic	0.6	0	Suspect Mutagenic (moderate reliability)	Mutagenic (moderate reliability)	Mutagenic (moderate reliability)	Mutagen (moderate reliability)

Table S7. *In silico* QSAR predictions of the Flutamide and TP found in RHWW concerning the Carcinogenicity as an endpoint by different

models provided by the VEGA QSAR v.1.1.4 software.

Id	SMILES	Carcinogenicity model (IRFMN/Antares) (version 1.0.0)	Carcinogenicity model (CAESAR) (version 2.1.9)	Carcinogenicity model (ISS) (version 1.0.2)	Carcinogenicity model (IRFMN/ISSCAN-CGX) (version 1.0.0)
Flutamide	O=C(Nc1ccc(c(c1)C(F)(F)F)[N+](=O)[O-])C(C)C	Carcinogen (EXPERIMENTAL value)	NON-Carcinogen (low reliability)	Carcinogen (moderate reliability)	Carcinogen (moderate reliability)
TP1	O=S(O)OC(C(=CO)NC(O)CO)=C(C=CO)C(F)(F)F	Carcinogen (moderate reliability)	NON-Carcinogen (low reliability)	NON-Carcinogen (low reliability)	Carcinogen (low reliability)
TP 2 a	O=S(O)OC(C(=CO)N(O)C(O)C)=C(C=CO)C(F)(F)F	Carcinogen (moderate reliability)	NON-Carcinogen (low reliability)	NON-Carcinogen (low reliability)	Carcinogen (low reliability)
TP 2 b	O=S(O)OC(=C(C=CO)N(O)C(O)C)C(=CO)C(F)(F)F	Carcinogen (moderate reliability)	Carcinogen (low reliability)	NON-Carcinogen (low reliability)	Carcinogen (low reliability)
TP 3 a	O=CC(O)=C(C(O)=C(C=O)NC(O)(O)C(OS(=O)O)(C)CO)C(F)(F)F	Carcinogen (low reliability)	NON-Carcinogen (low reliability)	Carcinogen (low reliability)	Carcinogen (low reliability)
TP 3 b	O=CC(O)=C(NC(O)(O)C(OS(=O)O)(C)CO)C(O)=C(C=O)C(F)(F)F	Carcinogen (low reliability)	NON-Carcinogen (low reliability)	Carcinogen (low reliability)	Carcinogen (low reliability)
TP 4	O=[N+]([O-])c1ccc(cc1C(F)(F)F)NC(OS(=O)O)C(C)C	Carcinogen (moderate reliability)	Carcinogen (low reliability)	Carcinogen (low reliability)	Carcinogen (low reliability)
TP 5	O=C(C=C)N(O)c1ccc(c(c1)C(F)(F)F)[N+](=O)[O-]	Carcinogen (low reliability)	Carcinogen (low reliability)	Carcinogen (moderate reliability)	Carcinogen (moderate reliability)
TP 6 and 7 a	O=[N+]([O-])c1c(O)cc(cc1C(F)(F)F)NCC(=C)C	Carcinogen (low reliability)	NON-Carcinogen (low reliability)	Carcinogen (low reliability)	Carcinogen (low reliability)
TP 6 and 7 b	O=[N+]([O-])c1cc(O)c(cc1C(F)(F)F)NCC(=C)C	Carcinogen (low reliability)	NON-Carcinogen (low reliability)	Carcinogen (low reliability)	Carcinogen (low reliability)
TP 6 and 7 c	O=[N+]([O-])c1ccc(NCC(=C)C)c(O)c1C(F)(F)F	Carcinogen (low reliability)	NON-Carcinogen (low reliability)	Carcinogen (low reliability)	Carcinogen (low reliability)
TP 8 a	O=C(Nc1ccc(O)c(c1)C(F)(F)F)C(C)C	Carcinogen (low reliability)	NON-Carcinogen (moderate reliability)	NON-Carcinogen (low reliability)	Carcinogen (moderate reliability)
TP 8 b	O=C(Nc1cc(O)cc(c1)C(F)(F)F)C(C)C	Carcinogen (moderate reliability)	NON-Carcinogen (low reliability)	NON-Carcinogen (low reliability)	Carcinogen (moderate reliability)
TP 8 c	O=C(Nc1cc(ccc1(O))C(F)(F)F)C(C)C	Carcinogen (low reliability)	NON-Carcinogen (low reliability)	NON-Carcinogen (low reliability)	Carcinogen (moderate reliability)
TP 8 d	O=C(Nc1cccc(c1(O))C(F)(F)F)C(C)C	Carcinogen (low reliability)	NON-Carcinogen (low reliability)	NON-Carcinogen (low reliability)	Carcinogen (moderate reliability)
TP 9	O=C(Nc1ccc(c(c1)C(F)(F)F)[N+](=O)[O-])C(C)CO	Carcinogen (moderate reliability)	Carcinogen (low reliability)	Carcinogen (low reliability)	Carcinogen (low reliability)
TP 10 a	O=C(Nc1cc(O)c(c(c1)C(F)(F)F)[N+](=O)[O-])C(OS(=O)=O)(C)C	Carcinogen (low reliability)	Carcinogen (low reliability)	Carcinogen (low reliability)	Carcinogen (low reliability)
TP 10 b	O=C(Nc1cc(c(cc1(O))[N+](=O)[O-])C(F)(F)F)C(OS(=O)=O)(C)C	Carcinogen (low reliability)	Carcinogen (low reliability)	Carcinogen (low reliability)	Carcinogen (low reliability)

TP 10 c	O=C(Nc1ccc(c(c1(O))C(F)(F)F)[N+](=O)[O-])C(OS(=O)=O)(C)C	Carcinogen (low reliability)	Carcinogen (low reliability)	Carcinogen (low reliability)	Carcinogen (low reliability)
TP 11	O=C(Nc1ccc(c(c1)C(F)(F)F)[N+](=O)[O-])C(O)(C)C	Carcinogen (moderate reliability)	Carcinogen (low reliability)	Carcinogen (moderate reliability)	Carcinogen (moderate reliability)
TP 12 a	O=C(C=C)Nc1cc(O)c(c(c1)C(F)(F)F)[N+](=O)[O-]	Carcinogen (low reliability)	Carcinogen (low reliability)	Carcinogen (moderate reliability)	Carcinogen (moderate reliability)
TP 12 b	O=C(C=C)Nc1cc(c(cc1(O))[N+](=O)[O-])C(F)(F)F	Carcinogen (low reliability)	Carcinogen (low reliability)	Carcinogen (moderate reliability)	Carcinogen (moderate reliability)
TP 12 c	O=C(C=C)Nc1ccc(c(c1(O))C(F)(F)F)[N+](=O)[O-]	Carcinogen (low reliability)	Carcinogen (low reliability)	Carcinogen (moderate reliability)	Carcinogen (moderate reliability)
TP 13 a	O=C(Nc1cc(O)c(c(c1)C(F)(F)F)[N+](=O)[O-])C(C)C	Carcinogen (low reliability)	Carcinogen (low reliability)	Carcinogen (low reliability)	Carcinogen (low reliability)
TP 13 b	O=C(Nc1cc(c(cc1(O))[N+](=O)[O-])C(F)(F)F)C(C)C	Carcinogen (low reliability)	Carcinogen (low reliability)	Carcinogen (low reliability)	Carcinogen (low reliability)
TP 13 c	O=C(Nc1ccc(c(c1(O))C(F)(F)F)[N+](=O)[O-])C(C)C	Carcinogen (low reliability)	Carcinogen (low reliability)	Carcinogen (low reliability)	Carcinogen (low reliability)

References

Faisal, M., Bouzid, H., Harraz, F.A., Ismail, A.A., Al-Sayari, S.A., Al-Assiri, M.S., 2015. Mesoporous Ag/ZnO multilayer films prepared by repeated spin-coating for enhancing its photonic efficiencies. Surf. Coatings Technol. 263, 44–53. https://doi.org/10.1016/j.surfcoat.2014.12.063

Hübner, U., von Gunten, U., Jekel, M., 2014. Evaluation of the persistence of transformation products from ozonation of trace organic compounds - A critical review. Wat. Res. 8, 150–170. https://doi.org/10.1016/j.watres.2014.09.051

International Conference on Harmonization (ICH), 2014. ICH Guideline M7- http://www.ich.org/fileadmin/Public_Web_Site/ICH_Products/Guidelines/Multidisciplinary/M7/M7_Step_4.pdf. Accessed on 02.11.2015.

Pizzo, F., Lombardo, A., Manganaro, A., Benfenati, E., 2013. In silico models for predicting ready biodegradability under REACH: A comparative study. Sci. Total Environ. 463–464, 161–168. https://doi.org/10.1016/j.scitotenv.2013.05.060

Prieto-Rodriguez, L., Miralles-Cuevas, S., Oller, I., Agüera, A., Puma, G.L., Malato, S., 2012. Treatment of emerging contaminants in wastewater treatment plants (WWTP) effluents by solar photocatalysis using low TiO2 concentrations. J. Hazard. Mater. 211–212, 131–137. https://doi.org/10.1016/j.jhazmat.2011.09.008

Sun, J.H., Sun, S.P., Fan, M.H., Guo, H.Q., Qiao, L.P., Sun, R.X., 2007. A kinetic study on the degradation of p-nitroaniline by Fenton oxidation process. J. Hazard. Mater. 148, 172–177. https://doi.org/10.1016/j.jhazmat.2007.02.022

US EPA, 2012. U.S. EPA. Estimation Programs Interface Suite™ for Microsoft® Windows, v 4.11. The United States Environmental Protection Agency, Washington, DC, USA.

Capítulo 2

Combinação dos processos foto-Fenton solar e adsorção para remoção do fármaco antineoplásico Flutamida e seus produtos de transformação em efluente hospitalar

INTRODUÇÃO

Os efluentes hospitalares são considerados um dos principais meios de contaminação ambiental por compostos farmacêuticos já que, em geral, essa água residual é equalizada e incorporada à rede de coleta de efluentes domésticos, assim, no melhor dos casos, sendo levado aos tratamento(s) convencional(is) das ETARs[70–73]. Como os processos secundários convencionais são limitados para a remediação de fármacos, surge à necessidade de empregar processos terciários para, assim, evitar a liberação desses micropoluentes. Nesse contexto, o tratamento terciário pode ser considerado uma etapa de "polimento" final, a qual deve garantir que o efluente já tratado esteja isento de fármacos e outros micropoluentes orgânicos e agentes infecciosos para sua liberação nos mananciais receptores.

Para o tratamento de efluentes hospitalares os AOPs, e em especial o processo foto-Fenton, vem ganhando destaque por ser um processo simples e que quando combinado com a energia solar, pode torna-se ambientalmente mais amigável. No entanto, para alcançar grandes taxas de degradação, ainda mais em efluentes hospitalares que são ricos em matérias orgânicas dissolvidas, são necessários uma quantidade de reagentes maiores quando comparados a efluentes menos complexos e ainda, um tempo de reação maior, elevando os custos do tratamento[74]. Assim, apesar das altas taxas de degradação que podem ser alcançadas para o(s) composto(s) original(is), nem sempre a mineralização completa é alcançada, o que pode levar à geração de compostos intermediários denominados TPs[75]. Os TPs gerados durante o tratamento são compostos que podem ser recalcitrantes (não biodegradáveis) e apresentar toxicidade ou potencial mutagênico e carcinogênico, além de elevada mobilidade, maior solubilidade, entre outros. Assim, a recalcitrância dos TPs pode inviabilizar o uso ou eficiência de tratamentos biológicos[46,76,77].

Uma alternativa para evitar a presença dos TPs gerados por AOPs ao final do tratamento é realizar a combinação com outro processo terciário, que nesse estudo foi o processo de adsorção. Esse acople pode ser uma estratégia viável devido à vantagens como: baixo custo e excelente desempenho para a remoção de uma ampla gama de analitos[78]. A vantagem da utilização do carvão ativo é que pode ser obtido a partir de fontes renováveis e também de resíduos de baixo valor comercial e transformá-los com um valor agregado[61,79]. Contudo, a sua aplicação em efluentes com alta carga de matéria orgânica

afeta a eficiência da adsorção, devido à competição pelos sítios ativos, assim, diminuindo a eficiência da remoção dos fármacos.

A aplicação de carvão ativo no processo de remoção de contaminantes de interesse emergente já é bem discutida na literatura[80–82]. Recentemente, Michel e colaboradores[83] realizaram o acople do processo foto-Fenton solar com o processo de adsorção fazendo uso de um carvão ativo comercial para remediar um efluente com um nível de toxicidade elevada.

OBJETIVOS

Avaliar a combinação do processo foto-Fenton solar com o processo de adsorção utilizando carvão ativo produzido a partir de uma fonte de biomassa renovável (caroço de abacate), para remoção residual da Flutamida e seus TPs empregando uma matriz de efluente hospitalar. Adicionalmente, o processo de adsorção será otimizado utilizando um planejamento experimental, para maximizar a remoção da Flutamida e seus TPs durante a etapa de tratamento via foto-Fenton solar.

PRINCIPAIS RESULTADOS

Ao realizar o tratamento do efluente hospitalar com as condições iniciais otimizadas no estudo apresentado no Capítulo 1 ($[Fe^{2+}]$ = 5 mg L^{-1} e $[H_2O_2]$ = 50 mg L^{-1} em pH= 5) foi obtida uma degradação de aproximadamente 20% da Flutamida presente inicialmente para um tempo de tratamento de aproximadamente t_{30W} = 140 min. Ainda, foi observada a formação de 10 TPs da Flutamida, os quais eram persistentes durante o AOP avaliado. Esse resultado com uma discreta degradação da Flutamida já era esperado pois o efluente em estudo é uma matriz complexa que apresenta um alto teor de matéria orgânica dissolvida. Para melhorar a *performance* do processo foto-Fenton solar, foi adotada a estratégia de realizar múltiplas adições de $[Fe^{2+}]$ = 5 mg L^{-1} em intervalos de 15 min, ou seja, em t_{30W} = 0 min, t_{30W} = 11,5 min e t_{30W} = 23,2 min), aumentando também a concentração inicial de $[H_2O_2]$ para 150 mg L^{-1}. Desta forma, foi obtida uma degradação primária da FLUT de 58% até o tempo final de tratamento (t_{30W} = 130 min). Para essa condição experimental otimizada, foram observados 13 TPs da Flutamida e se mostraram persistentes durante o processo.

Para identificação dos TPs, nesse estudo, foi adotada uma estratégia diferente da apresentada ao Capítulo 1. Nesse caso, a partir dos dados de massa exata obtidos no estudo prévio, foi construída uma base de dados para viabilizar a identificação dos TPs da Flutamida, como se estes fossem "*target compounds*" na complexa matriz de efluente hospitalar. Essa base de dados contém informações sobre: tempo de retenção, massas exatas teóricas e experimentais *(m/z),* íons moleculares associados aos seus íons fragmento característicos (se houvesse, um mínimo de 3 fragmentos) e DBE. Esse método de triagem predisse 10 TPs quando a primeira abordagem de tratamento foi avaliada e 13 TPs na segunda abordagem de tratamento proposta.

Em relação ao processo de adsorção com carvão ativo produzido a partir de caroço de abacate, foi realizada a otimização do tratamento com a aplicação do planejamento experimental Doehlert, com duas variáveis: tempo de contato do carvão ativo com a amostra (min) e a massa de carvão ativo (mg). Nesse planejamento 10 experimentos foram realizados, sendo 4 destas réplicas do ponto central.Com os resultados obtidos, e aplicando os tratamentos estatísticos apropriados (gráfico de Pareto, modelagem de superfície de reposta e gráfico de desejabilidade) observou-se que a condição otimizada do tratamento de adsorção era para um tempo de tratamento de 40 min e utilizando 14 mg de carvão ativo. Assim, obteve-se a remoção total de Flutamida e seus TPs. Ainda, altas taxas de adsorção da Flutamida e TPs que contém a presença de anéis aromáticas, sugerem que as interações π-π desempenham um papel significativo no processo. Já para os TPs que apresentam abertura do anel aromático taxas de remoção inferiores foram observadas, possivelmente devido à maior polaridade destas espécies.

O detalhamento dos métodos, resultados, discussões e conclusões relacionados com esse estudo estão apresentados no **Artigo 2** e **Material Suplementar 2**.

Combination of solar photo-Fenton and adsorption process for removal of the anticancer drug Flutamide and its transformation products from hospital wastewater

Alexandre Della-Flora, Marcelo L. Wilde, Pascal S. Thue, Diana Lima, Eder C. Lima, Carla Sirtori*

Instituto de Química, Universidade Federal do Rio Grande do Sul, Av. Bento Gonçalves 9500, CEP 91501-970, Porto Alegre, RS, Brazil

GRAPHICAL ABSTRACT
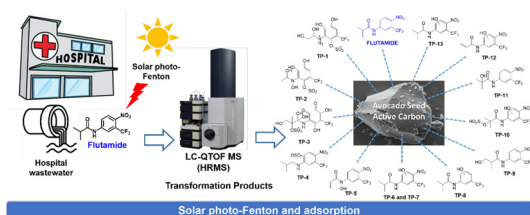
13 w x 4.92 h and 1500 dpi

ARTICLE INFO

ABSTRACT

The anti-cancer drug Flutamide (FLUT) is widely used and is of great environmental concern. The solar photo-Fenton (SPF) process can be an effective treatment for the removal of this type of micropollutant. The use of a single addition of 5 mg L^{-1} of Fe^{2+} and 50 mg L^{-1} of H_2O_2 achieved 20% primary degradation and only 3.05% mineralization. By using three additions of 5 mg L^{-1} Fe^{2+}, with an initial H_2O_2 concentration of 150 mg L^{-1}, 58% primary degradation was achieved, together with 12.07% mineralization. Consequently, thirteen transformation products (TPs) were formed. The SPF process was further combined with adsorption onto avocado seed activated carbon (ASAC) as an environmentally friendly approach for the removal of remained FLUT and the TPs. Doehlert design was used to assess the behavior of 13 TPs by optimizing the contact time and the adsorbent mass load. The optimal conditions for removal of FLUT and the TPs were 14 mg of ASAC and a contact time of 40 min. Remained FLUT and the TPs were totally removed using the adsorption process. The mechanisms of adsorption of FLUT and the TPs were strongly influenced by their polarity and π-π interactions of the TPs onto ASAC.

1. Introduction

Due to intense anthropogenic activity, many contaminants are present in the environment, including in aquatic environments (Burri et al., 2019; Warner et al., 2019). Contamination by pharmaceutical compounds has even been reported in aquifers (Di Lorenzo et al., 2019). The presence of such emerging contaminants, even at trace levels, can affect organisms that depend on water for their survival (Parrella et al., 2014; Grzesiuk et al., 2019). In rivers near major urban centers, the main route of the release of drugs into the aquatic surroundings is the hospital effluents. This release can be explained by the fact that wastewater treatment plants (WWTPs) are not explicitly designed for the removal of these compounds (Taheran et al., 2018; Wilkinson et al., 2017). Tertiary processes that have been investigated in recent years as

---

* Corresponding author.
E-mail address: carla.sirtori@ufrgs.br (C. Sirtori).

63

A. Della-Flora, et al.   Journal of Hazardous Materials 396 (2020) 122699

a way to eliminate these drugs include Advanced Oxidation Processes (AOPs) (Klavarioti et al., 2009; Mirzaei et al., 2017; Kanakaraju et al., 2018; Sun et al., 2018; Sun et al., 2020) for the treatment of wastewaters contaminated by pharmaceuticals.

Hospitals are significant contributors to environmental contamination by pharmaceuticals, although there is still insufficient knowledge about this environmental issue and, consequently, its effects on human health. Considered to be a 'hot-spot' of this type of contamination, hospital wastewater (HWW) is mostly discharged untreated into urban wastewater networks, reaching municipal wastewater treatment plants that are not equipped to remove complex compounds such as pharmaceuticals (Frédéric and Yves, 2014). Furthermore, in developing countries, such as Brazil, there is a lack of urban sanitation, so these micropollutants can be transported to surface waters (Tambosi et al., 2010; Philip et al., 2018; Sanganyado and Gwenzi, 2019).

There are several AOPs for the treatment of effluents contaminated by pharmaceuticals. The solar photo-Fenton (SPF) process has the main advantage of simplicity because it uses Fenton reagents combined with solar UV radiation, which also makes it more environmentally friendly (Lumbaque et al., 2019; Gernjak et al., 2006; Sirtori et al., 2009; Fiorentino et al., 2019). The hydroxyl radicals generated in the process are highly reactive and non-selective, making the process more efficient (Pignatello et al., 2006). However, despite high degradation rates of the parent compound, complete mineralization is not always achieved, which can lead to the generation of new transformation products (TPs). These TPs are compounds whose properties may be unknown and that are likely to be both more toxic and more stable than the parent compounds (Fatta-Kassinos et al., 2011; Osawa et al., 2019).

Therefore, in order to achieve a high rate of mineralization of an effluent, it is necessary to increase the reaction time and the quantity of reagents, hence increasing the cost of treatment (Durán et al., 2018). TPs may present non-biodegradable characteristics and specific toxicity, so biological processes may not be suitable for their removal (Wilde et al., 2018; Rastogi et al., 2014; Herrmann et al., 2015). To circumvent this, the use of a combination of processes can increase the efficiency of the treatment and maybe a way to remove these new compounds. Combinations of AOPs with other processes have been studied for the removal of pharmaceuticals (Brienza et al., 2019; Hou et al., 2019; Michael et al., 2019).

Adsorption has been investigated as an excellent option for the removal of micropollutants (Carmalin and Lima, 2018), offering advantages, including low cost, easy accessibility, and excellent performance (Zhu et al., 2017). Furthermore, the development of effective adsorbents from waste biomasses can make these methods environmentally friendly (Leite et al., 2018). Michael et al. (2019) used an SPF process in combination with adsorption onto activated carbon (AC), as a way to treat wastewater with high levels of toxicity. The use of activated carbon to remove contaminants of emerging concern has been described in other studies (Álvarez-Torrellas et al., 2017; Lima et al., 2019; Saucier et al., 2017). The advantages of this material include high surface area and the ability to remove compounds without the formation of byproducts, as well as reduction of the levels of dissolved organic carbon (DOC). Furthermore, activated carbon can be obtained from renewable waste biomasses (Carmalin and Lima, 2018; Rizzo et al., 2019; Silva et al., 2018). The presence of organic matter affects the adsorption efficiency by competing for the active sites onto AC, consequently decreasing its effectiveness (Altmann et al., 2014).

The non-steroidal drug Flutamide (FLUT) is chiefly used for therapy of cancer in the male prostate (Khan et al., 2015) and has been found at $\mu g\ L^{-1}$ concentrations in the aquatic environment (Ortiz de García et al., 2013). In France and Spain, the FLUT annual consumption has been estimated to be 521 and 1987.4 kg y^{-1}, respectively (Ortiz de García et al., 2013). There have been very few studies regarding the fates and effects of FLUT in the environment as well as their TPs tha tare originated in HWW.

There have also been few studies that have considered the

combination of AOPs with adsorption processes as environmentally friendly ways to remove the TPs formed. Therefore, this work aimed to evaluate the combination of the SPF process with adsorption using activated carbon produced from waste biomass, for the elimination of FLUT and the TPs generated during the SPF process, present in a complex matrix such as HWW. To this end, an approach employing experimental design with response surface methodology was used to optimize the conditions of the adsorption process for the removal of FLUT and the TPs.

2. Materials and methods

2.1. Chemicals

Flutamide (99.45%, CAS No. 13311-84-7) was acquired from Sigma-Aldrich. The reagents ammonium metavanadate, 1,10-phenanthroline, and ascorbic acid were purchased from Merck (Rio de Janeiro, Brazil). Hydrogen peroxide was acquired from Synth, and $FeSO_4.7H_2O$ was acquired from Neon (São Paulo, Brazil). The LC-MS grade organic solvents used for chromatography were obtained from Merck (Rio de Janeiro, Brazil). Aqueous solutions were prepared in ultrapure water (18.2 MΩ cm) obtained from a Milli-Q system (USA). All other chemicals used were furnished with analytical grade.

2.2. Solar photo-Fenton setup experiments

A mass of 100 mg of FLUT was dissolved in 1 mL of methanol in order to prepare stock solutions. The stock solution was diluted in ultrapure water to prepare the working solutions of FLUT (at 500 μg L^{-1} and 5 mg L^{-1}). A constant magnetic stirred 1 L cylindrical batch reactor was used to carry out the SPF process. Aliquots were sampled to evaluate the degradation of FLUT and further formation of TPs. The residual hydrogen peroxide (H_2O_2) was extinguished by the addition of an aliquot 200 μL (28%,w/v) of sodium hydrogen sulfide. The initial pH of the experiments was fixed at 5 that was adjusted using H_2SO_4 (0.5 mol L^{-1}). The ferrous iron and hydrogen peroxide initial concentrations were 5 and 50 mg L^{-1}, respectively.

Two strategies were used: (i) in a solution of FLUT, it was added an aliquot of 5 mg L^{-1} of Fe(II), in the absence of light, under magnetic stirring by 5 min. Then, an aliquot of 50 mg L^{-1} of H_2O_2 was added, and the solution was immediately exposed to solar irradiation; (ii) three sequential additions of Fe^{2+} were performed. The first addition of 5 mg L^{-1} was made in the dark, before the addition of H_2O_2 at an initial concentration of 150 mg L^{-1}. The system was then exposed to solar irradiation, and the second and third additions of 5 mg L^{-1} Fe^{2+} were performed after 15 and 30 min of irradiation, respectively.

Aliquots of the solutions were removed, filtered through 0.22 μm PTFE membrane filters (Millipore, Cork, Ireland), and analyzed by LC-QTOF MS. The solar UV radiation (W m^{-2}) was checked each 2 min intervals, using an ICEL SP-2000 solar energy meter. The monitored data were used to calculate t_{30W} (Equation (1)) (Prieto-Rodriguez et al., 2012):

$$t_{30W,n} = t_{30W,n-1} + \Delta t_n \frac{UV}{30} \frac{V_I}{V_t} \Delta t_n = t_n - t_{n-1} \qquad (1)$$

Where, $t_{30W,n}$ and $t_{30W,n-1}$ are the adjusted experimental times according to UV irradiation (kJ/L) at t_n and t_{n-1}, respectively; Δt_n is the experimental time between two sampling times; V_I is the irradiated volume, and V_t is the total volume. UV is the average incident solar ultraviolet irradiation measured between two sampling times. The value of 30 refers to a constant solar UV power of 30 W m^{-2}, corresponding to typical solar irradiation at around 12:00 h of a typical brightness day.

2.3. Kinetics of FLUT degradation

Usually, second-order kinetics is followed, considering the degradation of organic compounds by HO• (Equation (2)). When HO• is in excess, a pseudo-stationary state and apparent pseudo-first-order kinetics are obtained (Sun et al., 2007), which can be integrated into an exponential decay equation (Equation (3))

$$\frac{dC}{dt} = -\mathrm{k} \cdot [\mathrm{HO} \bullet][C] = k_{obs}[C] \qquad (2)$$

$$[C] = [C_0] \cdot e^{-k_{obs} \cdot t} \qquad (3)$$

Being C is the concentration of the target organics, [HO•] is the concentration of the hydroxyl radical, and k_{obs} is the observed kinetic rate constant.

The half-life time ($t_{\frac{1}{2}}$) of FLUT degradation was calculated according to Equation (4).

$$t_{\frac{1}{2}} = \frac{\ln 2}{k_{obs}} \qquad (4)$$

The fitting of the experimental data and determination of the degradation rate constants were performed by nonlinear regression using SigmaPlot v. 12 software (Systat Software, USA). ANOVA was used to assess the fitting data.

2.4. Instrumental analysis

Determination of the degradation of FLUT and accurate assignments of the TPs formed in the solar photo-Fenton procedure was obtained using a Shimadzu Nexera X2 LC system, which was coupled to a quadrupole time-of-flight mass spectrometer (Impact II, BrukerDaltonics). A C18 reverse-phase analytical column was used in the LC system. As mobile phases, it was used CH_3CN acidified with 0.1% HCOOH, and ultrapure water acidified with 0.1% HCOOH, that are designed as mobile-phase A, and B, respectively. The other operational conditions employed for the development and use of customized database (Cuervo Lumbaque et al., 2018) and FLUT and TPs identification by non-target analysis (Della-flora et al., 2020) were depicted elsewhere.

Analyses of Fe^{2+} and total iron were performed colorimetrically, employing 1,10-phenanthroline (ISO 6332, 1988). Hydrogen peroxide was determined spectrophotometrically using the ammonium metavanadate method (Nogueira et al., 2005).

2.5. Adsorption onto avocado seed activated carbon

The adsorption process was carried out as a final polishing step for the removal of FLUT and the TPs, using the sample obtained after t_{30W} = 120 min of SPF (pH 4), where most of the TPs were present, according to the LC-QTOF MS analysis. Avocado seed activated carbon (ASAC) was used as the adsorbent material due to its favorable characteristics (Leite et al., 2018). Batch adsorption experiments were performed in 50 mL Falcon tubes, under different experimental conditions (see Section 2.5.1). Samples of 20 mL of the solution containing FLUT and the TPs were added to 50 mL flasks containing the adsorbent, which had previously been dried for 24 h (Michael et al., 2019). After the adsorption procedure, the organics were determined in the liquid-phase using liquid chromatography quadrupole time-of-flight mass spectrometry as described in section 2.4.

Since there were no standards available for the TPs, it was not possible to determine some figures of merit for the adsorption processes, such as adsorption isotherms and thermodynamic parameters. Structure and property predictions and calculations employed the MarvinSketch plug-in from ChemAxon (http://www.chemaxon.com).

2.5.1. Doehlert experimental design for the adsorption process

Doehlert design is a response surface methodology that is widely used to optimize operating conditions (Ferreira et al., 2007a; Ferreira et al., 2007b). Two variables, namely the mass of adsorbent (X_1, mg) and the contact time (X_2, min), were selected as independent factors, using 5 and 3 levels, respectively. As a dependent factor (Y), the response adopted was the removal (%) of the summed peak areas, according to Equation (5):

$$Removal(\%) = 100 - \left(\sum \frac{A_o - A_f}{A_0} \right) \qquad (5)$$

Where, A_o is the initial area for the TPs in the sample after SPF, and A_f is the area for the TPs remaining in the supernatant after the adsorption test.

The lower (-1) and upper ($+1$) levels for each variable were established as corresponding to the minimum and maximum values of each independent variable in the experimental ranges studied, respectively. The independent variables (X_i) were calculated according to Equation (6) (Ferreira et al., 2007a; Ferreira et al., 2007b; Ellouze et al., 2017):

$$X_i = \frac{x_i - x_0}{\Delta x_i} \qquad (6)$$

Where X_i is the dimensionless value of the independent variable, x_i is the uncoded value of the independent variable, x_0 is the center point, and Δx_i is the difference value between the -1 and $+1$ levels (Ferreira et al., 2007a; Ferreira et al., 2007b; Ellouze et al., 2017).

A second-order polynomial model (Equation (7)) was used to fit the response variable (Y), employing the coded values determined using Equation (6):

$$Y = b_0 + b_1 X_1 + b_2 X_2 + b_{11} X_{11}^2 + b_{22} X_{22}^2 + b_{12} X_{12} \qquad (7)$$

Where the b_i coefficients are the estimation of the linear effect, the b_{ii} coefficients are the estimation of the quadratic effect, and b_{ij} provides information about the interactions between the variables (Ferreira et al., 2007a; Ferreira et al., 2007b; Ellouze et al., 2017).

3. Results and discussion

3.1. Primary elimination of FLUT using the solar photo-Fenton process applied to a real hospital wastewater

The degradation of FLUT was evaluated using an HWW matrix (Table S3, Supplementary Material). Two different approaches were used. Fig. 1A and B show the results for FLUT degradation and the formation of TPs using a single addition of 5 mg L^{-1} $[Fe^{2+}]_0$ and 50 mg L^{-1} $[H_2O_2]_0$. The degradation of FLUT followed zero-order kinetics, with $k_{obs} = 1.31 \times 10^{-3}$ min^{-1} (95% of confidence interval 7.4×10^{-4} to 1.88×10^{-3} min^{-1}) and r^2 of 0.998, achieving 20% primary degradation and only 3.05% mineralization. The $[Fe^{2+}]$ was reduced by 70%, the consumption of $[H_2O_2]$ was up to 71%, and total iron decreased by approximately 20% during the SPF process. Eight TPs were identified, with their profiles indicating that for most of the TPs, the areas increased during the process, with TP-13 showing a further transformation after t_{30W} = 120 min. The second approach investigated for the degradation of FLUT in the HWW matrix was based on three consecutive additions of ferrous iron, with initial concentrations of $[Fe^{2+}]_0$ and $[H_2O_2]_0$ of 5 and 150 mg L^{-1}, respectively. Three successive additions of 5 mg L^{-1} Fe^{2+} were made, at t_{30W} = 0 min, t_{30W} = 11.5 min, and t_{30W} = 23.2 min, totaling 15 mg L^{-1} of ferrous iron. As shown in Fig. 1C, the degradation of FLUT followed pseudo-first-order kinetics, with $k_{obs} = 6.52 \times 10^{-3}$ min^{-1} (confidence interval of 95%: 4.57×10^{-3} to 8.48×10^{-3} min^{-1}) and r^2 of 0.993, achieving 58% primary degradation and 12.07% mineralization. Approximately 57% of $[H_2O_2]_0$ was consumed during the SPF process. Both ferrous and total iron showed concentration decreases during the SPF process. Fig. 1D shows the profiles of the TPs during the SPF process with successive additions of ferrous iron. As can be observed, the profiles showed that

A. Della-Flora, et al.   Journal of Hazardous Materials 396 (2020) 122699

65
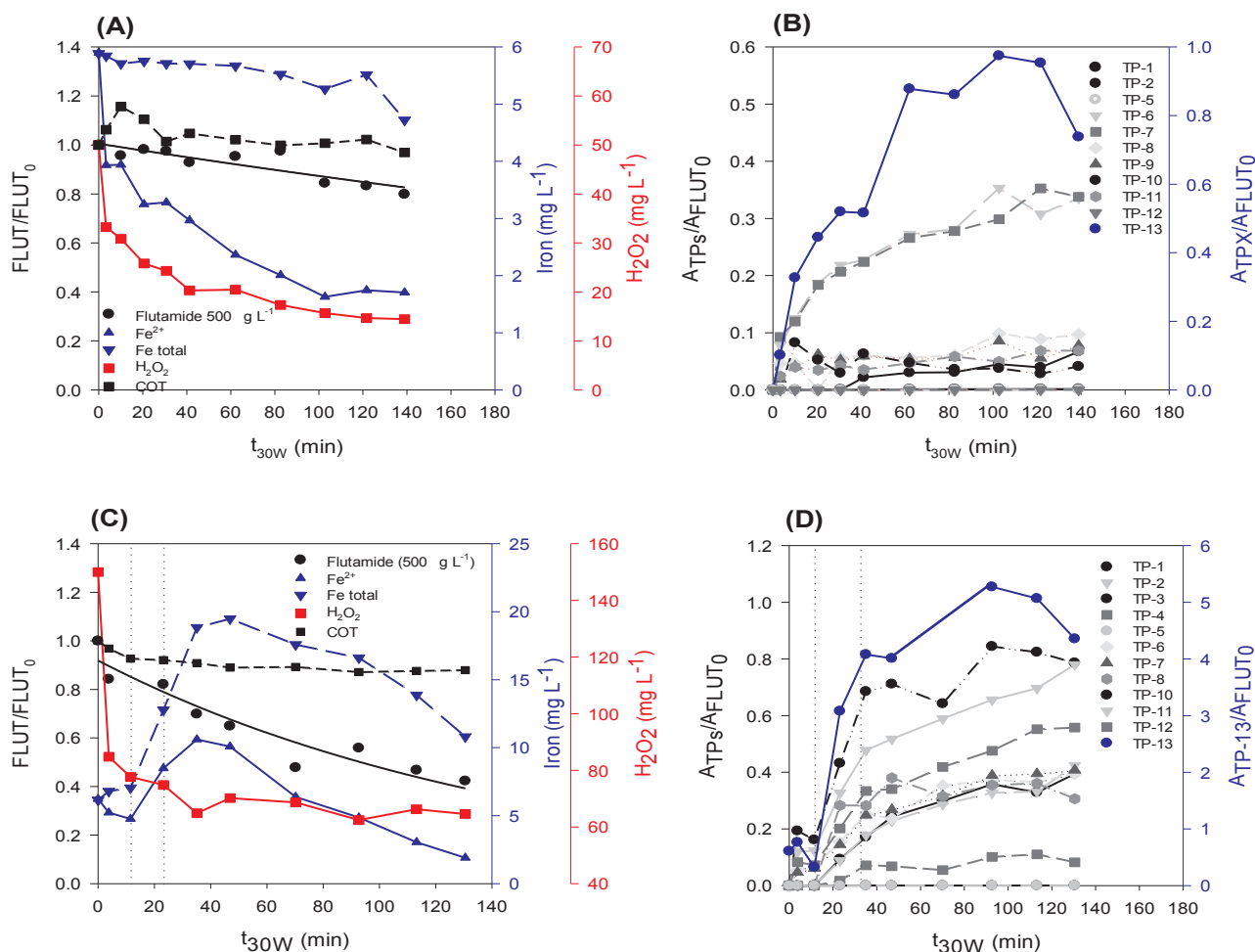
Fig. 1. Degradation of FLUT and formation of TPs in the HWW matrix. (A) Degradation of FLUT and the profile of Fe and H_2O_2 in HWW with a single addition of 5 mg L^{-1} $[Fe^{2+}]_0$ and 50 mg L^{-1} $[H_2O_2]_0$; (B) Formation of FLUT's TPs in HWW with a single addition of 5 mg L^{-1} $[Fe^{2+}]_0$ and 50 mg L^{-1} $[H_2O_2]_0$; (C) Degradation of FLUT and the profile of Fe and H_2O_2 in HWW with two successive additions of 5 mg L^{-1} $[Fe^{2+}]_0$ and 150 mg L^{-1} of $[H_2O_2]_0$; (D) Formation of FLUT's TPs in HWW with two successive additions of 5 mg L^{-1} $[Fe^{2+}]_0$ and 150 mg L^{-1} of $[H_2O_2]_0$. Dashed lines are referring to the two-addition times of 5 mg L^{-1} of $[Fe^{2+}]$.

most of the TPs formed during the degradation process were persistent. However, TP-13 showed a decrease in the area after t_{30W} = 102 min, indicating possible further transformation.

3.2. TPs identification

Identification of the TPs formed during the SPF process was performed using data obtained with liquid chromatography quadrupole time-of-flight mass spectrometry in negative ionization mode. In a first approach, the method used for identification was based on non-target analysis, resulting in the initial proposal of 13 TPs (Table 1). Once the structures of TPs had been proposed, a simplified version of a customized database was constructed in order to facilitate the identification of these TPs in a complex matrix such as HWW, using a suspect screening methodology (Cuervo Lumbaque et al., 2018). After the first approach for elucidation of the TPs, a purpose-built database was constructed considering the neutral formula of the TP [M], the theoretical and exact masses (m/z) of the negative ion $[M—H]^-$ and the qualifier ions (Q1-Q3), and the retention time (Rt) (Della-flora et al., 2020). The Rt parameter could only be used when the same chromatographic conditions were employed because there were no analytical standards for the TPs.

The screening method applied for FLUT and the TPs in HWW enabled the identification of 10 TPs for the SPF process carried out using a single addition of Fe^{2+} (5 mg L^{-1}) and 50 mg L^{-1} of H_2O_2, while 13 TPs

were identified in the SPF process performed using three consecutive additions of 5 mg L^{-1} Fe^{2+}, with 150 mg L^{-1} H_2O_2. The results are presented in Table 1, showing the exact masses, the molecular ion formula $[M—H]^-$, the error expressed in ppm, and the double bond equivalence (RDB) determined using the Bruker QTOF MS Compass DataAnalysis software.

Accordingly, MS data, it was possible to propose different mechanisms affecting the FLUT during the SPF process (Fig. 2), as well as the structures of the proposed TPs.

3.3. Avocado seed activated carbon (ASAC) as adsorbent

The physicochemical characteristics of the ASAC adsorbent have been reported previously (Leite et al., 2018; Leite et al., 2017), with S_{BET} surface areas ranging from 1122 to 1584 m^2 g^{-1} and mesopore volumes between 0.4753 and 0.6906 cm^3 g^{-1}. The pH_{pzc} values of ASAC were between 6.11 and 6.80, indicating that the surface of the adsorbent was close to neutrality. The acidic groups present on ASAC were more prevalent than the primary groups. The hydrophobicity-hydrophilicity ratio values were below 1.0, indicating a predominantly hydrophilic nature of the material (Leite et al., 2018).

Table 1

Accurate mass measurements of FLUT and the main TPs found by LC-QTOF MS by bbCID in negative ionization mode in HWW.

Compound	Rt (min)	Ion Formula [M-H]$^-$	Meas. m/z	m/z	error (ppm)	mSigma	RDB	TPs found in different treatments approaches with [Fe^{2+}] additions	
								Single addition	Multiple additions
TP-1	2.0	$C_9H_{11}F_3NO_7S$	334.0228	334.0214	−4.3	n.a.	3.5	X	X
		$C_8H_9F_3NO_2$	208.0593	208.0591	−0.8	83	3.5		
TP-2	3.3	$C_9H_{11}F_3NO_7S$	334.0204	334.0214	2.9	34.1	3.5	X	X
		$C_8H_{11}F_3NO_5S$	290.0306	290.0316	3.2	n.a.	2.5		
		$C_8H_9F_3NO_2$	208.0596	208.0591	−2.6	n.a.	3.5		
TP-3	3.5	$C_{11}H_{13}F_3NO_{10}S$	408.0224	408.0218	−1.5	28.6	4.5	-	X
		$C_{11}H_{10}F_3N_2O_2$	259.0696	259.0700	1.6	n.a.	6.5		
		$C_7H_2F_3O_3$	190.9958	190.9962	1.9	n.a.	5.5		
TP-4	4.1	$C_{11}H_{12}F_3N_2O_5S$	341.0428	341.0424	−1.2	n.a.	5.5	-	X
		$C_{11}H_{12}F_3N_2O_2$	261.0865	261.0856	−3.6	315.3	5.5		
TP-5	4.6	$C_{10}H_6F_3N_2O_4$	275.0280	275.0285	1.8	14.4	7.5	X	X
		$C_7H_4F_3N_2O_3$	221.0175	221.0179	1.9	n.a.	5.5		
		$C_7H_4F_3N_2O_2$	205.0224	205.0230	3.1	n.a.	5.5		
TP-6	4.8	$C_{11}H_8F_3N_2O_4$	289.0441	289.0441	0.2	47.3	7.5	X	X
		$C_8H_4F_3N_2O_3$	233.0181	233.0179	−1.0	n.a.	6.5		
		$C_8H_{15}F_2N_4O$	221.1211	221.1219	3.6	33	2.5		
		$C_7H_4F_3N_2O_2$	205.0233	205.0230	−1.5	32.2	5.5		
TP-7	4.9	$C_{11}H_8F_3N_2O_4$	289.0441	289.0441	0.1	15.3	7.5	X	X
		$C_8H_4F_3N_2O_3$	233.0174	233.0179	2.1	n.a.	6.5		
		$C_7H_4F_3N_2O_2$	205.0221	205.0230	4.4	45.4	5.5		
TP-8	5.2	$C_{11}H_{11}F_3NO_2$	246.0742	246.0747	1.8	29.8	5.5	-	X
		$C_8H_{11}F_3NO_3$	226.0686	226.0696	4.6	n.a.	2.5		
		$C_7H_4F_2NO$	156.0271	156.0266	−3.5	n.a.	5.5		
TP-9	5.6	$C_{11}H_{10}F_3N_2O_4$	291.0591	291.0598	2.2	n.a.	6.5	X	X
		$C_7H_4F_3N_2O_2$	205.0227	205.0230	1.5	4.2	5.5		
TP-10	5.8	$C_{11}H_{10}F_2N_2O_7S$	371.0162	371.0166	1.3	11.5	6.5	X	X
		$C_{11}H_{10}F_3N_2O_5$	307.0546	307.0547	0.2	n.a.	6.5		
		$C_{11}H_{10}F_3N_2O_4$	291.0592	291.0598	1	9.3	6.5		
		$C_7H_4F_3N_2O_2$	205.0229	205.0230	0.2	4.5	5.5		
TP-11	6.2	$C_{11}H_{10}F_3N_2O_4$	291.0602	291.0598	−1.6	n.a.	6.5	X	X
TP-12	6.6	$C_{10}H_6F_3N_2O_4$	275.0281	275.0285	1.5	76	7.5	X	X
		$C_7H_4F_3N_2O_2$	205.0226	205.0230	2	n.a.	5.5		
TP-13	6.8	$C_{11}H_{10}F_3N_2O_4$	291.0594	291.0598	1.4	4.6	6.5	X	X
		$C_7H_4F_3N_2O_3$	221.0182	221.0179	−1.4	4.9	5.5		
FLUT	7.0	$C_{11}H_{10}F_3N_2O_3$	275.0645	275.0649	1.1	3.6	6.5	X	X
		$C_{10}H_6F_3N_2O_3$	259.0341	259.0336	−1.9	n.a.	7.5		
		$C_7H_4F_3N_2O_2$	205.0229	205.0230	0.4	8.2	5.5		
		$C_7H_3F_3NO_2$	190.0123	190.0121	−1.3	313.5	5.5		

X means the presence in the sample.

– means absence in the sample.
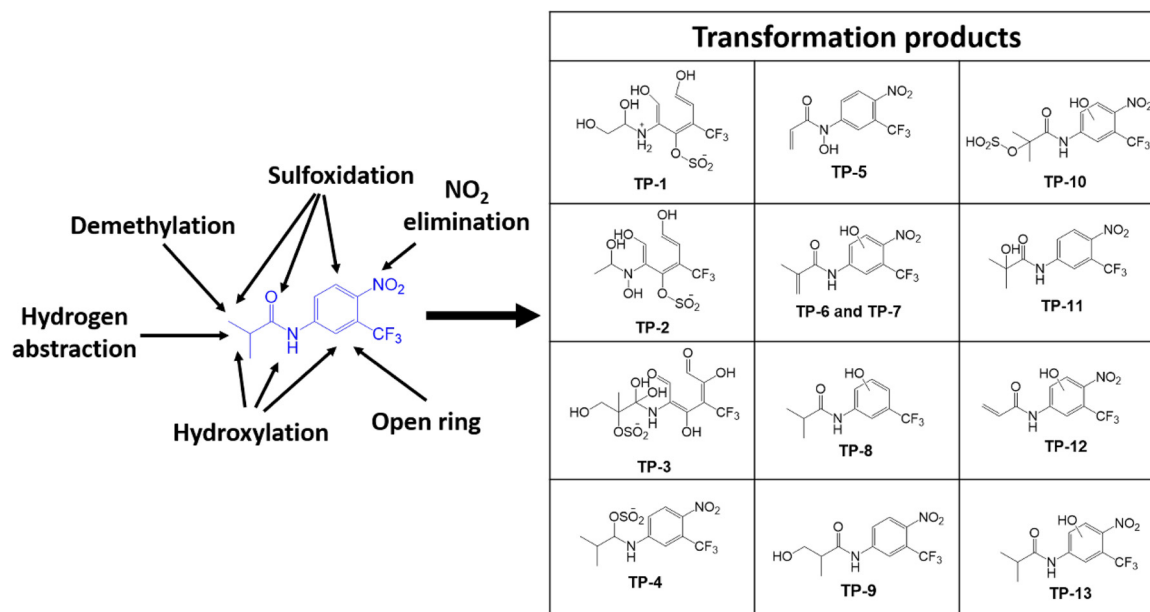
Fig. 2. Transformation products and its main species at pH 4.

Table 2

Doehlert experimental design and removal results of the adsorption tests of FLUT and TPs formed in HWW onto ASAC adsorbent.

Variables		Levels of variable 1				
Time (min)	Coded values	−1	−0.5	0	0.5	1
	Decoded values	5	20	35	50	65
		Levels of variable 2				
Mass (mg)	Coded values		−0.866	0	0.866	
	Decoded values		1	10.5	20	
Experimental design			Removal (%) of summed peak areas $((1-\Sigma(A_0-A_f/A_0))\times100)$			
Exp.	Time (min)	Mass (mg)	FLUT + TPs			
1	65	10.5	98.01			
2	50	20	98.29			
3	5	10.5	94.89			
4	20	1	84.27			
5	50	1	82.18			
6	20	20	97.79			
7	35	10.5	97.11			
8	35	10.5	96.89			
9	35	10.5	96.77			
10	35	10.5	96.85			

Experimental conditions: pH 4, 25 °C, 20 mL of HWW solution.

3.4. Experimental design for the adsorption of TPs present in the HWW matrix

There were no standards available for the TPs, so it was not possible to determine the adsorption kinetics and obtain adsorption isotherms. The adsorption kinetics and adsorption isotherms for ASAC used with other contaminants have been reported previously (Leite et al., 2018; Leite et al., 2017). Hence, in this study, the summed peak areas removal rate was employed $((1-\Sigma(A_0-A_f/A_0))\times100)$, given in % of FLUT + TPs. A multivariate experimental design based on a Doehlert matrix was applied in order to optimize the removal rate of FLUT and TPs (Table 2). The variables assessed were the contact time (min) and the mass loading of the adsorbent (mg). The pH of the adsorption tests was the final pH of the SPF process (pH ~4). The analytical response of the experimental design was determined according to Equation (5) (Della-Flora et al., 2020). As can be seen in Table 2, high removal rates (> 99%) were achieved.

A Pareto chart of the effects is shown in Fig. 3A. The results of the analysis of variance (ANOVA) are provided in the Supplementary Material (Text S1). The R-squared and R-adj values of the mathematical model were 0.988 and 0.973, respectively. The linear and quadratic variables of the adsorbent mass (mg) were the variables with statistically significant effects in the adsorption tests, while the contact time and the interaction between contact time and mass were not statistically significant ($p < 0.05$).

The equation for the fitting of the second-order model was obtained as follows:

$$Removal(\%) = 81.35 + 0.013X - 0.0005X^2 + 2.0537Y - 0.06824Y^2$$
$$+ 0.00455XY \qquad (8)$$

Where X and X^2 are the linear and quadratic coded values for the contact time (min), Y and Y^2 are the linear and quadratic coded values for the adsorbent mass (mg), and XY represents the interaction between contact time (min) and adsorbent mass (mg).

The model described above should be considered as case-specific, since the optimum conditions established in this study were for the adsorption of FLUT and the TPs present in the HWW matrix employed here. If the technique was applied to other wastewater matrices, the adsorption processes could present different responses and different optimum parameters. The ANOVA tables for the Doehlert design can be found in Text S1(Supplementary Material).

The response surface obtained for the adsorption of FLUT and the TPs onto ASAC is shown in Fig. 3B. The removal of FLUT and the TPs by adsorption showed a clear dependence on the adsorbent mass loading, with higher removal rates achieved by increasing the adsorbent mass. Although the effect of the contact time variable was not statistically significant, the response surface showed that a more extended contact time led to higher removal rates.

The effect of the adsorbent mass loading in the adsorption of micropollutants onto ASAC can be explained by the number of active sites on the surface of the activated carbon, which is responsible for the adsorption (Nazari et al., 2016). At the same time, the contact time is one of the main variables that need to be considered in order to make the adsorption process economically viable. Both variables (mass loading and contact time) affect the efficiency of the adsorbent material and the interaction mechanisms, which should ideally provide rapid adsorption equilibrium (Chen et al., 2010). High amounts of adsorbent and very long contact times can make the adsorption process expensivesothatits application on a large scale becomes unfeasible (Giménez et al., 2015).

Optimization can reduce costs by decreasing both the contact time and the amount of ASAC used in the adsorption process. In addition to the response surface, the desirability profile can be used to assist optimization processes using multivariate experimental design methods (Ferreira et al., 2007a; Ferreira et al., 2007b). In this case, the desirability of the responses is plotted by specifying the degrees of freedom for each variable and assuming a desirability scale from 0 (undesirable) to 1 (very desirable) (Ferreira et al., 2007a; Ferreira et al., 2007b). Fig. 4 shows the desirability profile applied to the Doehlert design for the optimization of contact time (min) and mass loading (mg) of ASAC adsorbent, using the summed peak areas $((1-\Sigma(A_0-A_f/A_0))\times100)$ to determine the removal of FLUT + TPs, where the removal responses were 82.17% (minimum), 90.23% (average), and 98.28% (maximum).

The desirability profile (Fig. 4) indicated that a 14 mg amount of the ASAC adsorbent should theoretically be the optimal amount for the removal of FLUT and its TPs. The desirability profile also indicated that the best contact time was 40 min, with adsorption equilibrium having already been achieved under the conditions studied, so no further treatment was required for the removal of FLUT and the TPs from the HWW after $t_{30W} = 120$ min.

Application of the optimized conditions determined by the Doehlert design led to the complete removal of FLUT and its TPs from the HWW matrix after $t_{30W} = 120$ min of SPF treatment at pH 4. In previous work, Leite et al. (2018) reported that ASAC presented a high surface area, resulting in high efficiency for the removal of micropollutants. In the present work, the amount of ASAC and the contact time were reduced, decreasing by about 17 mg for the ASAC adsorbent and 80 min for the contact time, compared to the initial conditions used by Leite et al. (2018). Therefore, the combination of SPF and ASAC adsorption provided a more efficient process, since it enabled the use of less material and shorter contact time. Besides, the SPF treatment provided a 70% higher removal of FLUT (Fig. 1C), while the complementary treatment using ASAC enabled total removal of FLUT and its TPs from HWW (Fig. S2, Supplementary Material).

In the work of Michael et al. (2019), SPF and adsorption enabled the removal of the target micropollutants. However, Michael et al. (2019) only considered the parent compounds, while the present study considered the removal of TPs formed during the SPF process. Furthermore, Michael et al. (2019)) used a domestic effluent that had already received activated sludge treatment and/or been filtered through a microfiltration membrane, while the present study used a raw HWW matrix that had not received any previous treatment (Table S3, Supplementary Material). This strategy directly influenced the SPF

(A)

(B)
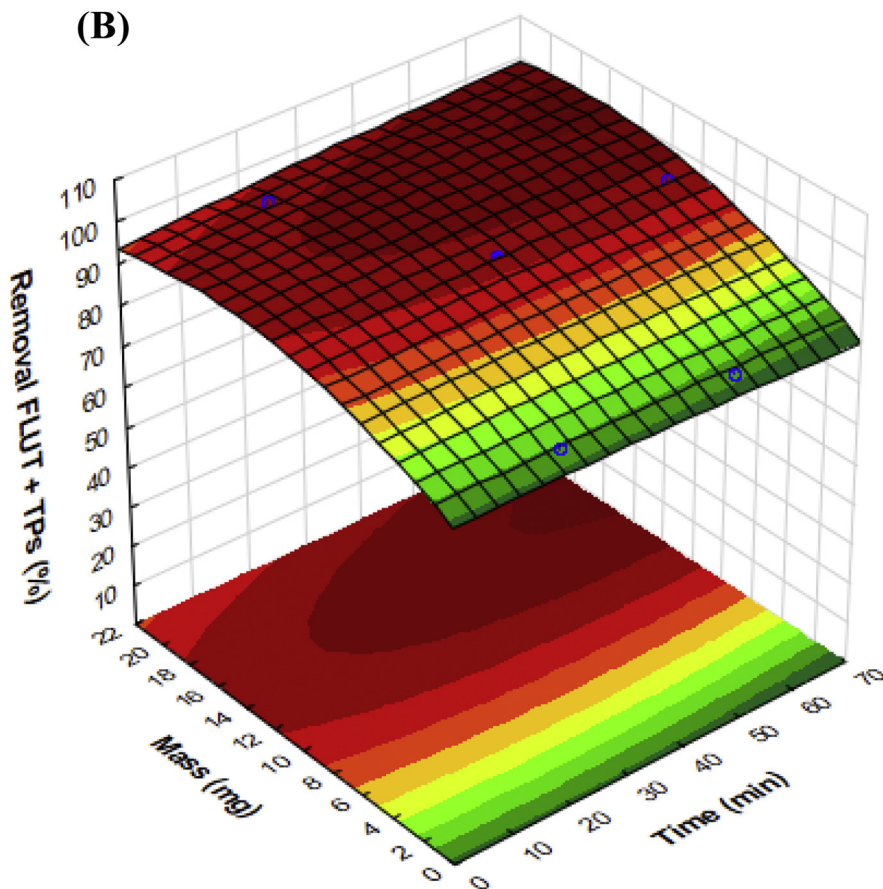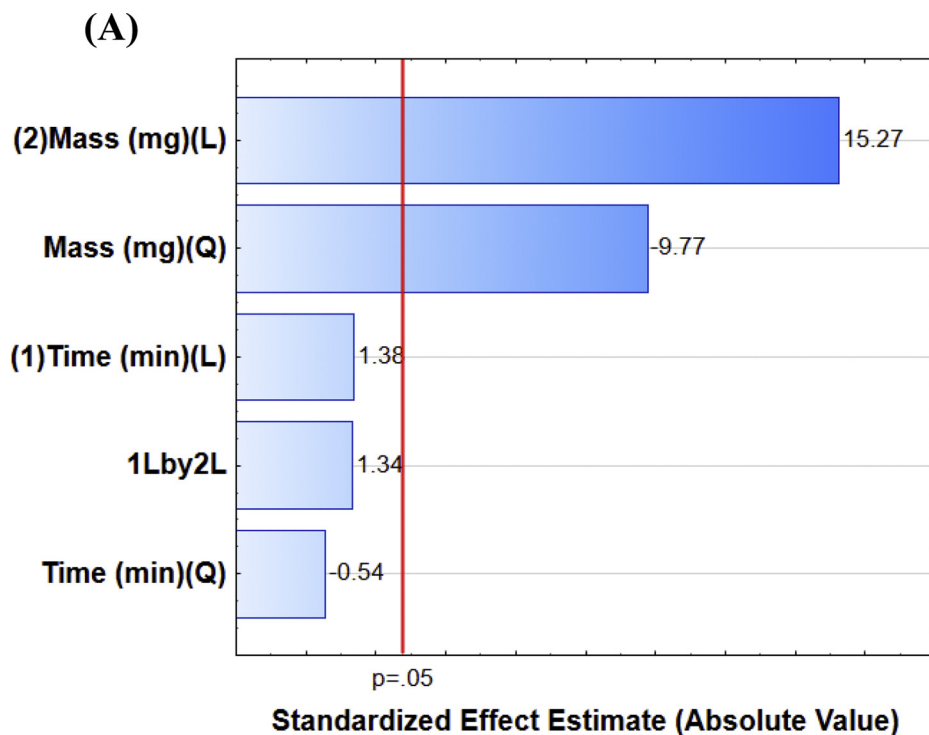
Fig. 3. (A) Pareto Chart of standardized effects of the main effects observed in the Doehlert design for adsorption of FLUT and TPs onto ASAC adsorbent. The vertical line refers the level of significance at $p = 0.05$. (B) Response surface showing the effect of mass (mg) vs. Contact time (min) on the adsorption of FLUT and TPs onto ASAC adsorbent.
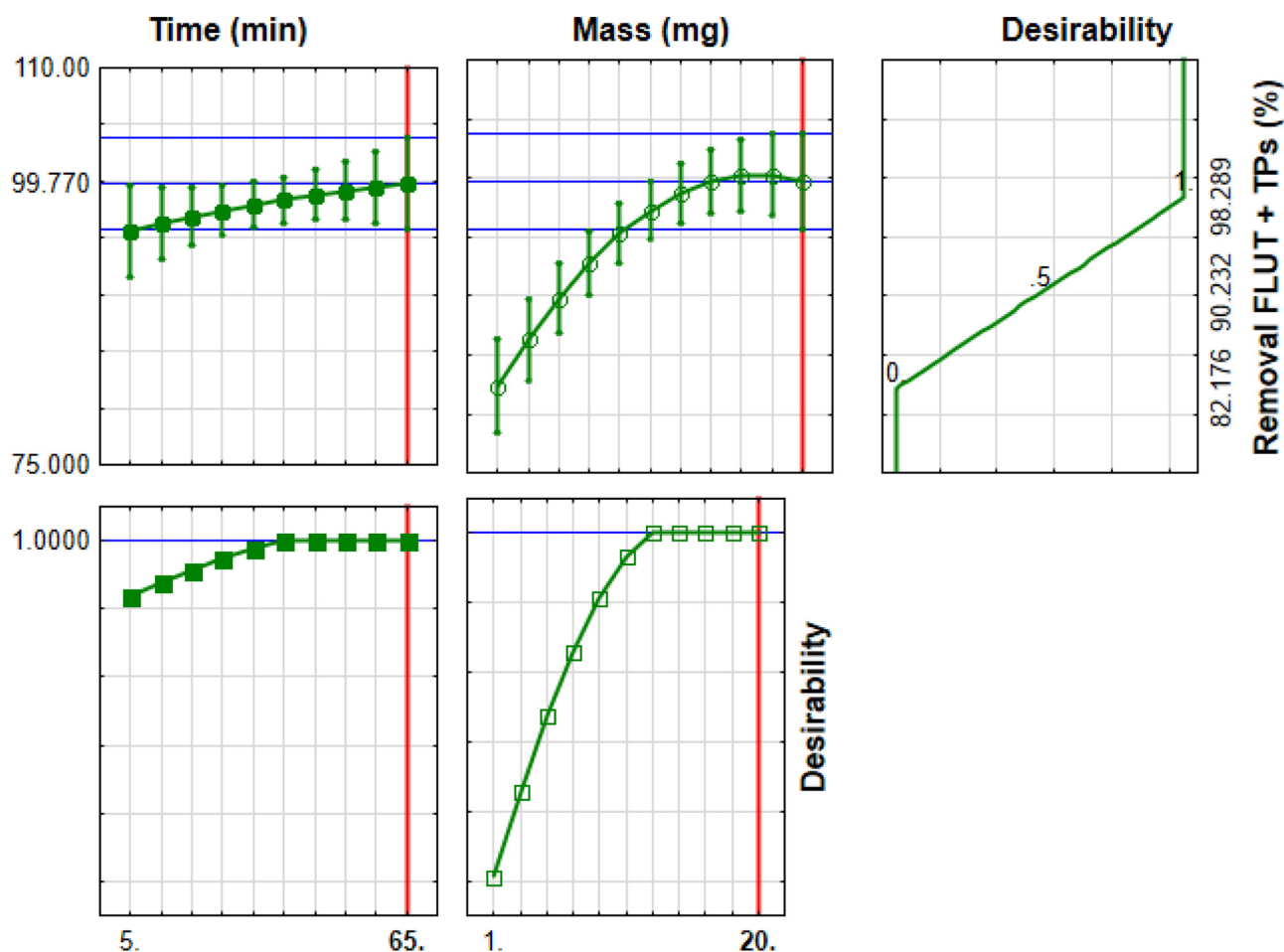
Fig. 4. Profiles for predicted values and the desirability function for the adsorption of FLUT and TPs onto ASAC adsorbent.

treatment time required for FLUT degradation, because the presence of organic matter and the cocktail of pharmaceuticals and other pollutants would result in competition with FLUT for the hydroxyl radicals generated in the SPF process. Therefore, it is evident that the SPF treatment time is a critical factor in the adsorption process, since Michael et al. (2019) used an SPF treatment time of t_{30W} = 30 min, at pH 2.9, whereas in the present study, the SPF treatment time was t_{30W} = 120 min, at pH 5. It is well known that Fenton/photo-Fenton processes are most efficient at pH between 2.8 and 3.0 (Pignatello et al., 2006). In the present work, the aim was to work at pH close to neutrality (pH 5), for two reasons: (i) the cost of reagents required to acidify/neutralize the effluent was low, and (ii) Brazilian legislation allows the disposal of effluents at pH 5-9 (Lumbaque et al., 2019; Benatti et al., 2006). The longer treatment time (t_{30W} = 120 min) was due to operation at pH near neutrality, at which the degradation of organic compounds was likely to be slower.

Regarding the use of adsorption onto activated carbon, Michael et al. (2019) employed a commercial activated carbon with a surface area of 1.100 m^2 g^{-1} and a contact time of 15 min, while the ASAC used as an adsorbent in the present study had a surface area of 1.432 m^2 g^{-1} and the contact time was 40 min.

Both adsorption processes were able to remove the micropollutants; however, in the present study, a statistical experimental design was performed for optimization of the experimental conditions.

3.4.1. Proposed mechanisms and interactions of FLUT and TPs during the adsorption onto ASAC

Fig. 5 shows the removal efficiencies for FLUT and each TP in the different Doehlert design experiments and under the optimal

experimental conditions (14 mg of ASAC and 40 min contact time). As the adsorbent characteristics were the same for all the TPs studied, the adsorption mechanisms and interactions on ASAC were likely to be most influenced by the physicochemical proprieties of the compounds and the interference/competition by organic compounds present in the wastewater matrix.

The overall adsorption process involves three general mechanisms, namely, diffusion, surface chemical reaction, and surface complexation (Saleem et al., 2019). The characteristics of both the adsorbent and the adsorbate determine these mechanisms. As can be seen in Table 3, a pattern concerning their physicochemical properties was observed in the adsorption of FLUT and the TPs onto the ASAC adsorbent. An attempt was made to obtain correlations between the removal rates of FLUT and the TPs and parameters, including molecular weight, log P, van der Waals, and polar surface areas, and van der Waals volume (the polar surface area divided by the van der Waals surface area).

The results revealed a pattern in the adsorption behaviors of FLUT and the TPs. Lower adsorption rates were observed for more polar TPs such as TP-1, TP-2, and TP-3. These TPs were predicted to present negative log P values, showing their polar character, with lower removal rates observed, even when the amount of adsorbent was increased and the adsorption contact time was extended. The highest removal rates for TP-1, TP-2, and TP-3 were achieved when 20 mg of ASAC was used (Exp. 6, Fig. 5). Complete removal of TP-3 was only achieved using 20 mg of ASAC and a 50 min contact time, indicating that despite the high polarity of TP-3, the adsorption onto ASAC occurred according to different mechanisms and interactions, such as hydrogen bonds and dipole-dipole interactions, as well as electron-donor-acceptor interactions.

70

A. Della-Flora, et al.   Journal of Hazardous Materials 396 (2020) 122699
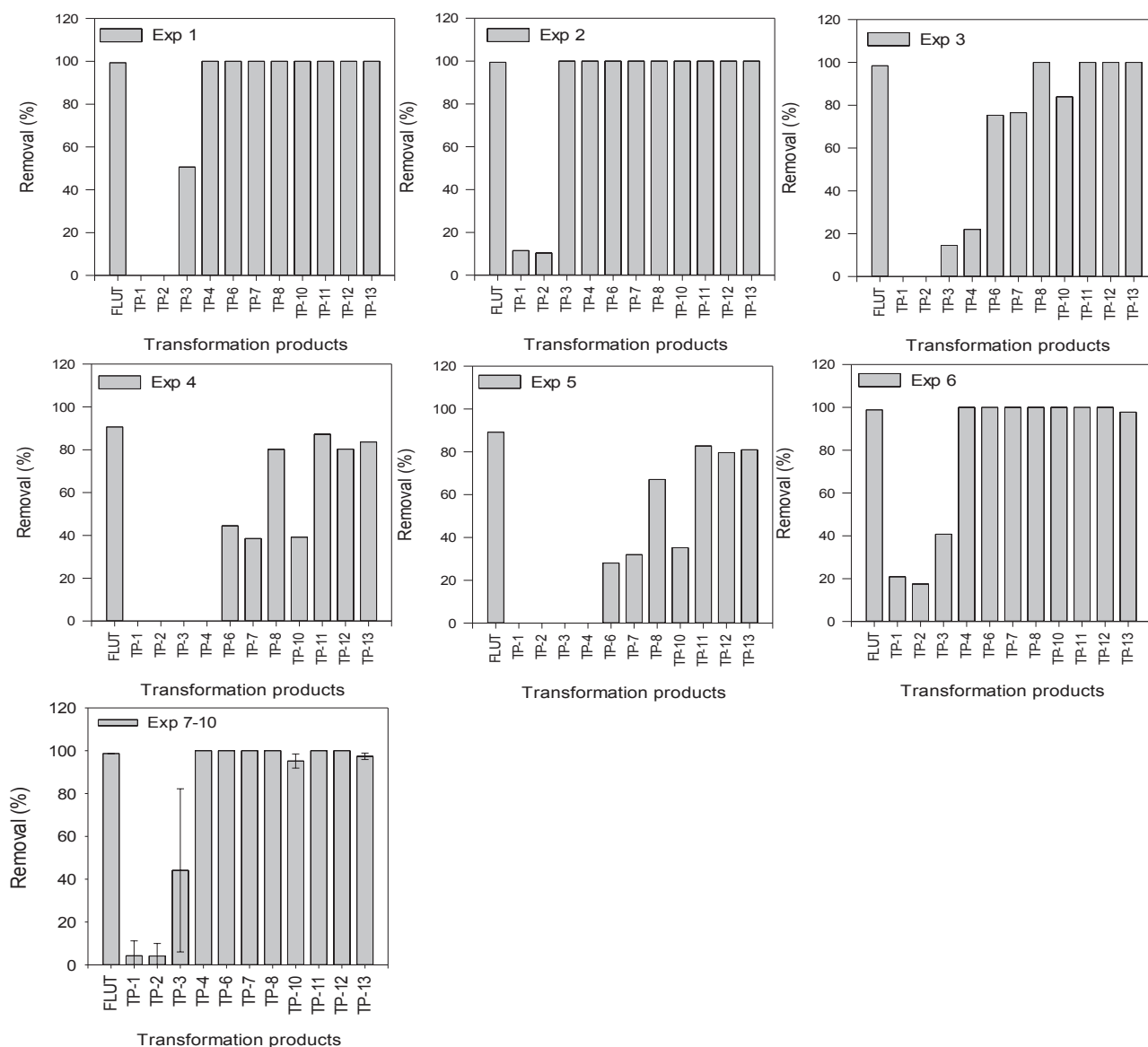
Fig. 5. Adsorption of FLUT and TPs onto ASAC adsorbent at each experiment of the Doehlert design. For the experimental conditions (Contact time vs. Mass load) of each experiment, see Table 2.

This behavior could also be related to the functional groups available on the ASAC surface. According to FTIR analysis of the ASAC adsorbent (Leite et al., 2018), the surface contains large amounts of polar groups (–OH, –COO, –O, and –NH), so a predominantly polar (hydrophilic) behavior was expected. As the functional groups on the ASAC surface were mostly protonated, H-bond interactions were favored. Besides, when compared to the other TPs studied, TP-1, TP-2, and TP-3 were predicted to have higher values for the polar surface area/van der Waals surface area ratio (> 0.4), at pH 7 (Table 3), indicating that physical interaction of the TPs with the adsorbent surface could occur as a result of their electrostatic potentials.

Despite having a predicted log P value of 3.00, TP-4 was predicted to be negatively charged (SO_3^-) at pH 4. Slower rates of removal of TP-4 were observed when a lower adsorbent mass was used (Fig. 5). Different from TP-1, TP-2, and TP-3, the TP-4 presented the basic structure of FLUT still intact, with only the attachment of an SO_3 group on the oxygen of the amide group oftheside chain. Therefore, faster removal rates were obtained with increases of the adsorbent amount and the contact time (Fig. 5). The main adsorption interactions that could occur on TP-4 were H-bonding, n-π, and π-π interactions, as well as dipole-

dipole interactions. Electron donor-acceptor interactions could also occur, since the surface of ASAC contains carbonyl groups able to interact with the aromatic ring of FLUT, with the aromatic ring acting as an e^- acceptor (Leite et al., 2018). Such interactions have been proposed for the adsorption of phenols by ASAC adsorbents (Leite et al., 2018).

Polarizability is the relative tendency of the molecule to form instantaneous dipoles, and the more stable each ionized site is, the more its vicinity is polarizable. Adsorption onto microporous activated carbon may depend on the electrostatic field when it is filled with organic compounds (electronic polarizability) (Selim and El-Nabarawy, 1980). Table 3 shows the predicted polarizabilities of FLUT and the TPs.

The pH affects both the nature of compounds and the surface properties of the adsorbent. The pH_{pzc} of ASAC is near neutrality, while the pH of the samples during the adsorption process was 4, and when pH < pH_{pzc}, the adsorbent surface is positively charged (Sekulic et al., 2019). The charges of pharmaceutical compounds and TPs are pKa dependent. FLUT was predicted to have a pKa of 12.81. Since the pH during the adsorption process was 4 (below pH_{pzc}), the majority of the microspecies structures of FLUT and the TPs were neutrally charged. The calculated percentage abundances of each species predominant at

71

A. Della-Flora, et al.   Journal of Hazardous Materials 396 (2020) 122699

Table 3
In silico predictions of some physical-chemical and 3D parameters of FLUT and the proposed structure of TPs.

Compound	Smiles	Log P[a]	Van der Waals surface area (Å², pH 7.0)[a]	Polar surface area (Å², pH 7.0)[a]	Van der Waals Volume (Å³)[a]	Polar surface area/Van der Waals surface area ratio (pH 7.0)[a]	Polarizability (Å³)	pKa[a]*
TP-1	OC(CO)NC(C(OS(O)=O)=C(C(F)(F)F)C = CO)=CO	-2.0	363.74	158.69	246.06	0.436	24.94	2.01/5.0
TP-2 a	OC(C)N(O)C(C(OS(O)=O)=C(C(F)(F)F)C = CO)=CO	-1.68	364.96	149.90	247.61	0.411	24.94	2.00/13.15
TP-2 b	OC(C)N(O)C(C = CO)=C(OS(O)=O)C(C(F)(F)F)=CO	-1.68	364.08	149.90	247.35	0.411	24.94	2.00/13.15
TP-3 a	CC(CO)(OS(O)=O)C(O)(O)NC(C(=O)=C(O)C(C(F)(F)F)F)=C(CO)C = O	-3.88	451.64	213.06	302.48	0.472	24.94	2.00/9.01
TP-3 b	CC(CO)(OS(O)=O)C(O)(O)NC(C(O)=C(C(F)(F)F)C(=O))=C(C(=O))O	-3.88	452.33	213.06	302.56	0.471	24.94	2.00/8.90
TP-4	CC(C(Nc1cc(C(F)(F)F)c([N+]([O-])=O)c(C(F)(F)F)c1)OS(O)(S)(O)=O)C	3.00	430.28	101.70	261.59	0.236	27.01	2.00/11.73
TP-6/7 a	C = CC(N(c1ccc([N+]([O-])=O)c(C(F)(F)F)c1)O)=O	2.88	341.50	92.47	219.55	0.271	22.59	7.04/-1.59
TP-6/7 b	CC(Nc1cc(C(F)(F)F)c([N+]([O-])=O)c(O)c1)=C	2.88	342.37	92.47	219.44	0.270	22.60	6.09/-1.5
TP 6/7 c	CC(Nc1cc(C(F)(F)F)c([N+]([O-])=O)cc1O)=C	2.88	339.92	92.47	219.62	0.272	22.60	6.1/-1.59
TP-8 a	CC(Nc1c(O)c(C(F)(F)F)cc([N+]([O-])=O)cc1)=C	3.03	332.71	49.33	204.13	0.242	20.72	8.29
TP-8 b	O = C(C(C)C)Nc1ccc(C(F)(F)F)c(O)c1	3.03	334.72	49.33	204.07	0.147	20.72	8.8
TP-8 c	O = C(C(C)C)Nc1ccc(C(F)(F)F)cc(O)c1	3.03	334.68	49.33	204.0	0.147	20.72	8.65
TP-8 d	O = C(C(C)C)Nc1ccc(C(F)(F)F)ccc1O	3.03	331.63	49.33	204.16	0.149	20.72	7.64
TP-10 a	O = C(C(C)C)Nc1cc(O)c(C(F)(F)F)cc(C(F)(F)F)ccc1	1.76	442.65	158.21	272.45	0.357	28.04	2.00/6.09/11.86
TP-10 b	O = C(C(C)CO)Nc1cc(C(F)(F)F)c([N+]([O-])=O)cc1	1.76	439.74	158.21	272.40	0.360	28.04	2.00/7.04/12.16
TP-10 c	O = C(C(C)C)OS(=O)=O)Nc1cc(C(F)(F)F)c([N+]([O-])=O)c(O)c1	1.76	439.90	158.21	272.52	0.360	28.04	2.00/6.10/12.18
TP-11	O = C(C(C)(C)OS(=O)=O)Nc1cc(C(F)(F)F)c([N+]([O-])=O)cc1O	2.21	372.87	92.47	227.18	0.248	22.86	11.79/13.99
TP-12 a	O = C(C(C)(C)OS(=O)=O)Nc1cc(O)c(C(F)(F)F)c([N+]([O-])=O)cc1	2.48	310.03	92.47	202.45	0.298	20.82	6.09/13.35
TP-12 b	O = C(C(O)(C))Nc1cc(C(F)(F)F)c([N+]([O-])=O)cc1	2.48	311.55	92.47	202.44	0.297	20.82	7.05/13.78
TP-12 c	O = C(Nc1cc(C(F)(F)F)c([N+]([O-])=O)c(O)c1)C = C	2.48	307.29	92.47	202.54	0.300	20.82	6.10/13.81
TP-13 a	O = C(Nc1cc(C(F)(F)F)c([N+]([O-])=O)c(O)c1)C = C	2.97	371.56	92.47	226.97	0.249	22.85	6.09/12.88
TP-13 b	O = C(Nc1c(O)c(C(F)(F)F)c([N+]([O-])=O)c1)C = C	2.97	370.86	92.47	226.84	0.249	22.85	7.06/13.26
TP-13 c	O = C(C(C)C)Nc1cc(C(F)(F)F)c([N+]([O-])=O)c(O)c1	2.97	369.14	92.47	226.90	0.250	22.85	6.12/13.29
FLUT	O = C(Nc1cc(C(F)(F)F)c([N+]([O-])=O)c1)C(C)C	3.27	360.07	72.24	218.58	0.20	22.13	12.81

calculated by Marvin Sketch plug-in 19.9 (www.chemaxon.com, 2019); * pKa₁/pKa₂.
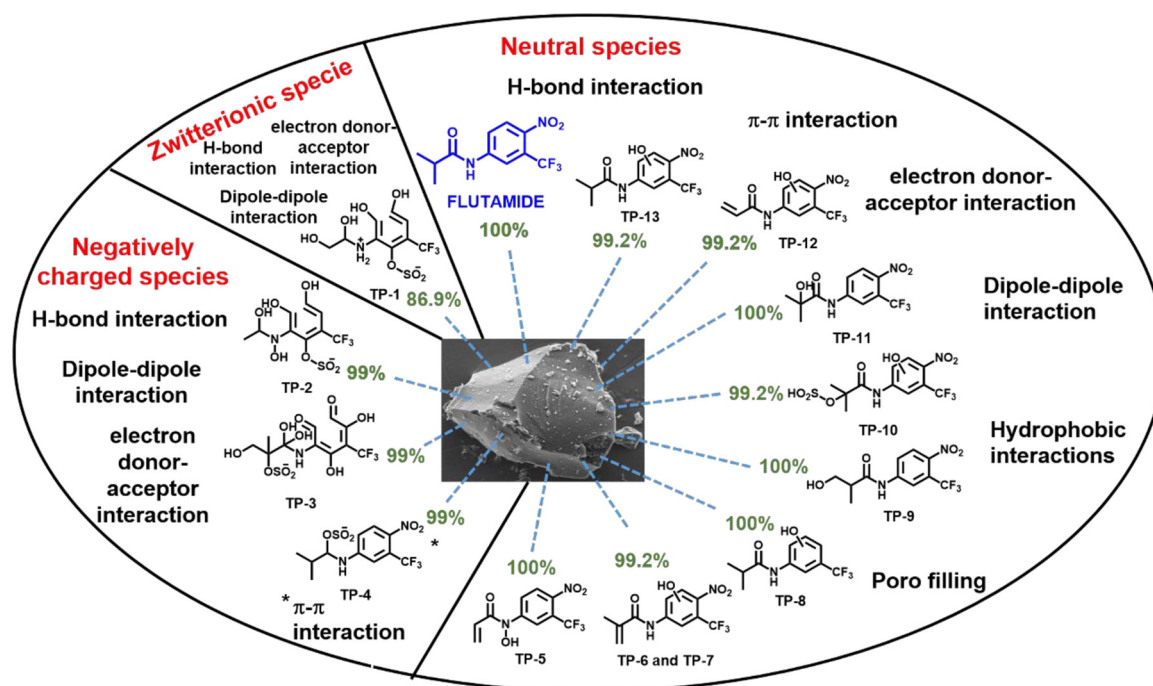
Fig. 6. Scanning electron microscopy of ASAC and proposed adsorption mechanisms and interaction of FLUT and TPs present after solar photo-Fenton treatment in a competitive and of HWW matrix. * In green, the percentage of the abundance of each specie at pH 4 calculated by Marvin Sketch plug-in 19.9 (www.chemaxon.com, 2019).

pH 4 are shown in Fig. 6. For the TPs that still retained the basic structure of FLUT, the neutral microspecies were predominant at pH 4, whereas the open-chain TPs (TP-1, TP-2, and TP-3) were predicted to have charged structures as the main microspecies. The TPs with the SO_3 group attached to the structure were negatively charged at pH 4, except for TP-1 and TP-10. TP-1 was predicted to have a zwitterionic structure, with the SO_3 group being negatively charged, while the secondary amine was positively charged.

All the other TPs (TP-6 to TP-13) were neutrally charged at pH 4. As shown in Table 3, these TPs were predicted to have log K_{OW} values between 2.21 and 3.03, except for TP-10, for which log K_{OW} was predicted to be 1.76. TP-10, TP-6, TP-7, TP-11, TP-12, and TP-13 were predicted to have polar surface area/van der Waals surface area ratio values between 0.147 and 0.3, with these ratios reflecting better adsorption onto ASAC. In the case of TP-10, the polar surface area/van der Waals surface area ratio was predicted to be around 0.36. Determination of the removal rates under the different conditions investigated (Fig. 5) showed that TP-10 presented lower removal rates in some cases, compared to the other TPs, mainly when smaller amounts of adsorbent and shorter contact times were used.

Therefore, the higher removal rates, even with shorter contact times and smaller amounts of ASAC, could be explained by the structural configurations of FLUT and the TPs, together with the mechanisms of adsorption on the ASAC surface. The latter included H-bonding, n-π, and π-π interactions, as well as dipole-dipole, electron donor-acceptor, and hydrophobic interactions, which could be related to the hydrophobicity of the material (Leite et al., 2018; Sekulic et al., 2019).

Fig. 6 shows the main microspecies of FLUT and the TPs at pH 4, the main mechanisms and interactions involved, and a scanning electron microscopy (SEM) image of the ASAC adsorbent.

4. Conclusions

The SPF process was combined with adsorption in order to remove FLUT and TPs from an HWW matrix. The SPF process was applied using two different approaches. The single addition approach (5 mg L^{-1} Fe^{2+} and 50 mg L^{-1} H_2O_2) achieved only 20% FLUT primary degradation and only 3.05% mineralization. The three Fe^{2+} additions approach (5 mg L^{-1} of Fe^{2+} each, with an initial H_2O_2 concentration of 150 mg L^{-1}) achieved 58% primary degradation and 12.07% mineralization. By using two different LC-QTOF MS strategies, namely non-target and screening using a customized database, it was possible to identify the presence of 13 TPs of FLUT formed in the HWW matrix during the SPF process.

In order to remove FLUT and the TPs from HWW, the SPF process was combined with adsorption using ASAC derived from waste biomass. The adsorption process was optimized using a Doehlert design, considering the variable's contact time and ASAC mass loading. The optimum conditions were 14 mg of ASAC and a contact time of 40 min. However, the highly polar open-ring TPs presented lower removal rates, even when the amount of adsorbent was increased. Higher removal rates were found for the TPs that still presented the aromatic ring, suggesting that π-π interactions played a significant role in the adsorption process. Therefore, this study showed that the combination of the SPF process with adsorption is an attractive option for the removal of persistent and toxic TPs from aqueous media.

Declaration of Competing Interest

The authors declare that they have no known competing financial interests or personal relationships that could have appeared to influence the work reported in this paper.

Acknowledgments

Appendix A. Supplementary data

Supplementary material related to this article can be found, in the online version, at doi:https://doi.org/10.1016/j.jhazmat.2020.122699.

References

Burri, N.M., Weatherl, R., Moeck, C., Schirmer, M., 2019. A review of threats to groundwater quality in the anthropocene. Sci. Total Environ. 684, 136–154. https://doi.org/10.1016/j.scitotenv.2019.05.236.

Warner, W., Licha, T., Nödler, K., 2019. Qualitative and quantitative use of micropollutants as source and process indicators. A review. Sci. Total Environ. 686, 75–89. https://doi.org/10.1016/j.scitotenv.2019.05.385.

Di Lorenzo, T., Di Cicco, M., Di Censo, D., Galante, A., Boscaro, F., Messana, G., 2019. D.M. Paola Galassi, Environmental risk assessment of propranolol in the groundwater bodies of Europe. Environ. Pollut. 255, 113189. https://doi.org/10.1016/j.envpol.2019.113189.

Parrella, A., Lavorgna, M., Criscuolo, E., Russo, C., Fiumano, V., Isidori, M., 2014. Acute and chronic toxicity of six anticancer drugs on rotifers and crustaceans. Chemosphere 115, 59–66. https://doi.org/10.1016/j.chemosphere.2014.01.013.

Grzesiuk, M., Bednarska, A., Mielecki, D., Garbicz, D., Marcinkowski, M., Pilžys, T., Malinowska, A., Świderska, B., Grzesiuk, E., 2019. Anticancer agents found in environment affect Daphnia at population, individual and molecular levels. Aquat. Toxicol. 215, 105288. https://doi.org/10.1016/j.aquatox.2019.105288.

Taheran, M., Naghdi, M., Brar, S.K., Verma, M., Surampalli, R.Y., 2018. Emerging contaminants: Here today, there tomorrow!. Environ. Nanotechnology, Monit. Manag. 10, 122–126. https://doi.org/10.1016/j.enmm.2018.05.010.

Wilkinson, J., Hooda, P.S., Barker, J., Barton, S., Swinden, J., 2017. Occurrence, fate and transformation of emerging contaminants in water: An overarching review of the field. Environ. Pollut. 231, 954–970. https://doi.org/10.1016/j.envpol.2017.08.032.

Klavarioti, M., Mantzavinos, D., Kassinos, D., 2009. Removal of residual pharmaceuticals from aqueous systems by advanced oxidation processes. Environ. Int. 35, 402–417.

Mirzaei, A., Chen, Z., Haghighat, F., Yerushalmi, L., 2017. Removal of pharmaceuticals from water by homo/heterogonous Fenton-type processes – A review. Chemosphere 174, 665–688. https://doi.org/10.1016/j.chemosphere.2017.02.019.

Kanakaraju, D., Glass, B.D., Oelgemöller, M., 2018. Advanced oxidation process-mediated removal of pharmaceuticals from water: A review. J. Environ. Manag. 219, 189–207. https://doi.org/10.1016/j.jenvman.2018.04.103.

Sun, S., Yao, H., Fu, W., Hua, L., Zhang, G., Zhang, W., 2018. Reactive Photo-Fenton ceramic membranes: Synthesis, characterization and antifouling performance. Water Res. 144, 690–698. https://doi.org/10.1016/j.watres.2018.08.002.

Sun, S., Yao, H., Fu, W., Xue, S., Zhang, W., 2020. Enhanced degradation of antibiotics by photo-fenton reactive membrane filtration. J. Hazard. Mater. 386, 121955. https://doi.org/10.1016/j.jhazmat.2019.121955.

Frédéric, O., Yves, P., 2014. Pharmaceuticals in hospital wastewater: Their ecotoxicity and contribution to the environmental hazard of the effluent. Chemosphere 115, 31–39. https://doi.org/10.1016/j.chemosphere.2014.01.016.

Tambosi, J.L., Yamanaka, L.Y., José, H.J., De Fátima Peralta Muniz Moreira, R., Schröder, H.F., 2010. Recent research data on the removal of pharmaceuticals from sewage treatment plants (STP). Quim. Nova. 33, 411–420. https://doi.org/10.1590/S0100-40422010000200032.

Philip, J.M., Aravind, U.K., Aravindakumar, C.T., 2018. Emerging contaminants in Indian environmental matrices – A review. Chemosphere 190, 307–326. https://doi.org/10.1016/j.chemosphere.2017.09.120.

Sanganyado, E., Gwenzi, W., 2019. Antibiotic resistance in drinking water systems: Occurrence, removal, and human health risks. Sci. Total Environ. 669, 785–797. https://doi.org/10.1016/j.scitotenv.2019.03.162.

Lumbaque, E.C., Becker, R.W., Salmoria Araújo, D.S., Dallegrave, A., Ost Fracari, T.O., Lavayen, V., Sirtori, C., 2019. Degradation of pharmaceuticals in different water matrices by a solar homo/heterogeneous photo-Fenton process over modified alginate spheres. Environ. Sci. Pollut. Res. 26, 6532–6544. https://doi.org/10.1007/s11356-018-04092-z.

Gernjak, W., Fuerhacker, M., Fern??ndez-Iba??ez, P., Blanco, J., Malato, S., Gernjak, W., Fuerhacker, M., Ferna, P., 2006. Solar photo-Fenton treatment - Process parameters and process control. Appl. Catal. B Environ. 64, 121–130. https://doi.org/10.1016/j.apcatb.2005.12.002.

Sirtori, C., Zapata, A., Oller, I., Gernjak, W., Agu, A., Malato, S., 2009. Solar Photo-Fenton as Finishing Step for Biological Treatment of a Pharmaceutical Wastewater. Environ. Sci. Technol. 43, 1185–1191.

Fiorentino, A., Esteban, B., Garrido-Cardenas, J.A., Kowalska, K., Rizzo, L., Aguera, A., Pérez, J.A.S., 2019. Effect of solar photo-Fenton process in raceway pond reactors at neutral pH on antibiotic resistance determinants in secondary treated urban wastewater. J. Hazard. Mater. 378, 120737. https://doi.org/10.1016/j.jhazmat.2019.06.014.

Pignatello, J.J., Oliveros, E., MacKay, A., 2006. Advanced Oxidation Processes for Organic Contaminant Destruction Based on the Fenton Reaction and Related Chemistry. Crit. Rev. Environ. Sci. Technol. 36, 1–84. https://doi.org/10.1080/10643380500326564.

Fatta-Kassinos, D., Vasquez, M.I., Kümmerer, K., 2011. Transformation products of pharmaceuticals in surface waters and wastewater formed during photolysis and advanced oxidation processes – Degradation, elucidation of byproducts and assessment of their biological potency. Chemosphere 85, 693–709. https://doi.org/10.1016/j.chemosphere.2011.06.082.

Osawa, R.A., Carvalho, A.P., Monteiro, O.C., Oliveira, M.C., Florêncio, M.H., 2019.

Degradation of duloxetine: Identification of transformation products by UHPLC-ESI (+)-HRMS/MS, in silico toxicity and wastewater analysis. J. Environ. Sci. (China). 82, 113–123. https://doi.org/10.1016/j.jes.2019.02.025.

Durán, A., Monteagudo, J.M., San Martín, I., 2018. Operation costs of the solar photocatalytic degradation of pharmaceuticals in water: A mini-review. Chemosphere 211, 482–488. https://doi.org/10.1016/j.chemosphere.2018.07.170.

Wilde, M.L., Menz, J., Leder, C., Kümmerer, K., 2018. Combination of experimental and in silico methods for the assessment of the phototransformation products of the antipsychotic drug/metabolite Mesoridazine. Sci. Total Environ. 618, 697–711. https://doi.org/10.1016/j.scitotenv.2017.08.040.

Rastogi, T., Leder, C., Kümmerer, K., 2014. Qualitative environmental risk assessment of photolytic transformation products of iodinated X-ray contrast agent diatrizoic acid. Sci. Total Environ. 482–483, 378–388. https://doi.org/10.1016/j.scitotenv.2014.02.139.

Herrmann, M., Menz, J., Olsson, O., Kümmerer, K., 2015. Identification of phototransformation products of the antiepileptic drug gabapentin: Biodegradability and initial assessment of toxicity. Wat. Res. 85, 11–21. https://doi.org/10.1016/j.watres.2015.08.004.

Brienza, M., Nir, S., Plantard, G., Goetz, V., Chiron, S., 2019. Combining micelle-clay sorption to solar photo-Fenton processes for domestic wastewater treatment. Environ. Sci. Pollut. Res. 26, 18971–18978. https://doi.org/10.1007/s11356-019-2491-3.

Hou, J., Chen, Z., Gao, J., Xie, Y., Li, L., Qin, S., Wang, Q., Mao, D., Luo, Y., 2019. Simultaneous removal of antibiotics and antibiotic resistance genes from pharmaceutical wastewater using the combinations of up-flow anaerobic sludge bed, anoxicoxic tank, and advanced oxidation technologies. Water Res. 159, 511–520. https://doi.org/10.1016/j.watres.2019.05.034.

Michael, S.G., Michael-Kordatou, I., Beretsou, V.G., Jäger, T., Michael, C., Schwartz, T., Fatta-Kassinos, D., 2019. Solar photo-Fenton oxidation followed by adsorption on activated carbon for the minimisation of antibiotic resistance determinants and toxicity present in urban wastewater. Appl. Catal. B Environ. 244, 871–880. https://doi.org/10.1016/j.apcatb.2018.12.030.

Carmalin, S.A., Lima, E.C., 2018. Removal of emerging contaminants from the environment by adsorption. Ecotoxicol. Environ. Saf. 150, 1–17. https://doi.org/10.1016/j.ecoenv.2017.12.026.

Zhu, S., Liu, Y., Liu, S., Zeng, G., Jiang, L., Tan, X., Zhou, L., Zeng, W., Li, T., Yang, C., 2017. Adsorption of emerging contaminant metformin using graphene oxide. Chemosphere 179, 20–28. https://doi.org/10.1016/j.chemosphere.2017.03.071.

Leite, A.B., Saucier, C., Lima, E.C., dos Reis, G.S., Umpierres, C.S., Mello, B.L., Shirmardi, M., Dias, S.L.P., Sampaio, C.H., 2018. Activated carbons from avocado seed: optimisation and application for removal of several emerging organic compounds. Environ. Sci. Pollut. Res. 25, 7647–7661. https://doi.org/10.1007/s11356-017-1105-9.

Álvarez-Torrellas, S., Peres, J.A., Gil-Álvarez, V., Ovejero, G., García, J., 2017. Effective adsorption of non-biodegradable pharmaceuticals from hospital wastewater with different carbon materials. Chem. Eng. J. 320, 319–329. https://doi.org/10.1016/j.cej.2017.03.077.

Lima, D.R., Lima, E.C., Umpierres, C.S., Thue, P.S., El-Chaghaby, G.A., da Silva, R.S., Pavan, F.A., Dias, S.L.P., Biron, C., 2019. Removal of amoxicillin from simulated hospital effluents by adsorption using activated carbons prepared from capsules of cashew of Para. Environ. Sci. Pollut. Res. 26, 16396–16408. https://doi.org/10.1007/s11356-019-04994-6.

Saucier, C., Karthickeyan, P., Ranjithkumar, V., Lima, E.C., 2017. G.S. dos Reis, I.A.S. de Brum, Efficient removal of amoxicillin and paracetamol from aqueous solutions using magnetic activated carbon. Environ. Sci. Pollut. Res. 24, 5918–5932. https://doi.org/10.1007/s11356-016-8304-7.

Rizzo, L., Malato, S., Antakyali, D., Beretsou, V.G., Đolić, M.B., Gernjak, W., Heath, E., Ivancev-Tumbas, I., Karaolia, P., Lado Ribeiro, A.R., Mascolo, G., Mcardell, C.S., Schaar, H., Silva, A.M.T.T., Fatta-kassinos, D., Maja, B.Đ., Gernjak, W., Heath, E., Ivancev-Tumbas, I., Karaolia, P., Lado, A.R., Mascolo, G., Mcardell, C.S., Schaar, H., Silva, A.M.T.T., Fatta-kassinos, D., 2019. Consolidated vs new advanced treatment methods for the removal of contaminants of emerging concern from urban wastewater. Sci. Total Environ. 655, 986–1008. https://doi.org/10.1016/j.scitotenv.2018.11.265.

Silva, C.P., Jaria, G., Otero, M., Esteves, V.I., Calisto, V., 2018. Waste-based alternative adsorbents for the remediation of pharmaceutical contaminated waters: Has a step forward already been taken? Bioresour. Technol. 250, 888–901. https://doi.org/10.1016/j.biortech.2017.11.102.

Altmann, J., Ruhl, A.S., Zietzschmann, F., Jekel, M., 2014. Direct comparison of ozonation and adsorption onto powdered activated carbon for micropollutant removal in advanced wastewater treatment. Water Res. 55, 185–193. https://doi.org/10.1016/j.watres.2014.02.025.

Khan, N., Nasser, H., Yan, J., Chung, F., Wu, H., 2015. Detection of flutamide in pharmaceutical dosage using higher electrospray ionization mass spectrometry (ESI-MS) tandem mass coupled with Soxhlet apparatus. Anal. Chem. Res. 3, 89–97. https://doi.org/10.1016/j.ancr.2015.01.001.

Ortiz de García, S., Pinto Pinto, G., García Encina, P., Irusta Mata, R., 2013. Consumption and occurrence of pharmaceutical and personal care products in the aquatic environment in Spain. Sci. Total Environ. 444, 451–465. https://doi.org/10.1016/j.scitotenv.2012.11.057.

Prieto-Rodríguez, L., Miralles-Cuevas, S., Oller, I., Agüera, A., Puma, G.L., Malato, S., 2012. Treatment of emerging contaminants in wastewater treatment plants (WWTP) effluents by solar photocatalysis using low TiO2 concentrations. J. Hazard. Mater. 211–212, 131–137. https://doi.org/10.1016/j.jhazmat.2011.09.008.

Sun, J.H., Sun, S.P., Fan, M.H., Guo, H.Q., Qiao, L.P., Sun, R.X., 2007. A kinetic study on the degradation of p-nitroaniline by Fenton oxidation process. J. Hazard. Mater. 148, 172–177. https://doi.org/10.1016/j.jhazmat.2007.02.022.

Cuervo Lumbaque, E., Cardoso, R.M., Dallegrave, A., Dos Santos, L.O., Ibáñez, M., Hernández, F., Sirtori, C., 2018. Pharmaceutical removal from different water matrixes by Fenton process at near-neutral pH: Doehlert design and transformation products identification by UHPLC-QTOF MS using a purpose-built database. J. Environ. Chem. Eng. 6, 3951–3961. https://doi.org/10.1016/j.jece.2018.05.051.

Della-Flora, A., Wilde, M.L., Pinto, I.D.F., Lima, E.C., Sirtori, C., 2020. Degradation of the anticancer drug flutamide by solar photo-Fenton treatment at near-neutral pH: Identification of transformation products and in silico (Q)SAR risk assessment. Environ. Res. 183, 109223. https://doi.org/10.1016/j.envres.2020.109223.

ISO 6332, 1988. Water quality - Determination of iron - Spectrometric method using 1,10-phenanthroline.

Nogueira, R.F.P., Oliveira, M.C., Paterlini, W.C., 2005. Simple and fast spectrophotometric determination of H_2O_2 in photo-Fenton reactions using metavanadate. Talanta 66, 86–91. https://doi.org/10.1016/j.talanta.2004.10.001.

Ferreira, S.L.C., Bruns, R.E., da Silva, E.G.P., dos Santos, W.N.L., Quintella, C.M., David, J.M., Andrade, J.B., Breitkreitz, M.C., Jardim, I.C.S.F., Barros Neto, B., 2007a. Statistical designs and response surface techniques for the optimization of chromatographic systems. J. Chromatogr. A 1158, 2–14. https://doi.org/10.1016/j.chroma.2007.03.051.

Ferreira, S.L.C., Bruns, R.E., Ferreira, H.S., Matos, G.D., David, J.M., Brandão, G.C., da Silva, E.G.P., Portugal, L.A., dos Reis, P.S., Souza, A.S., dos Santos, W.N.L., 2007b. Box-Behnken design: An alternative for the optimization of analytical methods. Anal. Chim. Acta. 597, 179–186. https://doi.org/10.1016/j.aca.2007.07.011.

Ellouze, S., Kessemtini, S., Clematis, D., Cerisola, G., Panizza, M., Elaoud, S.C., 2017. Application of Doehlert design to the electro-Fenton treatment of Bismarck Brown Y. J. Electroanal. Chem. 799, 34–39. https://doi.org/10.1016/j.jelechem.2017.05.042.

Leite, A.J.B, A, C.S., Thue, P.S., dos Reis, G.S., Dias, S.L., Lima, E.C., Vaghetti, J.C.P., Pavan, F.A., de Alencar, W.S., 2017. Activated carbon from avocado seeds for the removal of phenolic compounds from aqueous solutions. Desalin. Water Treat. 71, 168–181. https://doi.org/10.5004/dwt.2017.20540.

Nazari, G., Abolghasemi, H., Esmaieli, M., 2016. Batch adsorption of cephalexin antibiotic from aqueous solution by walnut shell-based activated carbon. J. Taiwan Inst. Chem. Eng. 58, 357–365. https://doi.org/10.1016/j.jtice.2015.06.006.

Chen, S., Zhang, J., Zhang, C., Yue, Q., Li, Y., Li, C., 2010. Equilibrium and kinetic studies of methyl orange and methyl violet adsorption on activated carbon derived from Phragmites australis. Desalination 252, 149–156. https://doi.org/10.1016/j.desal.2009.10.010.

Giménez, J., Bayarri, B., González, O., Malato, S., Peral, J., Esplugas, S., 2015. Advanced Oxidation Processes at Laboratory Scale: Environmental and Economic Impacts. ACS Sustain. Chem. Eng. 3188–3196.

Benatti, C.T., Tavares, C.R.G., Guedes, T.A., 2006. Optimization of Fenton's oxidation of chemical laboratory wastewaters using the response surface methodology. J. Environ. Manage. 80, 66–74. https://doi.org/10.1016/j.jenvman.2005.08.014.

Saleem, J., Bin Shahid, U., Hijab, M., Mackey, H., McKay, G., 2019. Production and applications of activated carbons as adsorbents from olive stones. Biomass Convers. Biorefinery. 9, 775–802. https://doi.org/10.1007/s13399-019-00473-7.

Selim, M.M., El-Nabarawy, T.A., 1980. The relation between the adsorption of hydrocarbons and their polarizabilities on active carbon. Surf. Technol. 10, 65–72.

Sekulic, M.T., Boskovic, N., Slavkovic, A., Garunovic, J., Kolakovic, S., Pap, S., 2019. Surface functionalised adsorbent for emerging pharmaceutical removal: Adsorption performance and mechanisms. Process Saf. Environ. Prot. 125, 50–63. https://doi.org/10.1016/j.psep.2019.03.007.

Supplementary Material

Combined solar photo-Fenton and adsorption process for removal of the anticancer drug Flutamide and its transformation products from hospital wastewater

Alexandre Della-Flora, Marcelo L. Wilde, Pascal S. Thue, Diana Lima, Eder C. Lima, and Carla Sirtori[*]

Instituto de Química, Universidade Federal do Rio Grande do Sul, Av. Bento Gonçalves 9500, CEP 91501-970 Porto Alegre, RS, Brazil.

Correspondingauthor: Prof. Carla Sirtori – carla.sirtori@ufrgs.br

Text S1. Doehlert design results

Table S1. Analysis of variance (ANOVA) for the Doehlert design of the adsorption process in the HWW matrix.

	SS	df	MS	F	p
Contact Time (min)(L)	1.7888	1	1.7888	1.8997	0.240184
Contact Time (min)(Q)	0.2702	1	0.2702	0.2869	0.620592
Mass (mg) (L)	219.5563	1	219.5563	233.1693	0.000107
Mass (mg) (Q)	89.8957	1	89.8957	95.4695	0.000615
1L by 2L	1.6779	1	1.6779	1.7820	0.252818
Error	3.7665	4	0.9416		
Total SS	316.9736	9			

Table S2. Effect estimates for the Doehlert design of the adsorption process in HWW matrixes.

	Effect	**Standard Error**	**t**	**p**	**Coefficient**	**Standard Error**
Mean/Interc.	96.90	0.48	199.72	0.000000	96.90	0.485185
(1) Time (min) (L)	0.77	0.56	1.38	0.240184	0.39	0.280122
Time (min) (Q)	-0.22	0.42	-0.54	0.620592	-0.11	0.210091
(2) Mass load (mg) (L)	14.82	0.97	15.27	0.000107	7.41	0.485185
Mass load (mg) (Q)	-12.32	1.26	-9.77	0.000615	-6.16	0.630274
1L by 2L	1.295	0.97	1.34	0.252818	0.65	0.485185

1 = variable one (Time)
2 = variable two (Mass load)
L = linear variavle
Q = quadratic variable
1L by 2L = interaction between the linear variables of
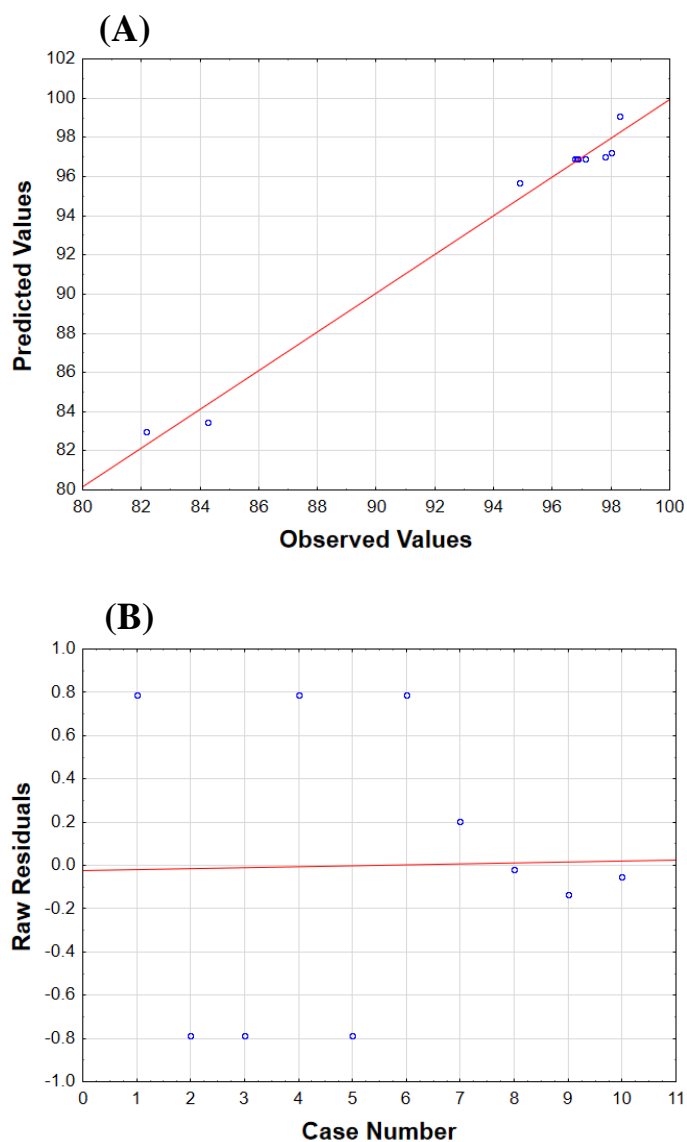
Figure S1. (A) Predicted *vs.* observed values for the Doehlert design of the adsorption of FLUT and TPs onto ASAC adsorbent. (B) Distribution of the Raw Residuals vs. Case numbers of the Doehlert design of the adsorption of FLUT and TPs onto ASAC adsorbent.

Physical-Chemical Characterization of HWW

Table S3. Physical-Chemical Characterization of HWW.

Parameters	HWW Matrix	Method	LD	LQ
pH	9.20	SMEWW 4500-H+ B	-	-
Conductivity (μS cm^{-1})	786.5	SMEWW 2510 B	1	0.2
COD (mg L^{-1} O$_2$)	252	SMEWW 5220 B	5	0.8
BOD (mg L^{-1} O$_2$)	123	SMEWW 5210 B	2	0.6
COD/BOD	0.4880	≥ 0.5 biodegradable (Lopes et al 2004)	-	-
TOC (mg L^{-1})	146.5	SMEWW 5310	1.68	3.99
Total Chloride (mg L^{-1})	47.4	SMEWW 4110 B	0.5	0.02
Total phosphate (mg L^{-1} PO$_4^{3-}$)	17.30	SMEWW 4500 P E	0.03	0.006
Total suspended solids (mg L^{-1})	119	SMEWW 2540 D	10	5
Total solids (mg L^{-1})	403	SMEWW 2540 B	10	5

SMEWW: standard methods for the examination of water and wastewater.(American Public Health Association)

Scheme of Solar photo-Fenton and adsorption process
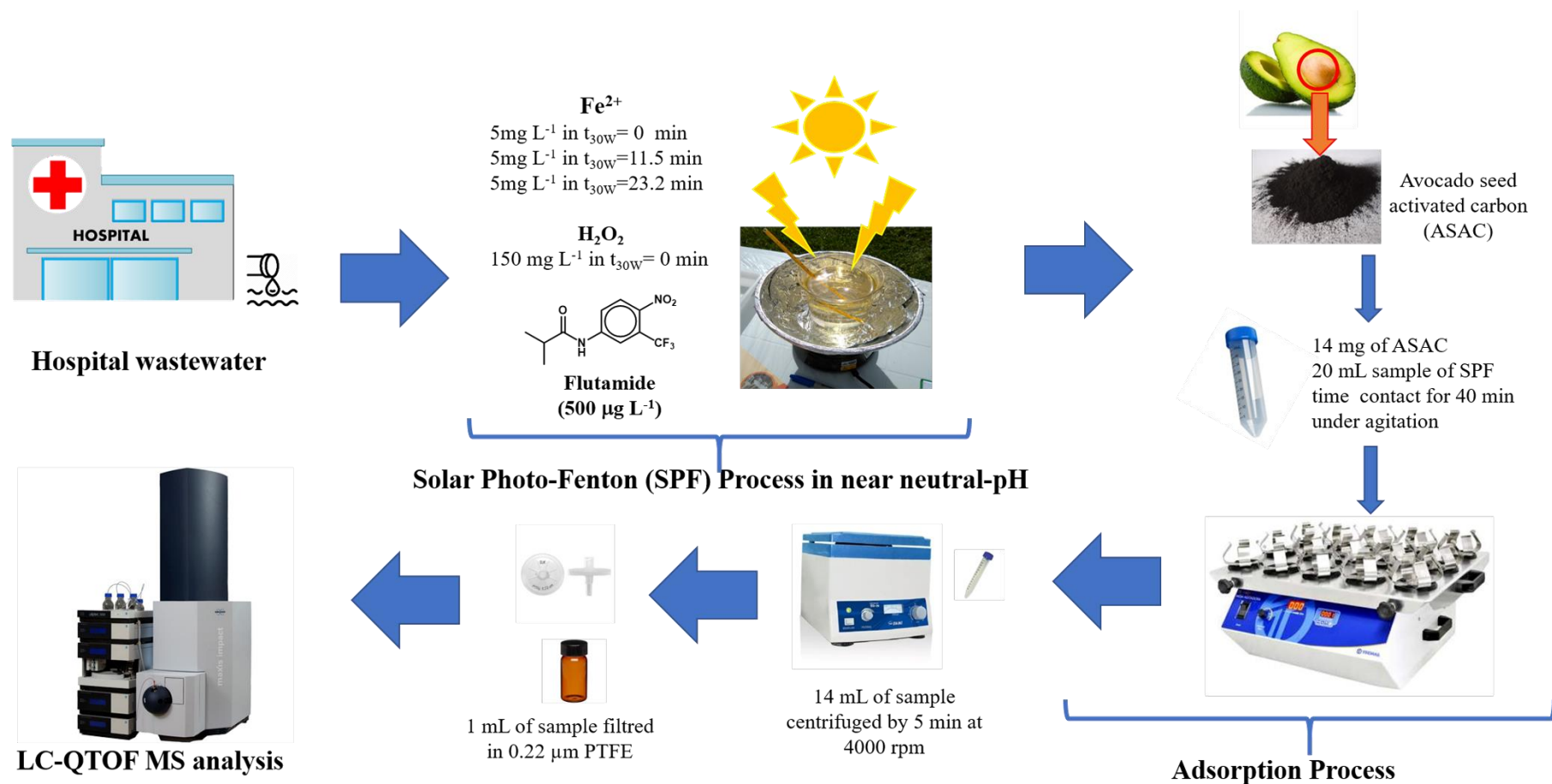
Figure S2. Scheme of the combined SPF process and adsorption process to remove FLUT and TPs.

References

American Public Health Association, American Water Works Association, Water Environmental Federation, 1998. Standard Methods for the examination of water and wastewater, 20th ed. ed. Washington.

Lopez, A., Pagano, M., Volpe, A., Di Pinto, A.C., 2004. Fenton's pre-treatment of mature landfill leachate. Chemosphere 54, 1005–1010. https://doi.org/10.1016/j.chemosphere.2003.09.015.

Capítulo 3

Combinação de processos terciários (foto-Fenton solar e adsorção) para o tratamento de efluentes hospitalares: remoção de fármacos e seus produtos de transformação

INTRODUÇÃO

O efluente hospitalar é uma matriz com alta carga de matéria orgânica e de micropoluentes de interesse emergente, principalmente fármacos das mais variadas classes. Em muitos países, ele é considerado um efluente industrial e precisa de tratamento no local de geração sendo, posteriormente, incorporado na rede de coleta de águas residuais doméstica. Por sua vez, em outros locais esse tipo de efluentes é aportado à rede de coleta de esgotos. Nas ETARs os efluentes passam por diferentes tipos de tratamentos sequenciais que têm por objetivo promover a redução de parâmetros macro, tais como: a demanda química de oxigênio (DQO), demanda bioquímica de oxigênio (DBO), sólidos suspensos, sólidos totais, dentre outros[6,84]. Contudo, em relação aos micropoluentes, como estes não são legislados, eles apenas são submetidos às diferentes etapas de tratamento, sem observar-se a sua redução ou eliminação ao final do processo[6,19]. A grande preocupação com os fármacos é que eles não estão presentes em forma individual, mas sim como uma mistura multicomponentes. Dessa forma, essa mescla de fármacos e metabólitos pode afetar significantemente os ecossistemas aquáticos[85–87]. Adicionalmente, analgésicos de fácil acesso,ou seja que são comercializados sem necessidade de prescrição médica, são uma das classes de compostos mais detectados nas águas residuais já tratadas pelas estações de tratamento, os quais podem apresentar efeito nocivos à fungos, bactérias e microrganismos dependentes do sistema aquático[88]. Outro fator preocupante está relacionado com a persistência dos fármacos no meio ambiente[89] uma vez que os tratamentos convencionais para potabilizar a água apresentam baixa eficiência na remoção desses microcontaminantes e que muitos dos fármacos têm sua administração de forma contínua, o que leva ao aporte continuado destes pelos usuários[90].

Nesse contexto, a utilização de tratamentos terciários vem sendo discutida e implementada em algumas regiões do mundo, nos últimos anos para viabilizar a remoção dos fármacos [61,91,92]. Diferentes estudos avaliaram tratamentos baseados no reagente de Fenton[93–95] e, também, os processos de adsorção, em especial com carvões ativos comerciais[39,41,82,96]. Assim, a combinação de processos terciários é uma temática recente de estudo que espera favorecer o sinergismo de diferentes tratamentos[97].

Adicionalmente o controle dos processos de tratamento requer o uso de técnicas analíticas instrumentais sofisticadas, em especial para acompanhar a eliminação dos fármacos

e se são gerados novos compostos (TPs) durante alguns dos processos de tratamento[98–100]. O uso de técnicas cromatográficas acopladas à espectrometria de massas de alta resolução, permite avaliar simultaneamente a eliminação dos fármacos e de (TPs). Esse processo pode ser automatizado fazendo uso de bases de dados especialmente construídas para a identificação de TPs[101–103].

OBJETIVO

Esse capítulo tem como finalidade avaliar o tratamento foto-Fenton solar de uma mistura de fármacos de nove compostos farmacêuticos (cloranfenicol, fluconazol, flutamida, furosemida, gemfibrozil, ibuprofeno, losartana, nimesulida e paracetamol) de diferentes características físico-químicas e funções terapêuticas presentes em efluente hospitalar e verificar a potencialidade de acoplamento do AOPs ao processo de adsorção para remoção dos fármacos e dos TPs. Ainda, para análise dos TPs foi construída uma base de dados de 127 TPs empregada na análise mediante a estratégia de triagem de suspeitos.

PRINCIPAIS RESULTADOS

Ao comparar a degradação da mistura de compostos farmacêuticos utilizando quatro abordagens: A) adição única de Fe^{2+} (5mg L^{-1}) e H_2O_2(50 mg L^{-1}) apenas no tempo inicial de tratamento; B) adição de H_2O_2(25 mg L^{-1}) e duas adições de Fe^{2+} (2,5 mg L^{-1} cada; uma em t_0 e outra em t = 10 min); C) adição de 50 mg L^{-1} de H_2O_2 e adição múltipla de Fe^{2+} (t_0 = 5 mg L^{-1}e outras duas adições de 2,5 mg L^{-1} nos tempos 5 e 10 min); D) adição única de 100 mg L^{-1} H_2O_2 e múltiplas adições de Fe^{2+} (no tempo inicial foram adicionados 5 mg L^{-1} e nos intervalos de 5 e 10 min 5 mg L^{-1})], a que apresentou melhor degradação foi a condição D. Nessa condição experimental, foram obtidas degradações superiores a 80% para o fluconazol e para os demais fármacos na ordem de 99%, em um tempo total de tratamento t_{30w}= 60 min. Ainda, nessa abordagem, todo o H_2O_2adicionado inicialmente, foi consumido. Em relação à formação de TPs durante o tratamento, o ápice de formação foi em t_{30w} = 15min. Já em t_{30w}= 45 min, se observa a degradação da maioria dos TPs observados em t_{30w} = 15min, com

exceção dos TPs do fluconazol que se mostram persistentes ao tratamento e são observados ainda no fim do tratamento t_{30W}= 60 min.

A construção da base de dados contendo informações de 127 TPs permitiu a identificação via triagem de suspeitos de 38 compostos. Nesse caso, foi observado que o cloranfenicol e losartana formavam 5 TPs. Para o fluconazol, furosemida e ibuprofeno foram observados quatro TPs. Para a flutamida, foram observados 8 TPs. O gemfibrozil formou apenas 1 TP e o paracetamol 2 TPs. Por fim, para a nimesulida foram identificados 3 TPs, e dois desses, tiveram suas estruturas químicas propostas.

A abordagem D foi selecionada e replicada até um t_{30W}= 15 min para avaliar o acople do processo foto-Fenton solar com a adsorção. Nesse tempo de foto-Fenton solar, foi encontrado um maior número de TPs, ou seja, optou-se por selecionar o pior cenário para o AOP para avaliar a performance do carvão ativo. Desta maneira, ao replicar as condições otimizadas para o processo de adsorção apresentadas no capítulo 2, foram obtidas taxas de remoção superiores a 99% para grande maioria dos compostos, com exceção dos TPs da flutamida que apresentam taxas de remoção próximas a 60%.

Foi realizado um teste para avaliar a redução do tempo de tratamento do processo de adsorção de 40 para 15 min. Essa possibilidade foi considerada pois, ao avaliar o gráfico de desejabilidade e gráfico de Pareto apresentados no capítulo 2, estes indicam que o tempo de adsorção não apresenta uma influência significativa na extração. Assim, foi reduzido o tempo de adsorção, sem alterar a eficiência do processo.

O detalhamento dos métodos, resultados, discussões e conclusões relacionados com esse estudo estão apresentados no **Artigo 3** e **Material Suplementar 3**.

Combination of tertiary solar photo-Fenton and adsorption processes in the treatment of hospital wastewater: The removal of pharmaceuticals and their transformation products

Alexandre Della-Flora , Marcelo L. Wilde , Diana Lima , Eder C. Lima , Carla Sirtori *

Instituto de Química, Universidade Federal do Rio Grande do Sul, Av. Bento Gonçalves 9500, CEP 91501-970 Porto Alegre, RS, Brazil

ARTICLE INFO

ABSTRACT

In this work, the degradation of a mixture of nine pharmaceuticals was performed in near environmental concentrations (500 μg L^{-1}) using hospital wastewater as the matrix and employing as a coupling strategy solar photo-Fenton (SPF) treatment followed by adsorption. Different SPF approaches were studied. The best condition chosen for the degradation of the pharmaceuticals by SPF was that which used an initial concentration of H_2O_2 of 100 mg L^{-1} and multiple additions of Fe^{2+} of 5 mg L^{-1} at times of t = 0, 5, and 10 min in hospital wastewater. Degradation of 80% was obtained for Fluconazole, whereas the degradation of other pharmaceuticals achieved 99% of primary elimination. Consequently, 38 Transformation Products (TPs) were generated by the SPF process. The combination of SPF with the adsorption process using avocado seed activated carbon (ASAC) as sorbent was used to prevent TPs reaching the aqueous environment. For this reason, the SPF process was stopped after 15 min; and within this time, the largest number of TPs (28 TPs) was observed. A volume of 20 mL of hospital wastewater (HWW) previously treated by SPF was combined with 14 mg ASAC, for 15 min of contact time. This coupling removed 30 of the 36 compounds (remaining pharmaceuticals and TPs), with an open-chain and highly polar TPs having a 50% and 60% removal for FLT TP2 and FLT TP3, respectively. With respect to compounds that present aromatic rings, these presented a 98–100% removal rate in the coupled processes, with π–π interactions as the main interaction mechanisms with ASAC.

1. Introduction

There is a type of pollution that has been worrying the scientific community: pharmaceuticals. Their short and long term effects on human health are uncertain. Even at μg L^{-1} levels, they can already affect organisms present in the environment as they are still biologically active even after excretion, furthermore, in the case of antibiotics, they can increase the spread of antimicrobial resistance [1–4]. The main contributor to this type of contamination is hospital wastewaters (HWW) [5]. The presence of pharmaceuticals in HWW is reported in the literature in the order of ng L^{-1} or μg L^{-1} [6,7]. In Brazil, the majority of the disposal of HWW is generally permitted into conventional sewage systems, with subsequent subjection to conventional treatments [8]. Despite this, unfortunately, not all residual wastewaters are collected for treatment in Brazil; with only 55% of domestic effluents being treated [9]. Conventional Sewage Treatment Plants (STPs) are not efficient for complete pharmaceutical removal. In general, STPs were designed using

primary and secondary treatments. In order to achieve the desired pharmaceutical removal, a tertiary treatment is necessary. According to Rodriguez-Mozaz et al. [10] tertiary treatment is the polishing step, which may ensure the removal of recalcitrant micropollutants, like pharmaceuticals and pharmaceutical metabolites. Moreover, tertiary treatment could contributes significantly to allow the inactivation and removal of pathogenic microorganisms from wastewaters [11].

Several tertiary treatments have been developed and researched for a huge variety of pharmaceutical compounds [12–14]. Advanced oxidation processes (AOPs) are gaining prominence due to the ability to remove different classes of pharmaceutical compounds [15–18]. Hydroxyl radicals are generated in situ in AOPs and are not selective. Among the AOPs, it is worth highlighting the processes that use Fenton reagents, a combination of Fe^{2+} and H_2O_2, to produce hydroxyl radicals. The great advantage of these processes is the ease of application, thus making them very versatile processes. When combined with UV radiation (photo-Fenton process), the efficiency of the process increases due

---

to the regeneration of the catalyst Fe^{3+} to Fe^{2+} [19]. Additionally, this process is directly affected by the pH, with acidic conditions (pH 2–4) being widely accepted as ideal for "traditional" Fenton and photo-Fenton processes. This acidic medium is necessary to guarantee the solubility of Fe^{2+} [19]. The photo-Fenton process becomes more environmental friendly when using solar radiation as a source of UV radiation, with the additional possibility of using pHs close to neutrality. According to Carra et al. [20] the work at circumneutral pH associate with multiple additions of Fe^{2+} (at intervals of 5 or 10 min) enables increasing the global efficiency of the treatment. Thus, when each fractionated amount of iron is added, Fe^{2+} reacts immediately with hydrogen peroxide, increasing the presence of hydroxyl radicals in the medium. Therefore, this strategy of working at near neutral pH combined with multiple additions of Fe^{2+} may present similar degradation results as the process performed in acid pH. Additionally, this strategy reduces the consumption of acids and bases to adjust the pH (initially and in the end of the "traditional" photo-Fenton process) and, sometimes, allowing treatment at the natural pH of the effluent [20–23]. Nonetheless, the main disadvantage of this type of application is when the process does not reach high mineralization levels, thus forming transformation products (TPs) [24, 25]. These TPs are compounds that have unknown properties. Moreover, these TPs could be more toxic, persistent, or bioaccumulative than their parent compound. Studies using *in silico* quantitative structure-activity relationships ((Q)SAR) have been used to increase information about the toxicity of these TPs [26–28].

The inevitable formation of TPs when achieving complete mineralization of pharmaceuticals through AOPs is difficult to handle, primarily if the process is carried out in complex matrices (e.g., HWW). In this sense, it would be possible to avoid the release of micropollutants, such as pharmaceuticals, into the environment by combining tertiary process treatments. Studies using a combination of SPF processes with other tertiary processes have removed recalcitrant pharmaceuticals [29–33]. In this way, the combination of nanofiltration with SPF using pilot plant systems can be an alternative in reducing 88% the treatment costs and 89% the hydrogen peroxide consumption [29]. In turn, Michael et al. [30] combined SPF process, performed in a CPC with treatment capacity of 100 L, with adsorption process using activated carbon and lab scale assay. The main results indicate an efficient disinfection of the effluent, with the complete elimination of toxicity and mitigation the presence of pharmaceuticals in the effluent [30]. The application of conventional biological treatments is efficient in reducing organic matter, macronutrients and micronutrients; however, for pharmaceuticals or TPs that are non-biodegradable, the removal is inefficient [34,35]. In turn, the adsorption process is very efficient in removing microcontaminants, due to its high surface area. The production of sorbent material from biomass can be considered as the main advantage of the adsorption process. The biomass may come from natural and renewable resources like avocado seeds, seed from *Caesalpinia ferrea*, grape seeds and peels, coconut shells, among others [36–38]. Moreover, these materials are not affected by pharmaceuticals and toxicological parameters of TPs, and their use has been recently evaluated as a single treatment for HWW [39]. Finally, it should be noted that the isolated use of both processes (AOPs or adsorption) has been extensively studied; however, the coupling of both treatment technologies is still rarely considered as an alternative for real wastewaters contaminated with pharmaceuticals and TPs.

This study's main objective is to evaluate the degradation of nine pharmaceuticals of different physical-chemical characteristics using the solar photo-Fenton process, assessing best treatment conditions for coupling with the adsorption process. In parallel, during the combined treatments, the TPs' formation/elimination was monitored through non-target screening using a purpose-built database containing up to 127 TPs.

2. Materials and methods

2.1. Chemicals

Chloramphenicol (CLO), fluconazole (FCZ), flutamide (FLT), furosemide (FRS), gemfibrozil (GFZ), ibuprofen (IBP), losartan (LOS), nimesulide (NMS), and paracetamol (PCT) were purchased from different suppliers with analytical grade (purity > 98.99%). Ammonium metavanadate, ascorbic acid, and 1,10-phenanthroline were purchased from Merck. Iron sulfate hexahydrate ($FeSO_4 \cdot 7H_2O$) was acquired from Reagen, and hydrogen peroxide (35% w/v) was purchased from Labsynth. Acetonitrile and methanol used for chromatographic analysis were of LC-MS grade and were purchased from Merck.

2.2. Solar photo-Fenton experiments

All drugs were weighed and dissolved together, in the same volumetric flask of 5 mL to prepare the stock solution (15 g L^{-1}). A mixture of acetonitrile and methanol (1:1, v/v) was used to ensure complete solubility. The HWW (see Tables S1 and S3 in the supplementary material) was fortified with 500 µg L^{-1} of each pharmaceutical using a volume of 33 µL of the stock solution. The pharmaceutical compounds selected for this study showing different physico-chemical characteristics and are representative from various pharmaceuticals classes. In this way, they could be employed as "model" compounds to evaluate the best strategy for the treatment of a real hospital effluent. The SPF was carried out in a cylindrical reactor with a volume capacity of 1 L, 0.897 m^2 of irradiation area, operated in batch mode (Fig. S1, supplementary material). In order to monitor the primary elimination of pharmaceuticals and TPs formation, aliquots were removed at predetermined experimental times for further LC-QTOF MS analysis. In addition, a volume of 200 µL sodium bisulfite (28%, w/v) was added to the sampled aliquots to quench the residual hydrogen peroxide. The initial pH condition of the SPF treatment was close to neutrality (pH 5.0). For this, the pH of the "raw" HWW (pH=9.2) (Table S1, supplementary material) was adjusted to pH 5.0 using H_2SO_4 (0.5 mol L^{-1}). With respect to the initial concentrations of Fe^{2+} and H_2O_2, four different approaches were evaluated: a) single addition, at the initial treatment time, of Fe^{2+} and H_2O_2 of 5 and 50 mg L^{-1}, respectively; b) a single addition of 25 mg L^{-1} H_2O_2 and multiple additions of Fe^{2+} (2.5 mg L^{-1} at initial treatment time and an additional concentration of 2.5 mg L^{-1} following 10 min of treatment); c) single addition of 50 mg L^{-1} H_2O_2 and multiple additions of Fe^{2+} (5 mg L^{-1} at initial treatment time and 2.5 mg L^{-1} at intervals of 5 and 10 min of treatment time); d) single addition of 100 mg L^{-1} H_2O_2 and multiple additions of Fe^{2+} (5 mg L^{-1} at initial treatment time and 5 mg L^{-1} at intervals of 5 and 10 min of treatment time). To ensure comparison of experiments on different days, the UV radiation (W m^{-2}) was monitored by a solar energy meter (ICEL SP-2000) at intervals of 2 min, so the total time of the experiment could be normalized using the $t_{30\,W}$ (Table S2, supplementary material) [19]. In addition, to verify whether the pharmaceuticals undergo hydrolysis or complexation with Fe^{2+}, experiments were carried out in the dark, at an initial pH of 5.0, with an initial concentration of 5 mg L^{-1} Fe^{2+} (only for complexation studies) and a total time of exposure of 60 min. Kinetic studies for the degradation of pharmaceuticals in SPF were performed using a pseudo-first-order kinetic model [40].

2.3. Instrumental analysis

The primary elimination of pharmaceuticals and TPs monitoring during the combined processes was performed using a liquid chromatography (LC) (Shimadzu-Nexera X2) system coupled with a hybrid mass analyzer Quadrupole-Time-Of-Flight (QTOF MS) (Impact II-Bruker Daltonics). Further details regarding instrumental conditions and the main parameters for provide TPs identification and the quantification method used to determine pharmaceuticals in this study are presented in

A. Della-Flora et al.   Journal of Environmental Chemical Engineering 9 (2021) 105666

87

the supplementary material (Text S3 and Table S3, respectively).

TPs identification formed during the SPF process in HWW were monitored using a purpose-built database appropriately developed for this study. An extensive review of each pharmaceutical TPs previously identified in current literature was carried out, and the database with information of 127 TPs (fragmentation pattern, molecular formula, and exact mass) was constructed. Such strategies have already been performed in other studies in our research group [41,42].

The determination of hydrogen peroxide was performed using the ammonium metavanadate method [43] and the total Fe using the 1,10 phenanthroline method [44]. Using properly calibrated equipment, mineralization was monitored using total organic carbon (TOC), with a multi N/C 2100S (Analytikjena) analyzer.

2.4. Adsorption using avocado seed for active carbon production

The adsorption process was carried out using the avocado seed as a raw material for activated carbon production. The process of obtaining activated carbon and its respective characterization has already been discussed in a previous study [37]. Similarly, the experimental conditions for the study in HWW were optimized in a previous study [45].

3. Results and discussion

3.1. Degradation of pharmaceuticals by SPF

Hydrolysis experiments were performed to check for possible pharmaceutical degradation. In batch 1 L reactor, an initial drug concentration of 500 µg L^{-1} in ultrapure water and pH 5 (experiment pH) was used to verify hydrolysis without adding Fenton reagents. An additional test was carried out to check the possibility of complexing formation between Fe^{2+} pharmaceuticals. The process was conducted by adding 5 mg L^{-1} of Fe^{2+} in an initial solution containing the mix of nine pharmaceuticals, each of them in a initial concentration of 500 µg L^{-1} in ultrapure water at pH 5 (experimental pH) but without adding H$_2$O$_2$. The total time of both tests was 60 min, in the dark, and aliquots were removed throughout the experiment. At the end of the hydrolysis experiment, a mere 10% decrease in the initial concentration of GFZ was observed, while for other pharmaceuticals, a decrease in initial concentration of around 5% was determined. As initial pharmaceutical concentrations were maintained at a constant in the presence of Fe^{2+} at the selected pH, the formation of possible complexes with the initial compounds was also not indicated by the experiment. These results demonstrate that the selected pharmaceuticals do not undergo hydrolysis or complexation in the experimental conditions evaluated in our study (Fig. S2, supplementary material).

The degradation process through SPF was based on four different approaches. The first approach, named approach "A", was carried out using a single addition of Fe^{2+} and H$_2$O$_2$ of 5 and 50 mg L^{-1}, respectively, only in the initial treatment time. In approach "A" (Fig. S3(A)), fast initial consumption of H$_2$O$_2$ ($\approx$30 mg L^{-1}) took place followed by very slow consumption throughout the treatment. This behavior may be related to the fact that in the first minutes of the process, there is a quick reaction between Fe^{2+} with H$_2$O$_2$ producing Fe^{3+}. Additionally, a decrease in total Fe concentration was observed (Fig. S3(A)), which may be associated with the iron complex formation and further precipitation.
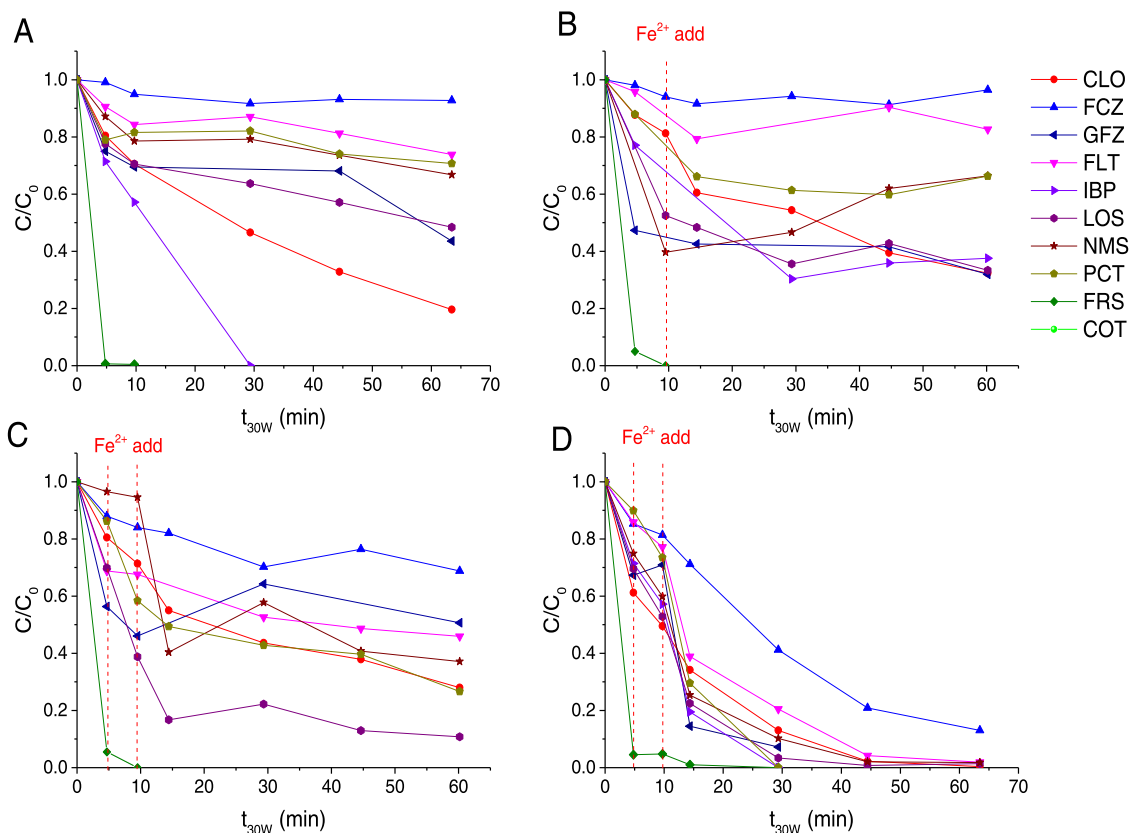
Fig. 1. Degradation profile of pharmaceuticals compounds in different SPF approaches. A) single addition of Fe^{2+} and H$_2$O$_2$ of 5 and 50 mg L^{-1} respectively only at the initial treatment time; B) addition H$_2$O$_2$ of 25 mg L^{-1} and multiple additions of Fe^{2+} (2.5 mg L^{-1} twice; one in t$_0$, and another in t = 10 min); C) addition of 50 mg L^{-1} de H$_2$O$_2$ and multiple addition of Fe^{2+} (t$_0$ = 5 mg L^{-1} and multiple additions of 2.5 mg L^{-1} in the times 5 and 10 min); D) single addition of 100 mg L^{-1} H$_2$O$_2$ and multiple additions of Fe^{2+} (in the initial time 5 mg L^{-1} were added and in the 5 and 10 min intervals of the experiment another 5 mg L^{-1} were added, respectively). Red dotted lines in (B), (C), and (D) indicated Fe^{2+} additions during the treatment time. (For interpretation of the references to colour in this figure legend, the reader is referred to the web version of this article.)

Besides the lower kinetic of Fe^{3+} to Fe^{2+} regeneration, iron complex formation and precipitation explain the slow H_2O_2 consumption up to the end of the SPF process in this approach. When comparing the H_2O_2 consumption with the primary elimination of pharmaceuticals (Fig. 1 (A)), it can be observed that there is a fast primary elimination of GFZ, LOS, CLO, and PCT above 20% with FRS elimination near 99% ($\approx$LOQ, see Table S3 in the supplementary material) in the first 5 min of treatment. Concerning the other parent compounds studied, after 60 min of SPF process, the primary elimination of GFZ and LOS reached close to 55%, whereas for FCZ it was 8%, while for FLT, PCT, IBP, and NMS, the primary elimination was in the range of 20–40%. Furthermore, the mineralization of 17% of the treatment was achieved.

In turn, approach "B" was carried out to reduce the initial concentration of H_2O_2 from 50 to 25 mg L^{-1} and multiple additions of Fe^{2+} (2.5 mg L^{-1} twice) was executed. Fig. S3(B) shows a rapid consumption of 15 mg L^{-1} H_2O_2 due to the first addition of Fe^{2+}. After the second Fe^{2+} aliquot addition, the consumption of 2.5 mg L^{-1} of H_2O_2 followed by a further slower H_2O_2 consumption was observed throughout the treatment. The behavior of total iron in the first 15 min of treatment remained constant. However, after $t_{30\ W}$= 30 min, there was a decrease in the total iron, which could be associated with possible loss by precipitation. The behavior of parent compounds in this approach (Fig. 1 (B)) showed a rapid degradation for LOS of 47%, and FRS was degraded below the LOD of the quantification method (Table S3, supplementary material) in $t_{30\ W}$= 10 min, whereas for CLO, GFZ, NMS, and PCT in $t_{30\ W}$= 15 min achieved a degradation of 40%, 57%, 47%, and 34%, respectively. At the end of treatment ($t_{30\ W}$=60 min), FCZ and FLT showed to be recalcitrant to the treatment achieving degradations of 3–18%, respectively. In relation to CLO, GFZ, IBP, and LOS, the degradation achieved were 67%, 68%, 62%, and 66%, respectively. Finally, the mineralization of approach "B" achieved 17% (the same value than approach A).

In approach "C", H_2O_2 initial concentration was maintained at 50 mg L^{-1}, with multiple Fe^{2+} additions ($t_0 = 5$ mg L^{-1} and 2.5 mg L^{-1} twice at 5 and 10 min) being performed. The H_2O_2 consumption profile (Fig. S3(C)) shows a rapid consumption of 25 mg L^{-1} of H_2O_2 followed by a slower consumption. The remaining H_2O_2 was approximately 18 mg L^{-1} in $t_{30\ W}$= 60 min. With respect to the total iron, the concentration behavior was constant. Concerning the primary elimination of the parent compounds (Fig. 1(C)), in 5 min of treatment time, approximately 20% of CLO was observed, whereas for GFZ and LOS a degradation of 44% and 30% were achieved, respectively. It was observed at $t_{30\ W} = 10$ min that the primary elimination of LOS increased from 30% to 61%, whereas for PCT, the primary elimination increased from 14% to 42%, and the FRS was degraded below the LOD. In the second addition of 2.5 mg L^{-1} of Fe^{2+}, NMS's primary elimination increased from 5% at $t_{30\ W}$ = 5 min to 60% $t_{30\ W}$= 10 min. At the end of the treatment ($t_{30\ W}$ = 60 min), the primary elimination of FCZ and FLT achieved was 31% and 54%, respectively. Concerning CLO, LOS, and PCT, the primary elimination was > 70%. However, the mineralization achieved for the approach "C" was only 10%.

Approach "D" was chosen to study the maximum amount of Fe^{2+} allowed by Brazilian legislation (15 mg L^{-1}) to be released in wastewater. The concentration of H_2O_2 was increased to 100 mg L^{-1} [46]. Fig. S3(D) (supplementary material) and indicated an immediate consumption of around 60% of H_2O_2 in the first 10 min of the SPF process. This behavior occurs due to the multiple additions of Fe^{2+}, increasing the catalyst's presence and producing extra HO• radicals compared to previous approaches. Furthermore, H_2O_2 was completely consumed by the end of treatment. This experimental condition's effect on the primary elimination of the pharmaceuticals studied is shown in Fig. 1(D). In the first 5 min of treatment time, rapid primary elimination of approximately 10% (PCT), 12% (FLT and FCZ), 22–32% (NMS, IBP, LOS, and GFZ), 39% (CLO), and 95% (FRS) was observed. After multiple successive additions of Fe^{2+}, degradation rates from 60% (FLT) to 93% (GFZ) were achieved. In $t_{30\ W}$ = 30 min, for FCZ, presented a degradation close to 60% while the other pharmaceuticals present a degradation above 80%. At the end of the treatment ($t_{30\ W}$=65 min), FCZ degradation reached about 80%, and 99% for the other pharmaceuticals ($\approx$LOQ, see Table S3 in supplementary material). Mineralization rate reached 22% in 45 min of treatment time (Fig. S3(D)), supplementary material).

Regarding the implications of HWW matrix for the mitigation of compounds studied, García-Muñoz et al. [47] observed for various AOPs that pharmaceuticals tend to be more reactive in comparison to other organic compounds commonly present in complex effluents. Additionally, studies indicate that ionic species frequently found in real complex matrices may act as sequestering agents for hydroxyl radicals, with less efficiency of pharmaceuticals degradation; or even, they may lead to the formation of less reactive radical species that would also imply a lesser reduction in the treatment of pharmaceuticals [48]. According to previous studies performed by our research group [25,45], the efficiency of the Fenton and photo-Fenton processes in HWW is affected by the presence of organic matter and different ionic species constituting the HWW. In turn, Bang et al. [49] observed that the degradation of microcontaminants has an opposite profile to the complexity of the aqueous matrix, represented by the chemical oxygen demand concentration. Therefore, the high reactivity of organic matter with hydroxyl radicals implies a less favorable performance of the treatment process, generally associated with an increase in the consumption of reagents and energy. The previous aspects may justify the results found in the present study, where the four approaches were carried out with a single mix of all selected pharmaceuticals only in a real HWW matrix.

3.2. Kinetical evaluation of the SPF process

Kinetical degradation of the pharmaceuticals compounds by SPF was studied in the four approaches. For FRS, it was not possible to determine the kinetic values due to the rapid elimination in all approaches performed. For LOS and NMS, during the approach "A", the kinetic adjustment of the degradation resulted in two stages of pseudo-first-order: a rapid primary degradation in the initial minutes, followed by a slower degradation. This same profile of degradation behavior is also observed for FCZ, GFZ, LOS, and NMS for approach "B", and in approach "C", for the pharmaceuticals CLO, FCZ, FLT, GFZ, and PCT. This behavior indicates that there is a rapid consumption of Fenton reagents in the initial minutes of the solar treatment, generating a rapid degradation of these pharmaceuticals and then a slower degradation throughout the treatment. For the other pharmaceuticals compounds in the various approaches, the degradation resulted in a kinetic adjustment that followed different pseudo-first-order models. Kinetic constant (k) values and r^2 can be seen in Tables S4-S7 (supplementary material).

3.3. Identification of TPs through SPF by means of LC-QTOF MS

To verify the formation of TPs by means of the SPF process in the different approaches studied, a purpose-built database was constructed with information from 127 TPs, provided by some articles reported in current literature and, in most cases, with an error less than 5 ppm. In our case, a total of 38 TPs were found in all approaches studied (see Table S8, supplementary material).

The degradation of CLO generated a total of five TPs (Fig. 2A). CLO TP2 ($C_{11}H_{11}Cl_2N_2O_6$, m/z 337.0001) and CLO TP3 ($C_{11}H_{11}Cl_2N_2O_6$, m/z 337.0012) are constitutional isomers and were formed through hydroxylation at different positions of the CLO molecule. According to Marson et al. [50], CLO TP6 is a product of the degradation of CLO TP2 and CLO TP3, formed through the elimination of $C_3H_5Cl_2NO_2$ (Fig. 2 (A)). Moreover, CLO TP16 ($C_{11}H_9Cl_2N_2O_5$, m/z 180.0302) was formed through hydrogen abstraction and double bond formation, which is evidenced by the increase in DBE when compared to CLO. Finally, CLO TP18 ($C_7H_4NO_4$, m/z 166.0141) was possibly formed from CLO TP3 throughout the aliphatic moiety elimination. Figs. S4-S7
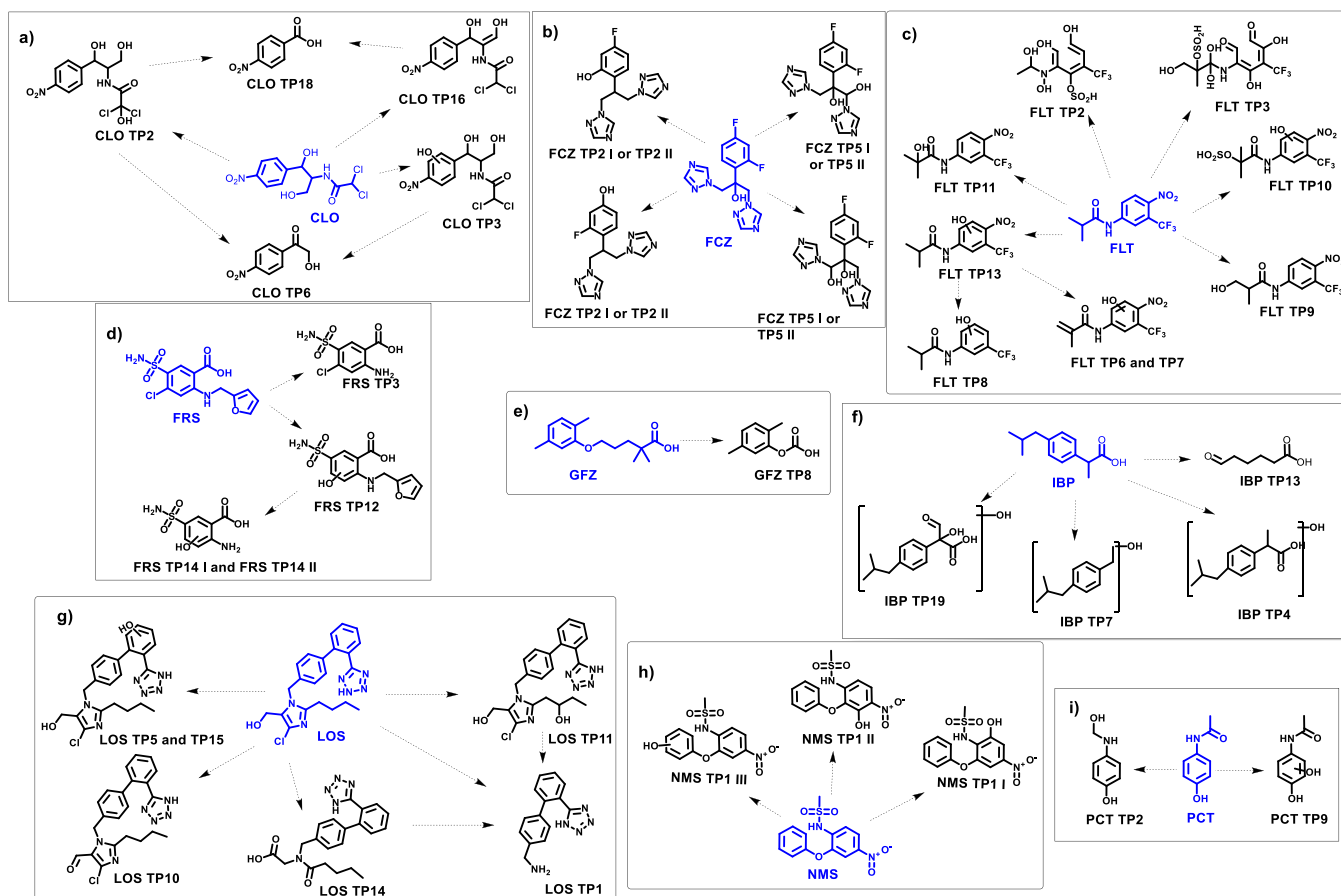
Fig. 2. TPs generated by SPF: a) CLO and TPs; b) FCZ and TPs; c) FLT and TPs; d) FRS and TPs; e) GFZ and GFZ TP8; f) IBP and TPs; g) LOS and TPs; h) NMS and TPs; i) PCT and TPs. In blue pharmaceutical compounds and TPs identified in black.

(supplementary material) show the CLO TPs profile (A/A$_0$, where A is the TP area and A$_0$ is the parent compound's initial area). Therefore, according to Fig. S4, it can also be considered that CLO TP6 and CLO TP18 could be the product of other TP by hydroxylation, followed by elimination of the aliphatic moiety because this TPs increasing in the final treatment time. Furthermore, CLO TPs were confirmed through ion fragments and retention time (Rt), which are associated, once the same conditions of analysis (chromatographic column, mobile phase composition and gradient, and equipment) were used in the study carried out previously by Marson et al. [50].

Four TPs were observed for FCZ. Two constitutional isomers with the same *m/z 303.1011* (FCZ TP2 I and FCZ TP2 II, C$_{13}$H$_{12}$FN$_6$O$_2$) throughout the purpose-built database and different Rt (2.5 and 3.0 min, respectively) were observed. These two TPs present a defluorination followed by a hydroxylation [51–53]. According to Lee et al. [54], through the frontier orbital theory, the position of the hydroxyl radical attack is governed by the radical reaction and its position is determined when the density of the sums of each electron occurs when they are in the highest occupied molecular orbital (HOMO) and in the lowest unoccupied molecular orbital (LUMO). In this context, one electron is in HOMO and another is in LUMO. Conversely, when electrolytic reactions take a place, the sum of electron densities are in HOMO (two electrons in HOMO) and, in turn, when nucleophilic reactions are performed, the sum of electron density is in LUMO (two electrons in LUMO). In accordance with Wan et al. [49], the positions in which fluorine is found in the FCZ molecule are those with the highest electronic density (one electron in HOMO and the other in LUMO), facilitating the radical reaction, and consequently favouring the hydroxylation in the position occupied previously for Fluor atom. In addition, two other constitutional isomers with the same *m/z* 321.0917 (C$_{13}$H$_{11}$F$_2$N$_6$O$_2$) FCZ TP5 I and FCZ

TP5 II but different Rts (2.62 and 2.84 min, respectively) have been reported [55]. The FCZ TP5 isomers have a hydroxyl addition, according to Hubicka et al. [55]. The methylene group in the triazole groups is more susceptible to hydroxyl attack. Conversely, for these four TPs mentioned, structural elucidations were not possible due to the lack of fragmentation pattern.

The degradation of FLT generated eight TPs. FLT TP2 (C$_9$H$_{11}$F$_3$NO$_7$S, *m/z* 334.0218), FLT TP3 (C$_{11}$H$_{13}$F$_3$NO$_{10}$S, *m/z* 408.0220), FLT TP6 (C$_{11}$H$_9$F$_3$N$_2$O$_4$, *m/z* 289.0439), FLT TP7 (C$_{11}$H$_8$F$_3$N$_2$O$_4$, *m/z* 289.0437), FLT TP8 (C$_{11}$H$_{11}$F$_3$NO$_2$, *m/z* 246.0745), FLT TP9 (C$_{11}$H$_{10}$F$_3$N$_2$O$_4$, *m/z* 291.0591), FLT TP10 (C$_{11}$H$_{10}$F$_3$N$_2$O$_7$S, *m/z* 371.0171), FLT TP11 (C$_{11}$H$_{10}$F$_3$N$_2$O$_4$, *m/z* 291.0591), and FLT TP13 (C$_{11}$H$_{10}$F$_3$N$_2$O$_4$, *m/z* 291.0598) were confirmed by the fragmentation pattern and mainly due to the retention time, as reported in a previous study [25]. According to Della-Flora et al. [25], the TPs are formed through different reactions, such as those with sulfur in their structure (FLT TP2, FLT TP3, and FLT TP10) are formed when NaHSO$_3$ is added to stop the reaction, being the end of treatment products. In addition, FLT TP13 was formed through hydroxylation in the aromatic ring, and FLT TP6 and FLT TP7 are products of the degradation of FLT TP13 (Fig. 2(C)) formed through hydrogen abstraction and double bond formation. Finally, the FLT TP8 was formed by eliminating the NO$_2$ group followed by hydroxylation in the aromatic ring.

FRS degradation resulted in a total of four identified TPs. FRS TP3 (C$_7$H$_6$ClN$_2$O$_4$S, *m/z* 248.9727), and FRS TP12 (C$_{12}$H$_{11}$N$_2$O$_6$S, *m/z* 311.0336) have been reported in the literature [56,57]. According to Katsura [57], FRS TP3 is 4-chloro-5-sulfamoyl-anthranilic acid (orsaluamine), a human metabolite FRS. The fragmentation pattern confirmed this TP. The formation of this TP occurs by the cleavage of the methyl furan bond, resulting in the formation of furfuryl alcohol plus saluamine

(FRS TP3). According to Katsura et al. [57], FRS TP12 undergoes a dechlorination step and hydroxyl addition in the same position. The fragmentation pattern found for this TP match with what was found in the literature [56,57]. Finally, two constitutional isomers with the same m/z 231.0081 ($C_7H_7N_2O_5S$) and Rts of 1.6 and 2.5 min were found for FRS TP14 I and FRS TP14 II, respectively. Jamiska et al. [56] commented that the formation of the FRS TP14 might result from the loss of the furanyl-methyl substituent, associated with the replacement of Cl by HO. Nonetheless, the exact position of the hydroxyl is difficult to state based on the fragmentation pattern information.

Concerning GFZ, a drug used to control cholesterol levels, only one TP was found in the SPF process. GFZ TP8 ($C_9H_9O_3$, m/z 165.0558) was referenced in a study by Chen et al. [58] with respect to the degradation of GFZ by heterogeneous photocatalysis. In that study, the formation of the superoxide anion leads to the formation of GFZ TP8. In processes that use TiO_2, this formation of the anions normal, but in processes that use Fenton reagents, the formations minor [59].

With regards to IBP, a widely used pharmaceutical for anti-inflammatory, analgesic, and other symptoms, four TPs were found in the SPF process. The IBP TP4 ($C_{13}H_{17}O_3$, m/z 221.1181) was formed by HO addition and this TP was only observed in the approach D. However, the position of this addition cannot be confirmed due to the lack of fragments [60]. The IBP TP7 ($C_{12}H_{17}O$, m/z 177.1285) was formed by decarboxylation and the addition of a hydroxyl [56,61]. The IBP TP13 ($C_6H_9O_3$, m/z 129.0558) was suggested with an aromatic ring opening [61]. Finally, the IBP TP19 ($C_{13}H_{15}O_5$, m/z 251.0923) was shown to contain the addition of two hydroxyls and one carbonyl group (addition of 3 oxygen) [62]. Nevertheless, Fabbri et al. [62] did not present any information that could justify the proposed structure. On the other hand, in our study, it was possible to predict hydroxyl and carbonyl groups' presence through the fragment m/z 149.0972 ($C_{10}H_{13}O$, error = −0.5 ppm).

Six TPs from LOS were identified. The imidazole ring-opening formed LOS TP1 ($C_{14}H_{12}N_5$, m/z 250.1100), and the fragment pattern found was the same as those reported in the literature [63]. Three LOS TPs isomers (LOS TP5, LOS TP11, and LOS TP15) were associated with the m/z 437.1498 ($C_{22}H_{22}ClN_6O_2$) and diverse Rts (4.95, 4.32, 4.82 min, respectively) given that all these TPs show an additional hydroxyl group in their chemical structures. LOS TP5 and LOS TP11 have characteristic fragment ions that are m/z 394.1328 ($C_{22}H_{21}ClN_3O_2$, error =1.8 ppm) and m/z 173.0487 ($C_7H_{10}ClN_2O$, error = −4.2 ppm), respectively [63]. For these two TPs, due to the fragmentation pattern/s, a structure is hereby proposed for one of them. The hydroxylation of LOS TP11 suggested being present on the butyl group. Such structural proposal was justified by the fragment ion of m/z 121.0300 (C_4H_8ClNO, error =−3.3 ppm) [63]. The other isomer, LOS TP15, was identified with the fragment ion m/z 279.1270 ($C_{15}H_{20}ClN_2O$, error= 0.4 ppm), which has not been reported previously. Based on the discrete fragmentation provided by bbCID(broadband collision-induced dissociation) data for LOS TP 15, it was impossible to elucidate the structure. LOS TP10 ($C_{22}H_{20}ClN_6O$, m/z 419.1386) presents an abstraction of hydrogen [63]. In this case, Serna-Galvis et al. [63] have suggest that the hydroxyl of the methyl group bonded to imidazole moiety is reduced to carbonyl. Conversely, in our study, the fragmentation profile was different from that published by Serna-Galvis et al. [63]. This might indicate that the TP observed in our study may be a constitutional isomer of the TP proposed by those authors. In LOS TP14($C_{21}H_{22}N_5O_3$, m/z 392.1740), the opening of pyrazole ring could be produced firstly due to the attack of hydroxyl radical, followed by the ring opening, with a loss of chloride amide and oxidation of secondary alcohols to ketone and primary alcohol to carboxyl group [64]. From the fragments reported by Carpinteiro et al. [64], the m/z 280.1092 ($C_{16}H_{14}N_3O_2$, error = 5.0 ppm) and m/z 252.103 ($C_{16}H_{14}NO_2$, error = −4.9 ppm) were found, confirming that TP.

Three constitutional isomers of NMS TP1 presenting an exact mass m/z 323.0343 ($C_{13}H_{11}N_2O_6S$, Rts 5.51, 5.73, and 5.94 min) were found.

These TPs have the HO addition in different positions of the aromatic ring. Koltsakidou et al. [28] found four isomers without a structural elucidation proposal for them. Conversely, in our study, the fragmentation pattern allowed us to propose the OH position of three isomers'. In the NMS TP1-I, the HO position was suggested at C7 (see Fig. S8, S9, and S10, supplementary material). According to the fragmentation pattern (Fig. S8, supplementary material), the m/z 243.0411 ($C_{12}H_7N_2O_4$, error = 1.8 ppm) demonstrates, firstly, the elimination of hydro-sulfonyl-methane moiety (-CH_3SO_2H). Subsequently, to stabilize the nitrogen (C2), a cycle was formed with oxygen (at C7), associated with the increment of one unit in the value of DBE (Fig. S8, supplementary material). In turn, NMS TP1-II ($C_{13}H_{11}N_2O_6S$, error = 1.9 ppm) showed a Rt of 5.73 min. In this case, the hydroxyl could be present in C4 (Fig. S9, supplementary material). This was justified by stabilizing the fragment m/z 134.0383 ($C_8H_6O_2$, error = 5.0 ppm) due to the aromatic ring's cleavage and the formation of a carbonyl moiety. Finally, the last isomer, the NMS TP1-III ($C_{13}H_{11}N_2O_6S$ error= 2.7 ppm), presented a Rt of 5.94 min and, possibly, presents the hydroxyl in somewhere in the aromatic ring at the positions of the C9–14 (Fig. S10, supplementary material).

Two TPs were found for PCT. One of them, PCT TP2 ($C_7H_8NO_2$, m/z 138.0556), was previously reported by Laurentiis et al. [65]. Nonetheless, the authors did not provide characteristic fragments in that study and did not make any proposition for this TP structure. PCT TP9 ($C_8H_8NO_3$, m/z 166.0509) has been reported in the literature with hydroxyl in its aromatic ring [65,66]. Unfortunately, in our study due to the limited fragmentation provided by bbCID, it was impossible to predict chemical structures for PCT TP2 and PCT TP9.

Among the SPF conditions evaluated, the total number of TPs (Fig. 3) observed in each different experiment, approach A presented the maximum number of TPs at $t_{30\,W}$ = 45 min of 23 TPs, whereas the minimum number of TPs was15 TPs at $t_{30\,W}$ = 60 min indicating stability and persistence for most compounds generated during SPF (Fig. S3, supplementary material). Concerning approaches B and C (Fig. 3), the number of TPs remained constant after reaching a peak at $t_{30\,W}$ = 15 min. As can be seen from Figs. S4 and S5 (supplementary material), the vast majority of their TPs achieve stability and persistence throughout the treatment. Finally, approach D presented the higher number of TPs (28) at $t_{30\,W}$ = 15 min and the lowest number of TPs (4) at $t_{30\,W}$ = 60 min. The TPs that are present at the end of the process, according to Fig. S7 (supplementary material) are: FLT TP13, FCZ TP2 II, FCZ TP2 I and FCZ TP5 I. Such behavior may be due to the degradation of the pharmaceuticals observed in Fig. 1D, where the addition of Fe^{2+}
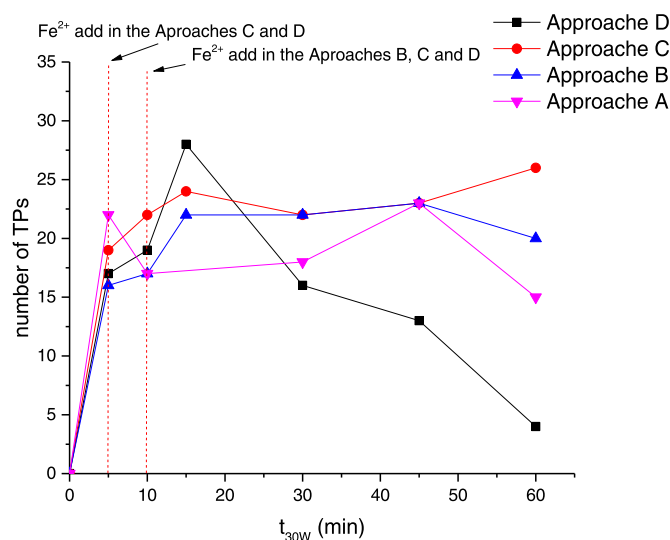
Fig. 3. Profile of the total TPs generated during different approaches evaluated by SPF.

increased the presence of hydroxyl radicals, which in turn increased the efficiency of the treatment that can be observed in Fig. S7 (supplementary material) of $t_{30\,W}$ = 30 min which shows a decay of TPs, indicating their degradation.

3.4. Combining treatments: SPF coupling with the adsorption process for removing TPs and remained pharmaceuticals

Approach D was selected at $t_{30\,W}$ = 15 min because at this treatment time the largest number of TPs (28) were identified. The idea was to simulate a condition where the SPF treatment achieved only partial degradation of the pharmaceuticals and generated many TPs. At this point, the efficiency of the coupling with the adsorption process was evaluated, with the "worst scenario" being simulated in the initial condition of the combined adsorption process. Thus, a new experiment was carried out, repeating the experimental condition and stopping the reaction at $t_{30\,W}$= 15 min, in order to carry out the adsorption process. The adsorption process was carried out by using avocado seed active carbon (ASAC), and the experimental conditions were optimized through a previous study [45], using 20 mL of sample, with 14 mg of ASAC in a contact time of 40 min, at a temperature of 25 ºC and pH 4. Moreover, tests to assess ASAC adsorption of the initial pharmaceutical mix in the HWW matrix were performed (see Table S11, supplementary material).

When analyzing the results of the combination of processes (Fig. 4), it is possible to observe a 40% and 60% removal for FLT TP2 and FLT TP3 while the removal of other compounds was between 98% and 100%. The compounds that present aromatic rings in their structures have high removal rates; however, for the opened chain TPs with polar characteristics, FLT TP2 and FLT TP3 present lower removal rates when compared to the other micropollutants with degradation values 46% and 62%, respectively. Despite the high removal rates for CLO, FCZ, and FLT, they are present in concentrations lower than LOD (Table S3, supplementary material). The complete removal indicated in this study is related to the detection sensitivity of the LC-QTOFMS in negative ionization mode (Table S3, supplementary material).

The efficiency of the adsorption process for removing pharmaceuticals and TPs is related to two main variables: the amount of activated

carbon mass and the activated carbon contact time. In our preceding study [45], it was noted that the optimization of ASAC for removal of FLT and its TPs do not have a significant degree of influence on the variable, the contact time of activated carbon and are therefore susceptible to decreasing the time without changing the efficiency of the adsorption process. Therefore, to verify the possibility of decreasing the total time of the adsorption process, another test was carried out to decrease the final treatment time to 15 min. As both treatments have similar removal results, a Student T-test was performed to assess whether the 15 min approach presents a significant degree of difference for the 40 min approach. As there was no significant difference (T_{calc}<T_{critc}) in the results presented in Table S10 (supplementary material), between the approaches, it was possible to decrease the time of the adsorption process to 15 min. Therefore, the Fig. 4 shows the result of the removal percentage for the combination of processes for the evaluated compounds.

The ASAC surfaces' characteristics make this AC positive due to its pH_{pzc} being close to neutrality [67]. This ensures electrostatic attraction on the ASAC surface due to the presence of deprotonated functional groups. The positively charged surface presence guarantees a Coulombic interaction for pharmaceuticals and TPs in their largest species at the negatively charged pH 4, favoring these compounds' adsorption [68]. This directly affects the molecules' binding mechanism, in which the positively charged surface has a stronger interaction with the anion and a strong repulsion with the cation [69]. In addition, as the experiments were carried out at pH 4, the degree of ionization and speciation of drugs and TPs were affected [70]. Fig. 5 shows the initial pharmaceuticals and TPs in their largest species at pH 4 in addition to the main adsorption mechanisms associated with their structures. With respect to negatively charged compounds FLT TP2 and FLT TP3, no significant removal was observed. This behavior is due to the fact that they are highly polar compounds and present interaction with water, making their removal difficult [71]. For the other two compounds that are negatively charged, an efficient removal was observed. Unlike open-chain TPs, CLO TP18 and IBP TP19 are TPs with aromatic rings, and the adsorption mechanisms involved are different. For pharmaceutical compounds and TPs containing aromatic rings, they show high removal rates (98–100%) because they are rich in electrons and can be in their neutral form,
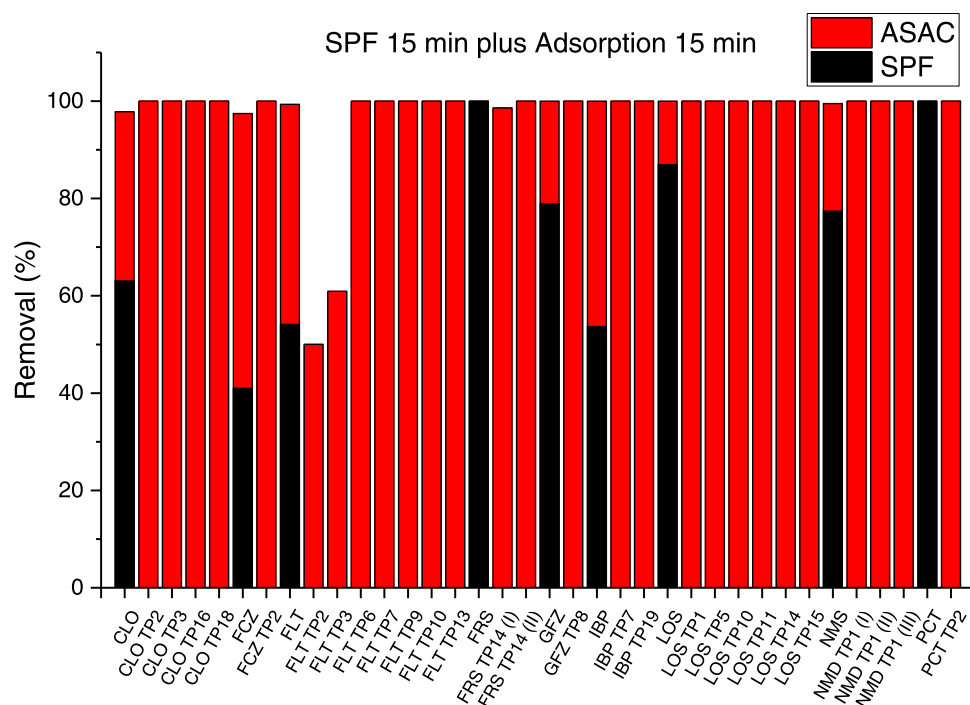
Fig. 4. Removal percentage after combining treatment processes using 15 min as contact time in the adsorption process.
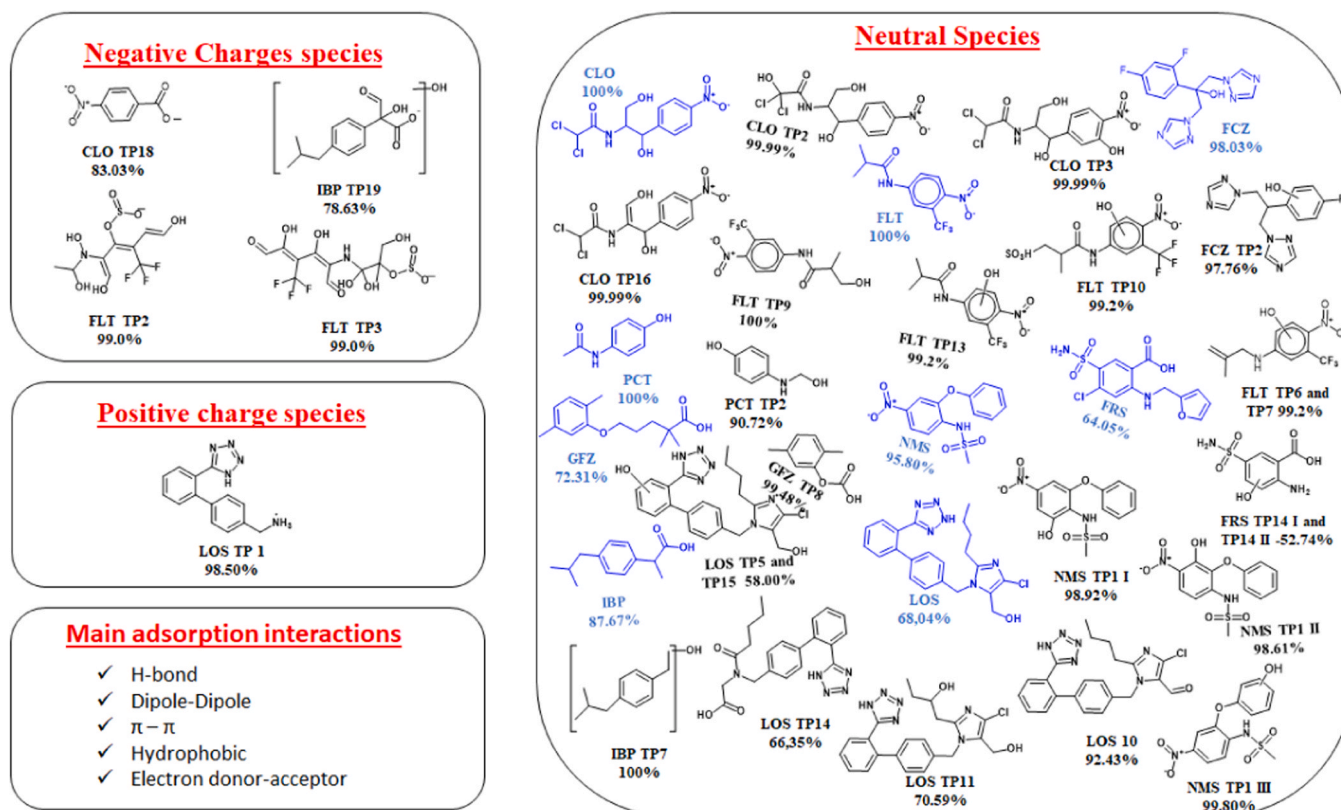
Fig. 5. Pharmaceuticals compounds and their TPs at pH 4, calculated by Marvin Sketch 20.14, and the adsorption process's main interactions. In blue pharmaceuticals and in black TPs.

leading to a low electrostatic interaction. The main mechanisms of these compounds are hydrophobic interactions, π-π interactions, dipole-dipole, electron donor-acceptor, and hydrogen bonds [69,72].

4. Conclusions

The SPF treatment was applied for the degradation of nine pharmaceuticals simultaneously in real hospital wastewater. Four different approaches were assessed to determine the best degradation profile for SPF treatment that was employed as pre-treatment. In SPF, Approach D presents the best degradation of the initial pharmaceuticals, at $t_{30w}= 65$ min. In these experimental conditions, FCZ presents a degradation rate of 80%, while for the other pharmaceuticals, a degradation of 99% ($\approx$LOQ) was observed in SPF treatment. Regarding the TPs generated by SPF, in the four approaches, a total of 38 different TPs were identified by a purpose-built database containing 127 TPs, and in approach D, at $t_{30\ W} = 15$ min thereby presenting the highest incidence of 28 TPs. Due to the high number of TPs formed and partial degradation of 29–99% for the initial pharmaceuticals under study, the treatment time of $t_{30\ W} = 15$ min was used to stop the SPF treatment and, later, to evaluate the combination with the adsorption process using ASAC.

The combination of the tertiary processes allowed the removal of 98–100% of the main micropollutants (initial pharmaceuticals + TPs). Nevertheless, some TPs like FLT TP2 and FLT TP3 presented a partial removal of 46% and 62%, respectively. This difference is associated with the fact that these two TPs present open chain and high polarity, presenting a strong interaction with water, unlike other micropollutants with aromatic rings and hydrophobicity. For initial pharmaceuticals and TPs with high removal rates, the main interactions are hydrophobic interactions, π-π, dipole-dipole, electron donor-acceptor, and hydrogen bonds. Finally, the possibility of reducing the ASAC contact time from 40 min to 15 min, makes this combination of processes, in the treatment of real hospital wastewater, a fast and efficient strategy with a period

time of 30 min.

CRediT authorship contribution statement

Alexandre Della-Flora: Investigation; Formal analysis; Writing - Original Draft; Visualization. **Marcelo L. Wilde:** Investigation; Formal analysis; Writing - Original Draft; Visualization. **Diana Lima:** Investigation. **Eder C. Lima:** Conceptualization; Writing - Original Draft; Supervision; Project administration. **Carla Sirtori:** Conceptualization; Writing - Original Draft; Supervision; Project administration; Funding acquisition.

Declaration of Competing Interest

The authors declare that they have no known competing financial interests or personal relationships that could have appeared to influence the work reported in this paper.

Acknowledgments

Appendix A. Supporting information

Supplementary data associated with this article can be found in the

online version at doi:10.1016/j.jece.2021.105666.

References

[1] K. Kümmerer, Pharmaceuticals in the environment, Annu. Rev. Environ. Resour. 35 (2010) 57–75, https://doi.org/10.1146/annurev-environ-052809-161223.

[2] A.J. Ebele, M. Abou-Elwafa Abdallah, S. Harrad, Pharmaceuticals and personal care products (PPCPs) in the freshwater aquatic environment, Emerg. Contam. 3 (2017) 1–16, https://doi.org/10.1016/j.emcon.2016.12.004.

[3] P. Grenni, V. Ancona, A. Barra Caracciolo, Ecological effects of antibiotics on natural ecosystems: a review, Microchem. J. 136 (2018) 25–39, https://doi.org/10.1016/j.microc.2017.02.006.

[4] Wellcome Trust, Initiatives for addressing antimicrobial resistance in the environment: current situation and challenges, 2018. ⟨https://wellcome.ac.uk/sites/default/files/antimicrobial-resistance-environment-report.pdf⟩.

[5] P. Verlicchi, A. Galletti, M. Petrovic, D. Barceló, Hospital effluents as a source of emerging pollutants: an overview of micropollutants and sustainable treatment options, J. Hydrol. 389 (2010) 416–428, https://doi.org/10.1016/j.jhydrol.2010.06.005.

[6] J. Xiang, M. Wu, J. Lei, C. Fu, J. Gu, G. Xu, The fate and risk assessment of psychiatric pharmaceuticals from psychiatric hospital effluent, Ecotoxicol. Environ. Saf. 150 (2018) 289–296, https://doi.org/10.1016/j.ecoenv.2017.12.049.

[7] S. Afsa, K. Hamden, P.A. Lara Martin, H. Ben Mansour, Occurrence of 40 pharmaceutically active compounds in hospital and urban wastewaters and their contribution to Mahdia coastal seawater contamination, Environ. Sci. Pollut. Res. 27 (2020) 1941–1955, https://doi.org/10.1007/s11356-019-06866-5.

[8] Brazil, Resolução – RDC/ANVISA no 306, de 7 de dezembro de 2004, 2004.

[9] BRASIL, ATLAS ESGOTOS Despoluição das Bacias Hidrográficas, (2020). ⟨http://atlasesgotos.ana.gov.br/⟩ (accessed March 23, 2020).

[10] S. Rodriguez-Mozaz, D. Lucas, D. Barceló, in: P. Verlicchi (Ed.), Full-Scale Plants for Dedicated Treatment of Hospital Effluents BT - Hospital Wastewaters: Characteristics, Management, Treatment and Environmental Risks, Springer International Publishing, Cham, 2018, pp. 189–208, https://doi.org/10.1007/698_2017_13.

[11] M.I. Polo-López, J.A.Sánchez Pérez, Perspectives of the solar photo-Fenton process against the spreading of pathogens, antibiotic-resistant bacteria and genes in the environment, Curr. Opin. Green Sustain. Chem. 27 (2021) 100416, https://doi.org/10.1016/j.cogsc.2020.100416.

[12] P. Verlicchi, M. Al Aukidy, E. Zambello, What have we learned from worldwide experiences on the management and treatment of hospital effluent? — an overview and a discussion on perspectives, Sci. Total Environ. 514 (2015) 467–491, https://doi.org/10.1016/j.scitotenv.2015.02.020.

[13] L. Rizzo, S. Malato, D. Antakyali, V.G. Beretsou, M.B. Đolić, W. Gernjak, E. Heath, I. Ivancev-Tumbas, P. Karaolia, A.R. Lado Ribeiro, G. Mascolo, C.S. McArdell, H. Schaar, A.M.T. Silva, D. Fatta-Kassinos, Consolidated vs new advanced treatment methods for the removal of contaminants of emerging concern from urban wastewater, Sci. Total Environ. 655 (2019) 986–1008, https://doi.org/10.1016/j.scitotenv.2018.11.265.

[14] N.A. Khan, S.U. Khan, S. Ahmed, I.H. Farooqi, M. Yousefi, A.A. Mohammadi, F. Changani, Recent trends in disposal and treatment technologies of emerging-pollutants- A critical review, Trends Anal. Chem. 122 (2020) 115744, https://doi.org/10.1016/j.trac.2019.115744.

[15] I. Carra, J.A. Sánchez-Pérez, S. Malato, O. Autin, B. Jefferson, P. Jarvis, Performance of different advanced oxidation processes for tertiary wastewater treatment to remove the pesticide acetamiprid, J. Chem. Technol. Biotechnol. 91 (2014) 72–81, https://doi.org/10.1002/jctb.4577.

[16] G. Shankaraiah, S. Poodari, D. Bhagawan, V. Himabindu, S. Vidyavathi, Degradation of antibiotic norfloxacin in aqueous solution using advanced oxidation processes (AOPs)—A comparative study, Desalin. Water Treat. 57 (2016) 27804–27815, https://doi.org/10.1080/19443994.2016.1176960.

[17] S. Miralles-Cuevas, D. Darowna, A. Wanag, S. Mozia, S. Malato, I. Oller, Comparison of UV/H2O2, UV/S2O82−, solar/Fe(II)/H2O2 and solar/Fe(II)/S2O82− at pilot plant scale for the elimination of micro-contaminants in natural water: An economic assessment, Chem. Eng. J. 310 (2017) 514–524, https://doi.org/10.1016/j.cej.2016.06.121.

[18] M. Roccamante, I. Salmerón, A. Ruiz, I. Oller, S. Malato, New approaches to solar Advanced Oxidation Processes for elimination of priority substances based on electrooxidation and ozonation at pilot plant scale, Catal. Today (2019) https://doi.org/10.1016/j.cattod.2019.04.014.

[19] S. Malato, P. Fernández-Ibáñez, M.I. Maldonado, J. Blanco, W. Gernjak, Decontamination and disinfection of water by solar photocatalysis: recent overview and trends, Catal. Today 147 (2009) 1–59, https://doi.org/10.1016/j.cattod.2009.06.018.

[20] I. Carra, J.L. Casas López, L. Santos-Juanes, S. Malato, J.A.Sánchez Pérez, Iron dosage as a strategy to operate the photo-Fenton process at initial neutral pH, Chem. Eng. J. 224 (2013) 67–74, https://doi.org/10.1016/j.cej.2012.09.065.

[21] E.C. Lumbaque, D.S. Araújo, T.M. Klein, E.R.L. Tiburtius, J. Argüello, C. Sirtori, Solar photo-Fenton-like process at neutral pH: Fe(III)-EDDS complex formation and optimization of experimental conditions for degradation of pharmaceuticals, Catal. Today 328 (2019) 259–266, https://doi.org/10.1016/j.cattod.2019.01.006.

[22] S. Arzate, M.C. Campos-Mañas, S. Miralles-Cuevas, A. Agüera, J.L. García Sánchez, J.A.S.ánchez Pérez, Removal of contaminants of emerging concern by continuous flow solar photo-Fenton process at neutral pH in open reactors, J. Environ. Manag. 261 (2020) 110265, https://doi.org/10.1016/j.jenvman.2020.110265.

[23] E.P. Costa, M. Roccamante, C.C. Amorim, I. Oller, J.A. Sánchez Pérez, S. Malato, New trend on open solar photoreactors to treat micropollutants by photo-Fenton at circumneutral pH: increasing optical pathway, Chem. Eng. J. 385 (2020), 123982, https://doi.org/10.1016/j.cej.2019.123982.

[24] I. Carra, C. Sirtori, L. Ponce-Robles, J.A. Sánchez Pérez, S. Malato, A. Agüera, Degradation and monitoring of acetamiprid, thiabendazole and their transformation products in an agro-food industry effluent during solar photo-Fenton treatment in a raceway pond reactor, Chemosphere 130 (2015) 73–81, https://doi.org/10.1016/j.chemosphere.2015.03.001.

[25] A. Della-flora, M.L. Wilde, I.D.F. Pinto, É.C. Lima, C. Sirtori, Degradation of the anticancer drug flutamide by solar photo-Fenton treatment at near-neutral pH: Identification of transformation products and in silico (Q)SAR risk assessment, Environ. Res. 183 (2020), 109223, https://doi.org/10.1016/j.envres.2020.109223.

[26] M.L. Wilde, J. Menz, C. Leder, K. Kümmerer, Combination of experimental and in silico methods for the assessment of the phototransformation products of the antipsychotic drug/metabolite Mesoridazine, Sci. Total Environ. 618 (2018) 697–711, https://doi.org/10.1016/j.scitotenv.2017.08.040.

[27] X. Ao, W. Sun, S. Li, C. Yang, C. Li, Z. Lu, Degradation of tetracycline by medium pressure UV-activated peroxymonosulfate process: influencing factors, degradation pathways, and toxicity evaluation, Chem. Eng. J. 361 (2019) 1053–1062, https://doi.org/10.1016/j.cej.2018.12.133.

[28] A Koltsakidou, M. Antonopoulou, E Evgenidou, I. Konstantinou, D. Lambropoulou, A comparative study on the photo-catalytic degradation of Cytarabine anticancer drug under Fe3+/H2O2, Fe3+/S2O82−, and [Fe(C2O4)3]3−/H2O2 processes. Kinetics, identification, and in silico toxicity assessment of generated transformation products, Environ. Sci. Pollut. Res. 26 (2019) 7772–7784, https://doi.org/10.1007/s11356-018-4019-2.

[29] S. Miralles-Cuevas, I. Oller, A. Ruiz Aguirre, J.A. Sánchez Pérez, S. Malato Rodríguez, Removal of pharmaceuticals at microg L−1 by combined nanofiltration and mild solar photo-Fenton, Chem. Eng. J. 239 (2014) 68–74, https://doi.org/10.1016/j.cej.2013.10.047.

[30] S. Miralles-Cuevas, I. Oller, J.A.S. Pérez, S. Malato, Application of solar photo-Fenton at circumneutral pH to nanofiltration concentrates for removal of pharmaceuticals in MWTP effluents, Environ. Sci. Pollut. Res. 22 (2015) 846–855, https://doi.org/10.1007/s11356-014-2871-2.

[31] M. Brienza, S. Nir, G. Plantard, V. Goetz, S. Chiron, Combining micelle-clay sorption to solar photo-Fenton processes for domestic wastewater treatment, Environ. Sci. Pollut. Res. 26 (2019) 18971–18978, https://doi.org/10.1007/s11356-018-2491-3.

[32] A. Gallego-Schmid, R.R.Z. Tarpani, S. Miralles-Cuevas, A. Cabrera-Reina, S. Malato, A. Azapagic, Environmental assessment of solar photo-Fenton processes in combination with nanofiltration for the removal of micro-contaminants from real wastewaters, Sci. Total Environ. 650 (2019) 2210–2220, https://doi.org/10.1016/j.scitotenv.2018.09.361.

[33] S.G. Michael, I. Michael-Kordatou, V.G. Beretsou, T. Jäger, C. Michael, T. Schwartz, D. Fatta-Kassinos, Solar photo-Fenton oxidation followed by adsorption on activated carbon for the minimisation of antibiotic resistance determinants and toxicity present in urban wastewater, Appl. Catal. B Environ. 244 (2019) 871–880, https://doi.org/10.1016/j.apcatb.2018.12.030.

[34] K.M. Onesios, J.T. Yu, E.J. Bouwer, Biodegradation and removal of pharmaceuticals and personal care products in treatment systems: a review, Biodegradation 20 (2009) 441–466, https://doi.org/10.1007/s10532-008-9237-8.

[35] L. Ferrando-Climent, S. Rodriguez-Mozaz, D. Barceló, Incidence of anticancer drugs in an aquatic urban system: from hospital effluents through urban wastewater to natural environment, Environ. Pollut. 193 (2014) 216–223, https://doi.org/10.1016/j.envpol.2014.07.002.

[36] C. Sophia A, E.C. Lima, Removal of emerging contaminants from the environment by adsorption, Ecotoxicol. Environ. Saf. 150 (2018) 1–17, https://doi.org/10.1016/j.ecoenv.2017.12.026.

[37] A.B. Leite, C. Saucier, E.C. Lima, G.S. dos Reis, C.S. Umpierres, B.L. Mello, M. Shirmardi, S.L.P. Dias, C.H. Sampaio, Activated carbons from avocado seed: optimisation and application for removal of several emerging organic compounds, Environ. Sci. Pollut. Res. 25 (2018) 7647–7661, https://doi.org/10.1007/s11356-017-1105-9.

[38] F.M. Kasperiski, E.C. Lima, C.S. Umpierres, G.S. dos Reis, P.S. Thue, D.R. Lima, S.L.P. Dias, C. Saucier, J.B. da Costa, Production of porous activated carbons from Caesalpinia ferrea seed pod wastes: highly efficient removal of captopril from aqueous solutions, J. Clean. Prod. 197 (2018) 919–929, https://doi.org/10.1016/j.jclepro.2018.06.146.

[39] D.R. Lima, A. Hosseini-Bandegharaei, P.S. Thue, E.C. Lima, Y.R.T. de Albuquerque, G.S. dos Reis, C.S. Umpierres, S.L.P. Dias, H.N. Tran, Efficient acetaminophen removal from water and hospital effluents treatment by activated carbons derived from Brazil nutshells, Colloids Surf. A Physicochem. Eng. Asp. 583 (2019) 123966, https://doi.org/10.1016/j.colsurfa.2019.123966.

[40] J.H. Sun, S.P. Sun, M.H. Fan, H.Q. Guo, L.P. Qiao, R.X. Sun, A kinetic study on the degradation of p-nitroaniline by Fenton oxidation process, J. Hazard. Mater. 148 (2007) 172–177, https://doi.org/10.1016/j.jhazmat.2007.02.022.

[41] E.C. Lumbaque, R.M. Cardoso, A. Dallegrave, L.O. dos Santos, M. Ibáñez, F. Hernández, C. Sirtori, Pharmaceutical removal from different water matrixes by Fenton process at near-neutral pH: Doehlert design and transformation products identification by UHPLC-QTOF MS using a purpose-built database, J. Environ. Chem. 6 (2018) 3951–3961, https://doi.org/10.1016/j.jece.2018.05.051.

[42] E.C. Lumbaque, M.L. Wilde, F.A. Lopes, E. de, S.A. Duarte, E.R.L. Tiburtius, M.B. Rodrigues, C. Sirtori, Degradation of a mixture of pharmaceuticals in hospital wastewater by a zero-valent scrap iron (ZVSI) combined reduction-oxidation

process, J. Water Process Eng. 37 (2020), 101410, https://doi.org/10.1016/j.jwpe.2020.101410.

[43] R.F.P. Nogueira, M.C. Oliveira, W.C. Paterlini, Simple and fast spectrophotometric determination of H_2O_2 in photo-Fenton reactions using metavanadate, Talanta 66 (2005) 86–91, https://doi.org/10.1016/j.talanta.2004.10.001.

[44] ISO 6332, Water quality - Determination of iron - Spectrometric method using 1,10-phenanthroline, 1988.

[45] A. Della-Flora, M.L. Wilde, P.S. Thue, D. Lima, E.C. Lima, C. Sirtori, Combination of solar photo-Fenton and adsorption process for removal of the anticancer drug Flutamide and its transformation products from hospital wastewater, J. Hazard. Mater. 396 (2020), 122699, https://doi.org/10.1016/j.jhazmat.2020.122699.

[46] Brazil, MINISTÉRIO DO MEIO AMBIENTE. CONSELHO NACIONAL DO MEIO AMBIENTE (CONAMA). RESOLUÇÃO No 430, DE 13 DE MAIO DE 2011, 2011.

[47] P. García-Muñoz, G. Pliego, J.A. Zazo, M. Munoz, Z.M. de Pedro, A. Bahamonde, J. A. Casas, Treatment of hospital wastewater through the CWPO-Photoassisted process catalyzed by ilmenite, J. Environ. Chem. Eng. 5 (2017) 4337–4343, https://doi.org/10.1016/j.jece.2017.08.023.

[48] G.M. Lanzafame, M. Sarakha, D. Fabbri, D. Vione, Degradation of methyl 2-aminobenzoate (methyl anthranilate) by H_2O_2/UV: effect of inorganic anions and derived radicals, Molecules 22 (2017) 619, https://doi.org/10.3390/molecules22040619.

[49] H. Bang, Y.M. Slokar, G. Ferrero, J.C. Kruithof, M.D. Kennedy, Removal of taste and odor causing compounds by UV/H_2O_2 treatment: effect of the organic and inorganic water matrix, Desalin. Water Treat. 57 (2016) 27485–27494, https://doi.org/10.1080/19443994.2016.1177274.

[50] E.O. Marson, C.E. Paniagua, N.M. Costa-Serge, R.M. Sousa, G.D. Silva, R.W. Becker, C. Sirtori, M.C.V.M. Starling, S.R. Carvalho, A.G. Trovó, Chemical and toxicological evaluation along with unprecedented transformation products during photolysis and heterogeneous photocatalysis of chloramphenicol in different aqueous matrices, Environ. Sci. Pollut. Res. (2020), https://doi.org/10.1007/s11356-020-09756-3.

[51] Z.-F. Chen, G.-G. Ying, Y.-X. Jiang, B. Yang, H.-J. Lai, Y.-S. Liu, C.-G. Pan, F.-Q. Peng, Photodegradation of the azole fungicide fluconazole in aqueous solution under UV-254: kinetics, mechanistic investigations and toxicity evaluation, Water Res. 52 (2014) 83–91, https://doi.org/10.1016/j.watres.2013.12.039.

[52] D. Wan, G. Zhang, Y. Chen, X. Lu, Y. Zuo, Photogeneration of hydroxyl radical in Fe (III)-citrate-oxalate system for the degradation of fluconazole: mechanism and products, Environ. Sci. Pollut. Res. 26 (2019) 8640–8649, https://doi.org/10.1007/s11356-019-04348-2.

[53] J.-F. Yang, L.-M. Yang, S.-B. Zhang, L.-H. Ou, C.-B. Liu, L.-Y. Zheng, Y.-F. Yang, G.-G. Ying, S.-L. Luo, Degradation of azole fungicide fluconazole in aqueous solution by thermally activated persulfate, Chem. Eng. J. 321 (2017) 113–122, https://doi.org/10.1016/j.cej.2017.03.103.

[54] B.-D. Lee, M. Iso, M. Hosomi, Prediction of Fenton oxidation positions in polycyclic aromatic hydrocarbons by Frontier electron density, Chemosphere 42 (2001) 431–435, https://doi.org/10.1016/S0045-6535(00)00061-8.

[55] U. Hubicka, J. Krzek, P. Zmudzki, B. Juromska-Witek, D. Motyl, A. Kryczyk, Determination of fluconazole and its oxidation products with kinetic evaluation under potassium permanganate treatment in acidic solutions by ultra performance liquid chromatography-tandem mass spectrometry, Acta Pol. Pharm. Drug Res. 76 (2019) 19–27, https://doi.org/10.32383/appdr/93513.

[56] A. Jakimska, M. Śliwka-Kaszyńska, J. Reszczyńska, J. Namieśnik, A. Kot-Wasik, Elucidation of transformation pathway of ketoprofen, ibuprofen, and furosemide in surface water and their occurrence in the aqueous environment using UHPLC-QTOF-MS, Anal. Bioanal. Chem. 406 (2014) 3667–3680, https://doi.org/10.1007/s00216-014-7614-1.

[57] S. Katsura, N. Yamada, A. Nakashima, S. Shiraishi, T. Furuishi, H. Ueda, Identification of furosemide photodegradation products in water–acetonitrile mixture, Chem. Pharm. Bull. 63 (2015) 617–627, https://doi.org/10.1248/cpb.c15-00122.

[58] P. Chen, F. Wang, Z.-F. Chen, Q. Zhang, Y. Su, L. Shen, K. Yao, Y. Liu, Z. Cai, W. Lv, G. Liu, Study on the photocatalytic mechanism and detoxicity of gemfibrozil by a sunlight-driven TiO2/carbon dots photocatalyst: the significant roles of reactive oxygen species, Appl. Catal. B Environ. 204 (2017) 250–259, https://doi.org/10.1016/j.apcatb.2016.11.040.

[59] S. Giannakis, M.I. Polo López, D. Spuhler, J.A. Sánchez Pérez, P. Fernández Ibáñez, C. Pulgarin, Solar disinfection is an augmentable, in situ-generated photo-Fenton reaction—Part 1: a review of the mechanisms and the fundamental aspects of the process, Appl. Catal. B Environ. 199 (2016) 199–223, https://doi.org/10.1016/j.apcatb.2016.06.009.

[60] Y. Xiang, J. Fang, C. Shang, Kinetics and pathways of ibuprofen degradation by the UV/chlorine advanced oxidation process, Water Res. 90 (2016) 301–308, https://doi.org/10.1016/j.watres.2015.11.069.

[61] I. Michael, A. Achilleos, D. Lambropoulou, V.O. Torrens, S. Pérez, M. Petrović, D. Barceló, D. Fatta-Kassinos, Proposed transformation pathway and evolution profile of diclofenac and ibuprofen transformation products during (sono) photocatalysis, Appl. Catal. B Environ. 147 (2014) 1015–1027, https://doi.org/10.1016/j.apcatb.2013.10.035.

[62] D. Fabbri, M.J. López-Muñoz, A. Daniele, C. Medana, P. Calza, Photocatalytic abatement of emerging pollutants in pure water and wastewater effluent by TiO2 and Ce-ZnO: degradation kinetics and assessment of transformation products, Photochem. Photobiol. Sci. 18 (2019) 845–852, https://doi.org/10.1039/C8PP00311D.

[63] E.A. Serna-Galvis, L. Isaza-Pineda, A. Moncayo-Lasso, F. Hernández, M. Ibáñez, R. A. Torres-Palma, Comparative degradation of two highly consumed antihypertensives in water by sonochemical process. Determination of the reaction zone, primary degradation products and theoretical calculations on the oxidative process, Ultrason. Sonochem. 58 (2019), 104635, https://doi.org/10.1016/j.ultsonch.2019.104635.

[64] I. Carpinteiro, G. Castro, I. Rodríguez, R. Cela, Free chlorine reactions of angiotensin II receptor antagonists: kinetics study, transformation products elucidation and in-silico ecotoxicity assessment, Sci. Total Environ. 647 (2019) 1000–1010, https://doi.org/10.1016/j.scitotenv.2018.08.082.

[65] E. De Laurentiis, C. Prasse, T.A. Ternes, M. Minella, V. Maurino, C. Minero, M. Sarakha, M. Brigante, D. Vione, Assessing the photochemical transformation pathways of acetaminophen relevant to surface waters: transformation kinetics, intermediates, and modelling, Water Res. 53 (2014) 235–248, https://doi.org/10.1016/j.watres.2014.01.016.

[66] N.H. El Najjar, A. Touffet, M. Deborde, R. Journel, N.K.V. Leitner, Kinetics of paracetamol oxidation by ozone and hydroxyl radicals, formation of transformation products and toxicity, Sep. Purif. Technol. 136 (2014) 137–143, https://doi.org/10.1016/j.seppur.2014.09.004.

[67] A.J.B. Leite, C.S.A., P.S. Thue, G.S. dos Reis, S.L. Dias, E.C. Lima, J.C.P. Vaghetti, F. A. Pavan, W.S. de Alencar, Activated carbon from avocado seeds for the removal of phenolic compounds from aqueous solutions. Water Treat. 71 (2017) 168–181, https://doi.org/10.5004/dwt.2017.20540.

[68] Y. Tong, P.J. McNamara, B.K. Mayer, Adsorption of organic micropollutants onto biochar: a review of relevant kinetics, mechanisms and equilibrium, Environ. Sci. Water Res. Technol. 5 (2019) 821–838, https://doi.org/10.1039/C8EW00938D.

[69] D. Chen, S. Xie, C. Chen, H. Quan, L. Hua, X. Luo, L. Guo, Activated biochar derived from pomelo peel as a high-capacity sorbent for removal of carbamazepine from aqueous solution, RSC Adv. 7 (2017) 54969–54979, https://doi.org/10.1039/C7RA10805B.

[70] M.B. Ahmed, J.L. Zhou, H.H. Ngo, W. Guo, Adsorptive removal of antibiotics from water and wastewater: progress and challenges, Sci. Total Environ. 532 (2015) 112–126, https://doi.org/10.1016/j.scitotenv.2015.05.130.

[71] L. Kovalova, D.R.U. Knappe, K. Lehnberg, C. Kazner, J. Hollender, Removal of highly polar micropollutants from wastewater by powdered activated carbon, Environ. Sci. Pollut. Res. 20 (2013) 3607–3615, https://doi.org/10.1007/s11356-012-1432-9.

[72] M.T. Sekulic, N. Boskovic, A. Slavkovic, J. Garunovic, S. Kolakovic, S. Pap, Surface functionalised adsorbent for emerging pharmaceutical removal: adsorption performance and mechanisms, Process Saf. Environ. Prot. 125 (2019) 50–63, https://doi.org/10.1016/j.psep.2019.03.007.

Supplementary Material

Combination of tertiary solar photo-Fenton and adsorption processes in the treatment of hospital wastewater: the removal of pharmaceuticals and their transformation products

Alexandre Della-Flora[a], Marcelo L. Wilde[a], Diana Lima[a], Éder C. Lima[a], and Carla Sirtori[a*]

Instituto de Química, Universidade Federal do Rio Grande do Sul, Av. Bento Gonçalves 9500, CEP 91501-970 Porto Alegre, RS, Brazil.

* Corresponding author: – carla.sirtori@ufrgs.br

Text S1. Physical-Chemical Characterization of HWW

Table S1. Physical-chemical characterization of HWW.

Parameters	Value	Method	LD	LQ
pH	9.2	SMEWW 4500-H+ B	-	-
Conductivity (μS cm^{-1})	838	SMEWW 2510 B	1	0.2
COD (mg L^{-1} O$_2$)	246	SMEWW 5220 B	5	0.8
BOD (mg L^{-1} O$_2$)	96	SMEWW 5210 B	2	0.6
BOD/COD	0.39	$\geq$ 0.5 biodegradable [1]	-	-
TOC (mg L^{-1})	149.8	SMEWW 5310	1.68	3.99
Total Chloride (mg L^{-1})	50.7	SMEWW 4110 B	0.5	0.02
Total phosphate (mg L^{-1} PO$_4^{3-}$)	18.50	SMEWW 4500 P E	0.03	0.006
Total suspended solids (mg L^{-1})	81	SMEWW 2540 D	10	5
Total solids (mg L^{-1})	313	SMEWW 2540 B	10	5

SMEWW: Standard Methods for the Examination of Water and Wastewater.

Text S2. Solar energy data

Table S2. Amount of energy irradiated during the SPF experiments.

Aproach A and D*		Aproach B and C*	
t_{30w} (min)	Q (kJ mol^{-1})	t_{30w} (min)	Q (kJ mol^{-1})
0.0	0.00	0.0	0.00
4.8	0.77	4.7	0.76
9.7	1.57	9.5	1.54
14.4	2.32	14.4	2.33
29.3	4.74	29.4	4.74
44.4	7.17	44.6	7.21
63.5	10.25	60.2	9.72

* The experiments were carried out simultaneously, Approach A and D on the first day

and Approach B and C on the second day.

Text S3. **LC-QTOF MS analysis**

For chromatographic separation, a mixture of acidified acetonitrile with 0.1% formic acid (A) and ultrapure water with 0.1% formic acid (B) was used in a constant flow of 0.5 mL min^{-1}. The separation gradient was defined using eluent A with an initial 5% and growing to 95% for 11 min, held for 1 min, thereafter was 5% A in 15 min, held for a further 5 min. The QTOF MS was operated in negative ionization mode, according to the following conditions: capillary at 2500 V, nebulizer at 4.5 bar, drying gas at 10 L min^{-1}, and gas temperature at 200 °C. The QTOF system was operated in broadband collision-induced dissociation (bbCID) acquisition mode, which simultaneously provides MS and MS/MS spectra. All MS information was obtained in scan mode in the range of *m/z* 50-1000. The bbCID mode was operated with two collision energies, low intensity of 25 eV to high intensity of 50 eV. A non-target approach was employed for the elucidation of TPs. The DataAnalysis v. 4.2 (Bruker Daltonik GmbH) software was used in the MS/MS data elucidation.

Table S3. Quantification method parameters used to determine pharmaceuticals in HWW.

Pharmaceuticals	Therapeutic class	Initial concentration in HWW before spiking ($\mu g\ L^{-1}$)	LOD ($\mu g\ L^{-1}$)	LOQ ($\mu g\ L^{-1}$)	Linear range ($\mu g\ L^{-1}$)	Equation	r^2
Chloramphenicol (CLO)	Antibiotics	< LOD	2.70	8.20	100 – 1000*	y = 682.28x + 105920*	0.996
					0.1 – 250**	y = 1120.6x + 3889**	0.9998
Fluconazole (FCZ)	Antifungal	51.44	4.90	14.85	50 – 1000*	y = 279.25x + 19691*	0.9936
					1 – 50**	y = 322.88x + 5153.6**	0.9944
Flutamide (FLT)	Chemotherapy	< LOD	2.71	8.22	25 – 1000*	y = 6136x + 189698	0.9918
					0.1 – 25**	y = 8722.8x + 30070	0.9982
Furosemide (FRS)	Diuretics	< LOD	6.80	20.60	50 – 1000*	y = 637.73x + 74402	0.9947
					1 – 50**	y = 901.54x + 12875	0.9893
Gemfibrozil (GFZ)	Lipid-regulating	< LOD	27.92	84.63	10 – 1000	y = 103.54x - 138.95	0.9982
Ibuprofen (IBP)	Analgesics/anti-inflammatory	< LOD	55.00	166.68	50 – 1000	y= 24.138x - 255.69	0.9965
Losartan (LOS)	Cardiovascular disease	7.35	1.45	4.42	10 – 1000*	y = 843.19x + 50078*	0.9932
					0.1 – 10**	y = 2462x + 2593.4**	0.9878
Nimesulide (NMS)	Anti-inflammatory	< LOD	0.364	1.10	25 – 1000*	y = 908.1x + 126054*	0.9935
					0.1 – 25**	y = 3969.5x + 9799.4**	0.9998
Paracetamol (PCT)	Analgesics/antipyretics	337.97	82.15	248.95	50 – 1000	y = 10.372x + 546.48	0.9922

*: high linear range; ****:** low linear range.

Text S4. Scheme of the solar photoreactor.

Total Solar Irradiance: 0.0897 m²
Total Volume Irradiance: 0.001 m³

Aluminum foil

Hospital wastewater 1L
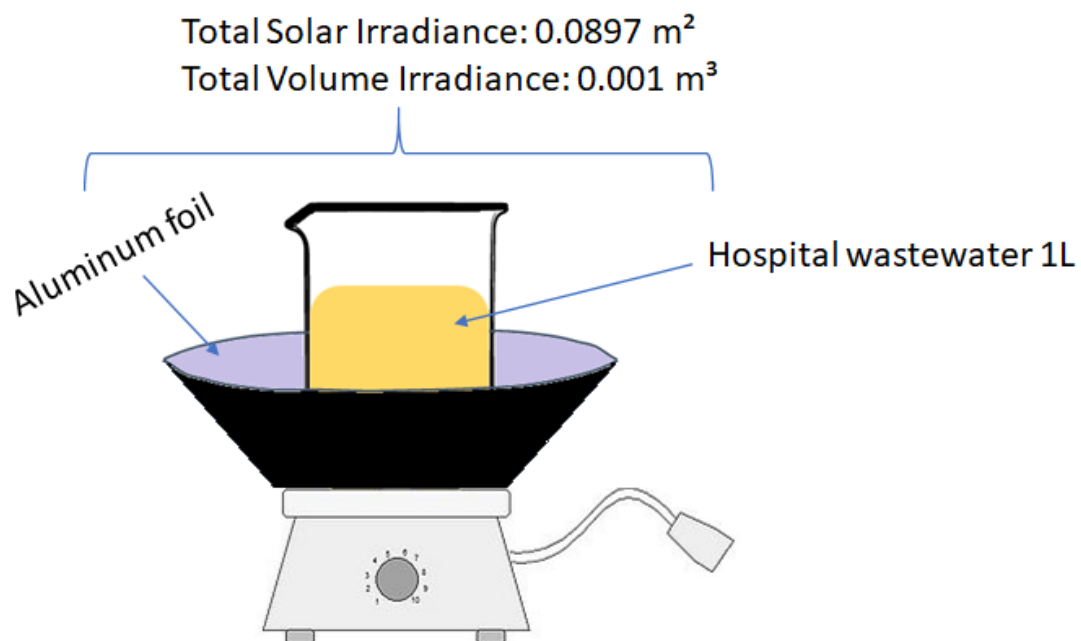
Figure S1. Scheme of solar batch phtoreactor employed in this study.

Text S4. Hydrolysis and iron complexation experiments
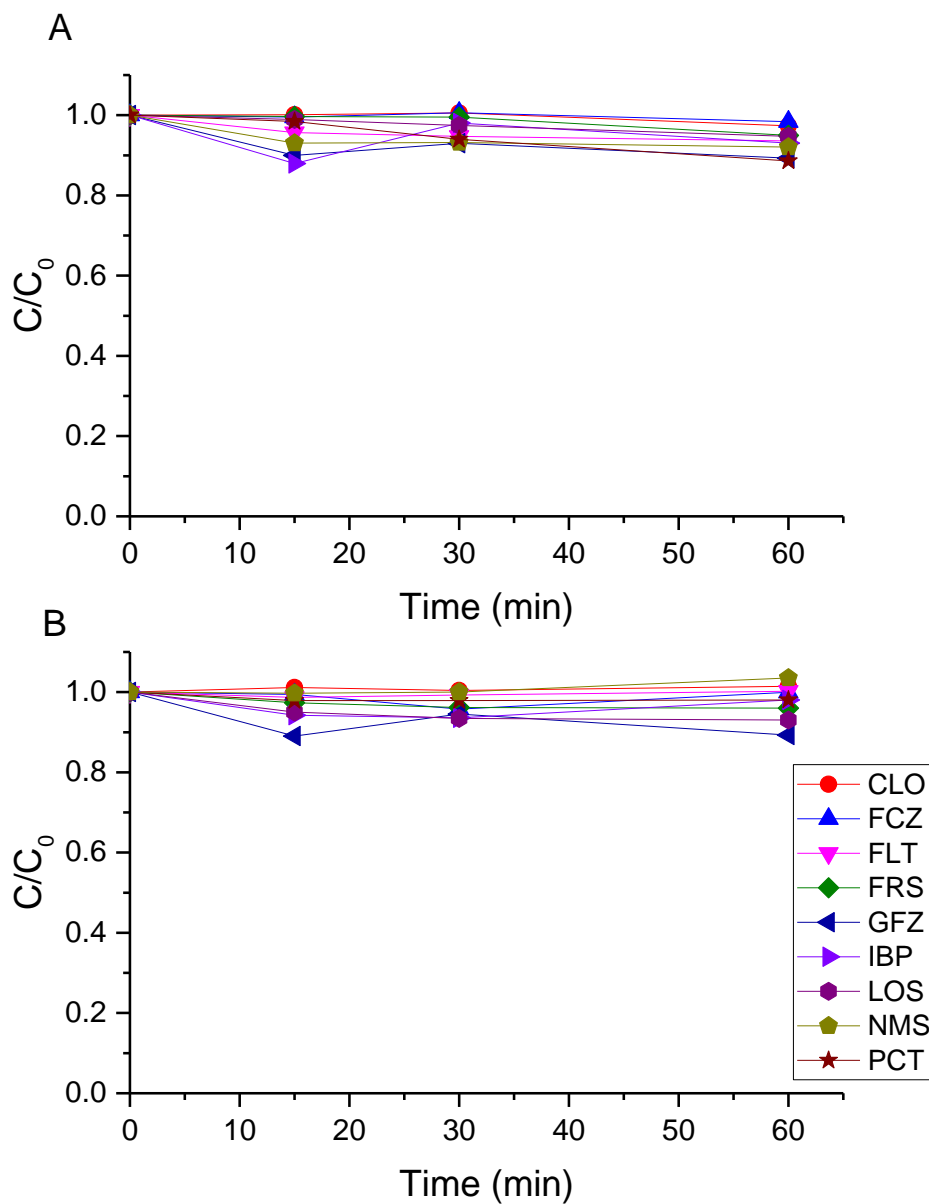
Figure S2. A) Hydrolysis experiments using an initial concentration of each pharmaceutical (500 µg L^{-1}) in ultrapure water and at pH 5; B) Iron-complexation experiment carried out by adding 5 mg L^{-1} of Fe^{2+} in a solution of each pharmaceutical (500 µg L^{-1}) in ultrapure water at pH 5 without adding H$_2$O$_2$.

Text S5. Kinetic information data from SPF approaches evaluated.

Table S4. Kinetic information data from approach A.

Compound	Equation	C_0	C_1	C_2	k_1 (min^{-1})	k_2 (min^{-1})	r^2
CLO	$y = C_1 + C_0 \cdot e^{-kt}$	0.811	0.161	-	0.120	-	0.990
FCZ	$y = C_1 + C_0 \cdot e^{-kt}$	0.096	0.913	-	0.037	-	0.868
FLT	$y = C_1 + C_0 \cdot e^{-kt}$	0.205	0.790	-	0.119	-	0.809
FRS	no kinetic equation	-	-	-	-	-	-
GFZ	$y = C_1 + C_0 \cdot e^{-kt}$	0.388	0.606	-	0.126	-	0.713
IBP	$y = C_1 + C_0 \cdot e^{-kt}$	0.337	0.667	-	0.126	-	0.932
LOS	$y = C_1 \cdot e^{-k_1 t} + C_2 \cdot e^{-k_2 t}$	-	0.254	0.747	0.451	0.008	0.997
NMS	$y = C_1 \cdot e^{-k_1 t} + C_2 \cdot e^{-k_2 t}$	-	0.178	0.823	0.325	0.004	0.970
PCT	$y = C_1 + C_0 \cdot e^{-kt}$	0.265	0.727	-	0.088	-	0.888

Condition: single addition of Fe^{2+} and H_2O_2 of 5 and 50 mg L^{-1}, respectively.

Table S5. Kinetic information data from approach B.

Compound	Equation	C_0	C_1	C_2	k_1 (min^{-1})	k_2 (min^{-1})	r^2
CLO	$y = C_1 + C_0 \cdot e^{-kt}$	0.732	0.268	-	0.039	-	0.974
FCZ	$y = C_1 \cdot e^{-k_1 t} + C_2 \cdot e^{-k_2 t}$	-	0.907	0.907	0.1088	2.65E^{-21}	
FLT	$y = C_1 + C_0 \cdot e^{-kt}$	1.1E^2	1.1E^2	-	2.2E^{-5}	-	0.922
FRS	no kinetic equation	-	-	-	-	-	-
GFZ	$y = C_1 \cdot e^{-k_1 t} + C_2 \cdot e^{-k_2 t}$	-	0.531	0.469	0.759	0.004	0.991
IBP	$y = C_1 + C_0 \cdot e^{-kt}$	0.674	0.338	-	0.107	-	0.983
LOS	$y = C_1 \cdot e^{-k_1 t} + C_2 \cdot e^{-k_2 t}$	-	0.568	0.431	0.167	0.003	0.982
NMS	$y = C_1 \cdot e^{-k_1 t} + C_2 \cdot e^{-k_2 t}$	0.856	0.364	-	10.8E^5	-	0.858
PCT	$y = C_1 + C_0 \cdot e^{-kt}$	0.617	0.397	-	0.118	-	0.963

Condition: addition H_2O_2 of 25 mg L^{-1} and multiple additions of Fe^{2+} (2x 2.5 mg L^{-1},

one in t_0, and another in t=10 min)

Table S6. Kinetic information data from approach C.

Compound	Equation	C_0	C_1	C_2	k_1 (min^{-1})	k_2 (min^{-1})	r^2
CLO	$y = C_1 \cdot e^{-k_1 t} + C_2 \cdot e^{-k_2 t}$	-	0.402	0.600	0.112	0.012	0.991
FCZ	$y = C_1 \cdot e^{-k_1 t} + C_2 \cdot e^{-k_2 t}$	-	0.133	0.867	0.353	0.004	0.986
FLT	$y = C_1 \cdot e^{-k_1 t} + C_2 \cdot e^{-k_2 t}$	-	0.292	0.707	0.775	0.008	0.989
FRS	no kinetic equation	-	-	-	-	-	-
GFZ	$y = C_1 \cdot e^{-k_1 t} + C_2 \cdot e^{-k_2 t}$	-	0.462	0.538	0.676	2.85E^{-19}	0.902
IBP	no kinetic equation	-	-	-	-	-	-
LOS	$y = C_1 + C_0 \cdot e^{-kt}$	0.538	0.462	-	0.709	-	0.906
NMS	$y = C_1 + C_0 \cdot e^{-kt}$	-0.021	1.065	-	0.018	-	0.974
PCT	$y = C_1 \cdot e^{-k_1 t} + C_2 \cdot e^{-k_2 t}$	-	0.528	0.498	0.498	0.008	0.961

Condition: addition of 50 mg L^{-1} de H_2O_2 and multiples addition of Fe^{2+} (t_0=5 mg L^{-1} and multiple additions of 2.5 mg L^{-1} at t_{30W}=5min and t_{30W}=10min);

Table S7. Kinetic information data from approach D.

Compound	Equation	C_0	k (min^{-1})	r^2
CLO	$y = C_0 \cdot e^{-kt}$	0.971	0.075	0.989
FCZ	$y = C_0 \cdot e^{-kt}$	1.035	0.037	0.974
FLT	$y = C_0 \cdot e^{-kt}$	1.065	0.058	0.957
FRS	no kinetic equation	-	-	-
GFZ	$y = C_0 \cdot e^{-kt}$	1.026	0.086	0.808
IBP	$y = C_0 \cdot e^{-kt}$	1.025	0.079	0.920
LOS	$y = C_0 \cdot e^{-kt}$	1.026	0.099	0.967
NMS	$y = C_0 \cdot e^{-kt}$	1.038	0.086	0.951
PCT	$y = C_0 \cdot e^{-kt}$	1.071	0.062	0.800

Condition: addition of 100 mg L^{-1} H_2O_2 and multiple additions of Fe^{2+} t_{30W}= 0 of 5 mg L^{-1} and two additions of 2.5 mg L^{-1} at t_{30W}=5min and t_{30W}=10min.

Text S6. The behavior of total Fe and H_2O_2 in SPF degradation for evaluated approaches.
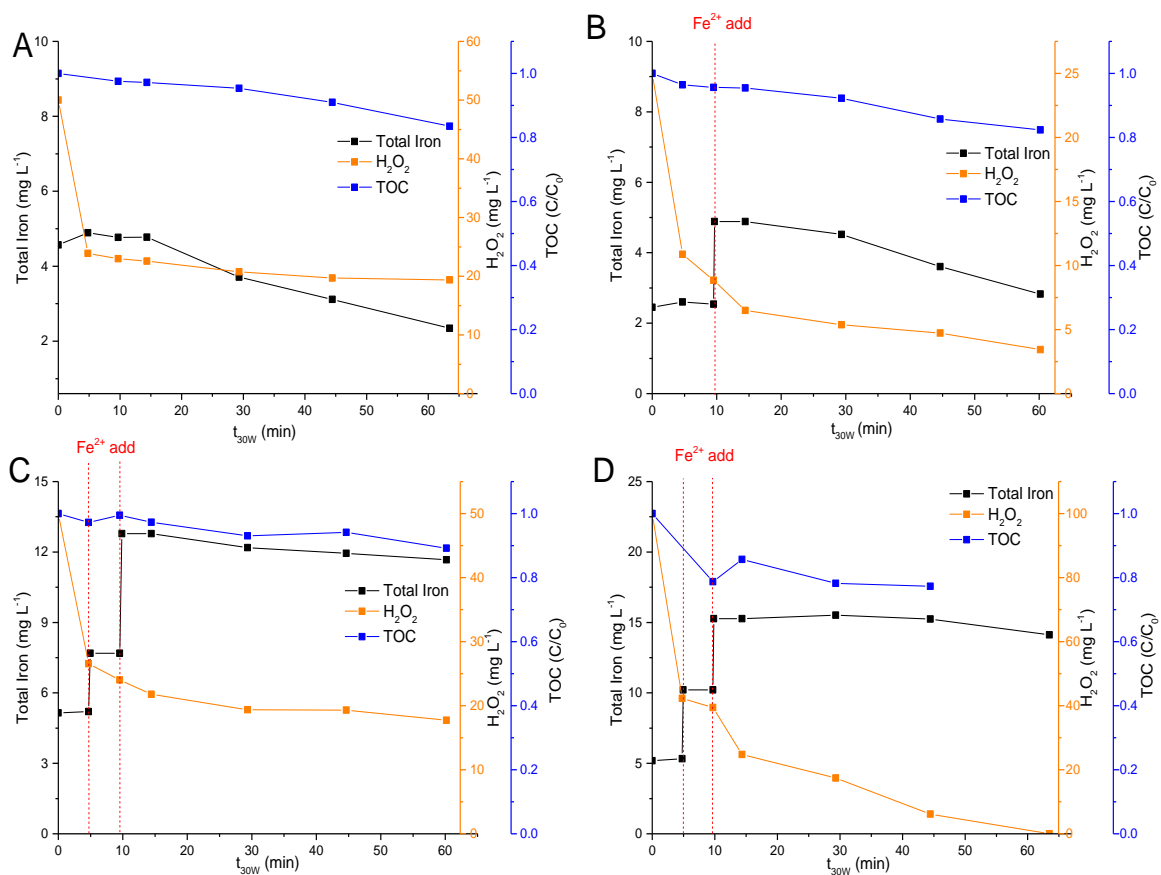
Figure S3. The behavior of total Fe and H_2O_2 in SPF degradation approaches A) single addition of Fe^{2+} and H_2O_2 of 5 and 50 mg L^{-1}; B) addition of H_2O_2 from 50 to 25 mg L^{-1} and multiple additions (2x 2.5 mg L^{-1}) Fe^{2+}; C) Addition of 50 mg L^{-1} of H_2O_2 and multiple additions of Fe^{2+} (t_0 = 5 mg L^{-1} and two additions of 2.5 mg L^{-1} at times 5 and 10 min); D) single addition of 100 mg L^{-1} H_2O_2 and multiple additions of Fe^{2+} (in the initial time 5 mg L^{-1} were added and in the 5, and 10 min intervals of the experiment another 5 mg L^{-1} were added, respectively. Red dotted lines in (B), (C), and (D) indicated Fe^{2+} additions during the treatment time.

Text S7. Degradation profile of pharmaceuticals and the formation of TPs during the SPF process of approaches.
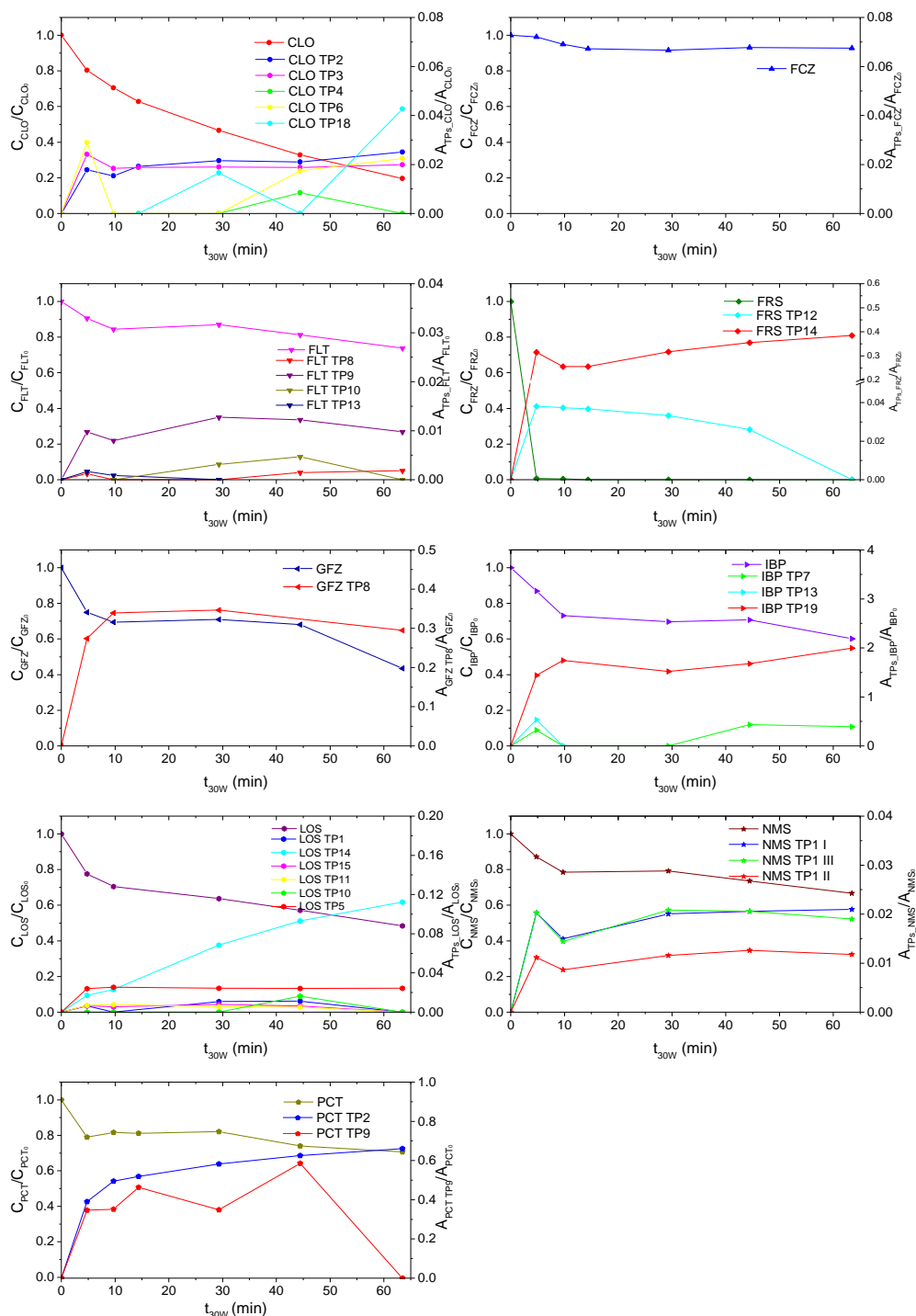
Figure S4. Degradation profile of pharmaceuticals and TPs' formation during the SPF process of approach A (single addition of Fe^{2+} and H_2O_2 of 5 and 50 mg L^{-1}, respectively).
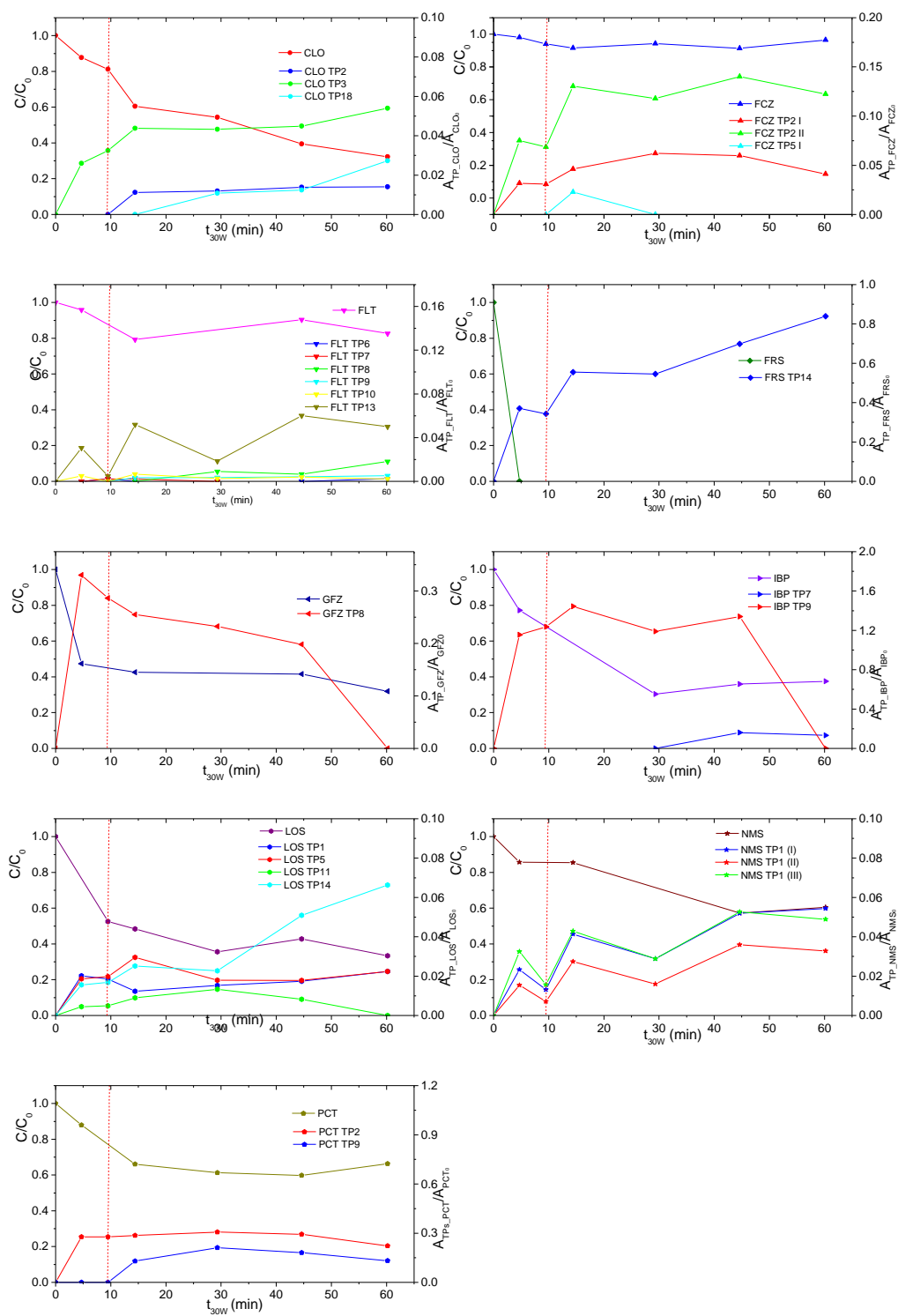
Figure S5. Degradation profile of pharmaceuticals and TPs' formation during the SPF process of approach B (addition of H_2O_2 from 50 to 25 mg L^{-1} and multiple additions of Fe^{2+} in t_{30W}=0min and t_{30W}= 10min of 2.5 mg L^{-1}).
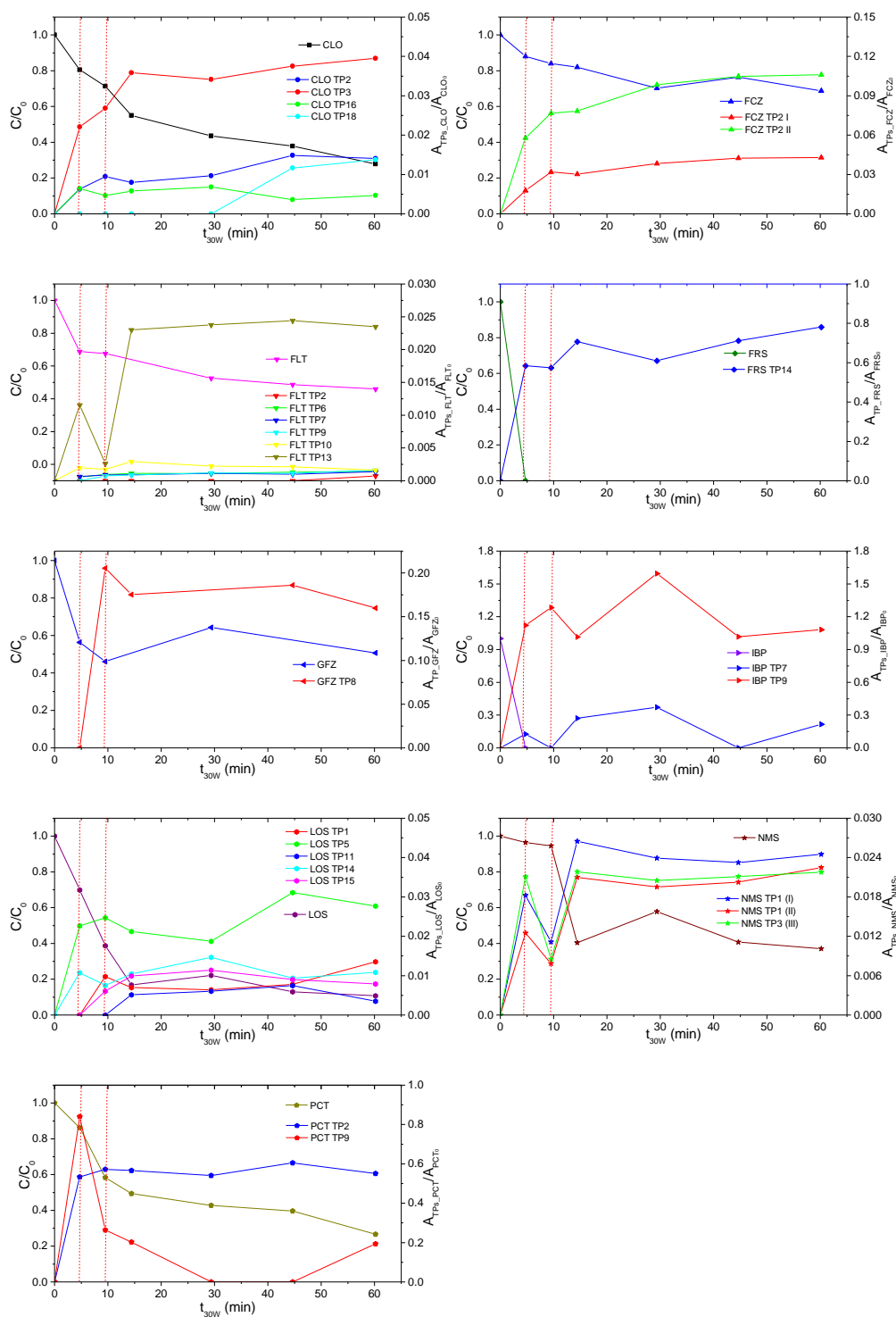
Figure S6. Degradation profile of pharmaceuticals and TPs' formation during the SPF process of approach C (addition of 50 mg L^{-1} of H$_2$O$_2$ and multiple additions of Fe^{2+} t$_{30W}$=0 of 5 mg L^{-1} and two additions of 2.5 mg L^{-1} at t$_{30W}$=5 min and t$_{30W}$=10 min).
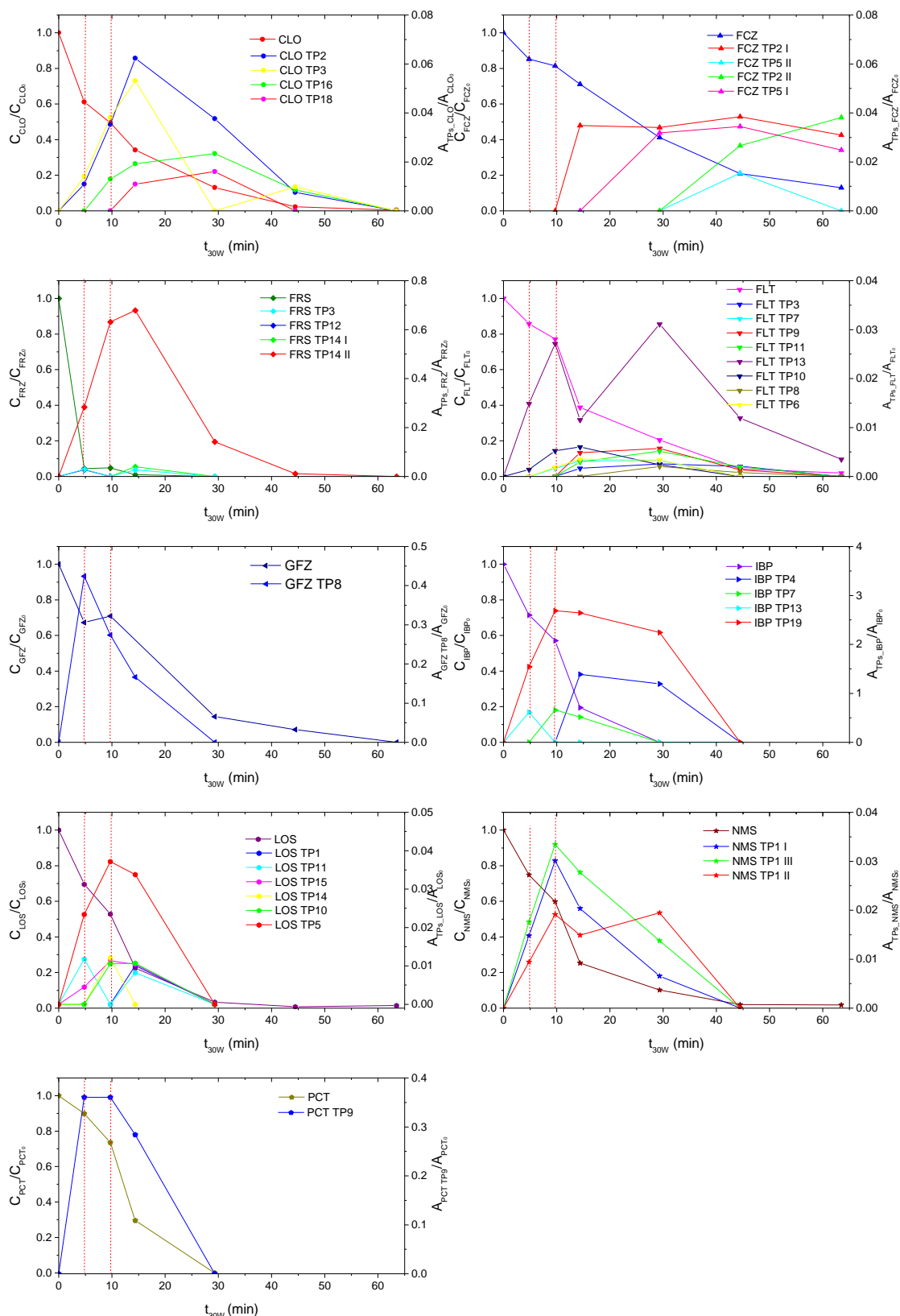
Figure S7. Degradation profile of pharmaceuticals and TPs' formation during the SPF process of approach D (addition of 100 mg L^{-1} H$_2$O$_2$ and multiple additions of Fe^{2+} t$_{30W}$= 0 of 5 mg L^{-1} and two additions of 2.5 mg L^{-1} at t$_{30W}$=5 min and t$_{30W}$=10 min).

Text S8. Accurate mass measurements of pharmaceuticals compounds and itsTPs found by LC-QTOF MS.

Table S8. Accurate mass measurements of pharmaceuticals compounds and itsTPs found by LC-QTOF MS by bbCID in negative ionization mode in HWW.

Compound	Rt (min)	Formula	Ion mass (m/z)		Error (ppm)	mSigma	DBE	Aproaches				Reference
			Experimental	Calculated				A	B	C	D	
CLO	4.19	$C_{11}H_{11}Cl_2N_2O_5$	321.0044	321.0051	1.9	9.9	6.5	✓	✓	✓	✓	
CLO TP2	3.93	$C_{11}H_{11}Cl_2N_2O_6$	337.0001	337.0000	-0.5	86.5	6.5	✓	✓	✓	✓	[2]
CLO TP3	4.02	$C_{11}H_{11}Cl_2N_2O_6$	337.0012	337.0000	-3.7	97.7	6.5	✓	✓	✓	✓	[2]
CLO TP6	2.39	$C_8H_6NO_4$	180.0302	180.0302	0.1	n.a.	6.5	✓				[2]
CLO TP16	3.50	$C_{11}H_9Cl_2N_2O_5$	318.9873	318.9894	6.6	117.1	6.5			✓	✓	[2]
CLO TP18	4.24	$C_7H_4NO_4$	166.0141	166.0146	2.8	36.9	6.5	✓	✓	✓	✓	[2]
FCZ	3.39	$C_{13}H_{12}F_2N_6O_1$	305.0986	305.0968	0.1	5.5	10.5	✓	✓	✓	✓	
FCZ TP2 I	2.46	$C_{13}H_{12}FN_6O_2$	303.1019	303.1011	-2.6	171.8	10.5		✓	✓	✓	[3]
FCZ TP2 II	3.02	$C_{13}H_{12}FN_6O_2$	303.1018	303.1011	-2.3	n.a.	10.5		✓	✓	✓	[3]
FCZ TP5 I	2.62	$C_{13}H_{11}F_2N_6O_2$	321.0905	321.0917	3.7	59.6	10.5		✓		✓	[4]
FCZ TP5 II	2.84	$C_{13}H_{11}F_2N_6O_2$	321.0932	321.0917	-4.5	96.2	10.5				✓	[4]
FLT	7.10	$C_{11}H_{10}F_3N_2O_3$	275.0649	275.0649	0.2	1.8	6.5	✓	✓	✓	✓	
FLT TP2	3.25	$C_9H_{11}F_3NO_7S$	334.0218	334.0214	−1,0	13.1	3.5			✓		[5]
FLT TP3	3.32	$C_{11}H_{13}F_3NO_{10}S$	408.0220	408.0218	-0.5	404.8	4.5				✓	[5]
FLT TP6	4.60	$C_{11}H_9F_3N_2O_4$	289.0439	289.0442	1	9.2	7.5		✓	✓	✓	[5]
FLT TP7	4.75	$C_{11}H_8F_3N_2O_4$	289.0437	289.0442	1.8	31	7.5		✓	✓	✓	[5]
FLT TP8	5.18	$C_{11}H_{11}F_3NO_2$	246.0745	246.0747	0.9	n.a.	5.5	✓	✓		✓	[5]
FLT TP9	5.61	$C_{11}H_{10}F_3N_2O_4$	291.0591	291.0598	2.5	30.2	6.5	✓	✓	✓	✓	[5]
FLT TP10	5.54	$C_{11}H_{10}F_3N_2O_7S$	371.0171	371.0166	-1.2	n.a.	6.5	✓	✓	✓	✓	[5]
FLT TP11	6.45	$C_{11}H_{10}F_3N_2O_4$	291.0591	291.0598	2.5	30.2	6.5				✓	[5]
FLT TP13	6.81	$C_{11}H_{10}F_3N_2O_4$	291.0598	291.0598	0	21.5	6.5	✓	✓	✓	✓	[5]

								C1	C2	C3	C4	Ref
FRS	4.98	$C_{12}H_{10}ClN_2O_5S$	329.0003	329.0004	0.4	20.3	8.5	✓	✓	✓	✓	
FRS TP3	2.48	$C_7H_6ClN_2O_4S$	248.9727	248.9742	6	39.6	5.5	✓			✓	[6–10]
FRS TP12	3.77	$C_{12}H_{11}N_2O_6S$	311.0336	311.0343	2.4	34	8.5				✓	[8]
FRS TP14 I	1.57	$C_7H_7N_2O_5S$	231.0078	231.0081	1.5	10.9	5.5				✓	[9]
FRS TP14 II	4.02	$C_7H_7N_2O_5S$	231.0077	231.0081	1.7	15.9	5.5	✓	✓	✓	✓	[9]
GFZ	8.10	$C_{15}H_{21}O_3$	249.1489	249.1496	2.8	5.9	5.5	✓	✓	✓	✓	
GFZ TP8	3.41	$C_9H_9O_3$	165.0558	165.0557	-0.6	n.a.	5.5	✓	✓	✓	✓	[11]
IBP	7.52	$C_{13}H_{17}O_2$	205.1232	205.1234	1.1	17.6	5.5	✓	✓	✓	✓	
IBP TP4	5.92	$C_{13}H_{17}O_3$	221.1181	221.1183	1.1	2.9	5.5				✓	[9,12,13]
IBP TP7	6.30	$C_{12}H_{17}O$	177.1285	177.1285	0.1	7.9	4.5	✓	✓	✓	✓	[9,12,14]
IBP TP13	1.55	$C_6H_9O_3$	129.0558	129.0557	-0.5	n.a.	2.5	✓			✓	[13,14]
IBP TP19	5.95	$C_{13}H_{15}O_5$	251.0923	251.0925	1	58.2	6.5	✓	✓	✓	✓	[14]
LOS	5.53	$C_{22}H_{22}ClN_6O$	421.1542	421.1549	1.8	6.1	14.5	✓	✓		✓	
LOS TP1	2.87	$C_{14}H_{12}N_5$	250.1100	250.1098	-0.6	22.9	11.5	✓	✓	✓	✓	[15]
LOS TP5	4.95	$C_{22}H_{22}ClN_6O_2$	437.1490	437.1498	1.9	41	14.5	✓	✓	✓	✓	[15]
LOS TP10	4.71	$C_{22}H_{20}ClN_6O$	419.1386	419.1393	1.5	37.6	15.5	✓			✓	[15]
LOS TP11	4.32	$C_{22}H_{22}ClN_6O_2$	437.1484	437.1498	3.3	432	14.5	✓	✓	✓	✓	[15]
LOS TP14	6.03	$C_{21}H_{22}N_5O_3$	392.1740	392.1728	-3	78.8	13.5	✓	✓	✓	✓	[16]
LOS TP15	4.82	$C_{22}H_{22}ClN_6O_2$	437.1507	437.1498	-1.9	240.9	14.5	✓		✓	✓	[15]
NMS	6.75	$C_{13}H_{11}N_2O_5S$	307.0388	307.0394	2.1	9.2	9.5	✓	✓	✓	✓	
NMS TP1 I	5.51	$C_{13}H_{11}N_2O_6S$	323.0342	323.0343	0.4	31.4	9.5	✓	✓	✓	✓	[17]
NMS TP1 II	5.73	$C_{13}H_{11}N_2O_6S$	323.0337	323.0343	1.9	44.3	9.5	✓	✓	✓	✓	[17]
NMS TP1 III	5.94	$C_{13}H_{11}N_2O_6S$	323.0335	323.0343	2.7	66.4	9.5	✓	✓	✓	✓	[17]
PCT	1.98	$C_8H_8NO_2$	150.0558	150.0561	1.8	7.3	5.5	✓	✓	✓	✓	
PCT TP2	2.42	$C_7H_8NO_2$	138.0556	138.0561	3	n.a.	4.5	✓	✓	✓		[18]
PCT TP9	1.75	$C_8H_8NO_3$	166.0509	166.0510	0.3	8.3	5.5	✓	✓	✓	✓	[18,19]

Text S9.HRMS elucidation of transformation products of Nimesulide formed through solar photo-Fenton

Figure S8.(A)Extraction ions chromatograms (EIC) of each fragment found for NMS TP1 I. (B)Mass spectrum, fragmentation pattern, and characteristic losses.

Figure S9.(A)Extraction ions chromatograms (EIC) of each fragment found for NMS TP1 II. (B)Mass spectrum, fragmentation pattern, and characteristic losses.

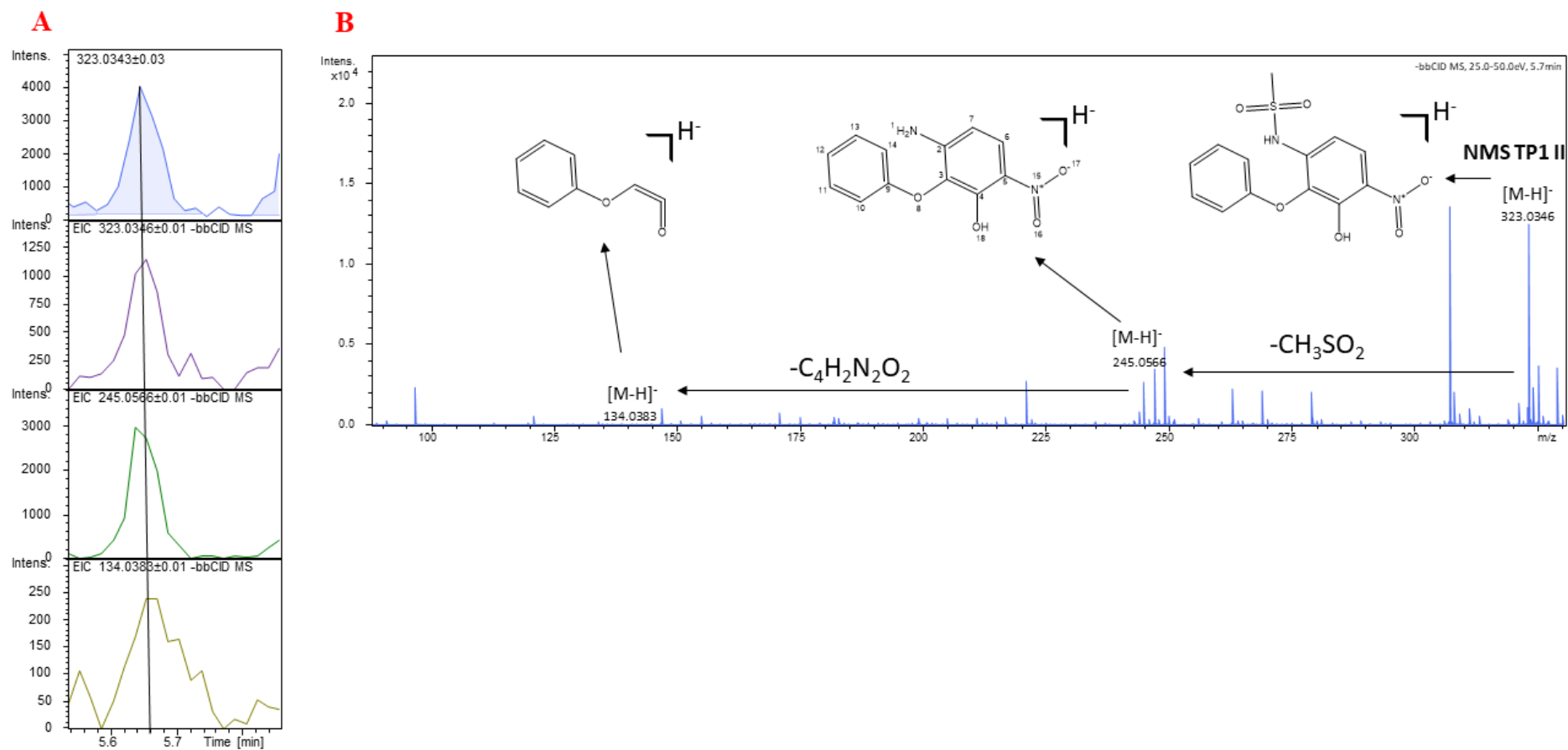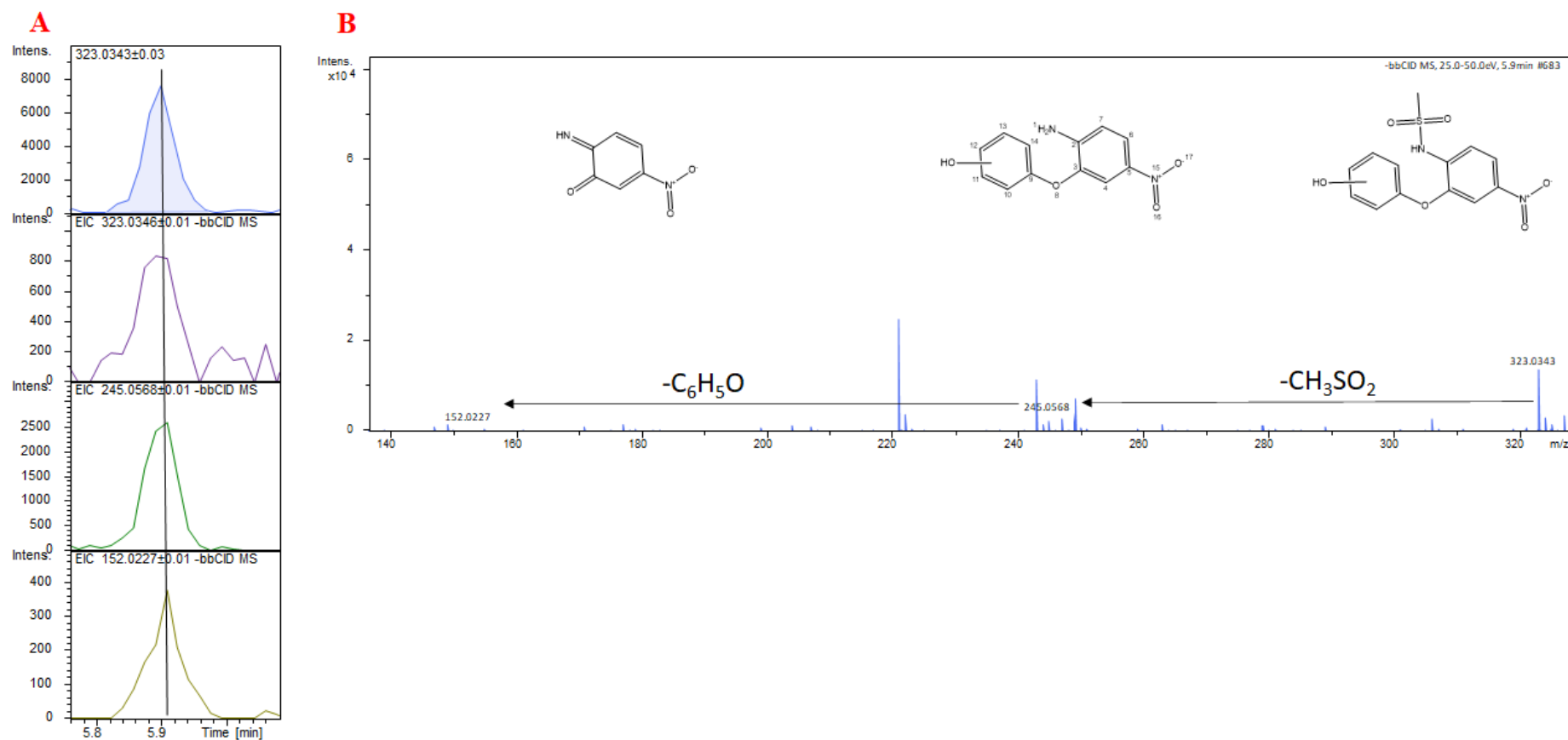**Figure S10**. (A)Extraction ions chromatograms (EIC) of each fragment found for NMS TP1 III. (B) Mass spectrum, fragmentation pattern, and characteristic losses.

Text S10. *In silico* predictions of some physical-chemical and 3D parameters of pharmaceutical compounds and theirTPs.

Table S9. *In silico* predictions of some physical-chemical and 3D parameters of pharmaceutical compounds and theirTPs.

Compound	Smiles	Log P[a]	Van der Waals surface area (Å², pH 7.0)[a]	Polar surface area (Å², pH 7.0)[a]	Van der Waals Volume (Å³)[a]	Polar surface area/Van der Waals surface area ratio (pH 7.0)[a]	Polarizability (Å³)	pKa[a]*
CLO	O=C(NC(CO)C(O)C1=CC=C([N+]([O-])=O)C=C1)C(Cl)Cl	0.88	385.75	112.70	249.06	0.45	27.82	8.69/13.55/15.09
CLO TP2	O=C(NC(CO)C(O)C1=CC=C([N+]([O-])=O)C=C1)C(Cl)(O)Cl	0.32	400.31	132.93	257.65	0.52	28.54	7.98/9.12
CLO TP3	O=C(NC(CO)C(O)C1=CC(O)=C([N+]([O-])=O)C=C1)C(Cl)Cl	0.29	394.43	135.76	257.54	0.53	28.26	6.59/8.83
CLO TP6	O=C(CO)C1=CC=C([N+]([O-])=O)C=C1	0.45	243.05	80.44	149.76	0.54	16.64	13.71
CLO TP16	O=C(N/C(C(O)C1=CC=C([N+]([O-])=O)C=C1)=C/O)C(Cl)Cl	0.60	354.50	155.53	241.42	0.64	27.28	8.10/13.47
CPC TP18	O=[N+](C1=CC=C(C(O)=O)C=C1)[O-]	1.52	208.96	83.27	132.66	0.63	14.56	3.31
FCZ	OC(CN1N=CN=C1)(C2=CC=C(F)C=C2F)CN3N=CN=C3	0.56	391.07	81.65	244.36	0.33	26.92	1.70/2.30/12.68
FCZ TP2-a	FC1=CC=C(C(CN2N=CN=C2)CN3N=CN=C3)C(O)=C1	0.47	382.66	81.65	239.21	0.34	27.04	1.75/2.36/8.81
FCZ TP2-b	FC1=CC(O)=CC=C1C(CN2N=CN=C2)CN3N=CN=C3	0.47	382.78	81.65	239.19	0.34	27.04	1.75/2.36/8.79
FCZ TP5-a	OC(C(O)N1N=CN=C1)(C2=CC=C(F)C=C2F)CN3N=CN=C3	-0.44	398.09	101.88	253.29	0.40	27.69	1.68/2.29/11.14/12.68
FCZ TP5-b	OC(CN4N=CN=C4)(C5=CC=C(F)C=C5F)C(O)N6N=CN=C6	-0.44	398.09	101.88	253.20	0.40	27.69	1.68/2.29/11.14/12.68
FRS	O=C(O)C1=CC(S(=O)(N)=O)=C(Cl)C=C1NCC2=CC=CO2	1.75	395.91	133.84	251.93	0.53	29.40	-1.52/4.25/9.83
FRS TP3	O=C(O)C1=CC(S(=O)(N)=O)=C(Cl)C=C1N	0.58	280.24	134.69	182.73	0.74	21.14	-0.27/4.38/9.86
FRS TP12-a	O=C(O)C1=CC(S(=O)(N)=O)=C(O)C=C1NCC2=CC=CO2	0.86	392.11	154.07	246.32	0.63	28.10	-1.51/4.51/7.50/11.54
FRS TP12-b	O=C(O)C3=CC(S(=O)(N)=O)=CC(O)=C3NCC4=CC=CO4	0.86	392.22	154.07	246.39	0.63	28.10	-0.47/3.92/9.08/11.15
FRS TP12-c	O=C(O)C5=C(O)C(S(=O)(N)=O)=CC=C5NCC6=CC=CO6	1.51	391.41	154.07	246.53	0.62	28.10	-1.30/2.96/8.56/11.57
FRS TP14-a	O=C(O)C1=CC(S(=O)(N)=O)=C(O)C=C1N	-0.22	275.82	154.92	177.20	0.87	19.84	-0.05/4.64/7.53/11.58
FRS TP14-b	O=C(O)C2=C(O)C(S(=O)(N)=O)=CC=C2N	0.43	274.73	154.92	177.30	0.87	19.84	0.10/3.17/8.62/11.60
FRS TP14-c	O=C(O)C3=CC(S(=O)(N)=O)=CC(O)=C3N	-0.22	275.41	154.92	177.30	0.87	19.84	0.65/4.05/9.17/11.18
GFZ	O=C(O)C(C)(C)CCCOC1=CC(C)=CC=C1C	4.39	439.98	49.36	255.10	0.19	27.82	4.42
GFZ TP8	CC1=CC=C(C)C(OC(O)=O)=C1	3.08	250.99	49.36	152.61	0.32	16.79	6.28
IBP	CC(C1=CC=C(CC(C)C)C=C1)C(O)=O	3.84	353.90	40.13	211.78	0.19	23.54	4.85
IBP TP4-a	CC(C)CC1=C(O)C=C(C(C)C(O)=O)C=C1	3.54	365.04	60.36	220.26	0.27	24.14	4.47/9.73
IBP TP4-b	CC(C)CC2=CC=C(O)C(C(C)C(O)=O)=C2	3.54	364.58	60.36	220.21	0.27	24.14	4.46/9.44
IBP TP4-c	CC(C)CC3=CC=C(C(C)C(O)=O)C(O)=C3	3.54	364.58	60.36	220.23	0.27	24.14	4.46/9.44
IBP TP4-d	CC(C)CC4=CC=C(C(C)C(O)=O)C=C4O	3.54	365.04	60.36	220.26	0.27	24.14	4.47/9.73
IBP TP4-e	CC(C)C(O)C1=CC=C(C(C)C(O)=O)C=C1	2.69	361.86	60.36	220.53	0.27	24.23	4.55/14.24
IBP TP4-f	CC(C)(O)CC2=CC=C(C(C)C(O)=O)C=C2	2.27	368.11	60.36	220.44	0.27	24.16	4.63/15.28
IBP TP4-g	CC(CO)CC3=CC=C(C(C)C(O)=O)C=C3	2.48	363.57	60.36	220.42	0.27	24.16	4.57/15.47
IBP TP4-h	CC(CO)CC4=CC=C(C(C)C(O)=O)C=C4	2.48	363.57	60.36	220.42	0.27	24.16	4.57/15.47
IBP TP7-a	CC(C)CC1=CC=C(CCO)C=C1	3.18	331.69	20.23	192.57	0.11	21.87	15.90
IBP TP7-b	CC(C)CC2=CC=C(C(O)C)C=C2	3.31	328.71	20.23	192.62	0.11	21.94	14.83
IBP TP7-c	CC(C)CC3=C(O)C=C(CC)C=C3	4.32	332.23	20.23	192.62	0.11	21.85	10.36

Name	SMILES							
IBP TP7-d	CC(C)CC4=CC(O)=C(CC)C=C4	4.32	322.09	20.23	192.39	0.11	21.85	10.37
IBP TP7-e	CC(C)CC5=CC=C(CC)C(O)=C5	4.32	332.09	20.23	192.30	0.11	21.85	10.37
IBP TP7-f	CC(C)CC6=CC=C(CC)C=C6O	4.32	332.23	20.23	192.35	0.11	21.85	10.36
IBP TP7-g	CC(C)C(O)C1=CC=C(CC)C=C1	3.47	328.90	20.23	192.71	0.10	21.94	14.27
IBP TP7-h	CC(C)(O)CC2=CC=C(CC)C=C2	3.15	335.64	20.23	192.71	0.10	21.87	15.30
IBP TP7-i	CC(CO)CC3=CC=C(CC)C=C3	3.26	330.81	20.23	192.51	0.11	21.87	15.47
IBP TP7-j	CC(CO)CC4=CC=C(CC)C=C4	3.26	330.81	20.23	192.51	0.11	21.87	15.47
IBP TP13	O=C(CCCCC=O)O	0.33	213.93	57.20	126.13	0.45	12.32	4.48
IBP TP19-a	CC(C)CC1=CC=C(C(C=O)(O)C(O)=O)C=C1O	1.98	371.64	97.66	213.47	0.46	24.89	3.43/9.59/11.77
IBP TP19-b	CC(C)CC2=C(O)C=C(C(C=O)(O)C(O)=O)C=C2	1.98	371.64	97.66	231.47	0.42	24.89	3.43/9.59/11.77
IBP TP19-c	CC(C)CC3=CC(O)=C(C(C=O)(O)C(O)=O)C=C3	1.98	370.51	97.66	231.47	0.42	24.89	3.43/9.88/11.75
IBP TP19-d	CC(C)CC4=CC=C(C(C=O)(O)C(O)=O)C(O)=C4	1.98	370.51	97.66	231.51	0.42	24.89	3.43/9.88/11.75
IBP TP19-e	CC(CO)CC1=CC=C(C(C=O)(O)C(O)=O)C=C1C	1.44	402.19	97.66	248.65	0.39	26.66	3.62/11.69
IBP TP19-f	CC(C)C(O)C2=CC=C(C(C=O)(O)C(O)=O)C=C2	1.13	368.22	97.66	231.76	0.42	24.98	3.50/11.69
IBP TP19-g	CC(C)(O)CC3=CC=C(C(C=O)(O)C(O)=O)C=C3	0.81	374.61	97.66	231.70	0.42	24.91	3.57/11.67
IBP TP19-h	CC(CO)CC4=CC=C(C(C=O)(O)C(O)=O)C=C4	0.93	370.24	97.66	231.66	0.42	24.91	3.52/11.68
LOS	OCC1=C(Cl)N=C(CCCC)N1CC2=CC=C(C3=CC=CC=C3C4=NNN=N4)C=C2	5.08	586.56	89.61	368.58	0.24	46.18	-1.45/3.85/5.85/14.22
LOS TP1	NCC1=CC=C(C2=CC=CC=C2C3=NN=NN3)C=C1	2.03	346.67	79.20	222.54	0.36	29.67	5.85/9.26
LOS TP5-a	OCC1=C(Cl)N=C(CCCC)N1CC2=CC=C(C3=C(O)C=CC=C3C4=NN=NN4)C=C2	4.12	597.62	109.84	376.91	0.29	46.79	3.85/5.82/9.23/14.22
LOS TP5-b	OCC5=C(Cl)N=C(CCCC)N5CC6=CC=C(C7=CC(O)=CC=C7C8=NN=NN8)C=C6	4.12	598.21	109.84	377.04	0.29	46.79	3.85/5.91/8.98/14.22
LOS TP5-c	OCC9=C(Cl)N=C(CCCC)N9CC%10=CC=C(C%11=CC=C(O)C=C%11C%12=NN=NN%12)C=C%10	4.12	598.42	109.84	376.98	0.29	46.79	3.85/5.81/9.41/14.22
LOS TP5-d	OCC1=C(Cl)N=C(CCCC)N1CC2=CC=C(C3=CC=CC(O)=C3C4=NN=NN4)C=C2	4.12	597.20	109.84	376.92	0.29	46.79	3.85/5.65/8.55/14.22
LOS TP10	O=CC1=C(Cl)N=C(CCCC)N1CC2=CC=C(C3=CC=CC=C3C4=NN=NN4)C=C2	4.90	569.80	86.45	362.30	0.24	45.63	2.83/5.85
LOS TP11	OCC1=C(Cl)N=C(CC(O)CC)N1CC2=CC=C(C3=CC=CC=C3C4=NN=NN4)C=C2	3.19	593.92	109.84	377.10	0.29	46.80	3.60/5.85/14.14/15.06
LOS TP14	OC(CN(CC1=CC=C(C2=CC=CC=C2C3=NN=NN3)C=C1)C(CCCC)=O)=O	3.14	564.98	122.00	355.16	0.34	42.67	4.30/5.86
LOS TP15-a	OCC1=C(Cl)N=C(CCCC)N1CC2=CC=C(C3=C(O)C=CC=C3C4=NN=NN4)C=C2	4.12	597.62	109.84	376.91	0.29	46.79	3.85/5.82/9.23/14.22
LOS TP15-b	OCC5=C(Cl)N=C(CCCC)N5CC6=CC=C(C7=CC(O)=CC=C7C8=NN=NN8)C=C6	4.12	598.21	109.84	377.04	0.29	46.79	3.85/5.91/8.98/14.22
LOS TP15-c	OCC9=C(Cl)N=C(CCCC)N9CC%10=CC=C(C%11=CC=C(O)C=C%11C%12=NN=NN%12)C=C%10	4.12	598.42	109.84	376.98	0.29	46.79	3.85/5.91/9.41/14.22
LOS TP15-d	OCC1=C(Cl)N=C(CCCC)N1CC2=CC=C(C3=CC=CC(O)=C3C4=NN=NN4)C=C2	4.12	597.20	109.84	376.92	0.29	46.79	3.85/5.85/8.55/14.22
NMS	CS(=O)(NC1=CC=C([N+]([O-])=O)C=C1OC2=CC=CC=C2)=O	1.79	406.45	104.12	249.13	0.42	29.45	6.70
NMS TP1 I	CS(=O)(NC1=C(O)C=C([N+]([O-])=O)C=C1OC2=CC=CC=C2)=O	2.13	413.75	127.18	257.55	0.49	29.85	5.96/6.68
NMS TP1 II	CS(=O)(NC1=CC=C([N+]([O-])=O)C(O)=C1OC2=CC=CC=C2)=O	1.48	413.23	127.18	257.60	0.49	29.85	5.85/6.91
NMS TP1 III	CS(=O)(NC1=CC=C([N+]([O-])=O)C=C1OC2=CC=CC(O)=C2)=O	1.48	417.60	124.35	257.55	0.48	30.11	6.69/9.10
PCT	CC(NC1=CC=C(O)C=C1)=O	0.91	222.91	49.33	138.08	0.36	15.82	9.46

PCT TP9-a	CC(NC1=CC=C(O)C=C1O)=O	0.60	232.91	69.56	146.61	0.47	16.46	8.72/10.62
PCT TP9-b	CC(NC2=CC=C(O)C(O)=C2)=O	0.60	232.68	69.56	146.63	0.47	16.46	9.13/12.57
PCT TP9-c	CC(NC3=CC(O)=C(O)C=C3)=O	0.60	232.68	69.56	146.59	0.47	16.46	9.13/12.57
PCT TP9-d	CC(NC4=C(O)C=C(O)C=C4)=O	0.60	232.91	69.56	146.66	0.47	16.46	8.72/10.36
PCT TP2	OCNC1=CC=C(O)C=C1	0.56	208.67	52.49	127.57	0.41	14.54	3.01/10.27/14.61

Calculated by Marvin Sketch 20.14; * pKa$_1$/pKa$_2$. FLT and its TPs were calculated in a study a previous study [20 b]

Text S11. Results of the comparison between the coupling processes were evaluated.

Table S10. Results for the adsorption process conditions studied.

Compounds	Approach 15 min		Approach 40 min		DF	|Tcalc|	t_{crit}
	Average	Variance	Average	Variance			
CLO	97.82	1.27	98.87	0.10	2	1.57	4.30
FCZ	97.47	1.46	98.13	0.27	3	0.87	3.18
FLT	99.35	0.04	99.41	0.03	4	0.39	2.78
FLT TP2	50.98	78.51	46.07	28.98	3	0.77	3.18
FLT TP3	67.89	44.83	62.28	8.62	1	1.12	12.71
FRS TP14 (I)	98.62	0.30	98.73	0.23	4	0.28	2.78
NMS	99.55	0.16	99.50	0.21	4	0.14	2.78

Average was calculated in triplicate (n=3). DF: Degrees of freedom.

Table S11. Preliminary evaluation of the adsorption in ASAC for the selected pharmaceuticals in HWW.

Pharmaceutical	Initial concentration ($\mu g\ L^{-1}$)	Adsorption 40 min		Adsorption 15 min	
		Final concentration ($\mu g\ L^{-1}$)	Removal (%)	Final concentration ($\mu g\ L^{-1}$)	Removal (%)
CLO	640.94	<LOQ	99.27	9.13	98.58
FCZ	595.14	<LOD	99.99	<LOQ	98.87
FLT	627.92	<LOD	99.73	<LOQ	99.50
FRS	735.42	31.46	95.72	54.41	92.60
GFZ	718.01	<LOD	100	<LOD	100
IBP	524.98	<LOQ	83.96	<LOQ	79.03
LOS	586.13	5.80	99.01	12.34	97.89
NMS	575.73	4.36	99.24	8.46	98.53
PCT	727.23	<LOQ	90.84	<LOQ	90.52

References

[1]   A. Lopez, M. Pagano, A. Volpe, A. Claudio Di Pinto, Fenton's pre-treatment of mature landfill leachate, Chemosphere. 54 (2004) 1005–1010.

https://doi.org/https://doi.org/10.1016/j.chemosphere.2003.09.015.

[2]   E.O. Marson, C.E. Paniagua, N.M. Costa-Serge, R.M. Sousa, G.D. Silva, R.W. Becker, C. Sirtori, M.C.V.M. Starling, S.R. Carvalho, A.G. Trovó, Chemical and toxicological evaluation along with unprecedented transformation products during photolysis and heterogeneous photocatalysis of chloramphenicol in different aqueous matrices, Environ. Sci. Pollut. Res. (2020).

[3]   G. Castro, J. Casado, I. Rodríguez, M. Ramil, A. Ferradás, R. Cela, Time-of-flight mass spectrometry assessment of fluconazole and climbazole UV and UV/H2O2 degradability: Kinetics study and transformation products elucidation, Water Res. 88 (2016) 681–690.
https://doi.org/https://doi.org/10.1016/j.watres.2015.10.053.

[4]   U. Hubicka, J. Krzek, P. Zmudzki, B. Juromska-Witek, D. Motyl, A. Kryczyk, Determination of fluconazole and its oxidation products with kinetic evaluation under potassium permanganate treatment in acidic solutions by ultra performance liquid chromatography-tandem mass spectrometry, Acta Pol. Pharm. - Drug Res. 76 (2019) 19–27. https://doi.org/10.32383/appdr/93513.

[5]   A. Della-flora, M.L. Wilde, I.D.F. Pinto, É.C. Lima, C. Sirtori, Degradation of the anticancer drug flutamide by solar photo-Fenton treatment at near-neutral pH: Identification of transformation products and in silico (Q)SAR risk assessment, Environ. Res. (2020). https://doi.org/10.1016/j.envres.2020.109223.

[6]   C. Laurencé, M. Rivard, I. Lachaise, J. Bensemhoun, T. Martens, Preparative access to transformation products (TPs) of furosemide: a versatile application of anodic oxidation, Tetrahedron. 67 (2011) 9518–9521.
https://doi.org/https://doi.org/10.1016/j.tet.2011.10.006.

[7]   G.R. Ibáñez, M. Bittner, Z. Toušová, M.C. Campos- Mañas, A. Agüera, J.L.C.

López, J.A.S. Pérez, K. Hilscherová, Does micropollutant removal by solar

photo- Fenton reduce ecotoxicity in municipal wastewater? A comprehensive

study at pilot scale open reactors, J. Chem. Technol. Biotechnol. 92 (2017) 2114–

2122. https://doi.org/10.1002/jctb.5212.

[8]   S. Katsura, N. Yamada, A. Nakashima, S. Shiraishi, T. Furuishi, H. Ueda,

Identification of Furosemide Photodegradation Products in Water–Acetonitrile

Mixture, Chem. Pharm. Bull. 63 (2015) 617–627.

https://doi.org/10.1248/cpb.c15-00122.

[9]   A. Jakimska, M. Śliwka-Kaszyńska, J. Reszczyńska, J. Namieśnik, A. Kot-

Wasik, Elucidation of transformation pathway of ketoprofen, ibuprofen, and

furosemide in surface water and their occurrence in the aqueous environment

using UHPLC-QTOF-MS, Anal. Bioanal. Chem. 406 (2014) 3667–3680.

https://doi.org/10.1007/s00216-014-7614-1.

[10]   C. Laurencé, M. Rivard, T. Martens, C. Morin, D. Buisson, S. Bourcier, M.

Sablier, M.A. Oturan, Anticipating the fate and impact of organic environmental

contaminants: A new approach applied to the pharmaceutical furosemide,

Chemosphere. 113 (2014) 193–199.

https://doi.org/https://doi.org/10.1016/j.chemosphere.2014.05.036.

[11]   P. Chen, F. Wang, Z.-F. Chen, Q. Zhang, Y. Su, L. Shen, K. Yao, Y. Liu, Z. Cai,

W. Lv, G. Liu, Study on the photocatalytic mechanism and detoxity of

gemfibrozil by a sunlight-driven TiO2/carbon dots photocatalyst: The significant

roles of reactive oxygen species, Appl. Catal. B Environ. 204 (2017) 250–259.

https://doi.org/https://doi.org/10.1016/j.apcatb.2016.11.040.

[12]   I. Michael, A. Achilleos, D. Lambropoulou, V.O. Torrens, S. Pérez, M. Petrović,

D. Barceló, D. Fatta-Kassinos, Proposed transformation pathway and evolution

profile of diclofenac and ibuprofen transformation products during

(sono)photocatalysis, Appl. Catal. B Environ. 147 (2014) 1015–1027.

https://doi.org/https://doi.org/10.1016/j.apcatb.2013.10.035.

[13]   Y. Xiang, J. Fang, C. Shang, Kinetics and pathways of ibuprofen degradation by

the UV/chlorine advanced oxidation process, Water Res. 90 (2016) 301–308.

https://doi.org/https://doi.org/10.1016/j.watres.2015.11.069.

[14]   D. Fabbri, M.J. López-Muñoz, A. Daniele, C. Medana, P. Calza, Photocatalytic

abatement of emerging pollutants in pure water and wastewater effluent by TiO2

and Ce-ZnO: degradation kinetics and assessment of transformation products,

Photochem. Photobiol. Sci. 18 (2019) 845–852.

https://doi.org/10.1039/C8PP00311D.

[15]   E.A. Serna-Galvis, L. Isaza-Pineda, A. Moncayo-Lasso, F. Hernández, M.

Ibáñez, R.A. Torres-Palma, Comparative degradation of two highly consumed

antihypertensives in water by sonochemical process. Determination of the

reaction zone, primary degradation products and theoretical calculations on the

oxidative process, Ultrason. Sonochem. 58 (2019) 104635.

https://doi.org/https://doi.org/10.1016/j.ultsonch.2019.104635.

[16]   I. Carpinteiro, G. Castro, I. Rodríguez, R. Cela, Free chlorine reactions of

angiotensin II receptor antagonists: Kinetics study, transformation products

elucidation and in-silico ecotoxicity assessment, Sci. Total Environ. 647 (2019)

1000–1010. https://doi.org/https://doi.org/10.1016/j.scitotenv.2018.08.082.

[17]   X. Sun, K.-L. Xue, X.-Y. Jiao, Q. Chen, L. Xu, H. Zheng, Y.-F. Ding,

Simultaneous determination of nimesulide and its four possible metabolites in

human plasma by LC–MS/MS and its application in a study of pharmacokinetics,

J. Chromatogr. B. 1027 (2016) 139–148.

https://doi.org/https://doi.org/10.1016/j.jchromb.2016.05.008.

[18] E. De Laurentiis, C. Prasse, T.A. Ternes, M. Minella, V. Maurino, C. Minero, M. Sarakha, M. Brigante, D. Vione, Assessing the photochemical transformation pathways of acetaminophen relevant to surface waters: Transformation kinetics, intermediates, and modelling, Water Res. 53 (2014) 235–248. https://doi.org/https://doi.org/10.1016/j.watres.2014.01.016.

[19] N.H. El Najjar, A. Touffet, M. Deborde, R. Journel, N.K.V. Leitner, Kinetics of paracetamol oxidation by ozone and hydroxyl radicals, formation of transformation products and toxicity, Sep. Purif. Technol. 136 (2014) 137–143. https://doi.org/https://doi.org/10.1016/j.seppur.2014.09.004.

[20] A. Della-Flora, M.L. Wilde, P.S. Thue, D. Lima, E.C. Lima, C. Sirtori, Combination of solar photo-Fenton and adsorption process for removal of the anticancer drug Flutamide and its transformation products from hospital wastewater, J. Hazard. Mater. 396 (2020) 122699. https://doi.org/https://doi.org/10.1016/j.jhazmat.2020.122699.

CONSIDERAÇÕES FINAIS

O uso de fármacos é essencial para melhorar a qualidade de vida e, sem dúvida, pode ser um dos fatores que tenha colaborado para a ampliação da expectativa de vida da população mundial com acesso a essa tecnologia nas últimas décadas. No entanto, quando os fármacos chegam aos diferentes compartimentos ambientais, por exemplo, por conta de limitações nos processos de tratamento convencionalmente empregados nas estações de tratamento de águas residuais, novas alternativas de processos de tratamento devem ser pesquisadas para viabilizar a remoção dos fármacos em águas e efluentes. Dentre as potenciais fontes de contaminação por fármacos, destacam-se os efluentes hospitalares. Tais efluentes são matrizes complexas que apresentam concentrações relativamente altas e variáveis de fármacos e seus metabólitos, que dependem a complexidade de atividades do centro de saúde, época do ano, dentre outros fatores. Além disso, podem apresentar uma carga orgânica elevada e, quando equalizados na própria instituição, podem apresentar alta carga de surfactantes e desinfetantes. Portanto, essa tese buscou avaliar uma estratégia alternativa para de remoção de fármacos e seus TPs por combinação de processos (foto-Fenton solar e adsorção) mediante estudos sequenciais que espera esclarecer os leitores quanto aos avanços e desafios dessa proposta.

O estudo detalhado no primeiro capítulo apresenta o tratamento por foto-Fenton solar do fármaco Flutamida, de forma isolada. Ainda, com o auxílio da cromatografia líquida de alta eficiência acoplada ao analisador de massas de alta resolução, foi possível identificar via método de estudo "clássico" 13 novos TPs, os quais apresentaram alertas de potenciais efeitos (carcinogenicidade, mutagenicidade, etc.) ao meio ambiente. Desse trabalho vale destacar que a Flutamida foi selecionada pela escassez de estudos na literatura. TPs de AOP da Flutamida foram por primeira vez relatados nesse estudo. A associação da identificação de TPs com sua avaliação por ferramentas (Q)SAR se configura também em uma abordagem valiosa e recente que vem sendo empregada no grupo de pesquisa já há algum tempo.

Por sua vez, o segundo capítulo se propõe a avaliara degradação da Flutamida via acople de processos (foto-Fenton solar e adsorção) em matriz de efluente hospitalar. Sob tais condições foram identificados 13 TPs da Flutamida no efluente hospitalar e quando combinados os processos (foto-Fenton solar seguido de adsorção utilizando o carvão ativo

produzido a partir de caroço de abacate), foram obtidas altas taxas de remoção para Flutamida e seus TPs. Por manterem intacto o anel aromático, a Flutamida e a maioria de seus TPs apresentam interações π-π, o que favoreceu a adsorção desses adsorvatos pelos sítios ativos do carvão ativo testado. Tão contrário, para os poucos TPs da Flutamida que apresentaram abertura do anel aromático, ou seja, eram mais polares, uma menor remoção foi observada. Adicionalmente, outro aspecto relevante a se destacar diz respeito ao uso de uma base de dados especialmente construída com os TPs identificados no estudo do capítulo 1, a qual permitiu via triagem de suspeitos a busca "automatizada" de TPs da Flutamida. Do ponto de vista analítico, essa estratégia de identificação de TPs representa um avanço muito interessante já que se utilizam as informações prévias que constam na base de dados de forma similar à informação obtida com a análise de padrões analíticos em análises de triagem alvo.

Por fim, o terceiro capítulo aumenta o escopo de fármacos modelo em estudo e, por consequência a geração de TPs de todos esses fármacos, na matriz de efluente hospitalar. A estratégia de identificação dos TPs se baseou em uma base de dados especialmente construída com dados do capítulo 1 e de estudos da literatura. Essa revisão gerou a informação de um total de 127 TPs. Tais TPs foram monitorados durante o estudo do acople de processos via triagem de suspeitos. Assim, a identificação de 38 TPs, sendo que duas novas estruturas químicas foram propostas para os TPs da Nimesulida, foi conseguido com tal trabalho. Em relação ao tratamento, o pior cenário no tratamento foto-Fentonsolar, ou seja, o que gerava maior número de TPs foi selecionado para acople à adsorção. Deste modo, o acople dos processos, resultou na remoção dos TPs e, se houvesse da carga residual dos fármacos iniciais.

Portanto, os resultados dessa tese defendida permitem indicar que a combinação do processo foto-Fenton solar e adsorção, como processos terciários, poderiam constituir-se em alternativas viáveis para remoção de fármacos e TPs de AOPs presentes em uma matriz complexa de efluente hospitalar.

DISPOSIÇÃO FINAL DOS RESÍDUOS

Todos os resíduos gerados durante os experimentos foram acondicionados em frascos adequados e devidamente identificados. Eles foram encaminhados para o Centro de Gestão e Tratamento de Resíduos Químicos (CGTRQ) do Instituto de Química da UFRGS, que contratam empresas terceirizadas para realizar o descarte adequado dos resíduos.

ATIVIDADES DE PRODUÇÃO INTELECTUALREALIZADAS DURANTE O DOUTORADO

ARTIGOS COMPLETOS PUBLICADOS RELACIONADOS À TESE

A. Della-flora, M.L. Wilde, I.D.F. Pinto, É.C. Lima, C. Sirtori, Degradation of the anticancer drug flutamide by solar photo-Fenton treatment at near-neutral pH: Identification of transformation products and *in silico* (Q)SAR risk assessment, Environ. Res. (2020). https://doi.org/10.1016/j.envres.2020.109223.

A. Della-Flora, M.L. Wilde, D. Lima, E.C. Lima, C. Sirtori, Combination of tertiary solar photo-Fenton and adsorption processes in the treatment of hospital wastewater: The removal of pharmaceuticals and their transformation products, J. Environ. Chem. Eng. 9 (2021) 105666. https://doi.org/https://doi.org/10.1016/j.jece.2021.105666.

A. Della-Flora, M.L. Wilde, P.S. Thue, D. Lima, E.C. Lima, C. Sirtori, Combination of solar photo-Fenton and adsorption process for removal of the anticancer drug Flutamide and its transformation products from hospital wastewater, J. Hazard. Mater. 396 (2020) 122699. https://doi.org/https://doi.org/10.1016/j.jhazmat.2020.122699.

A. Della-Flora, D. Scunderlick, M.L. Wilde, A.A. Gomes, E.C. Lima, C. Sirtori, In silico environmental risk assessment of fate and effects of pharmaceuticals and their TPs generated and treated by coupling tertiary processes in hospital wastewater. Environ. Sci. Water Res. Technol (2023) 9, 274-284. https://doi.org/10.1039/D2EW00518B.

ARTIGOS ORIUNDOS DE OUTROS TRABALHOS OU QUE FORAM DESENVOLVIDOS EM COLABORAÇAO

A. Della-Flora, R. Wielens Becker, S. Frederigi Benassi, A. Theodoro Toci, G.A. Cordeiro, M. Ibáñez, T. Portolés, F. Hernández, M. Boroski, C. Sirtori, Comprehensive investigation of pesticides in Brazilian surface water by high resolution mass spectrometry screening and gas

126

chromatography–mass spectrometry quantitative analysis, Sci. Total Environ. 669 (2019) 248–257. https://doi.org/https://doi.org/10.1016/j.scitotenv.2019.02.354.

F.P. Chaves, G. Gomes, **A. Della-Flora**, A. Dallegrave, C. Sirtori, E.M. Saggioro, D.M. Bila, Comparative endocrine disrupting compound removal from real wastewater by UV/Cl and UV/H_2O_2: Effect of pH, estrogenic activity, transformation products and toxicity, Sci. Total Environ. 746 (2020) 141041. https://doi.org/10.1016/j.scitotenv.2020.141041.

B.R. Gonçalves, **A. Della-Flora**, C. Sirtori, R.M.F. Sousa, M.C.V.M. Starling, J.A. Sánchez Pérez, E.M. Saggioro, S.F. Sales Junior, A.G. Trovó. Influence of water matrix components and peroxide sources on the transformation products and toxicity of tebuthiuron under UVC-based advanced oxidation processes, Sci. Total Environ. 859 (2023) 160120. http://dx.doi.org/10.1016/j.scitotenv.2022.160120.

TRABALHOS APRESENTADOS EM CONFERÊNCIAS

DELLA-FLORA, A.; GOMES, A. A.; SCUMDERLICK, D.; LIMA, EDER C.; SIRTORI, C. Chemometric analysis for screening of TPs generated during solar photo-Fenton process using QSAR data. 4to CONGRESO COLOMBIANO DE PROCESOS AVANZADOS DE OXIDACIÓN, Bogotá, 16/04/2021 (Apresentação Oral).

DELLA-FLORA, A.; WILDE, MARCELO L.; LIMA, EDER C.; SIRTORI, C.Application of adsorption for the removal TPs formed by solar photo-Fenton treatment in hospital wastewater. 2021. 4to CONGRESO COLOMBIANO DE PROCESOS AVANZADOS DE OXIDACIÓN, Bogotá, 16/04/2021 (Apresentação Oral).

DELLA-FLORA, A.; BECKER, R. W.; LIMA, E. C.; PINTO, I.D.F.; WILDE, M.L.; SIRTORI, C. Degradation of Flutamide by Solar Photo-Fenton Process at Near-Neutral pH and Transformation Products Identification. 2019. IV IBEROAMERICAN CONFERENCE ONADVANCED OXIDATION TECHNOLOGIES, Natal, 22/11/2019. (Apresentação Oral).

SCHWEIGERT, C.; **DELLA-FLORA, A**.; WILDE, MARCELO L.; PINTO, IGOR D.F.; LIMA, ÉDER C.; SIRTORI, C. Solar photo-Fenton degradation of Flutamide from water: Elucidation of transformation products by LC-QTOFMS. 2019. XIV Latin American Symposium on Environmental Analytical Chemistry, IX National Meeting on Environmental Chemistry, Bento Gonçalves 08/11/2019. (Apresentação Pôster).

WILDE, MARCELO L.; **DELLA-FLORA, A**; PINTO, I.D.F.; LIMA, E. C; SIRTORI, C. *In silico* quantitative structure-activity relationship (QSAR) approach for the assessment of environmental fate of the Flutamide its transformation products formed through solar photo-Fenton process. IV IBEROAMERICAN CONFERENCE ONADVANCED OXIDATION TECHNOLOGIES, Natal, 22/11/26Development of a routine quantification method for atrazine and their transformation products using dispersive liquid-liquid microextraction coupled with GC-MS. 2018. 7th CONFERENCE ON MASS SPECTROMETRY, Rio de Janeiro, 12/12/2018 (Apresentação Pôster).

SIRTORI, C.; **DELLA-FLORA, A.;** BECKER, R. W.; TOCI, ALINE T.; BOROSKI, M.; BENASSI, S. F.; CORDEIRO, G.A.; IBÁÑEZ, M.; HERNÁNDEZ, F. Investigation of pesticides in surface water from Brazil by combined use of UHPLC-QTOF MS screening and DLLME/GC-MS quantitative analysis. INTERNATIONAL CONFERENCE ONENVIRONMENTAL & FOOD MONITORING, Santiago Compostela, 22/06/2018 (Apresentação Pôster).

REFERÊNCIAS

[1] ANVISA, Medicamentos genéricos: estatísticas e listas, ANVISA. (2020). https://www.gov.br/anvisa/pt-br/assuntos/medicamentos/genericos/estatisticas (accessed August 11, 2022).

[2] B. Halling-Sørensen, S. Nors Nielsen, P.F. Lanzky, F. Ingerslev, H.C. Holten Lützhøft, S.E. Jørgensen, Occurrence, fate and effects of pharmaceutical substances in the environment- A review, Chemosphere. 36 (1998) 357–393. https://doi.org/https://doi.org/10.1016/S0045-6535(97)00354-8.

[3] T. Heberer, Occurrence, fate, and removal of pharmaceutical residues in the aquatic environment: a review of recent research data, Toxicol. Lett. 131 (2002) 5–17. https://doi.org/https://doi.org/10.1016/S0378-4274(02)00041-3.

[4] Brasil, Agência Nacional das Aguas (ANA), Atlas Esgotos - Despoluição de Bacias Hidrográficas., (2017). http://atlasesgotos.ana.gov.br (accessed August 11, 2022).

[5] S. Aydin, M.E. Aydin, A. Ulvi, H. Kilic, Antibiotics in hospital effluents: occurrence, contribution to urban wastewater, removal in a wastewater treatment plant, and environmental risk assessment, Environ. Sci. Pollut. Res. 26 (2019) 544–558. https://doi.org/10.1007/s11356-018-3563-0.

[6] P. Verlicchi, A. Galletti, M. Petrovic, D. Barceló, Hospital effluents as a source of emerging pollutants: An overview of micropollutants and sustainable treatment options, J. Hydrol. 389 (2010) 416–428. https://doi.org/https://doi.org/10.1016/j.jhydrol.2010.06.005.

[7] E. Carraro, S. Bonetta, C. Bertino, E. Lorenzi, S. Bonetta, G. Gilli, Hospital effluents management: Chemical, physical, microbiological risks and legislation in different countries, J. Environ. Manage. 168 (2016) 185–199. https://doi.org/https://doi.org/10.1016/j.jenvman.2015.11.021.

[8] M.I. Pariente, Y. Segura, S. Álvarez-Torrellas, J.A. Casas, Z.M. de Pedro, E. Diaz, J. García, M.J. López-Muñoz, J. Marugán, A.F. Mohedano, R. Molina, M. Munoz, C. Pablos, J.A. Perdigón-Melón, A.L. Petre, J.J. Rodríguez, M. Tobajas, F. Martínez,

Critical review of technologies for the on-site treatment of hospital wastewater: From conventional to combined advanced processes, J. Environ. Manage. 320 (2022) 115769. https://doi.org/https://doi.org/10.1016/j.jenvman.2022.115769.

[9]   D.M. Bila, M. Dezotti, Fármacos no meio ambiente, Quim. Nova. 26 (2003) 523–530. https://doi.org/10.1590/S0100-40422003000400015.

[10] N.H. Tran, M. Reinhard, K.Y.-H. Gin, Occurrence and fate of emerging contaminants in municipal wastewater treatment plants from different geographical regions-a review, Water Res. 133 (2018) 182–207. https://doi.org/10.1016/j.watres.2017.12.029.

[11] M. Patel, R. Kumar, K. Kishor, T. Mlsna, C.U. Pittman, D. Mohan, Pharmaceuticals of Emerging Concern in Aquatic Systems: Chemistry, Occurrence, Effects, and Removal Methods, Chem. Rev. 119 (2019) 3510–3673. https://doi.org/10.1021/acs.chemrev.8b00299.

[12] T. Deblonde, P. Hartemann, Environmental impact of medical prescriptions: assessing the risks and hazards of persistence, bioaccumulation and toxicity of pharmaceuticals, Public Health. 127 (2013) 312–317. https://doi.org/https://doi.org/10.1016/j.puhe.2013.01.026.

[13] M.I. Pariente, Y. Segura, S. Álvarez-Torrellas, J.A. Casas, Z.M. de Pedro, E. Diaz, J. García, M.J. López-Muñoz, J. Marugán, A.F. Mohedano, R. Molina, M. Munoz, C. Pablos, J.A. Perdigón-Melón, A.L. Petre, J.J. Rodríguez, M. Tobajas, F. Martínez, Critical review of technologies for the on-site treatment of hospital wastewater: From conventional to combined advanced processes, J. Environ. Manage. 320 (2022) 115769. https://doi.org/10.1016/j.jenvman.2022.115769.

[14] A. Mendoza, J. Aceña, S. Pérez, M. López de Alda, D. Barceló, A. Gil, Y. Valcárcel, Pharmaceuticals and iodinated contrast media in a hospital wastewater: A case study to analyse their presence and characterise their environmental risk and hazard, Environ. Res. 140 (2015) 225–241. https://doi.org/10.1016/j.envres.2015.04.003.

[15] W.-J. Sim, J.-W. Lee, J.-E. Oh, Occurrence and fate of pharmaceuticals in wastewater treatment plants and rivers in Korea, Environ. Pollut. 158 (2010) 1938–1947. https://doi.org/https://doi.org/10.1016/j.envpol.2009.10.036.

[16] A.J. Ebele, M. Abou-Elwafa Abdallah, S. Harrad, Pharmaceuticals and personal care products (PPCPs) in the freshwater aquatic environment, Emerg. Contam. 3 (2017) 1–16. https://doi.org/https://doi.org/10.1016/j.emcon.2016.12.004.

[17] N.A. Khan, S. Ahmed, I.H. Farooqi, I. Ali, V. Vambol, F. Changani, M. Yousefi, S. Vambol, S.U. Khan, A.H. Khan, Occurrence, sources and conventional treatment techniques for various antibiotics present in hospital wastewaters: A critical review, TrAC Trends Anal. Chem. 129 (2020) 115921. https://doi.org/https://doi.org/10.1016/j.trac.2020.115921.

[18] S. Rodriguez-Mozaz, S. Chamorro, E. Marti, B. Huerta, M. Gros, A. Sànchez-Melsió, C.M. Borrego, D. Barceló, J.L. Balcázar, Occurrence of antibiotics and antibiotic resistance genes in hospital and urban wastewaters and their impact on the receiving river, Water Res. 69 (2015) 234–242. https://doi.org/10.1016/j.watres.2014.11.021.

[19] P. Verlicchi, M. Al Aukidy, E. Zambello, Occurrence of pharmaceutical compounds in urban wastewater: Removal, mass load and environmental risk after a secondary treatment—A review, Sci. Total Environ. 429 (2012) 123–155. https://doi.org/10.1016/j.scitotenv.2012.04.028.

[20] Brasil, MINISTÉRIO DO MEIO AMBIENTE. CONSELHO NACIONAL DO MEIO AMBIENTE (CONAMA). RESOLUÇÃO No 430, DE 13 DE MAIO DE 2011, 2011.

[21] Brasil, Ministério do Meio Ambiente. Conselho Nacional do Meio Ambiente - CONAMA. Resolução nº 357, DE 17 DE MARÇO DE 2005, 2005.

[22] F.S. Souza, L.A. Féris, Hospital and Municipal Wastewater: Identification of Relevant Pharmaceutical Compounds, Water Environ. Res. 88 (2016) 871–877. https://doi.org/10.2175/106143016X14609975747603.

[23] S. Suarez, J.M. Lema, F. Omil, Pre-treatment of hospital wastewater by coagulation–flocculation and flotation, Bioresour. Technol. 100 (2009) 2138–2146. https://doi.org/10.1016/j.biortech.2008.11.015.

[24] UE, Commission Implementing Decision (EU) 2020/1161 of 4 August 2020 establishing a watch list of substances for Union-wide monitoring in the field of water

policy pursuant to Directive 2008/105/EC of the European Parliament and of the Council (notified under, (2020) 32–35. http://data.europa.eu/eli/dec_impl/2020/1161/oj.

[25] A.R. Ribeiro, O.C. Nunes, M.F.R. Pereira, A.M.T. Silva, An overview on the advanced oxidation processes applied for the treatment of water pollutants defined in the recently launched Directive 2013/39/EU, Environ. Int. 75 (2015) 33–51. https://doi.org/https://doi.org/10.1016/j.envint.2014.10.027.

[26] I. Oller, S. Malato, Photo-Fenton applied to the removal of pharmaceutical and other pollutants of emerging concern, Curr. Opin. Green Sustain. Chem. 29 (2021) 100458. https://doi.org/https://doi.org/10.1016/j.cogsc.2021.100458.

[27] S. Malato, P. Fernández-Ibáñez, M.I. Maldonado, J. Blanco, W. Gernjak, Decontamination and disinfection of water by solar photocatalysis: Recent overview and trends, Catal. Today. 147 (2009) 1–59. https://doi.org/https://doi.org/10.1016/j.cattod.2009.06.018.

[28] W. Huang, M. Brigante, F. Wu, K. Hanna, G. Mailhot, Development of a new homogenous photo-Fenton process using Fe(III)-EDDS complexes, J. Photochem. Photobiol. A Chem. 239 (2012) 17–23. https://doi.org/https://doi.org/10.1016/j.jphotochem.2012.04.018.

[29] S. Miralles-Cuevas, I. Oller, A. Ruiz Aguirre, J.A. Sánchez Pérez, S. Malato Rodríguez, Removal of pharmaceuticals at microg L−1 by combined nanofiltration and mild solar photo-Fenton, Chem. Eng. J. 239 (2014) 68–74. https://doi.org/https://doi.org/10.1016/j.cej.2013.10.047.

[30] S. Rahim Pouran, A.R. Abdul Aziz, W.M.A. Wan Daud, Review on the main advances in photo-Fenton oxidation system for recalcitrant wastewaters, J. Ind. Eng. Chem. 21 (2015) 53–69. https://doi.org/https://doi.org/10.1016/j.jiec.2014.05.005.

[31] L.O. Conte, A. V Schenone, O.M. Alfano, Ferrioxalate-assisted solar photo-Fenton degradation of a herbicide at pH conditions close to neutrality, Environ. Sci. Pollut. Res. 24 (2017) 6205–6212. https://doi.org/10.1007/s11356-016-6400-3.

[32]   A. Moncayo-Lasso, C. Pulgarin, N. Benítez, Degradation of DBPs' precursors in river water before and after slow sand filtration by photo-Fenton process at pH 5 in a solar CPC reactor, Water Res. 42 (2008) 4125–4132. https://doi.org/https://doi.org/10.1016/j.watres.2008.07.014.

[33]   B.M. Souza, M.W.C. Dezotti, R.A.R. Boaventura, V.J.P. Vilar, Intensification of a solar photo-Fenton reaction at near neutral pH with ferrioxalate complexes: A case study on diclofenac removal from aqueous solutions, Chem. Eng. J. 256 (2014) 448–457. https://doi.org/https://doi.org/10.1016/j.cej.2014.06.111.

[34]   O. Gomes Júnior, V.M. Silva, A.E.H. Machado, C. Sirtori, C.R. Lemos, A.M. Freitas, A.G. Trovó, Correlation between pH and molar iron/ligand ratio during ciprofloxacin degradation by photo-Fenton process: Identification of the main transformation products, J. Environ. Manage. 213 (2018) 20–26. https://doi.org/https://doi.org/10.1016/j.jenvman.2018.02.041.

[35]   P. Soriano-Molina, J.L. García Sánchez, O.M. Alfano, L.O. Conte, S. Malato, J.A. Sánchez Pérez, Mechanistic modeling of solar photo-Fenton process with Fe3+-EDDS at neutral pH, Appl. Catal. B Environ. 233 (2018) 234–242. https://doi.org/https://doi.org/10.1016/j.apcatb.2018.04.005.

[36]   S. Foteinis, J.M. Monteagudo, A. Durán, E. Chatzisymeon, Environmental sustainability of the solar photo-Fenton process for wastewater treatment and pharmaceuticals mineralization at semi-industrial scale, Sci. Total Environ. 612 (2018) 605–612. https://doi.org/https://doi.org/10.1016/j.scitotenv.2017.08.277.

[37]   S. Papoutsakis, F.F. Brites-Nóbrega, C. Pulgarin, S. Malato, Benefits and limitations of using Fe(III)-EDDS for the treatment of highly contaminated water at near-neutral pH, J. Photochem. Photobiol. A Chem. 303–304 (2015) 1–7. https://doi.org/https://doi.org/10.1016/j.jphotochem.2015.01.013.

[38]   F. Cecen, O. Aktas, Fundamentals of Adsorption onto Activated Carbon in Water and Wastewater Treatment, Act. Carbon Water Wastewater Treat. (2011) 13–41. https://doi.org/https://doi.org/10.1002/9783527639441.ch2.

[39]   C. Sophia A., E.C. Lima, Removal of emerging contaminants from the environment by

adsorption, Ecotoxicol. Environ. Saf. 150 (2018) 1–17.
https://doi.org/10.1016/j.ecoenv.2017.12.026.

[40]   C. Saucier, Preparação e caracterização de carvões ativos para remoção de compostos orgânicos de efluentes aquosos, Universodade Federal do Rio Grande do Sul - UFRGS., 2017.

[41]   S. Wong, N. Ngadi, I.M. Inuwa, O. Hassan, Recent advances in applications of activated carbon from biowaste for wastewater treatment: A short review, J. Clean. Prod. 175 (2018) 361–375.
https://doi.org/https://doi.org/10.1016/j.jclepro.2017.12.059.

[42]   I. Carra, C. Sirtori, L. Ponce-Robles, J.A. Sánchez Pérez, S. Malato, A. Agüera, Degradation and monitoring of acetamiprid, thiabendazole and their transformation products in an agro-food industry effluent during solar photo-Fenton treatment in a raceway pond reactor, Chemosphere. 130 (2015) 73–81.
https://doi.org/https://doi.org/10.1016/j.chemosphere.2015.03.001.

[43]   C. Sirtori, A. Zapata, W. Gernjak, S. Malato, A. Lopez, A. Agüera, Solar photo-Fenton degradation of nalidixic acid in waters and wastewaters of different composition. Analytical assessment by LC–TOF-MS, Water Res. 45 (2011) 1736–1744.
https://doi.org/https://doi.org/10.1016/j.watres.2010.11.023.

[44]   C. Sirtori, A. Zapata, S. Malato, A. Agüera, Formation of chlorinated by-products during photo-Fenton degradation of pyrimethanil under saline conditions. Influence on toxicity and biodegradability, J. Hazard. Mater. 217–218 (2012) 217–223.
https://doi.org/https://doi.org/10.1016/j.jhazmat.2012.03.017.

[45]   J. Menz, A.P. Toolaram, T. Rastogi, C. Leder, O. Olsson, K. Kümmerer, M. Schneider, Transformation products in the water cycle and the unsolved problem of their proactive assessment: A combined in vitro/in silico approach, Environ. Int. 98 (2017) 171–180. https://doi.org/https://doi.org/10.1016/j.envint.2016.11.003.

[46]   M.L. Wilde, J. Menz, C. Leder, K. Kümmerer, Combination of experimental and in silico methods for the assessment of the phototransformation products of the antipsychotic drug/metabolite Mesoridazine, Sci. Total Environ. 618 (2018) 697–711.

https://doi.org/10.1016/j.scitotenv.2017.08.040.

[47]   G.J. Myatt, E. Ahlberg, Y. Akahori, D. Allen, A. Amberg, L.T. Anger, A. Aptula, S. Auerbach, L. Beilke, P. Bellion, R. Benigni, J. Bercu, E.D. Booth, D. Bower, A. Brigo, N. Burden, Z. Cammerer, M.T.D. Cronin, K.P. Cross, L. Custer, M. Dettwiler, K. Dobo, K.A. Ford, M.C. Fortin, S.E. Gad-McDonald, N. Gellatly, V. Gervais, K.P. Glover, S. Glowienke, J. Van Gompel, S. Gutsell, B. Hardy, J.S. Harvey, J. Hillegass, M. Honma, J.-H. Hsieh, C.-W. Hsu, K. Hughes, C. Johnson, R. Jolly, D. Jones, R. Kemper, M.O. Kenyon, M.T. Kim, N.L. Kruhlak, S.A. Kulkarni, K. Kümmerer, P. Leavitt, B. Majer, S. Masten, S. Miller, J. Moser, M. Mumtaz, W. Muster, L. Neilson, T.I. Oprea, G. Patlewicz, A. Paulino, E. Lo Piparo, M. Powley, D.P. Quigley, M.V. Reddy, A.-N. Richarz, P. Ruiz, B. Schilter, R. Serafimova, W. Simpson, L. Stavitskaya, R. Stidl, D. Suarez-Rodriguez, D.T. Szabo, A. Teasdale, A. Trejo-Martin, J.-P. Valentin, A. Vuorinen, B.A. Wall, P. Watts, A.T. White, J. Wichard, K.L. Witt, A. Woolley, D. Woolley, C. Zwickl, C. Hasselgren, In silico toxicology protocols, Regul. Toxicol. Pharmacol. 96 (2018) 1–17. https://doi.org/https://doi.org/10.1016/j.yrtph.2018.04.014.

[48]   N. Abramenko, L. Kustov, L. Metelytsia, V. Kovalishyn, I. Tetko, W. Peijnenburg, A review of recent advances towards the development of QSAR models for toxicity assessment of ionic liquids, J. Hazard. Mater. 384 (2020) 121429. https://doi.org/10.1016/j.jhazmat.2019.121429.

[49]   B. Hensen, O. Olsson, K. Kümmerer, A strategy for an initial assessment of the ecotoxicological effects of transformation products of pesticides in aquatic systems following a tiered approach, Environ. Int. 137 (2020) 105533. https://doi.org/https://doi.org/10.1016/j.envint.2020.105533.

[50]   A.P. Toolaram, T. Haddad, C. Leder, K. Kümmerer, Initial hazard screening for genotoxicity of photo-transformation products of ciprofloxacin by applying a combination of experimental and in-silico testing, Environ. Pollut. 211 (2016) 148–156. https://doi.org/https://doi.org/10.1016/j.envpol.2015.12.040.

[51]   M. Irani, L.R. Rad, H. Pourahmad, I. Haririan, Optimization of the combined adsorption/photo-Fenton method for the simultaneous removal of phenol and

paracetamol in a binary system, Microporous Mesoporous Mater. 206 (2015) 1–7. https://doi.org/https://doi.org/10.1016/j.micromeso.2014.12.009.

[52] H. Bel Hadjltaief, A. Sdiri, W. Ltaief, P. Da Costa, M.E. Gálvez, M. Ben Zina, Efficient removal of cadmium and 2-chlorophenol in aqueous systems by natural clay: Adsorption and photo-Fenton degradation processes, Comptes Rendus Chim. 21 (2018) 253–262. https://doi.org/https://doi.org/10.1016/j.crci.2017.01.009.

[53] P. Verlicchi, Trends, new insights and perspectives in the treatment of hospital effluents, Curr. Opin. Environ. Sci. Heal. 19 (2021) 100217. https://doi.org/10.1016/j.coesh.2020.10.005.

[54] R.N. Brogden, S.P. Clissold, Flutamide: A review of its pharmacodynamic and pharmacokinetic properties, and therapeutic use in advanced prostatic cancer, Drup Aging. 1 (1991) 104–115. https://doi.org/10.2165/00003495-198938020-00003.

[55] K. Knapczyk-Stwora, A. Nynca, R.E. Ciereszko, L. Paukszto, J.P. Jastrzebski, E. Czaja, P. Witek, M. Koziorowski, M. Slomczynska, Flutamide-induced alterations in transcriptional profiling of neonatal porcine ovaries, J. Anim. Sci. Biotechnol. 10 (2019) 1–15. https://doi.org/10.1186/s40104-019-0340-y.

[56] J. Tian, L. Liu, Y. Han, Y. Yang, S. Jin, J. Yang, Effects of testosterone and flutamide on reproduction in Brachionus calyciflorus, Sci. Rep. 7 (2017) 1–7. https://doi.org/10.1038/s41598-017-05517-4.

[57] P. Yin, Y.W. Li, Q.L. Chen, Z.H. Liu, Diethylstilbestrol, flutamide and their combination impaired the spermatogenesis of male adult zebrafish through disrupting HPG axis, meiosis and apoptosis, Aquat. Toxicol. 185 (2017) 129–137. https://doi.org/10.1016/j.aquatox.2017.02.013.

[58] H. Franquet-Griell, C. Gómez-Canela, F. Ventura, S. Lacorte, Predicting concentrations of cytostatic drugs in sewage effluents and surface waters of Catalonia (NE Spain), Environ. Res. 138 (2015) 161–172. https://doi.org/https://doi.org/10.1016/j.envres.2015.02.015.

[59] ANVISA, Agência Nacional de Vigilância Sanitária. "Anuário estatistico do mercado

farmacêutico 2017.," 2018.
http://portal.anvisa.gov.br/documents/374947/3413536/Anuário+Estatístico+do+Merc
ado+Farmacêutico+-+2017/3179a522-1af4-4b4c-8014-cc25a90fb5a7.

[60]   T.H. Miller, K.T. Ng, S.T. Bury, S.E. Bury, N.R. Bury, L.P. Barron, Biomonitoring of
pesticides, pharmaceuticals and illicit drugs in a freshwater invertebrate to estimate
toxic or effect pressure, Environ. Int. 129 (2019) 595–606.
https://doi.org/https://doi.org/10.1016/j.envint.2019.04.038.

[61]   L. Rizzo, S. Malato, D. Antakyali, V.G. Beretsou, M.B. Đolić, W. Gernjak, E. Heath,
I. Ivancev-Tumbas, P. Karaolia, A.R. Lado Ribeiro, G. Mascolo, C.S. McArdell, H.
Schaar, A.M.T. Silva, D. Fatta-Kassinos, Consolidated vs new advanced treatment
methods for the removal of contaminants of emerging concern from urban wastewater,
Sci. Total Environ. 655 (2019) 986–1008.
https://doi.org/https://doi.org/10.1016/j.scitotenv.2018.11.265.

[62]   L.E. Afshar, N. Chaibakhsh, Z. Moradi-Shoeili, Treatment of wastewater containing
cytotoxic drugs by CoFe2O4 nanoparticles in Fenton/ozone oxidation process, Sep.
Sci. Technol. 53 (2018) 2671–2682. https://doi.org/10.1080/01496395.2018.1461113.

[63]   R. Wielens Becker, M.L. Wilde, D. Salmoria Araújo, D. Seibert Lüdtke, C. Sirtori,
Proposal of a new, fast, cheap, and easy method using DLLME for extraction and
preconcentration of diazepam and its transformation products generated by a solar
photo-Fenton process, Water Res. 184 (2020) 116183.
https://doi.org/https://doi.org/10.1016/j.watres.2020.116183.

[64]   E.C. Lumbaque, D.S. Araújo, T.M. Klein, E.R.L. Tiburtius, J. Argüello, C. Sirtori,
Solar photo-Fenton-like process at neutral pH: Fe(III)-EDDS complex formation and
optimization of experimental conditions for degradation of pharmaceuticals, Catal.
Today. 328 (2019) 259–266.
https://doi.org/https://doi.org/10.1016/j.cattod.2019.01.006.

[65]   P.C. Thomas, P. Bicherel, F.J. Bauer, How in silico and QSAR approaches can
increase confidence in environmental hazard and risk assessment, Integr. Environ.
Assess. Manag. 15 (2019) 40–50. https://doi.org/10.1002/ieam.4108.

[66]   F. Mansour, M. Al-Hindi, W. Saad, D. Salam, Environmental risk analysis and prioritization of pharmaceuticals in a developing world context, Sci. Total Environ. 557–558 (2016) 31–43. https://doi.org/10.1016/j.scitotenv.2016.03.023.

[67]   P. Sanabria, D. Scunderlick, M.L. Wilde, D.S. Lüdtke, C. Sirtori, Solar photo-Fenton treatment of the anti-cancer drug anastrozole in different aqueous matrices at near-neutral pH: Transformation products identification, pathways proposal, and in silico (Q)SAR risk assessment, Sci. Total Environ. 754 (2021) 142300. https://doi.org/10.1016/j.scitotenv.2020.142300.

[68]   C. Rücker, K. Kümmerer, Modeling and predicting aquatic aerobic biodegradation – a review from a user's perspective, Green Chem. 14 (2012) 875–887. https://doi.org/10.1039/C2GC16267A.

[69]   M. Chen, Z. Zhang, L. Zhu, N. Wang, H. Tang, Bisulfite-induced drastic enhancement of bisphenol A degradation in Fe^{3+}-H_2O_2 Fenton system, Chem. Eng. J. 361 (2019) 1190–1197. https://doi.org/10.1016/j.cej.2018.12.170.

[70]   M. Taheran, M. Naghdi, S.K. Brar, M. Verma, R.Y. Surampalli, Emerging contaminants: Here today, there tomorrow!, Environ. Nanotechnology, Monit. Manag. 10 (2018) 122–126. https://doi.org/10.1016/j.enmm.2018.05.010.

[71]   J. Wilkinson, P.S. Hooda, J. Barker, S. Barton, J. Swinden, Occurrence, fate and transformation of emerging contaminants in water: An overarching review of the field, Environ. Pollut. 231 (2017) 954–970. https://doi.org/10.1016/j.envpol.2017.08.032.

[72]   J.L. Wilkinson, A.B.A. Boxall, D.W. Kolpin, K.M.Y. Leung, W.S. Lai, C. Galbán-Malagón, A.D. Adell, J. Mondon, M. Metian, R.A. Marchant, A. Bouzas-Monroy, A. Cuni-Sanchez, A. Coors, P. Carriquiriborde, M. Rojo, C. Gordon, M. Cara, M. Moermond, T. Luarte, P. V., Y. Perikhanyan, C.S. Mahon, C.J. McGurk, H. Thilo, K. Tapos, I. Volga, G.-O. Jessica, T.J. L., G.D.F. Francisco, R.M.T. P., D. Victorien, G. Gildas, T. Oumar, B.J. M., K.L. E., W. Michelle, W. Donald, N. Romaric, P. Jaime, Y. Guang-Guo, C. Chang-Er, P. Martha, M.-L. Jina, O. Jean-Paul, P. John, I.S. A., W. Penelope, E.-S. Silvia, U.-K. Nikolina, M. Milena, F.-K. Despo, I.-T. Lida, B. Vladimíra, V. Jan, C.-B. María, K.B. A., G. Jeanne, C. Arnaud, G. Peter, K. Ilia, S.

Sven, L. Gerasimos, H.H. P., M. Molly, S. Thatikonda, L. Manisha, N. Anindrya, S. Adee, P. Nima, A. Ali, A. Omar, G.S. S., P. Francesco, C. Benny, T. Tom, Y.K. Marcellin, A. Bakhyt, B. Raikhan, O. Lydia, M.J. K., C. Peter, N. Victor, B.N. T., S. Sheck, A.A. Zaharin, L.L. Juen, N. Mahamoudane, T.S. T., O. Rik, O. Olatayo, A. Muhammad, I. Muhammad, A. Ziad, O. Aaron, M.-S.J. Manuel, C. María, de la C. Heidi, N. Ian, C. Fabio, G.A. Brima, K.B. M., C.-F. Vesna, G. Mitja, T. Melusi, C. Kyungho, K. Habyeong, L.J.L. Celestino, R. Andreu, A. Priyanie, S. Anna, H. Gisela, Z.A. K., K.A. C., J. Jheng-Jie, K. Rebecca, T. Madaka, T. Ulas, O.T. T., L.J. B., V. Yuliya, V. Yuriy, H. Horacio, P.-P. Andrés, S.D. B., F. Maritza, G. David, T. Charles, Pharmaceutical pollution of the world's rivers, Proc. Natl. Acad. Sci. 119 (2022) e2113947119. https://doi.org/10.1073/pnas.2113947119.

[73]   O. Frédéric, P. Yves, Pharmaceuticals in hospital wastewater: Their ecotoxicity and contribution to the environmental hazard of the effluent, Chemosphere. 115 (2014) 31–39. https://doi.org/10.1016/j.chemosphere.2014.01.016.

[74]   A. Durán, J.M. Monteagudo, I. San Martín, Operation costs of the solar photo-catalytic degradation of pharmaceuticals in water: A mini-review, Chemosphere. 211 (2018) 482–488. https://doi.org/https://doi.org/10.1016/j.chemosphere.2018.07.170.

[75]   D. Fatta-Kassinos, M.I. Vasquez, K. Kümmerer, Transformation products of pharmaceuticals in surface waters and wastewater formed during photolysis and advanced oxidation processes – Degradation, elucidation of byproducts and assessment of their biological potency, Chemosphere. 85 (2011) 693–709. https://doi.org/https://doi.org/10.1016/j.chemosphere.2011.06.082.

[76]   T. Rastogi, C. Leder, K. Kümmerer, Qualitative environmental risk assessment of photolytic transformation products of iodinated X-ray contrast agent diatrizoic acid, Sci. Total Environ. 482–483 (2014) 378–388. https://doi.org/10.1016/j.scitotenv.2014.02.139.

[77]   M. Herrmann, J. Menz, O. Olsson, K. Kümmerer, Identification of phototransformation products of the antiepileptic drug gabapentin: Biodegradability and initial assessment of toxicity, Wat. Res. 85 (2015) 11–21. https://doi.org/10.1016/j.watres.2015.08.004.

[78] S. Zhu, Y. Liu, S. Liu, G. Zeng, L. Jiang, X. Tan, L. Zhou, W. Zeng, T. Li, C. Yang, Adsorption of emerging contaminant metformin using graphene oxide, Chemosphere. 179 (2017) 20–28. https://doi.org/10.1016/j.chemosphere.2017.03.071.

[79] S.A. Carmalin, E.C. Lima, Removal of emerging contaminants from the environment by adsorption, Ecotoxicol. Environ. Saf. 150 (2018) 1–17. https://doi.org/10.1016/j.ecoenv.2017.12.026.

[80] S. Álvarez-Torrellas, J.A. Peres, V. Gil-Álvarez, G. Ovejero, J. García, Effective adsorption of non-biodegradable pharmaceuticals from hospital wastewater with different carbon materials, Chem. Eng. J. 320 (2017) 319–329. https://doi.org/10.1016/j.cej.2017.03.077.

[81] D.R. Lima, E.C. Lima, C.S. Umpierres, P.S. Thue, G.A. El-Chaghaby, R.S. da Silva, F.A. Pavan, S.L.P. Dias, C. Biron, Removal of amoxicillin from simulated hospital effluents by adsorption using activated carbons prepared from capsules of cashew of Para, Environ. Sci. Pollut. Res. 26 (2019) 16396–16408. https://doi.org/10.1007/s11356-019-04994-6.

[82] C. Saucier, P. Karthickeyan, V. Ranjithkumar, E.C. Lima, G.S. dos Reis, I.A.S. de Brum, Efficient removal of amoxicillin and paracetamol from aqueous solutions using magnetic activated carbon, Environ. Sci. Pollut. Res. 24 (2017) 5918–5932. https://doi.org/10.1007/s11356-016-8304-7.

[83] S.G. Michael, I. Michael-Kordatou, V.G. Beretsou, T. Jäger, C. Michael, T. Schwartz, D. Fatta-Kassinos, Solar photo-Fenton oxidation followed by adsorption on activated carbon for the minimisation of antibiotic resistance determinants and toxicity present in urban wastewater, Appl. Catal. B Environ. 244 (2019) 871–880. https://doi.org/https://doi.org/10.1016/j.apcatb.2018.12.030.

[84] N.A. Khan, S.U. Khan, S. Ahmed, I.H. Farooqi, M. Yousefi, A.A. Mohammadi, F. Changani, Recent trends in disposal and treatment technologies of emerging-pollutants- A critical review, TrAC Trends Anal. Chem. 122 (2020) 115744. https://doi.org/https://doi.org/10.1016/j.trac.2019.115744.

[85] M.-A. Vaudreuil, S. Vo Duy, G. Munoz, S. Sauvé, Pharmaceutical pollution of

hospital effluents and municipal wastewaters of Eastern Canada, Sci. Total Environ. 846 (2022) 157353. https://doi.org/10.1016/j.scitotenv.2022.157353.

[86] A. Nikolaou, S. Meric, D. Fatta, Occurrence patterns of pharmaceuticals in water and wastewater environments, Anal. Bioanal. Chem. 387 (2007) 1225–1234. https://doi.org/10.1007/s00216-006-1035-8.

[87] A.M. Botero-Coy, D. Martínez-Pachón, C. Boix, R.J. Rincón, N. Castillo, L.P. Arias-Marín, L. Manrique-Losada, R. Torres-Palma, A. Moncayo-Lasso, F. Hernández, 'An investigation into the occurrence and removal of pharmaceuticals in Colombian wastewater,' Sci. Total Environ. 642 (2018) 842–853. https://doi.org/https://doi.org/10.1016/j.scitotenv.2018.06.088.

[88] E. Brillas, A critical review on ibuprofen removal from synthetic waters, natural waters, and real wastewaters by advanced oxidation processes, Chemosphere. 286 (2022) 131849. https://doi.org/10.1016/j.chemosphere.2021.131849.

[89] A.V. Santos, C.F. Couto, Y.A.R. Lebron, V.R. Moreira, A.F.S. Foureaux, E.O. Reis, L.V. de S. Santos, L.H. de Andrade, M.C.S. Amaral, L.C. Lange, Occurrence and risk assessment of pharmaceutically active compounds in water supply systems in Brazil, Sci. Total Environ. 746 (2020) 141011. https://doi.org/10.1016/j.scitotenv.2020.141011.

[90] D. Simazaki, R. Kubota, T. Suzuki, M. Akiba, T. Nishimura, S. Kunikane, Occurrence of selected pharmaceuticals at drinking water purification plants in Japan and implications for human health, Water Res. 76 (2015) 187–200. https://doi.org/10.1016/j.watres.2015.02.059.

[91] A. Gogoi, P. Mazumder, V.K. Tyagi, G.G. Tushara Chaminda, A.K. An, M. Kumar, Occurrence and fate of emerging contaminants in water environment: A review, Groundw. Sustain. Dev. 6 (2018) 169–180. https://doi.org/10.1016/j.gsd.2017.12.009.

[92] S. Giannakis, K.-Y.A. Lin, F. Ghanbari, A review of the recent advances on the treatment of industrial wastewaters by Sulfate Radical-based Advanced Oxidation Processes (SR-AOPs), Chem. Eng. J. 406 (2021) 127083. https://doi.org/10.1016/j.cej.2020.127083.

[93] J. Hou, Z. Chen, J. Gao, Y. Xie, L. Li, S. Qin, Q. Wang, D. Mao, Y. Luo,
      Simultaneous removal of antibiotics and antibiotic resistance genes from
      pharmaceutical wastewater using the combinations of up-flow anaerobic sludge bed,
      anoxic-oxic tank, and advanced oxidation technologies, Water Res. 159 (2019) 511–
      520. https://doi.org/https://doi.org/10.1016/j.watres.2019.05.034.

[94] E.P. Costa, M. Roccamante, C.C. Amorim, I. Oller, J.A. Sánchez Pérez, S. Malato,
      New trend on open solar photoreactors to treat micropollutants by photo-Fenton at
      circumneutral pH: Increasing optical pathway, Chem. Eng. J. 385 (2020) 123982.
      https://doi.org/https://doi.org/10.1016/j.cej.2019.123982.

[95] G.R. Ibáñez, M. Bittner, Z. Toušová, M.C. Campos-Mañas, A. Agüera, J.L.C. López,
      J.A.S. Pérez, K. Hilscherová, Does micropollutant removal by solar photo-Fenton
      reduce ecotoxicity in municipal wastewater? A comprehensive study at pilot scale
      open reactors, J. Chem. Technol. Biotechnol. 92 (2017) 2114–2122.
      https://doi.org/10.1002/jctb.5212.

[96] A.B. Leite, C. Saucier, E.C. Lima, G.S. dos Reis, C.S. Umpierres, B.L. Mello, M.
      Shirmardi, S.L.P. Dias, C.H. Sampaio, Activated carbons from avocado seed:
      optimisation and application for removal of several emerging organic compounds,
      Environ. Sci. Pollut. Res. 25 (2018) 7647–7661. https://doi.org/10.1007/s11356-017-
      1105-9.

[97] S.G. Michael, I. Michael-Kordatou, V.G. Beretsou, T. Jäger, C. Michael, T. Schwartz,
      D. Fatta-Kassinos, Solar photo-Fenton oxidation followed by adsorption on activated
      carbon for the minimisation of antibiotic resistance determinants and toxicity present
      in urban wastewater, Appl. Catal. B Environ. 244 (2019) 871–880.
      https://doi.org/10.1016/j.apcatb.2018.12.030.

[98] N.A. Alygizakis, J. Urík, V.G. Beretsou, I. Kampouris, A. Galani, M. Oswaldova, T.
      Berendonk, P. Oswald, N.S. Thomaidis, J. Slobodnik, B. Vrana, D. Fatta-Kassinos,
      Evaluation of chemical and biological contaminants of emerging concern in treated
      wastewater intended for agricultural reuse, Environ. Int. 138 (2020) 105597.
      https://doi.org/10.1016/j.envint.2020.105597.

[99] R. Wielens Becker, M. Ibáñez, E. Cuervo Lumbaque, M.L. Wilde, T. Flores da Rosa, F. Hernández, C. Sirtori, Investigation of pharmaceuticals and their metabolites in Brazilian hospital wastewater by LC-QTOF MS screening combined with a preliminary exposure and in silico risk assessment, Sci. Total Environ. 699 (2020) 134218. https://doi.org/10.1016/j.scitotenv.2019.134218.

[100] M. Ibáñez, V. Borova, C. Boix, R. Aalizadeh, R. Bade, N.S. Thomaidis, F. Hernández, UHPLC-QTOF MS screening of pharmaceuticals and their metabolites in treated wastewater samples from Athens, J. Hazard. Mater. 323 (2017) 26–35. https://doi.org/10.1016/j.jhazmat.2016.03.078.

[101] K. Styszko, K. Proctor, E. Castrignanò, B. Kasprzyk-Hordern, Occurrence of pharmaceutical residues, personal care products, lifestyle chemicals, illicit drugs and metabolites in wastewater and receiving surface waters of Krakow agglomeration in South Poland, Sci. Total Environ. 768 (2021) 144360. https://doi.org/10.1016/j.scitotenv.2020.144360.

[102] R.M. Cardoso, R.W. Becker, L.A. Jachstet, D. Scunderlick, A. Dallegrave, A. Ruiz-Padillo, C. Sirtori, Qualitative evaluation of pharmaceuticals and metabolites in hospital effluent: Influence of sample preparation technique and outranking by environmental risk using the ELECTRE method, Sci. Total Environ. 834 (2022) 155119. https://doi.org/10.1016/j.scitotenv.2022.155119.

[103] F. Hernández, N. Calısto-Ulloa, C. Gómez-Fuentes, M. Gómez, J. Ferrer, G. González-Rocha, H. Bello-Toledo, A.M. Botero-Coy, C. Boıx, M. Ibáñez, M. Montory, Occurrence of antibiotics and bacterial resistance in wastewater and sea water from the Antarctic, J. Hazard. Mater. 363 (2019) 447–456. https://doi.org/10.1016/j.jhazmat.2018.07.027.